Zinc and zinc alloy composite coatings for corrosion protection and wear resistance

by

Tuaweri, Johnnie Tolumoye
M.Sc (Eng.) (Donetsk)

A doctoral thesis submitted in partial fulfilment of the requirements for the award of
Doctor of Philosophy of Loughborough University

Supervisor: Dr. G.D.Wilcox

Institute of Polymer Technology and Materials Engineering
Loughborough University

December 2005

SYNOPSIS

Zinc and its alloys are among the most widely utilised metallic coatings for the sacrificial protection of steel. Although excellent in this mode of protection, these coatings are often less durable when subjected to environments of combined wear and corrosion due to their intrinsic relative softness and ductility. A possible and fast growing way of improving the durability of these coating is by the codeposition of inert particles into the zinc and zinc-alloy matrix. The main aim of this research was therefore to improve the durability of zinc and zinc-nickel coatings by the incorporation of inert particles via electrolytic codeposition methods.

The first five chapters of this thesis comprise literature review on the electrodeposition of zinc, its alloys and composite electrodeposition in general. A major part of which was dedicated to the review of various conventional methods and parameters such as current density, agitation, temperature, solution composition, bath additives and pH usually investigated in electrodeposition.

The experimental work was principally based on DC electrodeposition and was aimed at understanding the deposition behaviour of zinc and zinc-nickel electrodeposition baths, conditions which influence them and solution compatibility to the introduction of silica particles

A systematic study on the deposition behaviour of both zinc/silica and zinc-nickel/silica composite baths was carried out with particular interest on the rate of particle incorporation and the influence of particles on zinc-nickel alloy deposition. The complimentary codeposition behaviour of the nickel and silica particles was observed. The influence of bath additives such as N,N Dimethyldodecylamine (NND) and sodium nitrate on the rate of silica incorporation was also studied. Both additives were found to improve the rate of particle incorporation for the zinc/silica. The morphologies and compositions of the coatings were analysed with the use of SEM and FEGSEM.

Corrosion performance studies were carried out in a neutral salt spray chamber and linear polarisation resistance methods used to determine barrier corrosion properties of the coatings. Anodic polarisation studies were also carried out. The results show an improvement in the corrosion performance of these coatings with the addition of silica particles

Reciprocating wear tests were used to determine the wear behaviour of the coatings in terms of weight loss. Improvement in wear resistance was not observed in the zinc/silica coatings probably due to the high content of silica in the coatings. Lower silica contents may be required for the desired improvements. However, there were obvious improvements in the wear behaviour of the zinc-nickel/silica coatings due to the presence of the silica particles.

Keywords

Composite, electrodeposition, zinc, zinc-nickel, N,N Dimethyldodecylamine, sacrificial coatings, corrosion resistance, wear resistance.

ACKNOWLEDGEMENTS

I would like to express my deepest gratitude to my supervisor, Dr. G.D. Wilcox for his concern, support, encouragement, patience and dedication in the supervision of this research work. Thanks also to Professor R. Faulkner my director of research.

I also want to thank my beloved wife and children, Pastor Lizzy, Toboulayefa, Gloria, Woyengipreye and Ebiegberi for their prayers, love and sacrifice throughout the period of this research work. Special thanks to my parents Mr J.O. Tuaweri and Mrs. M.P. Tuaweri for the love and sacrifice for my education. I also want to thank my sister and her husband Mrs Kens Walson and Mr Ken Walson for their love and support over the years.

I wish to specially thank Dr. Keming Chen for his invaluable discussions and support at all stages of this research work. Many thanks also to Mr. J.S. Bates, Mr. F. Page for their help with the FEGSEM and SEM analysis. Thanks also to my colleagues and friends on study fellowship at Loughborough University, Mr. Promise Mebine, Mr Emmanuel Adigio, Allen Ekubo, Mrs Ibiba Harry, Mrs Rhoda Gumus, Mr Osaisai and Mr. Cornelius Odigi for their encouragements.

My gratitude also extends to all the staff and students of IPTME for the friendly and supportive environment during the period of this research.

These acknowledgements are also extended to all that may have been directly or indirectly involved in this research that I happen to have overlooked.

Last, but not the least, I wish to thank the Bayelsa State Government for funding this research work.

Dedication

This work is dedicated to God almighty for "The earth is the Lord's, and the fullness thereof; the world and they that dwell therein" (Psalm 24:1).

NOMENCLATURE

CCE	Cathode current efficiency (%)
ΔW	Change in weight of deposit (g)
W_T	Theoretical weight of deposit (g)
I	Applied current (A)
t	Time (seconds.)
M_{Zn}	Molecular weight of zinc (g/mol)
n	Number of electrons involved in the reaction
E_{corr}	Corrosion potential (mV)
F_{Adh}	Adhesion force (N)
F_{Stagn}	Stagnation force (N)
F_{shear}	Shear force (N)
F_{fric}	Frictional force (N)
NND	N,N Dimethydodecylamine
Wt%	Weight percentage
J	Applied current density (A/dm^2)
A	Effective cathode surface area (dm^2)
VHN	Vickers hardness

CONTENTS

CHAPTER ONE

1 INTRODUCTION

The unique mechanical properties of mild steel have made it one of the most widely utilised engineering materials for several decades, consequently often exposing it to very severe working conditions. Although a lot of effort is being made to replace mild steel in many industries, probably due to its intrinsic weight, considerable efforts are equally being made to further improve its properties and durability either by developing better alloys or protective coatings capable of prolonging its lifespan with improved workability. Consequently, it continues to dominate as a major engineering material especially in the construction and automotive industries. However, a major drawback to carbon steel is that it suffers from various forms of corrosion and wear when subjected to certain aggressive environments, especially those containing aggressive pollutants and abrasive media.

Corrosion and wear are processes contributing to economic losses and pollution of our environment and are often associated with the degradation of metals and their alloys. This could occur in man-made as well as natural environments. Methods of corrosion control and wear resistance become more and more important as we become increasingly concerned about conserving our natural environment.

Electrodeposited (electroplated) coatings are one method widely utilised to confer protection to metallic surfaces. These coatings can consist of single metals, but also many binary and even ternary alloys can be deposited, producing in many cases, enhanced corrosion protection. A wide variety of metals can be successfully deposited in this manner ranging from noble metals such as gold and silver through to more base metals such as zinc and cadmium.

However, the use of cadmium is greatly discouraged in recent times, despite its good corrosion protection properties, due to its high toxicity.

Zinc has found widespread use as the basis of a whole range of sacrificial coatings for ferrous substrates. The metal can be applied by a variety of techniques, including hot- dipping, metal spraying, cementation, cladding and electrodeposition [1]. As a sacrificial coating under atmospheric conditions, zinc provides good protection to underlying ferrous substrates. However, more recently there has been much interest in the use of electrodeposited zinc alloys for similar end uses. These alloys are usually (but not exclusively) a combination of zinc and a so-called "iron block" metal. The most common examples are zinc-iron, zinc-nickel, zinc-cobalt, zinc-manganese and zinc-tin, the former three examples being the most widely reported, although zinc-manganese is probably not commercially available [1].

In recent years, the development of these zinc-based finishes has taken a new turn due to the increasing demand for more durable coatings. Research is beginning to focus on the study of new materials the metal matrix composite coatings. Electrochemical composite plating can produce these coatings, having improved properties compared to plain metal coatings. When inert particles are suspended in a metal electroplating electrolyte, they tend to codeposit with the metal matrix. Usually electrochemical composite plating is used to obtain metal coatings exhibiting a specific property of the particle material: for example, high abrasion resistance or low coefficient of friction [2]. Composite coating on a commercial scale is relatively new; the first commercial processes were established in the 1960s.

Although good for the sacrificial protection of steel, pure zinc coatings are generally ductile and unable to offer both corrosion and effective wear resistance properties, hence the need for further development of these zinc-based coatings.

The underlying aim of this research was therefore; to develop zinc and zinc-alloy coatings by incorporating second phase inert particles into their matrices and studying the behaviour of these composite coatings. A series of particulate species were considered and silica was subsequently selected as the second phase material. In this research, electrodeposited zinc,

zinc-nickel, zinc/silica and zinc-nickel/silica composite coatings have been studied. The effect of incorporation of silica has been examined and its suitability as an addition to electrolytes to produce zinc/silica and zinc-nickel/silica composite electrodeposits investigated.

The first part of this thesis attempts to explore existing literature on zinc and zinc-alloy composite electrodeposition with the initial section discussing the concept of sacrificial protection of steel. This is followed by the electrodeposition of zinc in general with particular attention to the different types of baths traditionally utilised in zinc electrodeposition. Previous works on deposit morphology, texture and crystallographic orientation of these coatings and their influence on the microstructure are studied. Influence of bath additives and impurities on zinc deposition is also presented. The next section in the literature review centres on the fundamental principles of alloy electrodeposition giving priority to the iron group metals such as Zn-Ni, Zn-Fe, Zn-Co, Zn-Mn and Zn-Sn. The culminating section of the literature review is dedicated to the crux of the research; this being composite electrodeposition, embracing methods of particle incorporation, electroless and electrolytic composite coatings, and various parameters influencing composite electrodeposition. Wear resistant coatings are also discussed.

The second part of this thesis outlines the experimental procedures employed to execute the project. The first section begins with the study of zinc electrodeposition. Determination of current efficiency of the different types of bath with particular attention on the influence of the various conventional electrodeposition parameters is discussed. This is then followed by zinc-nickel electrodeposition from both chloride and sulphate acid baths. For the purpose of industrial applications, sulphate baths were selected for further investigations. The next stage of the experimental techniques section is the composite electrodeposition of zinc/silica, and zinc-nickel/silica. The importance of particle suspension was recognised for effective particle incorporation. Bath agitation was therefore given particular attention in most of the composite electrodeposition experiments carried out with either magnetic stirring or by vibratory agitation. Cathodic polarisation studies were carried out to produce a mechanistic understanding of the deposition behaviour of the composite system. Details are then given of corrosion tests carried out on the coatings namely the use of a neutral salt spray chamber in

accordance with ASTM B117. The corrosion rates of zinc, zinc-nickel, zinc/silica and zinc-nickel/silica coatings were investigated. Anodic polarisation studies were also carried out in 3.5% and 5.0% NaCl solutions to include mechanistic information regarding the corrosion behaviour of these coatings. Finally, wear tests were carried out to ascertain the wear resistance behaviour of these coatings particularly those containing silica particles.

The third and last part of this thesis contains five chapters of results and discussions, conclusions, future work, references and an appendix.

CHAPTER TWO

2 ZINC

Zinc is a silvery white metal with a relatively low melting point (419 °C) and boiling point (907 °C). The strength and hardness of unalloyed zinc is greater than tin and lead, but appreciably less than that of aluminium and copper. It cannot be used in stressed applications due to its low creep resistance. Except when very pure, zinc is brittle at ordinary temperatures but malleable above 100 °C and can readily be rolled. The metal is amenable to most forming operations. A major application of zinc is as an alloying addition to copper, forming the range of copper alloys called brasses. One of the most useful characteristics of zinc is its resistance to atmospheric corrosion, and one of its main applications thus being for the protection of steelwork [3].

The excellent resistance of zinc to corrosion in many environments and its ability to protect steel galvanically account for its successful use and performance in a myriad of applications. A large percentage of the total consumption of zinc is for applications where resistance to corrosion is a major requirement. The balance is used where mechanical properties, ease of fabrication, or cost may be of greater importance as in zinc die-casting and parts fabricated from rolled zinc and zinc alloys [4]. Although most applications of the metal are under pressure from possible substitutes, the demand continues to grow, and there can be little doubt that it will be used in quantity for many years to come. If demand continues at the present rate, however, the availability of sufficient high-grade concentrate, on which the industry now mainly depends, will be threatened [3].

2.1 Mechanism of corrosion and corrosion protection

The corrosion of zinc is an electrochemical process in which zinc is oxidized with simultaneous reduction of hydrogen ions or dissolved oxygen in the electrolyte. When zinc corrodes in pure water, up to four species can be present over the complete range of potential and pH: Zn, Zn^{2+}, $Zn(OH)_2$ and ZnO_2^{2-} [5]. The oxidation follows the following reaction and the potential deduced from the Nernst equation as shown in equation 1 below:

$Zn = Zn^{2+} + 2e^-$ $E = -0.76 + 0.0295 \log [Zn^{2+}]$ V_{SHE} **(eqn.1)**

Where $[Zn^{2+}] = 10^{-6}$ M.

Zinc owes its high degree of resistance to atmospheric corrosion to the formation of insoluble basic carbonate films. The most important factors, which control the rate at which zinc corrodes in atmospheric exposure, are: the duration and frequency of moisture contact; the rate at which the surface dries; and the extent of industrial pollution of the atmosphere [4]. As earlier mentioned, one of the most important uses of zinc in corrosion control is as a coating for steel such as in galvanising. As long as the coating is continuous and impervious, the corrosion behaviour will be similar to that of solid zinc. But should the coating become perforated or discontinuous as a result of corrosion or mechanical damage, a galvanic cell will be formed in the presence of moisture or other electrically conducting solutions. The difference in electrochemical potential between the zinc and steel causes an electric current to flow through the cell. This current is a measure of galvanic corrosion, and the more active metal (least noble) will be the anode and will corrode in proportion to the magnitude of the current and the period of exposure. In most solutions, zinc is anodic to steel and suffers accelerated corrosion, while the steel is galvanically protected. This mechanism is also referred to as sacrificial corrosion; that is, the zinc is sacrificed in order to protect the steel. Corrosion in such a situation is a desirable effect because it operates to prolong the life of the steel that is being protected. In practice, corrosion products formed as a result of the flow of current through the galvanic cell may deposit in small discontinuities in the coating and serve to stifle further corrosion just as films of corrosion products protect solid zinc surfaces. Therefore in spite of the increased corrosion of zinc by the flow of galvanic current, the mechanism that is responsible for the inherent corrosion resistance of zinc also contributes to the excellent protective action provided by zinc coatings [4].

2.2 Effect of atmospheric pollutants on zinc

For a long time the degradation of most metals in the atmosphere was attributed to the deteriorative effect of sulphur dioxide and in special environments also to chlorides. They received thorough attention in atmospheric corrosion research and are the most extensively studied pollutants [6].

In the first step of corrosion, the atmospheric corrosion of zinc leads to a thin surface layer of zinc hydroxide. After a few months of exposure in medium polluted atmospheres zinc carbonate, zinc hydroxide, hydrozincite ($Zn_5(OH)_6(CO_3)_2$) and zinc oxide are formed, the later being the thermodynamically most stable corrosion product in the zinc/H_2O-system. Due to the protective action of the corrosion layer formed, the corrosion rate slows down somewhat. In moderately polluted atmosphere zinc hydroxy sulphates such as $Zn_4SO_4(OH)_6.nH_2O$ and in marine site zinc hydroxy chlorides, with a comparatively low water-solubility have been found as components of the corrosion layers. The presence of high levels of sulphur dioxide or chloride concentrations leads to the dissolution of the protective layer and to the formation of corrosion products with a good water solubility. Generally, sulphate-based zinc compounds are more soluble than their choride-based counterparts and therefore expected to corrode quicker. Recent results [6] from environments with comparatively low sulphur dioxide pollution levels have shown that the decrease in corrosion rate with time is rather small and therefore the protective properties of the corrosion layer are also low, even in less polluted atmospheres. The formation of water-soluble zinc sulphate among other factors is responsible for the comparatively high soluble sulphate and zinc ion concentrations found in aqueous extracts of the corrosion products.

Laboratory exposures conducted by HENRIKSEN [7] at high relative humidity (95 %) with nitrogen dioxide as the single pollutant showed that its effect on weight gain is considerably smaller compared to that of sulphur dioxide. Also for combinations of these gases practically the same weight gain resulted as with nitrogen dioxide alone. Laboratory experiments with ozone are rare. However, SVENSSEN [8] conducted experiments with ozone and combination

of sulphur dioxide and ozone and found a negligible effect for ozone in the absence of sulphur dioxide, while the combination with sulphur dioxide resulted in a corrosion accelerating effect at 70% as well as 95% relative humidity compared to the effect of sulphur dioxide alone.

In the presence of sulphur dioxide and its combination with nitrogen, zinc hydroxides, zinc carbonate and zinc oxide, zinc sulphate and basic sulphates, as well as water-soluble nitrates were found [8]. The corrosion products in the presence of the single pollutants nitrogen dioxide and ozone are not well known. However, the presence of nitrates and nitrites were reported [8] in water rinses of experiments with nitrogen dioxide.

CHAPTER THREE

3 ZINC ELECTRODEPOSITION

Electrodeposited zinc and zinc-based coatings find extensive use in applications such as, amongst others, the corrosion protection of steel in the automotive industry. Usually the mechanical and chemical properties are improved by alloying [9]. The manufactured material usually meet standards of five years' resistance to "appearance" deterioration and 10-years resistance to the perforation of the underlying basis metal [10]. Many producers and investigators assume that the service life of the electrogalvanised layers is directly proportional to their thickness only. However, the corrosion characteristics are strongly determined by the texture and microstructure obtained, that, in turn, depends on the specific deposition procedure employed. The electrochemical deposition of zinc has been widely investigated using various approaches, which has effectively lead to the preparation of coatings that differ in their macro and micro-structure, texture density, uniformity and corrosion resistance [11-13]. It is however, noted [14] that electrodeposited films' texture, apart from the corrosion behaviour, can noticeably affect a variety of properties such as paintability, formability and wear resistance.

A wide variety of plating bath composition has been employed in electrogalvanizing to control the growth of cathode deposits, inhibiting the formation of dendrites and to produce fine-grained, smoother deposits [15]. Until recently nearly all zinc electroplating was carried out using cyanide baths. However, the effluent toxicity is a cause for concern and as a result newer less toxic baths have been developed [16]. These can be broadly classified as alkaline or acid types. The alkaline type baths are usually used for zinc plating steel pressings and many still contain cyanide, albeit at reduced levels. Many of the acid type baths utilise zinc sulphate and are normally used to electroplate cast iron and malleable irons. The main disadvantages of the acid type baths are that they are corrosive so care has to be taken to protect operators and

equipment and these baths generally exhibit poor current efficiency. A review of the relative merits of the zincate containing baths has been published by WILCOX AND MITCHELL [16]

In general, the results obtained from acid, neutral and alkaline electrolytic baths occasionally bear contradictory conclusions, however, zinc electrodeposition can be described as weakly inhibited process involving a fast even autocatalytic electron transfer rate [14]. In zincate solutions as well as in certain acid media such as Leclanche cell electrolyte, it is known that several complex ions are in chemical equilibria. EPELBOIN et al [17] modelled the electrocrystallization of zinc involving an autocatalytic step. They noted that the mechanism of electrocrystallization is more complicated in alkaline medium than in acid medium. According to them, with a Leclanche electrolyte, decrease in pH gives rise to a decrease in cathodic polarization at low current values, which is contrary to the inhibiting effect of hydrogen adsorption. On the other hand, with the acid solution, which is known to form complexes with zinc much less readily than the Leclanche cell electrolyte, a decrease of the pH actually entails an increase in the inhibiting effect of hydrogen adsorption [17]. Furthermore, their model accounted for the influence of hydrogen evolution on the efficiency of the electrocrystallization of zinc stating that both in acid and alkaline medium, the efficiency of electrocrystallization is actually an increasing function of current while a decrease in pH leads to a decrease of the efficiency at constant current.

Electroplating normally takes place under a DC regime, however, improved smoothness by means of pulse plating, a periodically interrupted process in which a certain duty cycle of cathodic potential/current is employed [14,18,19]. A variation of the latter method is the periodic-reverse mode in which the polarity is periodically reversed so that the metal is alternatively plated and anodically dissolved [14]. As reported by VASILOKOPOULOS et al [14] due to the absence of any rigorous theory on electrocrystallization, simplified, though useful approaches, have been proposed in order to cope with the complexity of growth mechanisms. Thus, the inhibition intensity together with the ratio of apparent cathodic current density of the bulk concentration of metallic ions to be discharged, constitute, in most cases, very useful parameters in order to describe the electrocrystallization process and the resulting crystal configuration. These parameters may be correlated, in general, to the observed order of

nucleation and further the mode of crystal growth. VELINOV et al [20] found that in the zinc electrocrystallization process two types of inhibition occur, primary and secondary (autoinhibition). They reported that the conditions for cathode deposit formation and consequently crystallite orientation are significantly altered by hydrogen codischarge. In general, the crystalline forms and crystal orientation of metal deposit result from a competition between growth parallel and perpendicular to the deposition substrate, both determined by supersaturation (expressed by cathodic overvoltage), which characterises the process in a complicated manner [15]. A high 'out' growth rate normal to the substrate leads to a fibrous structure whilst an increased rate of lateral growth may lead to the development of large "facets" parallel to the substrate.

3.1 Electrodeposition from acid sulphate baths

Zinc deposition has been extensively investigated under various operating conditions depending on the application considered or the aims chosen. A sulphate medium is fairly popular in the electrometallurgy of zinc even though alkaline electrolytes or cyanide-containing baths are commonly used for industrial purposes. Sulphate media most often consist of zinc sulphate in the presence of sulphuric acid or sulphates of metal ions such as sodium and aluminium [12]. Most relevant papers underline the effect of pH on the kinetics of the process due to the likely role of H^+ in the case of acidic solutions. Besides, the reduction process can be interpreted using two different approaches:

(i) The macroscopic approach. The macroscopic approach is based on voltammetric curves obtained using classical devices such as the rotating disk electrode (*RDE*). The reductive deposition is represented as the exchange of two electrons. For the case of zinc sulphate containing solutions, KAHANDA AND TOMKIEWICZ [21] modelled the reduction as the simultaneous transfer of two electrons. According to other studies, zinc deposition is the product of two successive electron transfers [22], the first being rate determining step.

(ii) The " physical" approach. In the 1970s WIART et al. [17] suggested a more complex reaction scheme for zinc deposition and the value of the numerous parameters involved could be examined using several electrochemical techniques. As observed by EPELBOIN et al [23], an S-shaped *i-E* curve can be obtained for high zinc concentration showing multiple steady-

states characterised by the existence of three currents at a given potential. Secondly, the reduction of the divalent zinc was shown to be linked to hydrogen evolution, especially in acidic media: hydrogen adsorption onto the electrode was found to have an inhibiting action on zinc electrocrystallization. Also WIART et al [17] considered the competitive adsorption of monovalent zinc Zn^+ and ZnA, where A is the anion, the nature of which depends on the electrolyte.

The effect of zinc and acid concentration on current efficiency has been reported [24]. According to the authors, increasing the zinc concentration (decreasing the acid concentration) increased the current efficiency in a non-linear fashion and that the highest rate of increase occurred when the zinc concentration was increased from 42 to 50 g/l. The observation that the current efficiency increases as the acid concentration decreases is mainly due to the increase in zinc deposition reaction rate as the number of zinc ions in the electrolyte rises. Also, since the number of H^+ ions in solution decreases, the rate of hydrogen evolution reaction is reduced. Both of these factors improve the current efficiency [24].

3.2 Electrodeposition from chloride baths

One of the reasons why sulphuric acid has been widely used in hydrometallurgical treatment for the extraction of zinc from zinc ore or waste is because of the ease of electrowinning zinc from sulphate solutions. However, from the viewpoint of leaching, hydrochloric acid is a very efficient lixicant [25]. In spite of the advantages of high leaching efficiency and the relatively clean residue, it is rarely utilised due to the problem of chloride electrolysis, producing chlorine, which eventually leads to the loss of hydrochloric acid. As reported by BAIK AND FRAY [25], the few studies of zinc electrodeposition in chloride solutions have all produced chlorine gas and that the higher solubility and electrical conductivity of $ZnCl_2$ to decrease solution resistance are further advantages over sulphate electrolysis. Utilising these advantages, THOMAS AND FRAY [26] conducted the electrolysis in high concentration (18-35 wt%) of zinc chloride with high current densities (220-250 mA/cm^2) achieving 90% current efficiency (CE). However, leachate solutions are usually below 18% $ZnCl_2$ which means that lower current densities have to be used. According to BAIK AND FRAY [25], a better

alternative to the metal chloride treatment with recovery of hydrochloric acid would be a two-compartment cell divided by a cation exchange membrane. In this case, zinc is deposited at the cathode, oxygen is liberated at the anode and hydrogen ions pass from the anolyte (sulphate solution) to the catholyte (chloride solution) through the cation selective membrane. According to the authors, preliminary investigations, without using airsparging, produced dendrite-like growths which were predominant in all the deposits. Dendrites can be avoided by using air-sparging but this has undesirable effects, that is, water and acid loss by evaporation coupled with additional costs for the installation and maintenance of the sparging line. In high acid solutions, the air sparging would cause a toxic atmosphere containing hydrochloric acid. To avoid air sparging, levelling agents were used. Various kinds of levelling agents including proteinous additives [27] and alkyl ammonium chlorides have already been found to be effective in making dense coatings.

3.3 Effect of additives

The influence of various types of organic additives on the kinetics of zinc electrodeposition has been reported [27-31]. Such additives have been widely employed to counteract the harmful effects of different metallic impurities. They act either by increasing the induction period, by complexing the harmful impurities or by suppressing the hydrogen evolution reaction, which is facilitated by the presence of such impurities [29]. Apart from their inhibitive effect on metal ion impurities, certain organic additives (perfluorocarboxylic acids) tends to increase the current efficiency, decrease power consumption and produce better surface morphologies [29] for zinc electrodeposits. MACKINNON AND BRANNEN [27] reported that organic additives control deposit growth by inhibiting the formation of dendrites and by producing fine-grains, smoother deposits, perhaps by causing the deposition of metals in clusters on the points of high current density, thereby reducing the currents at these points. Although the precise mechanism by which this is achieved is not known, the following facts have been established:

(a) The additives assume a net positive charge and migrate to the cathode where they are adsorbed;

(b) Their actual presence in the deposit is exceedingly small and is difficult to confirm analytically.

Columnar deposit growth is eliminated by their presence in the electrolyte;

The composition of the electrolyte tends to alter the electrochemistry of the organic additive [27].

Reports in the literature indicate that the influence of colloids and surface-active substances on the zinc chloride electrolyte is less effective than with sulphate [32]. BRESSAN AND WIART [33] have shown that tetrabutylammonium bromide (NBu_4Br) is effective in inhibiting dendrite formation during zinc deposition from the Leclanche cell electrolyte: 2.67M NH_4Cl, 0.72M $ZnCl_2$, pH adjusted to 5.2 with NH_4OH. Previously, DIGGLE AND DAMJANOVIC [34] showed that NBu_4Br was effective in suppressing dendritic growth and producing compact zinc deposits from alkaline zincate. An earlier study on the structure of one hour zinc deposits electrowon from synthetic zinc chloride electrolyte [35] showed that the deposits were characterised by a morphology which featured clusters of large platelets with rounded edges and by a preferred orientation (002), (103), (105). According to BAIK AND FRAY [25] gelatin as a levelling agent was found to be effective for zinc deposition in these solutions. Without air sparging, and with mild stirring only, dense and flat deposits resulted. The presence of an organic additive was reported [27] to be essential for the electrowinning of smooth, compact, dendrite-free zinc deposits from chloride media. The effect of aluminium sulphate, animal glue and extracts of horse-chestnuts (HCE) on zinc electrowining from a weak sulphate electrolyte has been reported [30]. According to the authors the conjoint use of $Al_2(SO_4)_3$, animal glue and HCE results in smooth, slightly bright deposits, showing a beneficial effect for the mixture on zinc electrodeposition. These additives are thought to inhibit the discharge rate of impurity metal ions, such as copper, and lead, whose deposition is diffusion controlled [30].

3.4 Texture and morphology of zinc electrodeposits

The texture and morphology of zinc electrodeposits prepared under direct current (DC) and pulse current (PC) plating conditions from an acidic sulphate bath on low carbon steel

cathodes has been reported [14]. According to the author, variation of DC deposition current from very low (0.5 A/dm^2) to moderately high values (40 A/dm^2), results in changes in texture, grain structure, and surface morphology of deposited films, depending on the adopted acidic bath pH (2.0-4.5) and that PC plating effectively modifies the properties obtained, within a limited range of conditions; however, at high current densities PC's resemblance to DC plating was reported [14]. McBREEN [36] studied the morphology of zinc deposits formed under conditions of randomly varying potential as well as the effect of additives and substrates on morphology. He found that by superimposing a small potential oscillation, the morphology of the deposit was greatly improved. McBREEN AND GANNON [37] found that by superimposing a square wave potential the zinc nucleation rate was increased and the deposit morphology modified.

According to JIRICNY et al [38], current density and hydrodynamics are known to play a role in determining the nature of electrodeposit. These variables have been studied by many authors using rotating disc electrodes for the deposition of zinc from chloride and sulphate electrolytes [38]. According to JIRICNY et al it was found that smooth deposits were always obtained (in both laminar and turbulent flow) above 80 ± 10 mA/cm^2 (in 1M $ZnSO_4$ solution) or when the current was pulsed. Below these limits striated deposits were formed with the striations parallel to the flow direction. An explanation [39] is that the nucleation and growth rates of zinc crystals are dependent on overpotential (i.e current density). Consequently, higher current densities (even the momentary ones of current pulsing) result in numerous zinc nuclei across the whole surface of the electrode. The macroscopically smooth deposit is then the result of the inter-growth of these crystallites. At low current densities nucleation proceeds slowly, compared to crystal growth, and the few nuclei that form grow to large protrusions before encountering their neighbours [38].

3.4.1 Effect of crystallographic texture on zinc electrodeposit

Literature data on the effect of crystallographic texture on the properties of zinc and zinc–based coated steel sheets are contradictory. LINDSAY et al [10] reported on the relationship between crystallographic texture and formability based on laboratory and industrially

produced samples. The zinc coatings electrodeposited under laboratory conditions from a sulphate electrolyte were of two types. Coatings with basal (001) planes oriented parallel to the surface of the substrate easily underwent a substantial elongation under deep drawing. Coatings with pyramidal oriented parallel to the surface of the substrate quickly underwent intergranular or transgranular fracture under conditions of deep drawing and bending. On the contrary, commercial zinc deposit electrodeposited from a sulphate electrolyte having their pyramidal planes oriented parallel to the surface of the substrate, also retained their integrity under conditions of deep drawing and bending. LINDSAY et al [10] suggested that the difference in performance of industrial and laboratory zinc coatings could be related to the grain size. RANGARAJAN et al [40] reported that thicker electrogalvanised zinc coatings had a marked texture on the surface with a larger percentage of grains with (112) planes parallel to the surface. They concluded that with this texture, the basal plane, being the primary slip planes in hexagonal close packed (hcp) zinc, were favourably oriented for high resolved shear stress when subjected to uniaxial tension. They observed that as the coatings were strained the grains with the (112) planes parallel to the surface slipped and rotated, causing a significant change in texture. So in contradiction to the results of LINDSAY et al, RANGARAJAN et al [40] found the (112) texture to be favourable to plastic deformation. However, it is reported by XINGPU YE et al [13] that neither the hypothesis proposed by LINDSAY et al nor the conclusions on the experiments by RANGARAJAN et al [40] were satisfactory in their investigations.

3.5 Influence of microstructure on ductility

Concerning the influence of microstructure on ductility, ROGERS [41] stated that the following structural effects must be considered: the nucleation of voids, dislocation interaction, the presence of holes and particles and the embrittling effect of a special distribution of the softer phase in a two phase system. It is known that particles such as solid, organic or inorganic substances, additive and side reaction products present in the plating bath may codeposit with zinc during electrodeposition. The inclusion of such particles in the coating affects ductility [10].

3.6 Effect of impurities

Impurities in the electrolyte have an influence on morphology, and this is thought to result in effects on current efficiency and cathodic polarization [42]. Unfortunately, impurity effects are complex; some impurities exhibit synergy when added to zinc electrolytes in combination. Some impurities exhibit an induction period before they become detrimental to zinc electrodeposition by promoting redissolution of zinc and loss of current efficiency [43-44]. Because redissolution begins in pits formed in the deposit, a possible means of extending this induction period is to seek conditions where a smooth, level deposit, free of dendrites is obtained. FUKUBAYASHI [45] showed that the induction time was a function of the impurity concentration and that it was inversely dependent on the impurity concentration and temperature.

JAKSIC [46] investigated the initiation and development of the spongy growth of zinc and its suppression in the electrowinning of zinc from binary chloride systems. According to him, several types of metallic impurities result in the appearance of spongy zinc: (a) impurities such as copper which grow independently and locally and further perturb the growth surface; (b) impurities such as nickel and cobalt which are codeposited as an alloy with zinc and, after attaining a critical content in the growth surface, affect either the mossy growth or dissolution of zinc with the evolution of hydrogen; (c) impurities such as molybdate which create dense compact bright zinc deposits and suppress the detrimental effects of other impurities, and in particular neutralize the synergistic effects of iron, nickel and cobalt.

It has been pointed out [47] that mossy deposits grow whenever the exchange current density approaches or exceeds the limiting current and hence the formation of spongy zinc is a feature of chloride and bromide solutions rather than sulphate and alkaline media. It has also been reported [48] that spongy zinc consists of a large number of small microcrystals with the same lattice characteristics as those of the compact growth mode. Some impurities and additives promote and facilitate the mossy growth of zinc whereas others retard or even suppress it, thus creating various induction periods for spongy electrogrowth (synergistic amplification and counteraction effects).

3.6.1 Effect of cupric ions on zinc macromorphology

The electrode potential of copper is much more positive than that of zinc and hence its impurity effect is of marked significance. According to JAKSIC [46], one of the most characteristic impurity codeposition effects was found when cupric ions were present as a minor component of the acidic binary zinc chloride solutions. The induction time [49] for copper as the minor component appears to be relatively long (30min-1hr at 10 mA/cm^2). Scanning electron microscopy (SEM) analysis revealed the presence of small globular grains resembling cauliflowers at the bottom of equiangular spiral grooves in the zinc electrodeposit on the rotating disk electrode (RDE) after a certain induction period probably due to the flow regime induced by the RDE. This implies that the zinc deposited prior to the codeposition of copper globules at disproportionately low cupric ion content is homogeneous and exhibits typical electrogrowth from binary chloride solutions [38]. The induction time decreases with increasing cupric ion concentration. The copper globules appear to catalyse hydrogen evolution so that eventually the deposit takes on the typical mossy form. The detrimental effect of the cupric ions would have been even more pronounced if the zinc had been added as nitrates rather than chloride or sulphate, when both ions would have contributed to the development of the spongy appearance of the zinc deposit [50].

3.6.2 Effect of iron on zinc macromorphology

Both the iron (II) and iron (III) species exhibit a catalytic effect on zinc mossy growth. Although it has been reported [51] that iron is extremely detrimental to zinc electrogrowth, particularly from halide electrolytes, its effect as a minor component in reagent grade $ZnCl_2$ solution has a rather long induction period (at least 2 hr at 10 mA/cm^2). Ferric ions produce a rather more compact zinc deposit consisting of very small crystals as the precursors of further nucleation. However, small amounts of ferric ions sometimes have a dramatic effect on the growth surface and promote the rapid development of characteristic spongy zinc. This evidence of a synergistic impurity effect is usually associated with the presence of sub-microlevels of an additional unknown impurity, originating from the reagent grade chemicals [43]. The spongy growth appears to depend on the pH value and current density in addition to the impurity content and the deposition time. The iron impurity effect becomes very

pronounced above pH 4.5 in $ZnCl_2$ solutions and the induction period for mossy growth increases with increasing current density as is typical for concentration polarization. A pH change as small as 0.2 pH units and a doubling of the current doubles the induction period and hence postpones mossy growth on a new substrate. However, once mossy growth has started it cannot be suppressed by a change in the pH or the reaction rate.

The growth mechanism of spongy zinc, particularly when affected by iron impurities, shows characteristic mass transfer features. As reported by JAKSIC [46], the mossy deposit spreads from the centre of rotation towards the edge of the RDE. It appears earlier at lower current densities, which is characteristic of concentration polarization because of higher current densities the effect is suppressed and retarded (the induction period is increased). The initial number of grains in the spongy growth appears to be a linear function of the impurity content, but their size depends on the deposition time and the surface area increases at an exponential rate, which is typical for autocatalytic processes. Alternatively, there could be a combined electrocatalytic effect associated with hydrogen evolution. Thus, whereas copper impurities participate directly in the development of the zinc growth surface, iron impurities appear to have an indirect catalytic effect which is much more efficient and characteristic.

3.6.3 Effect of molybdate on suppressing mossy zinc electrogrowth

It is reported [46] that molybdate ions reduce onto iron, cobalt, titanium, and graphite substrates, with a low faradaic yield, and produce MoO_2 which has a high electrocatalytic activity towards the hydrogen evolution reaction (HER) and which is further reduced by codeposition to a form of molybdenum black. The synergistic electrocatalytic effect of molybdenum with cobalt nickel and/or iron exceeds even that of the noble metals in activity towards the HER, so that investigation of the composite impurity effects with these metals would be of interest. It was expected that the deposition of molybdenum black would be accompanied by hydrogen evolution, as has been observed in deposition onto iron, nickel and titanium. This would be expected to enhance the mossy zinc electrogrowth, as in the case of copper, because of local increase in the hydrogen evolution rates at active centres. Similarly, the synergistic electrocatalytic effect of combination of various metals with molybdenum (Co-

Mo, Fe-Mo and Ni-Mo) was expected to be more pronounced. However, quite opposite and unexpected results were obtained [46]. The addition of molybdate alone resulted in much more compact bright zinc electrogrowths at very high current yields (approaching 100%), i.e molybdate appears to be a brightener.

The addition of molybdate provides an improved surface morphology, a bright compact zinc deposit, more uniform electrogrowth and reduced autodissolution, and more significantly, the interaction of molybdate with iron impurities prevent the growth of spongy zinc. The iron impurities promote the formation of a mossy deposit whereas molybdate promotes a compact rather dense electrodeposit and thereby suppress sponginess.

3.6.4 Effect of some other transition metal impurities

Nickel and cobalt, which are more electropositive than zinc, are common detrimental impurities in zinc electrowinning from both sulphate and halide baths [49]. At low impurity contents (1-10 ppm) nickel first deposits alone at its well-defined limiting current plateau and then at higher current densities, forms an alloy with zinc. The presence of a small amount of nickel has little effect on the surface morphology of zinc after deposition for 1 hr at low deposition rate (10 mA/cm^2), and the deposit appears slightly more dense and compact. However, the combined effect of nickel and iron is very pronounced and leads to rapid growth of spongy zinc all over the surface. Thus the effect of low nickel impurity content is to exhibit a rather long induction time and the spongy deposit appears only at a critical nickel content on the growth surface. In other words, the nickel impurity effect depends on its concentration in the solution and on the growing surface, and therefore on the depositon time and the current density.

Whereas copper is codeposited independently on the zinc growth surface after a characteristic induction time and then imposes its detrimental impurity effect, cobalt and nickel first alloy with zinc and then emerge at some critical content in the growing surface to promote spongy growth and reduce the faradaic yields for zinc electrodeposition [46].

CHAPTER FOUR

4 ZINC-ALLOY ELECTRODEPOSITION

4.1 Introduction

A wide range of binary and ternary alloy coatings are produced industrially by electrodeposition [52], the most important being zinc alloys, tin alloys, nickel alloys and noble metal alloys (see figure 4.1).

As pointed out by BRENNER [52], the composition of electrodeposited alloys depends on many factors and differs usually from the composition of the electrolyte. BRENNER [52] distinguishes ''normal'' and ''abnormal'' co-deposition behaviour. In the first case 'the relative proportions of the metals in the electrodeposited alloy are quantitatively that expected on the basis of the equilibrium potentials of the metals against the solution' [52]. Normal codeposition is further subdivided into 'regular' codeposition (diffusion control), 'irregular' codeposition (activation control) and 'equilibrium' codeposition. Irregular (activation control) codeposition appears to involve intermediate species which catalyse the reduction of the nobler component often at low cathode polarisations whilst diffusion control appears to be dependent on the concentration of ionic species and the rate of their migration in the diffuse double layer. In 'abnormal' codeposition according to BRENNER, the deposit composition differs from that expected from equilibrium considerations. This type of behaviour includes 'anomalous' and 'induced' codeposition. In anomalous codeposition the less noble component deposits preferentially and its relative concentration in the alloy is higher than in the electrolyte. Induced codeposition means that a given element can be co-deposited to form an alloy, but cannot be deposited in pure form. Tungsten and molybdenum are examples [53]. BRENNER's [52] classification is based mainly on thermodynamic considerations. Whilst it describes different experimental observations, its usefulness in terms of scientific

understanding of alloy deposition phenomena is limited because it does not sufficiently take into account charge transfer kinetics and mass transport [53]

The mixed potential theory, originally developed by Wagner and Traud as reported by LANDOLT [53], is commonly applied to corrosion. It states that the measured current in an electrochemical system is equal to the sum of the partial anodic and cathodic currents [53]. The application of mixed potential theory to alloy deposition provides a framework for the appreciation of the relative importance of thermodynamic and kinetic factors on resulting alloy composition. Kinetic and thermodyamic factors which influence codeposition include conductivity, solubility, free energy of the system, enthalpy, entropy and temperature. Indeed, it becomes readily apparent that the chemical composition of an alloy will normally differ from that of the electrolyte and will generally depend as much on kinetics as on thermodynamic quantities. For example, the occurrence of a so-called anomalous codeposition is a natural consequence of certain types of kinetic behaviour of the alloy components. In practice anomalous codeposition is observed with many alloy systems, including zinc alloys and iron alloys. Permalloy (Ni-20%Fe) used in the electronic industry for its magnetic properties, is probably the most thoroughly investigated example. Iron the less noble component, deposits preferentially, its deposition rate being partially or fully controlled by mass transport.

In corrosion, it is customary to assume (although this may not always be supported by experiment) that the behaviour of the mixed system can be predicted from knowledge of the individual kinetics of the components. In alloy plating the situation is not always that simple because of possible interaction between partial reactions. LANDOLT [53] distinguished between three types of codeposition behaviour: non-interactive codeposition, charge transfer-coupled codeposition and mass transport coupled codeposition. In non-interactive systems the partial currents are largely independent of each other and the alloy composition can be predicted from the pure metals. For charge transfer couple systems the value of the partial current of a given alloy component differs from that observed during deposition of the component in its pure state. For example, during the deposition of a zinc-nickel alloy from a sulphate electrolyte the deposition rate of nickel is slowed down drastically by the presence of

zinc. LANDOLT [53] observes that for a given potential, the partial current density for nickel during alloy deposition is much lower than the current density measured during deposition of the pure metal. Zinc, on the other hand is not significantly affected by the presence of nickel. The author further suggests that the observed inhibition effect due to the presence of zinc might be related to competitive adsorption of reaction intermediates influencing the surface coverage of nickel. In some cases, a given metal may have a catalytic effect on a codepositing alloy component. This situation is referred to as catalysed codeposition [53].

Mass transport coupled codeposition refers to situations where the rate of codeposition of a given alloy component depends on the mass transport of a species being consumed or produced at the cathode due to codeposition of another component. For example, concurrent hydrogen formation can lead to an increase of pH in the cathodic diffusion layer, which may change metal deposition kinetics, or cations of different components may compete for the same ligand to form complexes. Charge transfer kinetics may or may not be coupled in such situations.

Many metals deposit with concurrent hydrogen evolution. This leads to consumption of protons or to the formation of OH^- ions at the cathode, which may cause a local increase of pH in the cathodic diffusion layer. The extent of depletion of H^+ or accumulation of OH^- depends on mass transport conditions and on the buffering capacity of the electrolyte. If the rate of charge transfer of one of the depositing species at the electrode is pH dependent (for example if it involves hydrolysed ions of the type MOH^+) a change in local pH can influence the relative deposition rate of alloy components and hence the resulting alloy composition.

Many industrially used plating electrolytes use complexing agents. Their presence shifts the equilibrium potentials and influences charge transfer rates. Furthermore, the formation of complexes often avoids hydroxide precipitation. In alloy plating, the codepositing metal ions may compete for ligands and the concentration of certain complexed species may depend on that of codepositing ions. MATHIAS AND CHAPMAN [55] modelled the deposition of zinc-nickel alloys from a chloride electrolyte taking into account equilibria between different zinc chloride complexes. The nickel was assumed not to complex. The authors were able to

calculate concentration profiles from different zinc chloride species and for Ni^{+} or Ni^{2+}. Interestingly the concentration of the latter ion increased at the cathode because of migration [53]. The theoretical model permitted the prediction of alloy composition as a function of current density and convection rate, but several empirical assumptions with regards to charge transfer kinetics had to be made to fit experimental data.

Mixed potential theory provides a useful framework for the theoretical modelling of alloy plating, provided one takes into account the possibility that partial reactions may be coupled. For non-interactive systems quantitative predictions of alloy compositions can be achieved from knowledge of behaviour of the individual components under given mass transport conditions. Unfortunately, for charge transfer couple systems useful kinetic expressions are not readily available and theoretical modelling most often relies on the use of adjustable parameters [53].

According to Gabe as reported by WATERHOUSE AND NIKU-LARI [54], if a successful process of alloy deposition is to be established it is a pre-requisite that a stable solution of both metal ions can be obtained with deposit composition being relatively insensitive to changing deposition conditions (current density, pH, temperature etc). The author further noted that solution replenishment is best achieved by using soluble anodes of the same composition as the deposit, for which the electrode efficiencies must be almost equal. The following criteria were enumerated for an acceptable process;

- The operating parameters should be flexible, not too specific or rigid and should be of a conventional nature; such parameters include those mentioned above, together with the use of addition agents and agitation.
- The replenishment of solution, either by chemical or by use of soluble anodes, should be simple.
- The alloy deposit should be of consistent and reproducible composition; structure and variations in physical properties should be systematic and controllable.
- The deposit should meet a need or use to be a commercial proposition.
- The solution should be stable whilst worked or left idle.
- The effluent problems associated with the solution should be acceptable.

4.2 Zinc-nickel electrodeposition

4.2.1 Introduction

Electrodeposited alloy films can provide desirable surface properties when compared with single-metal films, but alloy deposits can be difficult to apply because of the need to control uniformity of composition, thickness, and microstructure [55]

It has been reported [56-57] that the maximum protective ability of Zn-Ni is reached with a nickel content between 10 and 15%. In particular, Zn-Ni alloy coatings are considered a less polluting alternative to cadmium [58]. According to ABIBSI et al [59], zinc-nickel alloys can be obtained using plating baths of different composition and operating conditions, e.g chloride, sulphate, ammoniacal, sulphate-sulphamate, sulphate-chloride, pyrophosphate and cyanide. Usually Zn-Ni deposits obtained from cyanide solutions have a lower nickel content than their counterparts from cyanide- free systems and due to the undesirable characteristics of cyanide may therefore be eliminated when considering coating for maximum corrosion resistance. Most studies regarding the codeposition of zinc-nickel have been made with acid baths containing simple salts of the metals. However, many commercial baths contain ammonium chloride, which causes effluent treatment problems and is also undesirable because of the negative environmental impact of ammonia [59]. Since the range of nickel concentrations for maximum corrosion resistance is relatively narrow, it is essential that small changes in operating conditions do not lead to substantial changes in nickel concentration from the optimum [59].

The electrodeposition of Zn-Ni alloy is generally a codeposition of the anomalous type, according to Brenner's definition [52], since the less noble metal zinc deposits preferentially and its percentage in the deposit is higher than that in the electrolyte. However, as reported by BAJAT et al [60], codeposition of Zn and Ni is not always anomalous since, at low current densities, it is possible to obtain normal deposition where Ni deposits preferentially to Zn. Therefore, there is a transitional current density that has to be reached in order to start anomalous codeposition. Many attempts have been made to explain the anomalous

codeposition of alloys, but there is still no universally accepted theory. At first, anomalous codeposition was attributed to the pH increase at the cathode surface being able to induce zinc hydroxide precipitation, which inhibits nickel discharge [61]. This theory does not explain the strong inhibition of nickel reduction observed in the normal deposition region, the high current efficiency during anomalous deposition and the increase in the nickel content of the alloy with increasing pH [62]. Recently, Zn-Ni codeposition was studied by means of polarisation curves and impedance spectroscopy measurements both in chloride [63] and in sulphate baths [62]. Even though metal cations can form chloro-complexes in chloride electrolyte [55], in contrast to what happens in sulphate electrolyte, the reaction models proposed are substantially similar and involve several adsorbed intermediates. In particular, at low cathodic polarisation (normal codeposition) the deposition of nickel-rich alloys was attributed to a mixed intermediate ($ZnNi^{+}_{ad}$), which catalyses the reduction of Ni^{2+} ions. At high cathodic polarizations (anomalous codepositon) zinc preferential discharge is attributed to the intermediate Zn^{+}_{ad}, catalyst for the deposition of zinc rich deposits [58].

4.2.2 Effect of plating variables on zinc-nickel electrodeposition

The operating conditions such as current density, pH , organic additives, buffer capacity, concentration of solution components, lead to changes in the kinetics of electrodeposition, composition and morphology of the coatings, as well as in their physico-mechanical characteristics [64].

4.2.2.1 Effect of current density

The effect of current density on the percentage of nickel in Zn-Ni electrodeposits has been reported [59,60,64]. FRATESI AND ROVENTI [64] reported that coherent and homogeneous coatings were obtained with current densities of up to 100 mA/cm^2 and that above that value the deposit appeared less uniform and dendritic along the edges of the sample. They further noted that the percentage of nickel in the alloys was approximately constant over a wide current density range and increased strongly at the lowest current density values. In a comparative study of two types of baths, BAJAT et al [60] reported that electrodeposition from a chloride bath leads to an alloy having a larger content of nickel than the alloy deposited

from a sulphate solution, as well as a deposition with greater current efficiency. In agreement with [64] these authors also noted that the percentage of Ni remains almost constant regardless of the deposition current density within a broad range of current densities, for both deposition solutions. However, ABIBSI et al [59] noted that cathode current efficiency for alloy deposition decreased with increasing current density. ALFANTAZI et al [65] investigated the effect of pulse plating on Zn-Ni alloy electrodeposition and observed that an increase in peak current density resulted in only a slight increase in the nickel content from 12-14 wt% Ni. This, according to them, is consistent with the results presented by KNODLER et al [66] who reported that the nickel content of the deposit is more or less independent of the peak current density at relatively high zinc content in the bath (10 g/dm^3). JESSEN et al [67] studied the effect of average current density on the grain size of Zn-Ni alloy produced by D.C. plating technique. They found that increasing the average current density from 1 to 8 A/dm^2 resulted in considerable grain refinement.

4.2.2.2 Effect of temperature

ABIBSI et al [59] have investigated the effect of increasing temperature on the rate of nickel deposition during zinc-nickel electrodeposition. They found that as the temperature increased, the nickel content in the deposit also increased. ALFANTAZI et al [65] also studied the effect of temperature on the characteristics of the deposit in the range of 25 to 80 °C and observed that the nickel content initially increased as the temperature increased form 25 to 60 °C and then increased much more rapidly for temperatures between 60 to 80 °C.

The effect of temperature on the morphology of Zn-Ni electrodeposits has also been reported [65]. Deposits produced at 25 °C had a rough surface morphology and the structure contained a fine-grained matrix of γ-phase and coarse η-phase crystals. Whereas, deposits produced at 40 °C were much smoother, consisting entirely of the γ-phase with a nodular fine-grained structure morphology and grain size in the range of 0.5 to 2 μm. The iron group metals are generally characterized by very low current densities, unlike zinc, which shows high exchange current densities. Strong influence of temperature on the transition current density has been reported by FRATESI AND ROVENTI [64]. They note that the transition current increases

with increase in bath temperature, confirming the key role played by the temperature dependent kinetics parameters. This hypothesis is supported by MATHIAS et al [55] who using the Roehl bath (pH 1.6), found that the electrodeposition of zinc-nickel alloy is anomalous even though the hydrogen evolution current is not high enough to raise the interfacial pH much above the bulk pH, as would be necessary for the formation of zinc hydroxide. These authors calculated that the zinc exchange current density is five orders of magnitude higher than that of nickel and attributed the anomalous codeposition to the intrinsically slow nickel kinetics [64].

4.2.2.3 Effect of pH

The effect pH on the deposition behaviour of zinc-nickel with different bath formulations has been reported [59,64,68-69]. According to ZHONGDA et al [69], when the pH is increased from 1.5 to 5.8, polarization curves for zinc-nickel codeposition are shifted towards less negative potentials and that this result may be explained by the hydroxide suppression mechanism put forward by DAHMS AND CROLL [70]. With lower pH of the solution, the formation of a hydroxide surface film during codeposition has also been reported [69], i.e with a higher rate of hydrogen evolution, which would cause a local increase in pH. The change in polarisation curves for Zn-Ni deposition due to changes in pH is probably as a result of the fact that an increase in pH (especially above 3.3) causes significant catalysis of Zn-Ni deposition with a simultaneous decrease of nickel in the coating and that this effect is related to the nature and concentration of complexed species [68].

4.2.3 Properties of zinc-nickel electrodeposits

4.2.3.1 Corrosion resistance

The corrosion resistance of Zn-Ni electrodeposits have been widely reported [1,57,68,71-77]. Change of corrosion current as a function of nickel content has also been reported [71]. The coatings that have approximately 13% nickel show the lowest corrosion current, whereas, coatings with nickel content higher than 15% quickly become more noble than the steel substrate [57] and show a high corrosion current. This is the result of surface nickel

enrichment due to a standard dezincification process [1,57]. It has also been reported [71] that the corrosion potential increases as the nickel content in the deposit increases and that the coating which consists of 13.5% Ni, for instance, has a corrosion potential of –969 mV vs SCE. However, as the nickel content increases up to 42%, the corrosion potential also increases up to –749 mV vs SCE. According to WATSON as reported by WILCOX AND GABE [1] nickel slows down the dehydration of zinc hydroxide $Zn(OH)_2$ a product of the corrosion, into ZnO. The hydroxide has a lower level of electronic conductivity than the oxide, so the reaction of the cathodic oxygen reduction is weaker than for the oxide, and corrosion is therefore slower [57].

The influence of texture, stress in the coating, phase composition, and chemical composition has also been reported [71]. These microstructural parameters all change when the processing conditions are modified, and therefore, it is difficult to separate the role each of the above parameters has on the corrosion resistance.

In WATSON's findings, as reviewed by WILCOX AND GABE [1], alloys of 10-17% nickel are single γ-phase coatings. Furthermore, coatings of less than 10% are a mixture of γ- and η-phases, whilst nickel contents greater than 17% are a mixture of γ- and α-phases. However, PARK AND SZPUNAR [71] noted that the γ-phase starts to form at nickel contents above 15%. According to them, the η-phase dominates when the nickel content is around 13%, whereas coatings have the η+ γ dual phase at about 15 % of nickel. The formation of a dual phase is thought to be responsible for the sudden increase in corrosion current at this nickel percentage range. It was concluded that zinc-nickel coatings consisting of the η-phase at the lower nickel content of 13-15% have better corrosion resistance than the coatings consisting of the γ-secondary phase that has higher than 15% nickel content. ALFANTAZI [65] observed that zinc-nickel coating consisting of a single γ-phase, have lower corrosion resistance once the nickel content exceeds 20%. He also proposed that in the pulse-plated zinc-nickel coatings, the best corrosion resistance is observed in the coatings having a nickel content of 14-20%, which consist of the single γ-phase. At a similar range of nickel content, the DC plated zinc-nickel coatings consist of the η+ γ dual phase. PARK AND SZPUNAR [71] therefore argue that in the case of pulse plating, the absence of the η-phase is attributed to the selective

dissolution of the η-phase during pulse-off time caused by the local electrochemical cell between the γ-phase and the η-phase [74]. The authors noted that since the γ-phase is electrochemically nobler than the η-phase, the local cell between the two phases promotes the formation of a single γ-phase.

4.3 Zinc-iron electrodeposition

During recent years the use of slightly more noble zinc alloy coatings such as Zn-Ni, Zn-Co and Zn-Fe has increased due to the reported superior corrosion performance of these coatings in most environments compared to pure zinc. Several investigators have carried out work on the electrodeposition of Zn-Fe [78-81]. Zinc-iron not only offers improved cathodic protection of mild steel compared to pure zinc, it can also offer better weldability and paintability, which is of primary concern in the automobile industry, one of the main end users of electrogalvanised steel sheet. These properties depend on the phase structure of the deposits [80]. Optimum corrosion resistance is normally reported for Zn-Fe containing 15-20 wt% Fe, whereas the best paintability is achieved with coatings containing 60-80 wt % Fe [78].

Apart from its corrosion resistance, paintability and weldability properties, recent studies have focused on the electrodeposition of Zn-Fe alloy electrodeposits because iron is a relatively cheap metal compared to the other possible alloying elements like nickel and cobalt, making the chemistry of the Zn-Fe plating bath cheaper than most other plating electrolytes [79].

Either chloride or sulphate based baths can be used to deposit zinc-iron alloys, but both tend to suffer from the formation of ferric ions in solution, usually in the form of ferric hydroxide [82]. Fe^{2+} is inherently unstable and will normally oxidise to Fe^{3+} reducing the current efficiency during electroplating. According to JENSEN et al, [79] bath ageing ($Fe^{2+} \rightarrow Fe^{3+}$) can be observed by the plating solution changing colour from bright green to yellow and finally brown. At this stage the main portion of the current applied during electroplating is spent on the reduction of ferric ions i.e current efficiency is very low. They further stated that addition of an antioxidant, ascorbic acid, extended bath life from a few hours to several weeks.

This combined with mild steel anodes, kept the bath stability at a level sufficient for long-term use.

DAHMS et al [70] in attempting to explain the electrodeposition mechanism of Zn-Fe noted that anomalous codeposition for the Zn-Fe system under certain specific conditions, is as a result of a local barrier layer forming closely adjacent to the cathode surface. A local rise in pH due to an overpotential for reduction of water forms hydroxide ions and hydrogen gas, is believed to cause the formation of zinc hydroxide film, which hinders the free diffusion of the more noble metal ions, in this case Fe^{2+}, to the cathode surface, whereby the composition of the electrodeposited Zn-Fe alloy becomes rich in the less noble metal zinc.

4.4 Zinc-cobalt

Electrodeposited zinc alloyed with a low percentage of cobalt, (< 1%) is a commercially viable option from the point of view of low cost and better corrosion resistance characteristics than the existing conventional zinc coating systems [83-84].

Zinc-cobalt alloys share many similarities with zinc-nickel alloys, and are beginning to find use in the aerospace industry. Usually, ammonia-free mild acid-chloride electrolytes are used, which give deposits containing 0.25-0.9 wt.% cobalt. Such solutions predominate in the U.S.A. A single zinc anode is used, and cobalt ions are replenished by adding small amounts of cobalt salt.

Alkaline, cyanide-free solutions are less widely used, but alloy compositions of up to 4 wt% cobalt have been reported. Like the acid solution, only zinc anodes are used, and cobalt levels are maintained in solution by periodic addition of cobalt salts [82].

According to SHORT et al [72], 4-8 wt% cobalt gives optimum corrosion resistance. However, for commercial reasons alloys containing much less cobalt (between 0.6 and 1.2 wt%) are used. Additional corrosion resistance can be achieved by chromate passivation of the deposits, with blue, yellow, green and black coloured films being possible. However, the olive

drab colour attainable with chromated cadmium is not possible on zinc-cobalt alloys containing greater than 0.4 wt% cobalt, although the colours are more stable than that of cadmium [82].

Effects of some plating parameters on Zn-Co electrodeposition have been investigated by ABD EL REHIM et al [85]. According to them, the Co% in the alloy increases with increase of either its content in the bath or of the bath temperature and increases with decreasing current density or decreasing pH. This is in agreement with NARASIMHAMURTHY et al [83] who stated that the percentage of Co in the alloy decreased with increase in current density. Hardness of the deposit was attributed to higher content of cobalt in the alloy whilst the morphology of alloy deposits was reported to be dependent on the amount of cobalt in the deposit.

4.4.1 Corrosion mechanism of Zn-Co alloy coating

TU et al [86] reported that the corrosion product of Zn-Co alloy is mainly composed of $ZnCl_2.4Zn(OH)_2.H_2O$ and a small amount of $3Zn(OH)_2.ZnCO_3$ and ZnO; whereas that of Zn is mainly composed of ZnO and a small amount of $ZnCl_2.4Zn(OH)_2.H_2O$ from a neutral salt spray corrosion product analysis. While analysis of the corrosion products revealed the presence of complex salts of zinc hydroxide in the corrosion products of Zn-Co and Zn. According to them, when Zn-Co alloy coating is exposed to the atmosphere, the surface will be oxidized like that of a zinc coating, and at the same time a protective film of $Zn(OH)_2.ZnCO_3$ will be generated on the surface. Because the cobalt in Zn-Co alloy is comparatively stable and not easily oxidized, it will become zero valent and exist in the state of atoms. It is the existence of the cobalt atoms that play the role of inhibiting further corrosion in the coating. They further stated that when Zn-Co alloy coating is corroded, the cobalt promotes a corrosion product in the form of a complex salt ($-Zn(OH)_2$). The film is comparatively compact and stable, and the electroconductivity is poor, which will inhibit corrosion effectively.

4.5 Zinc-manganese electrodeposition

In the research and development activity on zinc-alloy electroplating, there is growing interest in the zinc-manganese system. These alloys show synergistic effect with better corrosion resistance than the individual metals [87-90]. This is probably due to the formation of a Mn oxide layer affecting the catalytic activity for cathodic oxygen reduction. In addition, the alloying elements are entirely acceptable from an environmental point of view, and they provide the opportunity of implementing the as-plated Zn-Mn alloy. However, MULLER et al [90] reported that this deposition process has important drawbacks: (a) with most electrolytes, high Mn contents are only achieved at high current densities, much higher than necessary to protect small pieces; (b) the current efficiencies of the process are intrinsically low, particularly at high current densities when the percentage of manganese is high; and (c) it is difficult to obtain coatings with a satisfactory quality because dependence of the alloys' composition on current density is very pronounced and this leads to non-uniform deposits. Zn-Mn layers can be electrodeposited from a sulphate bath, from a sulphate bath containing citrates and from a fluoroborate bath. Although, the use of an acid chloride bath has been reported [88], the sulphate-citrate bath is the one most used for the electrodeposition of high-Mn alloys [91]. Variations of bath composition, temperature, pH and current density affect the Mn content in the alloy, the current efficiency, quality and appearance of the coating. According to earlier investigations as reported by WILCOX AND PETERSEN [87], the manganese content of the electrodeposit increase with increase in current density, cathode current efficiency fell. Bath temperature appeared to have clear effects on electrodeposit quality. Approximately room temperature conditions promoted the best deposits, with higher temperatures producing a commensurate fall in deposit quality.

The loss of zinc from alloy coatings on exposure to a corrosive environment reduces their effectiveness as sacrificial coatings. Zinc-manganese coatings do not suffer from this problem but are difficult to electroplate as described above and its lack of throwing power. Published data indicate that a manganese content of more than 50% is required if significant improvements in corrosion protection are to be achieved [92].

Recently, BOZZINI et al, [91] investigated the effect of thiocarbamide (TCA) on the sulphate-citrate bath, particularly on: composition, crystal structure, morphology, mechanical properties and corrosion behaviour of Zn-Mn alloy coatings. According to them TCA was chosen since cathodic adsorption of this additive might give rise to a partial inhibition of zinc deposition, which could enhance the Mn content in the coatings.They further noted that as far as the structure of Zn-Mn alloy is concerned, the use of TCA gives rise to the formation of nanocrystalline ε-phase electrodeposited coatings which might be related to the measured improvements in mechanical properties. They also observed that the presence of of TCA influences the morphology of Zn-Mn coatings, clusters of ε-phase globular crystallites tends to develop. Earlier work by SULCIUS et al, [93], has clearly illustrated the effect of adding selenates to sulphate-citrate formulations to increase the manganese content of alloy deposits. It was reported that selenium was found in the alloy electrodeposits up to 0.17 wt%. However, recent investigations by BOZZINI et al, [91] reported that addition of TCA reduces hydrogen damage compared to Se-containing additives. Earlier investigations on hydrogen permeation during Zn-Mn alloy plating by SRINIVASAN et al, [88] reported that the porosity of the deposit increases in the following order: Zn-Mn(14.3%), Zn-Mn(2.4%), Zn-Mn(24.8%) and Zn-Mn (37.5%). According to them, this is in agreement with the corrosion data obtained which indicates that Zn-Mn alloy deposits with low manganese contents show better performance than pure zinc deposits.

4.6 Zinc-tin electrodeposition

About 20 different electrodeposited tin alloys are known and Zn-Sn is one of them. These coatings are used both as functional and as protective-decorative plate. They offer improved corrosion resistance, good solderability and ductility [94-97]. The outstanding corrosion protection for steel is reportedly [96] due to the combined barrier protection of tin with the galvanic protection of zinc, without the bulky corrosion products associated with wholly zinc deposits. They also have low electrical contact resistance and are not subject to bimetallic corrosion [98]. In some cases they can replace not only zinc but also cadmium and allergenic nickel coatings [94,98]. Zinc coatings when exposed to adverse atmospheric conditions starts to dissolve, leading to the formation of basic salts. Tin coatings resists atmospheric influence,

but are quite porous and since tin is cathodic with respect to steel substrate, the efficiency of corrosion protection depends on the porosity of the coatings [95].

There are several compositions, which are suggested to offer the best corrosion resistance and protective effect. Zn-Sn alloy coatings with high tin content are highly resistant, provided they have been deposited as a continuous layer. The addition of Sn to improve the resistance of the coating against tarnishing, enhances the solderability and elasticity, and increases the anti-friction properties. Previous investigations provide evidence that tin-25%zinc plates are better than pure zinc in humid atmosphere tests [94]. Similarly, in other studies, [96-97] it has been reported that alloy coatings with 70-80% Sn by weight and 20-30% Zn by weight has the best mechanical and corrosion protection properties. Tin-zinc electrodeposition has been investigated using different bath systems [96-97], at different pH values and using different complexing agents and additives, in order to replace the contaminant cyanide baths used in industrial processes for tin-zinc alloy plating. According to ASHIRU and SHIROKOFF [96], tin-zinc deposits obtained from the stannate/zincate bath is fine-grained, semi-bright, and shows considerable improvement over the tin-zinc deposit from the previously used cyanide plating process.

CHAPTER FIVE

5 COMPOSITE COATINGS

5.1 Introduction to composite materials

In the continuing quest for improved performance, which may be specified by various criteria including less weight, more strength and lower cost, currently used materials frequently reach the limit of their usefulness. Thus material scientists, engineers and scientist are always striving to produce either improved traditional materials or completely new materials. Composites are an example of the latter category. Although the underlying concept of composite materials goes back to antiquity, the technology was essentially developed and most of the progress occurred in the last decades.

Composite materials are largely multiphase materials, made up from two or more phases, whose mechanical performance and properties are designed to be superior to those of the constituent materials acting independently. The continuous phase in a composite is referred to as the matrix, while the other phase, or phases, provide reinforcement. The reinforcement materials can often be found in the form of fibre, whisker or platelet-reinforced materials, particulate composites such as dispersion-strengthened alloys and cermets, laminates and sandwich materials [82].

Various methods such as powder metallurgy, metal spraying, internal oxidation and co-precipitation are utilised to produce metallic composites. For example, metal spraying involves the melting of metallic powders usually sprayed onto surfaces by a gas stream, with composites being obtained by adding inert particles into the powder blend. Production of composites containing very fine dispersed oxides can be achieved by selective oxidation of metals and alloys, while composites produced by the co-precipitation method require a mixture containing easily reducible metal salt and colloidal oxide dispersion. The composite

is formed through the reduction of the metal salt that produces a mixture of very fine metal and oxide powders, which can then be processed by conventional powder metallurgy techniques.

Composite electrodeposition of inert particles suspended in a plating bath by agitation can be traced back to the late 1950s and resulted in patents in the early 1960s. This work was followed by major developments in Germany, particularly with respect to Ni-SiC coatings for the trochoid surfaces of wankel engine components for wear resistance. Due to their high wear resistance and low cost of ceramic powder, Ni-SiC composites have been investigated to the greatest extent and successfully commercialised for the protection of friction parts [99]. In the U.K, notable developments included wear resistant coatings at BAJ Vickers in the late 1960s and early 1970s. The advantages of co-deposition are clear, since the technique offers an elegant way to combine the characteristics of different metallic and non-metallic materials in a controlled fashion [100]. Recently, SIMMONS [82] outlined the advantages of electrolytic and electroless composite deposition as follows:

- Only a limited financial investment is necessary to adapt a conventional production cell.
- A wide range of composites can be obtained by selecting different types of inert particles like metal oxides, metal carbides or organic compounds.
- Control of the production conditions permits smooth deposits with dimensions as required, resulting in minimal post-treatment.
- No heat-treatment of the part is required, and thus thermal damage of the components to be coated is avoided.
- When compared to metal spraying, more complex geometrical forms can be coated successfully, but highest uniformity of thickness is obtained by electroless plating.

The main limitations of these electrolytic and electroless techniques according to him, are the grain size of the second phase particles and a limited rate of codeposition.

5.2 Models and methods of particle incorporation

Until recently, a definition of 'inclusion layer' was not difficult to formulate: an inclusion layer was defined as a metal in which inert (usually polymer or ceramic) particles are dispersed by means of electrodeposition [100]. This definition is no longer valid because dispersion layers may be precipitated from polymer solutions rather than from dispersions of the particles in an electrolyte [100]. Nevertheless, interest in electrodeposited composite coatings have continued to increase rapidly mainly due to their expected new engineering applications. Such coatings are produced by codeposition of inert particles and a metal matrix from electrolytic baths [101]. In general, three mechanisms, namely, mechanical inclusion, electrophoresis, and adsorption of inert particles onto the cathode are proposed to explain the codeposition behaviour [101].

KEES and FRANK [100] noted that there are two strategies for the incorporation of particles into growing metal deposits. The first and largest group according to them uses 'physical dispersion' of the inert particles in the plating bath. The mechanism of incorporation of particles was then explained by a model, which considers adsorption of cations at the particle surface and transportation to, then reduction on the cathode surface. They further noted that a second deposition strategy arranges for the particles to have artificially high positive values of the zeta potential. This is achieved by adding suitable cationic substances, which adsorb strongly at the particle surface. In the case of 'physical dispersion' plating baths, an important contribution to the theory for codeposition of dispersed particles in metallic coatings was derived by GUGLIELMI [102].

5.2.1 Guglielmi's model [102]

Guglielmi's model is based on two consecutive adsorption steps at the cathode surface. The first, which is physical in character, produces a layer of loosely adsorbed particles with a relatively high surface coverage. The second step, which is considered to be electric field assisted (and therefore, potential dependent) gives rise to strong adsorption of the particles onto the cathode. The inclusion deposits grow as the adsorbed particles continue to be built in

to the electrodepositing metal matrix. The mathematical treatment by GUGLIELMI [102] gives a relationship between the current density and the concentration of the particles in the liquid and the metal layer. He showed that the volume fraction of codeposited particles could either increase or decrease with increase in current density. This will depend on the strength of the interaction between the particles and the cathode surface. If the interaction is strong, the volume fraction will increase with current density, if it is weak the volume fraction decreases [103]. However, important process parameters, such as hydrodynamics, particle form, particle size and particle size distribution, were not considered in this model.

5.2.2 Model of Kariapper and Foster [103]

A slightly different approach to that of Guglielmi was adopted in this model where it was assumed that only those particles with impact velocity below a critical value would be candidates for codeposition. They concluded that composite coatings could be produced from acid electrolytes if the particles in suspension acquire a positive surface charge by the adsorption of metal ions. These metal ions are thought to have a dual role. On adsorption onto the surface of the particle, they enhance the attraction and subsequent migration of the particles to the cathode due to electrostatic force, and assist in the creation of an efficient mechanical bond between particles and the cathode surface. The effect of agitation and current density on the volume fraction of particles in the deposit was also stressed. They noted that the effect of agitation and current density became less pronounced as the volume fraction of particles in the plating solution is increased. They argued that if V_p = volume fraction of particles in deposit and C = volume fraction of particles in suspension, then

$$dV_p / dt = \frac{kC}{1+kC} \qquad \textbf{(eqn. 5.1)}$$

Where

k = measure of the interaction between particle and cathode surface

In this model, they attempted to establish a mathematical relationship between k and factors that influences it. Such factors includes:

Electrostatic attraction, which was considered to be a function of the adsorbed charge (q) on the particle and the potential field at the cathode (V).

Physical bond, which was considered to be dependent on the rate of metal deposited. That is area of metal/particle interface. It was assumed that if bond strength per unit area is (A) and current density is (i) then the physical bond would be a function of Ai^2.

The interaction would depend on mechanical factor (M) such as size and density of the particles and the rate of agitation.

Therefore:

$$k = \lambda(qV + Ai^2 - M) \qquad \textbf{(eqn. 5.2)}$$

$$dV_p / dt = \frac{N\lambda(qV + Ai^2 - M)C}{1 + (qV + Ai^2 - M)C} \qquad \textbf{(eqn.5. 3)}$$

Where,

λ= constant

N = number of collisions of particles suitable for codeposition/second.

They noted that k would then be affected by current density and/ or agitation.

5.2.3 Model of Celis, Roos and Buelens [103]

Another useful contribution to an understanding of the incorporation of particles has been made at Leuven University. CELIS et al [104] developed a mathematical model describing the mechanism of electrolytic codeposition of particles with a metallic matrix. They proposed that an adsorbed layer of ionic species is created around the inert particles at the time the particles are added to the plating solution or during the pre-treatment of these particles in ionic solutions. Furthermore, the reduction of these adsorbed ionic species is required for the incorporation of particles in the metallic matrix. They postulated several fundamental steps in the codeposition process, as shown in the boundary layer diagram of Fig (5.1). During transport to the cathode, the particles have to proceed through five consecutive stages, namely formation of ionic cloud, convection towards the cathode, diffusion through the hydrodynamic

boundary layer, then adsorption and reduction at the electrode surface, before particles can be embedded in the metal.

5.2.4 Bozzini's model [105]

BOZZINI [105] proposed a simple approach to the problem of predicting the effects of the dispersion of non-conducting particles, electrokinetic behaviour of the bath and operating conditions on the stability of cathode morphology. He stated that even though variations of all the considered variables have a bearing on the growth stability, the most important single effect is polarisation. The deposition of metal with high polarisation makes codeposition possible and renders viable the achievement of sufficiently smooth and thick materials whilst metals deposited at low overvoltage are mostly associated with unsuccessful composite plating.

5.2.5 Two-step particle incorporation [106]

Attempts to increase the incorporation of co-deposited particles using various surfactants in an electrolytic bath have been reported by many researchers [100,107-108]. However, surfactant molecules adsorbed on a particle (as well as the free surfactant) can codeposit with the metal, which can lead to highly stressed and brittle deposits in some cases [100]. Also, the usual particle loading in a classical plating bath needs to be high in order to disperse a high vol. % of particles into a metal matrix. This might increase the cost of production of the composite coating.

As an alternative to the previously employed methods of particle incorporation, a simple two-step technique in order to disperse a high vol. % of ceramic particles into a nickel matrix has been proposed [106] (see Fig 5.2). According to the authors [106], a uniform film of ceramic particles was first electrophoretically deposited on an iron plate. Nickel was then electrodeposited in the second step onto the substrate covered with the film of these ceramic particles [106]. The two-step procedure consequently leads to the preferential deposition of nickel through the pores of the film prepared in the first step. It grows in and around the grains of the particles and hence, the inter-granular spaces are completely occupied by the deposited

nickel in the second step with the ceramic particles tightly held and bonded within the matrix [106].

5.3 Electroless composite coatings

Electroless plating is a chemical reduction process, which depends on the catalytic reduction of a metallic ion from an aqueous solution containing a reducing agent, and the subsequent deposition of the metal without the use of electricity [109]. Electroless composite deposition was first patented by Metzger as reported by SIMMONS [82] and was based on a nickel-phosphorus matrix. Initial attempts made to produce such deposits were not successful and often resulted in decomposition of the bath [109]. Dispersion of finely divided particles increase the surface area loading of the electroless plating bath by 800 times than normally acceptable conventional electroless plating and this ultimately leads to homogeneous decomposition of the bath [110]. Other matrix metals deposited in this way include copper and cobalt. Among the variety of metals that can be plated using this method, electroless nickel has proved its supremacy for producing coatings with excellent corrosion and wear resistance [109]. Since the baths used for electroless deposition are closely dependent upon surface area in their operation, they are regularly filtered to remove any soluble contaminants that may lead to autocatalytic decomposition of the solution, and/or imperfections in the deposit [82]. Typical baths contain a number of different additives, such as complexing agents, buffers, brighteners and stabilisers, in order to control the speed of metal deposition and to avoid solution decomposition. Electroless coatings can be applied to many substrate types, such as metals, alloys, or non-conductors with excellent thickness uniformity, even on complex shaped components. An essential advantage of preparing composite coatings by electroless deposition compared to electrocodeposition is that the former allows accurate reproduction of the base geometry and eliminates the need for subsequent mechanical finishing.

FEDSTEIN et al [111] stated that it is possible to codeposit more than one particle type from the same solution, producing a greater range of opportunities for end use. Generally, the percentage of entrapped particles increases with increased bath content and increased

temperature. Temperature also increases matrix deposition rates, although the addition of particles causes deposition rates to be reduced.

5.3.1 Electroless nickel composite coatings

Composite electroless nickel coatings are still a developing and promising area of metal finishing with extensive potential for the aerospace industries. The primary reason for the growth of electroless nickel coatings are its property of corrosion and wear resistance, lubricity, uniformity, and its ability to replace toxic chromium and cadmium plating processes. However, it is pertinent to note that there are also toxicity issues with nickel now. Electroless nickel is often deposited as an alloy, with four 'ranges' commonly available: low (1-4% phosphorus), medium (6-8% phosphorus), high (10-12% phosphorus), and nickel-boron (0.5-3% boron). Each of these give coatings offering varying degrees of hardness, corrosion resistance, magnetism, solderability, brightness, internal stress and lubricity, allowing the coating to be tailored according to the physical properties desired [82].

Particle size ranging from 1-10 μm can be used with this system [112], with performance benefits possible when two different particle sizes are used in one bath. This is thought to be due to smaller particles filling spaces between the larger particles.

FELDSTEIN [112] also reported that the codeposition of particles within electroless nickel coatings can dramatically enhance existing characteristics and even add new properties. These capabilities according to him are making composite electroless nickel coatings increasingly advantageous for:

Facilitating the use of new substrate materials, such as titanium, aluminium, lower-cost steel alloys, ceramics and plastics. The benefits of this capability are of special interest to aerospace and airline applications where lighter and more durable, or less expensive materials are desirable and are made practical with such a surface treatment.

Replacing environmentally problematic coatings, such as electroplated chromium.

Allowing higher productivity of manufacturing equipment with greater speeds, less wear and less maintenance-related downtime.

Ever more demanding usage conditions requiring, for example less wear or lower friction.

Electroless nickel composites can be divided into a number of categories according to their commercial applications, such as wear resistance, self-lubrication etc. Of these, wear resistance is the most common application. Selection of the correct particle specification (i.e size, shape, density and type) is governed by a number of factors, including the specific wear mechanism expected. Typical particles codeposited for wear resistance are diamond, silicon carbide, alumina, tungsten carbide, boron carbide or chromium carbide.

Lubricious (low friction) coatings also offer wear resistance, but are considered to belong to a different category due to their extra beneficial characteristics, such as dry lubrication, improved release properties and repellence of contaminants like oil and water. Of the particles added for lubricity purposes, PTFE has received the most widespread commercial interest. However, PTFE degrades at approximately 450 ^{o}C, and is not suited for use at temperatures above this. In such circumstances, other materials should be used, such as molybdenum disulphide, graphite or boron nitride. Another advantage of these materials is that they are harder, more wear resistant and have higher load bearing capabilities. Boron nitride, in particular, has excellent load bearing properties and is able to withstand temperatures up to 3000 ^{o}C depending upon the atmosphere. NISHIRA AND TAKANO [113], in their work on electroless Ni-P/PTFE composites, noted that as PTFE content was increased, the overall hardness was reduced. SIMMONS [82] reported that the 'Niflor^{TM}' process developed by Ebdon in conjunction with Fothergill Engineered Surfaces Limited is one of the commercialised electroless nickel/PTFE composite coating systems currently available today.

5.4 Electrolytic Composite coatings

Electrolytic codeposition, namely the incorporation of inert particles suspended in a plating bath, into a metal matrix during electrolysis has since 1969 been presented in the literature as an alternative method to more conventional techniques for the production of composite coatings [114]. The method offers the possibility of producing smooth deposits with desirable dimensions and variable properties. STOJAK and TALBOT [115] outlined the advantages of

electrocodeposition over other coating methods as the uniformity of deposition for complex shapes, reduction of wastes often encountered in dipping or spraying techniques, low levels of contamination, and ability to process parts continuously.

A wide range of composite films has been used for a variety of applications by tailoring the composition via electrodeposition. These films have been used to protect against abrasion, oxidation, and hot corrosion; to provide lubrication; or to create a high hardness surface for cutting or grinding tools.

As with conventional electrolytic deposition, the matrix of electrodeposited composite coating can be in the form of a pure metal or an alloy. The second phase can be in the form of a powder or fibre (either oriented or of random orientation) and either conducting or non-conducting, depending upon the intended application. This is summarised in Figure 5.3. It is important that the second phase material is insoluble in the electrolyte to be used, and that it can be wetted. Due to problems keeping large particles in suspension, an upper size limit of 40 μm diameter was stated by CELIS AND ROOS [116]. As stated by ZHITOMIRSKY [117] electrolytic deposition produces colloidal particles in cathodic reactions for subsequent deposition. The electrodeposition process according to them includes mass transport, accumulation of particles near the electrode and their coagulation to form a cathodic deposit.

SIMMONS [82], outlined the following techniques for the production of electrolytic composite coatings

The conventional suspension techniques, in which particles are continuously kept in suspension, chemically or mechanically, allowing the formation of a composite coating on the cathode during electroplating.

The sedimentation technique, in which particles are periodically disturbed by vigorous agitation and allowed to sediment again on a horizontal surface during electrodeposition has the advantage that higher incorporation rates can be achieved when compared with normal suspension technique. Also by periodic agitation/ sedimentation, it is possible to get layered deposits.

5.4.1 Parameters affecting composite electrodeposition

Whilst a significant amount of research has been conducted on composite electrodeposition, most of the work has focused on maximising particle incorporation or improving a specific property of the codepositing film. The improvement of a specific film property is related to the particular application, i.e better corrosion or oxidation resistance, lower wear rates, and overall increase in the longevity of the coating.

The amount of particles codeposited with metals depends on a number of factors. These include hydrodynamics, current density, bath composition, particle characteristics, temperature, bath agitation, addition agents present in the solution, and particle loading in the suspension.

5.4.1.1 Effect of current density

STOJAK AND TALBOT [115] in their investigations on electrocodeposition of alumina particles within a copper matrix stated that the most influential process parameter on the resulting particle incorporation (as long as there is sufficient particle loading in suspension) appears to be the percentage of the limiting current density the process is operating at. This inherently involves the system hydrodynamics and overpotential. According to them, particle incorporation increases with increasing current density for all rotational rates and particle loadings in suspension until about 20-25% of the limiting current density is attained. In this region, the rate-determining step for codeposition appears to be the reduction of metallic ions adsorbed onto the alumina particles. Then incorporation decreases with an increasing rate of metal deposition, and then remains relatively constant until about 90% of the limiting current density is attained when incorporation drops significantly. With a stationary cathode, incorporation increases with increasing current density to a maximum at about 15% of the limiting current density, and then decreases rapidly until a value of about 25% of the limiting current density. It was further stated that the relative effects of other variables can be evaluated more clearly when related to the limiting current density. Similarly, BOZZINI [105] in his model emphasized the importance of polarisation in particle composite electrodepositon. He stated that even though variations of all the considered variables have a bearing on the growth

stability, the most important single effect is polarisation. HOVESTAD AND JANSSEN [2] also mentioned that, along with the particle concentration in solution, current density is possibly the most widely investigated parameter. CELIS AND ROOS [116] noted a general trend of decreasing codeposition as current density was increased, whilst an increase was reported for a Ni/SiC composite. It was stated that either effect could be obtained, depending upon electrolysis conditions. Other investigators [118-119] have also reported the improved rate of particle incorporation with increasing current density. However, YEH and WAN [119] noted that the vol.% of particles co-deposited initially increased with increasing current density, attained a maximum and then decreased.

5.4.1.2 Effect of pH

Control of pH values may be important in producing deposits with specific properties.
In view of this, effect of pH on composite electrodeposition has been widely researched [118, 120-121]. Investigating a Ni-SiC system, WANG and WEI [118] found that in the strong acid region ($pH \leq 2$), the embedded SiC content is lower than 0.5%. When the pH of the suspension becomes weakly acid, SiC content increases until the pH=6. Above pH=6, the coating loses its surface brightness and cannot form a dense layer. Similarly, HAMID and GHAYAD [120] studied the codepostion behaviour of Ni-polyethylene and reported that the volume percent of polyethylene (PE) incorporation increases with pH up to 4; further increase markedly lowered the incorporation of PE in the composite. This decrease was attributed to a decrease in efficiency of nickel deposition and an increase in viscosity of the plating solution. Although what happens to the SiC particles at pH>6 is not mentioned, it is likely that beyond this pH, the agglomeration of SiC particles could start to take place. TAKAHASHI et al [121] investigated the effect of a SiO_2 colloid on the electrodeposition of zinc-iron group metal alloy composites. They reported that the agglomeration of SiO_2 on the cathode was due to the pH increase, because this colloid is agglomerated at neutral pH. ASLANDIS et al [122] investigated the electrolytic codeposition of silica and titania modified silica with zinc. They reported that the codeposition of pure silica with zinc increased with increasing pH in the range 1 to 4.4. At a pH of 4.4, pure silica carried more zinc ions in their double layer than at the pH of 1.1. However, they noted that titania modified silica carried even more adsorbed

zinc ions in their double layer and therefore codeposited better with zinc at higher pH than in the case of pure silica. The higher codeposition of titania modified silica with zinc at higher pH was therefore attributed to the higher dielectric constant of titania and the associated larger number of ions adsorption onto titania modified silica than pure silica.

Variation of pH, as earlier mentioned appears to yield varied results. Work by YEH AND WAN [123] who investigated the effect of ion adsorption on the codeposition of SiC from a Watts type nickel bath, attempted to explain this phenomenon. They found that SiC powders catalysed the adsorption of hydrogen atoms and significantly increased hydrogen evolution at a pH$\leq$ 2. This pH corresponded to the point of zero charge for SiC in sodium chloride solution. They, therefore, concluded that the powder content of the deposited layer and the current efficiency for nickel reduction were both notably decreased at pH lower than two when SiC particles were present in the electrolyte. YEH AND WAN [123] also reported the effect of increase in pH on the rate of nickel ion adsorption onto the particles in a watts nickel plating bath. According to them, increase in pH from 1.5 to 4.0 produced a corresponding increase in nickel ions adsorption onto the particle surface. Furthermore, current efficiency was also found to increase within the same range of pH (1.5-4.0).

5.4.1.3 Effect of agitation and type

Bath agitation plays a very significant role in electrodeposition. Its significance is further stressed in composite electrodeposition where the need to keep particles in suspension for effective particle incorporation is of primary importance. Recently, GABE [124] outlined the purposes of agitation as follows.

To avoid stagnation- dispersing products and delivering reactants.

To increase deposition rates- stirring and thus thinning of the electrode diffusion layer.

To dissipate heat from the surface-equilibration of the deposition conditions.

To incorporate particles in the coatings- composite coating production.

To modify deposit properties- grain size, stress, hardness etc control.

He distinguished various types of agitation currently utilised in electrodeposition. These include air agitation, rotational stir, eductor agitation and vibratory agitation. Whichever

utilised, in composite electrodeposition the rate of agitation and type of flow determines, to a large extent, the amount of particles incorporated in the composite electrodeposit. Recently, the use of vibratory agitation has found increasing favour amongst several investigators [125-127] due to the fact that particles are maintained in suspension without swirling and gross turbulence. KALANTARY AND GABE [126] concluded that with vibratory agitation particles could be codeposited in an electrodeposit in a uniform manner although the absence of shear mixing action may allow particle agglomeration. Two forms of fluid flow were identified; laminar and turbulent. However, they did not recommend a laminar flow as particle dispersion for composite plating is effective only near the turbulent region with maximum incorporation taking place near the laminar to turbulent transition. JOHAL et al [125] reported that the mechanism of codeposition is widely agreed to take place in three stages of which the first stage is agitation dominated. Thus agitation must have two effects on codeposition. Firstly, it ensures that particles are delivered to the growing cathode surface from suspension in solution-thus an increase in agitation would be expected to increase the collision frequency of particles with the cathode surface. Secondly, they noted that it may also sweep away particles which are not rapidly incorporated in the growing cathode or are unable to remain adsorbed on the surface in the presence of excessive agitation shear stresses, thus collision contact time might be involved in the second criteria. It was also argued that a corollary of this must be increasing current density, which could increase the rate of incorporation of particles in the electrodeposit. However, the pre-requisite condition is that the particles are well dispersed in solution, a condition usually achieved by agitation.

The use of the Rotating Disk Electrode (RDE) has been reported [128]. According to MULLER et al [128], at low rotation speeds the fluid flow induced by the RDE is not capable of transporting all the particles to the cathode and, when the rotating speed is too high, the rate of particle removal becomes greater than that of attachment at certain sites on the electrode. This is probably due to the predominant laminar flow at most practical rotation speeds and could lead to poor rates of particle incorporation. Agitation using mechanical stirring has also been widely reported [129-131]. GAY et al [130] while studying the electrodeposition behaviour of Ag-ZrO_2, observed that the vol.% of ZrO_2 incorporated increased with increase

in stirring rate until it attained a maximum value and then decreased considerably. Similar observations have been made by other researchers [129,132].

5.4.1.4 Effect of temperature

Temperature appears to affect different systems in different ways [82]. KIM AND YOO [132] reported that the temperature of the electrolyte affects the plating process. They noted that the highest vol. % of SiC was obtained at 50 °C. According to them, the temperature for obtaining the highest vol.% of codeposited SiC is independent of the particles size. WANG AND WEI [118] also reported the effect of temperature on the streaming current of Al_2O_3 and ZrO_2 in a $Ni/Al_2O_3/ZrO_2$ system. Streaming current appears to be a measure of the migratory behaviour of particles as a function of the density of metal ions on the surface of the particles due to the applied voltage. They observed that the two powders were positively charged and their streaming current readings were nearly constant as the temperature of the plating solution was increased.

HAMID AND GHAYA [120] reported the influence of temperature on the vol.% incorporation of polyethylene in a nickel matrix with increasing temperature. They stated that the polyethylene incorporation increased from 12 vol.% at 25 °C to 30 vol.% at 50 °C and that with further increase in the temperature, a decreasing trend was observed, which resulted from the decrease in current efficiency of the bath. However, ZHU [127] observed a decreasing trend of SiC incorporation with increase in temperature from 25 to 60 °C with the highest vol.% of SiC incorporation at 25 °C in a Cu/SiC composite system in the presence of additives. According to them the observed decrease in SiC incorporation was due to the fact that the adhesive force between SiC particles and the cathode decreased as the viscosity of the plating solution decreased due to increase in temperature. Besides, the additive desorbed from the surface of SiC more easily due to high temperature. So that increasing the temperature of the plating solution decreased the codeposition of SiC and Cu ion on the cathode

KIM AND YOO [132] also investigated the effect of temperature on the plating process of Ni/SiC. They reported that the highest vol.% of SiC was obtained at 50 °C and concluded that

the temperature for obtaining the highest vol.% of codeposited SiC is independent of the particle size.

5.4.1.5 Effect of particle loading and size

The effect of particle loading is one parameter that has been widely investigated [127-136]. Several of these authors reported that rate of particle incorporation increases with increase in particle concentration in the bath until it attains a maximum value and then decreases with further increase in the bath concentration of particles. HAMID [134] while studying the codeposition behaviour of Zn-Co-TiO_2 noted that the increase in codeposition of TiO_2 at higher concentrations is attributed to the greater adsorption of TiO_2 on the surface of the cathode. He further stated that once the particles are adsorbed, metal begins building around the cathode, slowly encapsulating and incorporating the TiO_2. With further addition, the particles appeared to agglomerate in the bath and a decreasing trend was observed. Similar observations have been reported by other researchers [128], although the agglomeration of particles was attributed to insufficient stirring to keep all particles in suspension.

Literature about the effect of particle size is fairly contradictory. KIM AND YOO [132] reported that the codeposited SiC content increased as the particle size increased up to 14.0 μm. Beyond this particle size, the codeposited SiC content decreased. Contrary to this observation, GARCIA et al [135] reported that the codeposition efficiency does not decrease with decreasing particle size. Rather, at a given number density of particles in the plating solution, the codeposition efficiency increases with decreasing particle size. The term 'effective particle concentration' has been introduced while describing the effect of particle loading on the rate of particle incorporation. WANG et al [129] defined the effective particle concentration as the ratio of the weight of suspended particles in the plating solution to the volume of the plating solution. They noted that decrease in the vol.% of talc incorporated above 25 g/l resulted from the dropping of its effective bath concentration, which was caused by the agglomeration of the particles in the bath because of its bad wettability. Similarly, GHORBANI et al [131] also reported that in high concentrations of graphite (60-100 g/l)

because of the agglomeration of particles in the bath, the effective particle concentration is constant which resulted in constant vol.% of graphite in the composite coating.

5.4.1.6 Surfactants and Electrophoresis

To have a better understanding of the behaviour of surface active additives and the way they enhance electro-codepositon in colloidal systems of ionic solutions, it is pertinent to discuss the electrical double layer and the phenomenon of electrophoresis.

When a surface is placed in an ionic solution, an electrical potential develops at the solution/surface interface. If a positively charged electrode is placed in a solution containing both positively and negatively charged ions, only negatively charged ions are attracted to the surface. This in turn leads to a build up of negative ions in the solution near the surface so that a new charge exists. Since the system as a whole should be electrically neutral, the total net charge on the surface is balanced by the charge set up within the solution. Thus a double layer of charge exists, one localised at the surface, and the other developed in a region extending into the solution.

Even if a solid is not an electrical conductor, an electrical double layer can still form. The main origin for double layer formation on both organic and inorganic surfaces is by the specific adsorption of ions. In such cases, charge is located entirely on the surface, with no charge being held within the bulk of the solid as is the case for conductors. Therefore counter ions form the Helmhotz and diffuse double layers within the solution. It is this way electrical double layers form around solid particle suspensions or colloidally dispersed materials

Surfactant' is an abbreviation of a surface active agent, which literally means active at a surface [136-137]. A surfactant was therefore defined as a substance which in solution, particularly aqueous solution, tends to congregate at the bounding surfaces, i.e the air-solution interface, the walls of the containing vessel and the liquid-liquid interface, if a second phase is present. As a result, the various interfacial tensions are reduced. The reason for this behaviour is that the surfactant molecule contains two structurally distinct parts, one of which is

hydrophilic while the other is hydrophobic [138]. Surfactants are generally classified according to the nature of their hydrophilic parts, anionic surfactant in which the hydrophilic part carries a negative charge, non-ionic surfactant in which the hydrophilic part is uncharged, cationic surfactant in which the hydrophilic part carries a positive charge and an amphoteric surfactant in which the hydrophilic part carries both positive and negative charges [138].

The task of choosing a surfactant in composite electrodeposition is a daunting one as several considerations have to be made before making an appropriate choice. Such considerations may include, the nature, size and type of the second phase material, nature of the bath-aqueous or non-aqueous, composition of the bath, ionic concentration of the bath, intended application of the coating, the type of hydrophilic group on the surfactant. However, the primary aim for the use of surfactants in composite electrodeposition is to enhance codeposition of the second phase material.

Recently, the availability of ever decreasing particle sizes has expanded potential metal matrix composite applications [139]. Submicrometre size particles dispersed into a metal matrix not only promote homogeneity of the composite due to the increase in metal-particle contact surface area, but also would be a necessity for use as composite materials in micro devices. Since components of these devices are of micro scale, the second phase material in the metal matrix needs to be an order of magnitude smaller; thus, up to nanomeric requirement [139]. However, the reduction of the particle size will decrease the codeposition content of the particles [135,140]. According to the literature, the smaller the particle size, the more difficult for the particles to embed in the depositing layer [141]. FRANSAER et al [142] stated that the development of composite plating with nano-sized particles is hampered by the following two problems. In aqueous plating electrolytes, particles easily agglomerate due to the compression of the diffuse double layer surrounding the particles by the high ionic strength. According to them, this effect is even more pronounced for particles of submicron size as the shearing forces on the agglomerates created by agitation of the plating bath decreases with particle size. As a consequence, the codeposition of agglomerated particles takes place and the anticipated mechanical, chemical and/or physical properties of the composite coatings are not reached. It has also been reported that particle aggregation affects particle codeposition and in industrial

practice it can lead to sedimentation or creaming of particles in storage tanks and clogging of tubes [143]. GARCIA et al [135] showed that the highest volume fraction of codeposited SiC was achieved with 5 μm particles rather than with 0.7 or 0.3 μm particles. WANG AND WEI [118] also reported that ultra-fine SiC was more difficult to codeposit than the coarse SiC and that the rate determination step is controlled by the transferal process of loose adsorption to strong adsorption. Their results implied that the adsorption on the electrode surface of ultra-fine SiC particles is more difficult than that of the coarse SiC particles. It appears that the size of inert particles seems to play a significant role but it is still not clear why inert particles of smaller size are difficult to embed in the deposition layer [141]. To overcome the aforementioned problems of particles agglomeration and consequent poor incorporation, the use of surfactants has drawn the attention of several researchers [100,140-144] in composite electrodeposition.

The use of cationic surfactants seems to be favoured probably due to their positive charge and therefore a greater tendency to be attracted towards the cathode. HOVESTAD et al [143] while investigating the electrochemical deposition of zinc-polystyrene composites in the presence of surfactants reported that addition of cetylpyridinium chloride, a cationic surfactant, prevented aggregation and enhanced polystyrene codeposition. According to them, other surfactants also increased suspension stability but diminished polystyrene codeposition, irrespective of their charge. They related the effect of surfactant to possible changes in surface roughness of zinc due to surfactant adsorbed on the electrode. The enhanced codeposition behaviour of SiC in the presence of cetyltrimethylammonium bromide (CTAB) has been reported [140-141]. According to HOU et al [140] addition of CTAB cannot only disperse the SiC particles well in the electrolyte leading to better homogeneously distributed SiC particles in the matrix, but also enhances the SiC vol.% embedded in the codeposited layer. Similarly, GER [141] reported that addition of CTAB could reduce the agglomeration of SiC particles in the plating bath so that a high percentage of uniformly distributed SiC particles can be deposited. Furthermore, he stated that the adsorption of surfactant CTAB on the SiC particles increases with increasing concentration of CTAB. The influence of the hydrophobic tail length of a cationic surfactant containing an azobenzene group (AZTAB) on the extent of co-deposition of SiC particles with nickel has also been reported [144]. They showed that an

AZTAB with a shorter tail could co-deposit a higher amount of SiC particles than the surfactant with a longer tail. It was assumed that the difference in efficiencies for maximum codeposition of particles with nickel is due to the difference in the rate of desorption. of these azo-cationic surfactants from the particle surface during the codeposition process [144]. HAMID AND OMAR [145] attempted to establish a relationship between anionic/non-ionic surfactants and the electrodeposition of nickel-polytetrafluoroethylene polymer. They noted that the adsorption of an anionic surfactant on nickel cations and the ability to stabilise a dispersion of the PTFE particles appears to be a function of micellar composition.

Apart from electrolytic codeposition of inert particles from a bath containing dissolved ionic species and colloidal second phase materials, particle incorporation could also be effected electrophoretically. ZHITOMIRSKY [146] carried out an extensive overview of the production of ceramic films using cathodic electrodeposition. He divided the process of ceramic film formation into two processes namely cathodic electrodeposition and electrophoretic deposition. Electrophoretic deposition was defined as a process in which ceramic particles, suspended in a liquid medium, migrate in an electric field and deposit on an electrode. According to him ceramic films must be electrically charged to permit forming by electrophoretic deposition. The charge on a colloidal particle could originate from various sources, such as from adsorbed simple organic ions or from dispersants. This implies that the use of surfactants is important in composite electrodeposition as well as in composite electrophoretic deposition.

5.5 Properties of composite coatings [2, 116]

As mentioned earlier in this chapter, the codeposition of inert particles with a metal can improve the coating's physical properties and even provide new characteristics. This makes composite coatings particularly useful, for the following reasons.

Coatings can now be applied to materials such as titanium, aluminium, lower-cost steels, ceramic and polymers (electroless techniques) where previously this was rather difficult or impossible. The benefits of this capability are of special interest to aerospace application

where lighter, more durable, or less expensive materials are desirable and are made practical with such surface treatments.

Replacement of environmentally harmful coating processes, such as electroplated chromium.

Higher productivity of manufacturing equipment with greater speeds, less wear and less maintenance-related downtime.

Surfaces can endure ever more damaging usage conditions requiring less wear or where, for example lower friction are required.

Electrodeposited composite coatings are particularly used in areas where improved characteristics such as wear resistance, corrosion resistance or self-lubrication, are required and of importance.

5.5.1 Corrosion resistance

A major application of composite coatings is in the production of corrosion resistant coatings. Zinc and zinc alloy electrodeposited steel sheets have been used for automobile bodies due to their high corrosion resistance [147]. Composite coatings with SiO_2 or Al_2O_3 particles are known to show good corrosion resistance and paintability. For example HIRAMATSU et al [148] have reported an improvement in the corrosion resistance and paintability of zinc electrodeposit composite with SiO_2. Other reasearchers [122, 149] have also reported the improved corrosion resistance of zinc- based SiO_2 composite coatings. HASHIMOTO AND ABE [149] attempted to explain the corrosion resistance mechanism of zinc-silica composite electrodeposits. According to them, at the early stage of the corrosion process, zinc hydroxychloride is formed on the SiO_2-rich region as the protective corrosion product and surrounds the SiO_2-poor phase. They noted that SiO_2 may have stimulated the formation of the protective corrosion product and supported the corrosion products. Furthermore, the protective products decelerated the corrosion rate of the SiO_2-poor phase. The corrosion resistance of Zn-SiO_2 was attributed to the formation of protective products in the composite layer supported by SiO_2. ABE et al [150] reported the improved corrosion resistance of these coating in the presence of some nitrogen compounds. According to them, nitrogen compounds dispersed into the plating layer fill gaps between plated metal grains and silica particles in the coating layer,

thus resulting in a denser surface. BECH-NIELSEN [151] reported that the rate of corrosion of electroplated zinc in near-neutral chloride solution can be lowered by as much as 75% by adding fine, inert particles of substances such as MnO_2, Fe_3O_4, SiC, and TiN. He attributed the corrosion resistance of inert particles in a zinc matrix to the formation of a physical barrier, shielding the zinc surface against aggressive species. ASLANDIS et al [122] reported that for zinc coatings receiving a subsequent paint layer, the better corrosion resistance does not derive solely from the dispersed particles present in the bulk of the zinc, but originates, in part, from the interlocking between the codeposited particles and the subsequently applied paint layer. TAKAHASHI et al [121] have reported the effect of SiO_2 on the corrosion resistance of Zn-Fe group alloys. According to them, Zn-Fe-SiO_2 showed a slightly better corrosion resistance than Zn-Fe. Zn-Cr-SiO_2 composite was reported to show excellent corrosion resistance. However, the SiO_2 had only a small effect on the corrosion resistance, whilst the effect of Cr was remarkably large. In their investigations, KIMOTO et al [152] reported that although the corrosion resistance of zinc electroplated steel sheets is improved by the dispersion of oxide particles such as SiO_2, Al_2O_3 and TiO_2, it is not only affected by the codeposition ratio but also by the characteristic of the oxide particles and microstructure of codeposition. HAMID [134] has made a comparison of the corrosion resistance of Zn, Zn-Co, and Zn-Co-TiO_2 in a salt spray cabinet. According to them, the zinc coated sample shows a small percentage of red rust at 400 hours whilst Zn-4% Co shows a small percentage of red rust at 500 hours and Zn-Co-TiO_2 showed no sign of red rust after 500 hours. This means that the presence of cobalt and titanium oxide improved the corrosion resistance of galvanized steel. However, 400 hours time to 5% red rust for ordinary zinc as reported by these authors is quite unusual, except the coating thickness was significantly higher than 8 μm. Corrosion of zinc and zinc-alloys is generally assessed against the time required for the coating to show either white or red rust. White corrosion indicates partial depletion of the zinc in the protective film formed on the steel substrate. Red rust shows complete depletion, plus corrosion of the steel substrate. Furthermore, they attributed the high corrosion resistance of Zn-Co-TiO_2 to the formation of $ZnCl_2$, $Zn(OH)_2$ in a network form and to support of the corrosion products by the dispersed TiO_2 particles.

HAMID AND GHAYAD [120] reported the corrosion resistant behaviour of Ni-polyethylene. According to them potentiodynamic polarisation studies of steel, nickel and nickel-composites containing different volume percent of polyethylene (PE) shows that the uncoated steel gives the highest corrosion rate (9.0 m/year). This value was decreased up to 0.62 m/year for steel coated with nickel. A further decrease in corrosion rate was obtained up on the addition of polyethylene polymer to the nickel. They noted that the corrosion rate of Ni-PE composites decreased with increase in PE volume percent up to 0.03 m/year with 30 vol.% PE. The decrease in corrosion rate was attributed to the presence of polyethylene particles in the nickel deposit, which lead to a decrease in its porosity.

Recently, ROSSI et al [153] characterised the corrosion resistant properties of nickel/PTFE, phosphate/MoS_2 and bronze/PTFE electroless composite coating on carbon steel. According to them electroless nickel coatings showed the best protection properties with good barrier properties, because of their coating structure: an external layer, which contains PTFE particles improving tribological properties, and an inner nickel layer, which protects against corrosion because of the barrier effect. PTFE- coated sintered bronze samples showed limited corrosion resistance due to the high number of defects present. Furthermore, they reported that the application of a MoS_2 polymer-embedded layer improved the characteristics of phosphate conversion coatings, which, by themselves, cannot assure good protection. They also reported salt spray corrosion results on these coatings, which revealed that the nickel coating showed very good corrosion protection: only after approximately 20 days did the first corrosion attack appear on the substrate. Other nickel samples showed some localised attack only after 30 days. The good corrosion behaviour was attributed to the high quality of the coating and to its high thickness. They noted that the presence of dual layer nickel coatings might be important in that the inner coating (without PTFE particles) could provide a better corrosion protection and improve the coating/substrate adhesion [154]. In fact, the presence of particles could decrease the corrosion protection because the codeposited particles could represent a defect site, allowing possible electrolyte infiltration [155]. Furthermore, ROSSI et al [153] reported that bronze particles within a PTFE matrix resulted in very poor behaviour: after some days of exposure, a blistering phenomenon appeared. According to them, this system acts like a polymeric layer where the solution penetrates through the coating defects and reaches the

substrate, weakening the adhesion to the substrate. For the phophate steel, corrosion was said to have occurred in a short time (1 day), nevertheless the extent of the attacked area remained constant for several days. This behaviour was attributed to non-regular morphology characterised by the presence of several defects, which are due to the limited and non-uniform thickness [156]. The MoS_2-based coatings presented a equivocal behaviour: some samples showed very good resistance, with no evidence of corrosion after 30 days of exposure; while other samples showed several blisters and presented some corrosion attack after a short time. The authors [153] therefore concluded that the nickel-phosphorus coating containing PTFE particles showed good protection properties because of the dual nature of the coating: the outer layer includes PTFE particles (self-lubricating properties), the inner one increases the barrier-effect, whilst the bronze-PTFE coatings presented limited barrier protection effect which was attributed to the high porosity and defectiveness of the coating. Bronze particles, are electrochemically more noble than the steel, this could be a cause of galvanic coupling, which increases the corrosion rate. The application of a MoS_2 layer enhances the corrosion protection properties of the phosphate conversion layer, which was not able to offer sufficient protection by itself, through a decrease of defects present. BALARAJU et al [109] also reported the corrosion resistant properties of Ni-P composite coatings. According to them, evaluation of the corrosion resistance of Ni-P-Si_3N_4, Ni-P-CeO_2 and Ni-P-TiO_2 composite coatings by electrochemical impedance spectroscopy suggest that these coatings provide better corrosion resistance than plain electroless Ni-P coatings.

The properties and structure of electrodeposited RE-Ni-W-B-SiC composite coatings has been reported by GUO AND ZHU [157]. RE in the composite appears to have been added as an additive in the form RE(CeO_2). This additive was said to have enhanced the hardness and wear resistance of the composite coating. They claimed that the corrosion resistance of Ni-B based composite coatings against sulphuric acid is not as good as that of Ni-P based composite coatings, but superior to those of stainless steel and hard chromium coatings. The second phase particle in both cases was SiC. Also, the corrosion resistance of Ni-B based composite coatings against alkaline solution was good.

5.5.2 Wear resistance

One possibility to increase the durability and performance of materials for different applications is to protect them using composite coatings [106]. Highly wear resistant coatings are required in different fields of technology such as transportation, machine and device construction, machine tools and aircraft [120]. In recent years, ABDEL HAMID et al [120,145,153] have reported that polymer particles such as PTFE and polycarbon monofluoride $(CF)_n$ can be deposited from electroplating and electroless plating baths. These compounds are used for coatings with 'non-stick' characteristics and low coefficient of friction. The production of wear resistant coatings by the electrolytic codeposition of suspended inert particles in an electrolytic bath has been widely reported [106, 120, 129-131, 135,140,144]. In their work on the two-step preparation of composite electrodeposits of Ni/BN and Ni/Al_2O_3, SHRESTHA et al [106] reported that, regardless of the method of preparation, the Ni/BN composite coatings had a better wear-resistant performance than the Ni/Al_2O_3 coatings. The two-step method involved the initial electrophoretic deposition of the ceramic particles onto the substrate. Nickel was then electrodeposited in the second step onto the substrate covered with the film of ceramic particles. According to them, all composite coatings prepared by the two-step method showed substantially better wear resistance than those prepared by the single step method. They assumed that the better anti-wear performance of the composite coatings prepared by the two-step method was due, not only to the higher volumetric content of the particles, but also the manner in which these particles were incorporated within the metal matrix. HAMID AND GHAYAD [120] reported the wear behaviour of ordinary Ni and Ni-polyethylene composite electrodeposit. According to them, the wear rate of Ni-polyethylene deposits was markedly lower than Ni deposit. They observed that the incorporation of polyethylene improves the abrasive wear resistance of nickel and its microhardness in the range between 460 and 700 VHN depending on the amount of particles incorporated whilst coatings without polyethylene exhibited the lowest hardness values of 230 VHN. WANG et al [129] produced electrocomposite coatings consisting of Al_2O_3, CaF_2 and talc particles with copper-tin alloy by means of conventional electrodeposition techniques. According to them the presence of particles greatly improved the hardness and wear resistance of composite coatings. From the hardness values they reported, it shows that hardness of the various electrodeposits increased in the following order: Al_2O_3-Cu(Sn) >CaF_2-Cu(Sn) > Talc-

Cu(Sn) >Cu(Sn) and the wear rate of these coatings was much less than that of copper-tin alloy coatings. According to them, the hardness and wear resistance of composite coatings are dependent on the hardness of the incorporated particles and that composite coating containing harder particles (e.g Al_2O_3) are of greater hardness and wear resistance. GAY et al [130] characterised Ag-ZrO_2 electrodeposits. They reported that composite coatings deposited with a volume % of up to 8% ZrO_2 presented high hardness and low friction coefficients and a notable increase in wear resistance. For incorporation rates less than 5.4 %, the volume of material removed from the composite coatings during wear tests was approximately twice that obtained without particles. This result was attributed to a weak adhesion of particle agglomerates embedded in the composite matrix. For a higher volume % of particles in the deposits (between 8.4% and 9.2%) when the number of agglomerated particles is diminished, the volume of matter removed was considerably reduced. They therefore concluded that the wear resistance of the composite Ag-ZrO_2 coating is influenced by the percentage of particles embedded in the coating. GHORBANI et al [131] produced brass-graphite composites and characterised their tribological properties. These authors noted that an increase in the amount of graphite in the deposit lead to a decrease in the coefficient of friction, but also to an increase in weight loss in wear tests. Furthermore, when graphite content in the coating reached 3.7 (vol.%), weight loss increased by approximately 30% but coefficient of friction decreased by approximately 35%. It was therefore concluded that graphite content in the composite electrodeposits influenced the weight loss in the wear tests and coefficient of friction depends on the graphite content, load, distance and speed of the 'block on ring' tester during the wear test. The coating containing approximately 3.7 (vol.%) graphite had the best tribological properties.

Recently GARCIA et al [135] investigated the sliding wear behaviour of Ni-SiC composite electrodeposits with different particle sizes. According to them, the wear properties of Ni-SiC composite coatings depended on the volume occupied by the reinforcing particles, as well as their number density. Higher volume percent or number density of codeposited particles lowered the wear resistance. Whilst decrease in particle size, affected the wear resistance in a positive way. Similarly, HOU et al [140] reported that the wear resistance of the deposited layer increases with increase in SiC vol.% since the SiC particles provide both dispersion

strength and particle strength. According to these authors, as long as the particles in the coating layer are well distributed, the wear resistance was expected to be enhanced. Indeed, it is known that the hardness and other mechanical properties of metal matrix composites depend in general on the amount and size of the dispersed phase, apart from the mechanical characteristics of the matrix, particles and interfaces. That amount and size of particles defines two kinds of reinforcing mechanisms in metal matrix composite materials, namely dispersion-strengthening and particle strengthening. A dispersion strengthened composite is characterized by a dispersion of fine particles with a particle diameter ranging from 0.01 to 1 μm, and 1 to 15 vol. % of particles. In this case the matrix carries the load and the fine particles impede the motion of dislocation. A particle-reinforced composite contains more than 20 vol.% of particles larger than 1 μm. The inter-particle spacing is less than 5 μm, and the load is carried by both the matrix and the particles. Strengthening is achieved because particles restrain matrix deformation by mechanical forces [135]. These authors further noted that the abrasive wear of metal matrix composite increases with increasing amount and size of abrasive particles, as does the hardness of the metal matrix composites. Therefore, in composite plating, a decrease in the size of particle codeposited is, in both cases positive. However, an increase in the number density of codeposited particles produces higher hardness and mechanical strength, but also an increase in abrasion wear when reinforcing particles are pulled out of the composite coatings during sliding wear.

5.5.3 Lubricity and solid lubricants [158]

In recent years, several new solid lubricants and new lubrication concepts have been developed to achieve better lubricity and longer wear life in demanding tribological applications. Most of the traditional solid lubricants were prepared in the form of metal, ceramic and polymer-matrix composites. They have been used successfully in various engineering applications. Recent progress in thin-film deposition technologies has led to the synthesis of new generations of adaptive, self-lubricating coatings with composite or multilayered architectures, by using duplex/multiplex surface treatments [158].

When service conditions in tribological applications become severe, solid lubricants may be the only choice for controlling friction and wear. According to HOLMBERG et al [159] a general design appraisal of the tribological requirements of a coated-surface contact can be formulated as follows.

The initial coefficient of friction (CF), the steady-state, and the friction instability must not exceed certain design values.

The wear of the contacting surfaces, including the coated one, must not exceed certain design values.

The lifetime of the system must, with a specified probability, be longer than the required lifetime. The lifetime limit of the system may be defined as the time when even one of the earlier requirements is not maintained.

In conclusion, it is apparent from the literature review that a lot has been done to improve the properties of conventional metallic coatings by embedding second phase materials into their matrices using various methods. However, not much appears to have been carried out to incorporate silica particles into zinc and zinc-nickel alloy matrices. The main aim of this project therefore, was to explore possible ways of incorporating various amounts and sizes of silica particles into zinc and zinc-nickel alloys and investigate their corrosion and mechanical properties.

Preliminary investigations on this project were aimed at identifying a suitable approach towards the production of uniform and adherent zinc and zinc-nickel electrodeposits and subsequently composite electrodeposits on the addition of inert particles into an electrolyte. Consequently, as vital parameters in enhancing the production of such electrodeposits, cathode preparation, bath formulations, methods of agitation and cathode current efficiency were given particular attention in this work. Hull cell studies were also carried out to investigate electrolyte properties. Knowledge of the corrosion and wear properties of the electrodeposits was crucial. To achieve this, corrosion/electrochemical studies such as neutral salt spray, linear polarisation resistance, cathodic polarisation and anodic polarisation studies were carried out. Also, studies on the wear behaviour of the electrodeposits were undertaken. The investigations were therefore focused mainly on studying various deposition parameters

extensively investigated in the literature and their effects on both the electrodeposition behaviour, corrosion and mechanical properties of the zinc and zinc-nickel composites.

CHAPTER SIX

6 EXPERIMENTAL

6.1 Introduction

This chapter contains comprehensive descriptions of the various methods and steps taken to achieve the objectives of this project. It includes methods of cathode preparation, bath formulations, determination of electrolyte properties, optimisation of conventional electrodeposition procedures and parameters such as bath agitation, type of agitation, current density and temperature. Also, Hull cell studies, coating characterisation, corrosion/electrochemical tests and finally methods used to determine the wear behaviour of the coatings are described.

6.2 Cathode preparation

Apart from Hull cell investigations where copper cathodes were utilised, all other cathode material used in this work was mild steel sheet. Three different sizes were used in most of the experiments at various instances. The sizes were 2.5cm x 4cm, 5cm x 5cm and 7.6cm x 10.2cm depending on the type of test required. Two methods of surface pre-treatment were used. Most of the samples used in the production of zinc and zinc-nickel deposits were degreased using acetone while samples used in the production of composite electrodeposition were subjected to electrochemical degreasing. In the first case, prior to electroplating, the steel sample was degreased using acetone and pickled in 50 vol.% hydrochloricic acid to remove any surface scale or oxide. After pickling, the panels were washed with running tap water to remove possible acid residues, and then deionised water to remove any hard water salts present on the surface from the previous washing stage. The panels were then dried and weighed. Chemically inert tape was used to blank off the backs of all the panels, and to provide a pre-determined area on which the deposit could form. In the second case, the back of

each panel was blanked off with chemically inert tape and the surface onto which deposits could form was pre-determined. The panels were then washed with detergent. Panels were then subjected to electrochemical cathodic cleaning in a bath containing 25.0 g/l of NaOH, 25.0 g/l of Na_2CO_3 and 50.0 g/l of Na_3PO_4 and etched in 50 vol.% hydrochloric acid for approximately 20 seconds, washed in running tap water and then in deionised water. It was then transferred immediately into the bath for plating to avoid re-oxidation of the surface.

6.3 Zinc Electrodeposition

6.3.1 Bath Preparation

Zinc was electrodeposited from additive-free, aqueous solutions composed of standard laboratory reagents. A 1 litre beaker was half-filled with deionised water and the appropriate quantity of reagent added gradually with mild agitation initially and then more vigorously, as the concentration of the solution increased to enhance dissolution. Measurements of pH were carried out using a HI-8424 digital pH meter, and adjusted accordingly using sodium hydroxide (10 % solution) or concentrated sulphuric acid. The solution was finally made up to 1 litre. The whole process was carried out at room temperature (approximately 22 °C). The various solution formulations are as follows:

1)	Alkaline zinc [160]	10 g/l ZnO
		105 g/l NaOH
		pH = 14.0
2)	Acid zinc (I) [160]	250 g/l $ZnSO_4.7H_2O$
		80 g/l Na_2SO_4
		pH = 2.0-4.4
3)	Acid zinc (II)	350 g/l $ZnSO_4.7H_2O$
		30 g/l $Al_2(SO_4)_3.6H_2O$
		pH = 2.3

6.3.2 Determination of cathode current efficiency and deposit thickness

Cathode current efficiency and deposit thickness of zinc electrodeposits were measured gravimetrically. Pre-weighed samples after plating were first rinsed immediately in running tap water, immersed in acetone, dried in a stream of warm air and then weighed again to determine the weight gain. Cathode current efficiency and deposit thickness were subsequently calculated using the following formulae:

$$\text{Cathode Current efficiency (CCE)} = \frac{\Delta W}{W_T} - \times 100\% \qquad \textbf{(eqn.6.1)}$$

Where,

CCE – Cathode current efficiency (%)

ΔW – Change in weight after plating (g)

W_T - Theoretical weight of deposit (g)

Whilst;

$$W_T = \frac{I \times t \times M_{Zn}}{n \times F} \qquad \textbf{(eqn.6.2)}$$

Where I = Current (A)

t = Time (second)

M_{Zn} = Molecular weight of zinc (g/mol)

F = Faradays const (96,500 C/mol)

n = Number of electrons involved in the reaction

6.4 Zinc-nickel electrodeposition

6.4.1 Electrolyte preparation

The solutions were prepared using deionised water and standard laboratory reagents. Three different types of solution were used in the case of zinc-nickel electrodeposition based on SIMMONS' [82] formulations. This was to investigate various characteristics such as, throwing power and current efficiency of the individual electrolytes to determine a suitable

electrolyte. However, the composition of the acid zinc-nickel (chloride based) solution was subsequently changed by progressive addition of 5 g/l of $NiCl_2.6H_2O$ whilst studying the effect of metal ion concentration in the bath on the nickel content of the deposit. The various bath formulations used for zinc-nickel electrodeposition are given below:

1(a)	Acid zinc-nickel (I)	264.5 g/l $ZnSO_4.7H_2O$
		350 g/l $NiSO_4.6H_2O$
		pH=3.5-4.0
(b)	Acid zinc-nickel (II)	288.0 g/l $ZnSO_4.7H_2O$
		184.0 g/l $NiSO_4.6H_2O$
		pH = 3.8
2)	Acid zinc-nickel (III) [59]	62.5 g/l $ZnCl_2$
		60.7 g/l $NiCl_2.6H_2O$
		200 g/l NH_4Cl
		pH = 3.5

6.4.2 Determination of cathode current efficiency

Determination of cathode current efficiency for zinc-nickel electrodeposition was basically the same as that of pure zinc. However, in the binary alloy system, influence of each of the individual metal ion present in the solution on the rate of deposition of the other was considered. The percentage compositions of individual metals in the deposit were obtained using a SEM fitted with an energy dispersive X-ray spectrometer (EDX). Pre-weighed samples were rinsed with deionised water after plating and dried in a hot stream of air. The dried samples were weighed again to obtain the weight gain. The cathode current efficiency was determined using the following expression:

$$CCE = \frac{\Delta W (wt\%_{Ni} / M_{Ni} + wt\%_{Zn} / M_{Zn}) \times 2F}{jAt} \times 100\% \quad \textbf{(eqn.6.3)}$$

Where:

CCE cathode current efficiency, (%)

ΔW change in weigth after plating, (g)

$wt\%_{Ni}$, $wt\%_{Zn}$ weight percentages of nickel and zinc in the deposit

$wt\%_{Ni} + wt\%_{Zn} = 100\ \%$

M_{Ni}, M_{Zn} atomic weight of nickel and zinc (g/mol)

F = Faraday constant (96500 C/mol)

j = applied current density (A/dm^2)

A = effective cathode surface area (dm^2)

t = plating duration (second)

6.5 Composite electrodeposition

6.5.1 Bath preparation

Electrolytes for the production of zinc-silica and zinc-nickel-silica electrodeposits were also prepared from similar acid sulphate baths as was the case of pure zinc and alloy zinc-nickel baths with the following standard laboratory reagents . Note that the type and concentration silica particles varied with individual baths and can be seen from the figures.

1) Zinc-silica

a) 250g/l $ZnSO_4.7H_2O$,
80g/l Na_2SO_4
pH = 2.0-2.5

b) 1.4 x 10^3 Mol/m^3 $ZnSO_4.7H_2O$
0.53 x 10^3 Mol/m^3 Na_2SO_4
2.81 x 10^3 Mol/m^3 $SnSO_4$
0.3 x 10^3 g/m^3 SiO_2 [147]

2) Zinc-nickel-silica

a) 57.5 g/l $ZnSO_4.7H_2O$,

131.4 g/l $NiSO_4.6H_2O$

71.02 g/l Na_2SO_4

pH = 2.0-2.5

b) 57.5 g/l $ZnSO_4.7H_2O$

131.4 g/l $NiSO_4.6H_2O$

161.9 g/l $Na_2SO_4.10H_2O$

pH = 2.0-2.5

With a magnetic stirrer, the electrolytes were vigorously stirred for a minimum of 30min. to enhance effective dissolution of the salts. Silica particles were then added into the electrolytes in the desired proportions. Two types of silica particles were utilised in this work. Silica particles with an average size of 20 nm in a 40% aqueous colloidal suspension with density of 1.3 g/cm^2 and 2 μm particles in the form a powder were utilised. The particles were utilised as received from Alfa Aesar with no further pre-treatment or surface modification. N,N-dimethyldodecylamine ($CH_3(CH_2)_{11}N(CH_3)_2$) – 97% (Aldrich) cationic surfactant with a molecular weight of 213.41 g hereafter abbreviated as NND was the major additive investigated in this work. Instead of coating particles with NND before adding to the electroplating bath, the NND was added directly into the individual baths since the particles were received in two different forms: colloidal (20 nm) and powder (2 μm). This anomaly could have made it difficult to modify their surfaces with NND in a consistent manner prior to electroplating bath make-up. In the case of zinc-silica electrodeposition with 2 μm silica particles, the optimum concentration of NND was established at 2.5 ml/l and was added into the individual baths as required.

6.5.2 Electrodeposition procedure

Experiments on the electrolytic codeposition of zinc-silica and zinc-nickel-silica were carried out using a simple electrolytic cell and associated control equipment, which was made up of a power supply unit, two electrode supports, mild steel cathode, and a zinc anode. The range of current densities and pH was 1 to 30 A/dm^2 and 2.0-2.6 respectively. Effect of current density

at both low and high current densities on the rate of particle incorporation was investigated. Agitation as a means of keeping particles in suspension and enhancement of deposition rates was also investigated. Bath temperature was kept constant at 50 °C in the case of zinc-silica and 60 °C in that of zinc-nickel/silica. All the electrodeposition experiments were carried out galvanostatically using DC currents both at high and low current densities. The anode material was 99% zinc foil.

6.5.3 Agitation techniques [82]

Agitation remains an important parameter in composite electrodeposition. It is one of the most widely investigated parameters in this type of electrodeposition. Two types of agitation were given particular attention in this work-mechanical stirring and vibratory agitation.

6.5.3.1 Mechanical stirring [82]

Bath agitation was effected using a polymer coated mechanical stirrer 'paddle', placed in the bottom of the electrolytic cell. This was driven by a standard laboratory bench-top stirring plate, having variable motor speed. Length of the stirrer was varied according to the volume of solution being agitated, with longer length 'paddles' being used for larger volumes of solution and vice-versa.

6.5.3.2 Vibratory agitation [82]

A Chemap A.G. laboratory vibromixer motor, model E-1, in conjuction with a 4.5cm perforated agitator-disc was used to effect the vibratory agitation in one litre of solution. The mixing process was largely due to the geometry of the mixing agitator disk, which consisted of several equally sized truncated cones. A schematic representation of the experimental apparatus is shown in Figure 6.1, whilst Figure 6.2 shows a photograph of the actual apparatus used with additional features such as the water bath housing the beaker containing the electrolyte to maintain constant temperature of the bath. Photograph of the agitator disc is shown in Figure 6.3. The reciprocatory motion of these truncated cones is capable of producing a jet at the narrow end in an incompressible fluid thereby causing a pumping effect

based on the venturi phenomenon. This 'jet-flow' pumping action is beneficial in suspending fine particles within a solution. Vibrational amplitude was controlled by means of a Zenith Variac. Calibration was based entirely upon previous works by KALANTARY [161].

6.5.4 Determination of deposit thickness

A weight gain method was used to determine deposit thickness by measuring the uncoated and coated masses of each sample. The difference between these and the theoretical deposit mass, which were calculated from Faraday's Law, were compared. A mean value of deposit thickness was deduced and percentage cathode current efficiency determined accordingly. All deposits were set approximately at 8 μm nominal thickness.

6.5.5 Morphology and composition analysis

Surface morphology studies were carried out using in some cases a Cambridge 360 scanning electron microscope and in others, a Leo model 1530 field emission gun scanning electron microscope (FEGSEM). The ability of these devices to display secondary and back-scattered images made it easier for the interpretation of surface features. These functions, combined with energy dispersive X-ray analysis techniques to satisfactorily characterise the coatings. Coating cross-sections were produced by edge mounting in a polyfast resin prior to metallographic polishing. Samples were then subjected to various stages of polishing with suspensions of 6 μm and finally 1 μm sized diamond particles.

Size distribution of the 20 nm and 2 μm particles was investigated using the Field emission gun scanning electron microscope (FEGSEM) after being sputter coated with gold to provide a thin conducting film over their surfaces. Apart from being used for morphological investigations, these equipment were used to analyse the deposit composition each being fitted with an X-ray energy dispersive analysis system (EDX) and the weight percentage of silicon obtained was converted to the weight percentage of silica.

6.5.6 Hull-cell studies

The Hull cell is an analytical electrochemical cell designed with trapezoidal geometry to incorporate a range of current densities [162]. It was designed to examine electroplating rather than mass production processes. In the present work, Hull cell tests were carried out for electrolytes detailed in sections 6.3.1, 6.4.1 and 6.5.1. The standard volume capacity of the Hull cell used was 267 ml with fixed dimensions. The dimensions of the single plate copper cathode were 10cm × 6cm. Ranges of currents between 1 - 5 A were applied at different durations to determine the range of current densities that produced visually acceptable coatings.

6.5.7 Corrosion/electrochemical tests

The practical approach adopted in this work to evaluate the integrity of the electrodeposits in terms of corrosion resistance consisted of the conventional neutral salt spray and linear polarisation resistance methods.

6.5.7.1 Neutral salt spray testing

Neutral salt-spray corrosion investigations were conducted according to ASTM B117. A.C.W. Equipment Ltd, salt-spray cabinet, model number SF 450-CASS under constant humidity conditions, at 35 °C and in a 5 % sodium chloride solution was utilised. All samples tested had nominally 8 μm thick coatings. The edges of each sample were securely masked with inert tape. In most of the samples, effective surface area exposed to the salt fog was approximately 52.5 cm^2. Time to 5% red rust was used to describe the level of corrosion resistance of each sample. However, it should be noted that this only indicates the time to first noticing red rust appearance close to or at the centre of approximately 52.5 cm^2 surface area of each sample investigated.

6.5.7.2 Linear polarisation resistance testing

A systematic investigation of linear polarisation resistance (LPR) studies were conducted for zinc and zinc-nickel alloys, both with and without silica particles. Polarisation was achieved

using an ACM Instruments computer controlled potentiostat, model Auto Tafel HP, linked to a personal computer. Each test was carried out on a panel blanked off with chemically inert tape to expose an area of 10 cm^2 (2.5 cm x 4 cm). These panels were then immersed in 350 ml of fresh 5 % NaCl solution and left for approximately 25 minutes to allow an equilibrium state to be obtained within the test cell, before polarisation. Each sample was polarised from -25 mV to +25 mV either side of its open circuit rest potential at a scan rate of 6 mV/min. The reference electrode was a Russell SRR5 saturated calomel supplied with a salt bridge. The salt bridge consisted of a length of rubber tube connected to a fritted glass end-piece, and was filled with saturated potassium chloride solution to provide a suitable conductive medium. Use of the salt bridge prevented possible poisoning of the electrode due to species formed in the test cell. A sheet of platinium foil 25 cm^2 (5cm x 5cm) was used as the counter electrode. No special pre-treatment of this was carried out, except for periodic cleaning with a scotch-brite pad. All experiments were conducted in a Faraday cage in order to prevent any atmospheric electromagnetic noise interfering with the results. Data obtained from the tests was then converted to a Microsoft Excel file, using the supplied ACM computer software. The converted files were then imported into the said spreadsheet software and analysed manually by finding the tangent of the plotted curve at zero overpotential.

6.5.7.3 Cathodic and anodic polarisation

Equipment used for the cathodic and anodic polarisation experiments were identical to that utilised for the linear polarisation resistance studies (section 6.9.2) with the exception of the counter electrode material being platinium in the case of anodic polarisation. In the cathodic process, counter electrode material used was 99% pure zinc foil. Pure zinc foil was utilised in order to maintain conditions very similar to those in the actual electrodeposition bath. Each of these different sets of polarisation studies was conducted in order to obtain mechanistic data for metal deposition and corrosion reactions. As was the case in linear polarisation resistance studies, the volume of electrolyte was 350 ml

Cathodic polarisation studies were carried out on mild steel panels to aid a mechanistic understanding of the separate influences of N,N-dimethyldodecylamine (NND) and silica on

zinc electrodeposition at a sweep rate of 30 mV/min. Both dilute and concentrated electrolytes were utilised for studying the effect of silica whilst only a dilute bath was utilised in the case of NND. Dilute baths were employed in order to achieve well-defined deposition behaviour in the polarisation curves as opposed to solutions with high zinc levels where metal reduction peaks are less clear. The various bath compositions are given below:

Solution 1- 10 g/l $ZnSO_4.7H_2O$

Solution 2- 10 g/l $ZnSO_4.7H_2O$ + 13 g/l SiO_2

Solution 3- 250 g/l $ZnSO_4.7H_2O$

Solution 4- 250 g/l $ZnSO_4.7H_2O$ + 13 g/l SiO_2

Solution 5- 10 g/l $ZnSO_4.7H_2O$ + 80 g/l Na_2SO_4 + 0.04 ml/l NND

Solution 6- 10 g/l $ZnSO_4.7H_2O$ + 80 g/l Na_2SO_4 + 0.2 ml/l NND

The same equipment as described in the case of linear polarisation resistance was also used in anodic polarisation studies. These investigations were conducted on zinc, zinc-nickel, zinc-silica and zinc-nickel-silica composite electrodeposits. The primary aim of which was to obtain a mechanistic data on the dissolution behaviour of these electrodeposits. The electrolyte was 5% NaCl solution. Samples were prepared as previously described in sections 6.2 and 6.5.2. However, the sample surface area in this case was 0.8 cm^2. Prior to polarisation, samples were allowed to equilibrate for approximately twenty-five minutes. On attaining equilibrium rest potential, samples were polarised from –50 mV cathodic to the rest potential to a potential of 1500 mV with a sweep rate of 120 mV/min. Anodic polarisation was conducted from –50 mV in the cathodic region for ease of identification of the start of anodic polarisation.

6.6 Wear studies

The test method utilised here to determine the wear behaviour of zinc, zinc-nickel, zinc-silica and zinc-nickel-silica composite electrodeposits was based on a linear reciprocating ball-on-flat plane geometry described in ASTM Standards, designation; G 133-95. The direction of the relative motion between the sliding surfaces reverses in a periodic fashion such that the sliding occurs back and forth and in a straight line.

6.6.1 Materials

The test materials as mentioned earlier were zinc, zinc-nickel, zinc-silica and zinc-nickel-silica composite electrodeposits produced from an acid sulphate bath. The counter material consisted a hardened stainless ball bearing with a diameter of approximately 12 mm.

6.6.2 Description of wear rig

The wear rig used in the investigations was custom made. The entire wear procedure involved the reciprocatory motion of a compartment with the test sample rigidly fitted to its base against a stationary steel ball bearing with a normal load applied to it. A schematic representation of the wear compartment is shown in Figure 6.4.

Figure 6.4 shows the schematic arrangement of the reciprocating ball-on-flat test used here on a custom made machine. The ball with a spherical tip was rigidly clamped to a ball holder to avoid slippage during the test. The ball holder was also rigidly fixed so that the periodic reversal in the sliding direction did not result in tilting or other misalignments of the contact. Use of a spherical tip alleviates the alignment problems associated with flat-ended balls sliding on flat surfaces. The diameter of the ball was 12 mm. The sample was held tightly onto the base of the lubricant bath (without any lubricants), which moved back and forth against the tip of the stationary ball bearing. A scotch yoke drive mechanism provided a smooth, sinusoidal velocity profile for the flat specimen relative to the ball without the need for the motor to stop and reverse direction periodically.

6.6.3 Wear testing procedure

As earlier mentioned, the wear tests were conducted on an oscillating slider wear rig (Figure 6.4) under dry (unlubricated) conditions at room temperature. Depending on the type of coating studied, the normal load was varied. Generally, the range of loads applied was between 0.8-25 N. The relative humidity was 40% and the lengths of stroke approximately 2.5 cm. Prior to wear testing, samples were washed, dried with hot air and ultrasonically cleaned

in acetone for 2 minutes and dried again in a hot stream of air. The flat samples were then rigidly screwed to the base of the lubricating bath. After being screwed in place, a final cleansing was done by wiping with acetone using cotton swabs. This was to ensure that no surface contaminants in form of minute particles capable of enhancing the wear process remained on the surface of the sample. The spherical steel ball bearing already clamped to its holder (see Figure 6.4) was then gently lowered onto the flat specimen ensuring that the reciprocating drive shaft motion was horizontal and parallel to the surface of the flat specimen. The desired load was then applied. The wear process was then started. The degree of wear resistance was based mainly on weight loss. Each friction pair (ball and flat specimen) was cleaned ultrasonically in acetone before and after each test to remove any possible surface contaminants and wear debris. The weight loss of the coatings was obtained by measuring the sample weight before and after each test, using an electrical balance with 0.01 mg accuracy. Three replicate wear tests were carried out for each specimen condition so as to minimise data scattering, and the average of the three replicate test results are reported in this work. The morphologies of the wear tracks were studied using a scanning electron microscope (SEM). The morphologies of the wear tracks were studied using a scanning electron microscope (SEM) with energy dispersive X-ray (EDX) analysis.

CHAPTER SEVEN

7 ZINC AND ZINC-NICKEL ELECTRODEPOSITION

In this section, the electrodeposition behaviour of zinc and zinc-nickel alloys when subjected to various electrodeposition parameters such as current density, temperature, pH, bath agitation and type of bath is presented. Morphological characteristics of these deposits, as a function of the aforementioned parameters, are also presented.

7.1 Zinc

7.1.1 Investigation of electrolyte properties

The suitability of an electrolyte for the production of an electrodeposit intended for a specific purpose is often measured by various parameters such as throwing power and current efficiency. Amongst others, acid and alkaline non-cyanide baths are the most widely utilised in recent years for the electrodeposition of zinc. Preliminary investigations were therefore carried out mainly on these two types of baths. This was to determine the suitability of each of these electrolytes for the purpose of electrodeposition of zinc, zinc-based alloys, and subsequently zinc alloy composites. The main parameters that were considered, as mentioned earlier, included the current efficiency of the bath, current density, agitation, temperature and pH. It is noteworthy also, that cathode current efficiency on its own is largely dependent on the other parameters. Results of the preliminary investigations on the properties of an alkaline and an acid bath are shown in tables 7.1 and 7.2 respectively. Current efficiency of the acid bath with relatively higher metal ion content was found to be significantly higher than that of the alkaline bath. This is probably due to the limiting current density of the alkaline bath as compared to the acid bath. The acid bath tends to show excellent cathode current efficiency at all the current densities investigated. Electrodeposits from the acid bath were also found to be

coherent and visually acceptable. In contrast, electrodeposits produced from the alkaline bath were porous, incoherent and visually unacceptable. Since cathode current efficiency of each bath was deduced by method of weight gain, it is highly probable that the weight gain of the electrodeposits from the alkaline baths could be inconsistent due to the poor integrity of these coatings. Therefore, the results presented here may not be completely reliable. However, with bath agitation, improvement in cathode current efficiencies in the range of 48 to 92% was obtained with the alkaline bath. These results seem to agree, in part, with earlier reports [163] that the cathode current efficiency for zinc deposition from alkaline zinc electrolytes varies in the range of 60-90%, depending on the electrolyte composition and plating conditions. The obviously low cathode current efficiency of the alkaline bath was probably due to hydrogen overpotential and consequent inhibition of zinc deposition reaction at the surface of the cathode. As mentioned earlier, another possible reason for the lower cathode current efficiency of this bath could be as a result of its low limiting current density due to the low concentration of metal ions. The limiting current density of zinc deposition is largely a function of its metal ion concentration amongst others. Since the main reactions at the cathode during electrodeposition is a competition between zinc reduction and hydrogen evolution, as the limiting current density is approached during zinc deposition, the zinc ion concentration near the cathode is quickly depleted and the cathode reaction shifts from zinc deposition to hydrogen evolution [164]. This could result in the deposition of a mixture of zinc and zinc hydroxide or zinc oxides [31] due to pH increase in the vicinity of the cathode. The Pourbaix diagram in Figure 2.1 gives a better insight to possible states of zinc and the products of its corrosion in an aqueous medium as a function solution pH. At pH< 7 zinc appears to exist in the ionised form Zn^{2+} . As the pH becomes greater than 7 the oxide ZnO is stable (although not shown in the Pourbaix diagram). Further increase results in the formation of $Zn(OH)_2$. At higher pH values $Zn(OH)_2$ ionises to form ZnO_2^{2-} . See the various reactions leading to the formation of these products in [5]. The acid bath was consequently chosen for further investigations on the effect of agitation, current density, pH, and temperature due to its excellent cathode current efficiency and ability to produce acceptable coatings.

Table 7.1 Current efficiency of zinc electrodeposition from an alkaline bath containing 10g/l ZnO, 105 g/l NaOH, pH 13.

S/N	Current density (A/dm^2)	Current efficiency (%)	
		Magnetic stirring (rpm)	Without Agitation
1	2.1	48	36
2	2.2	67	29
3	2.3	70	32
4	2.5	74	16
5	5.0	92	12

Table 7.2 Current efficiency of zinc electrodeposition from an acid bath containing 250 g/l $ZnSO_4.7H_2O$, 80 g/l Na_2SO_4, pH 2.8 with agitation using magnetic stirrer.

Sample	Current Density (A/dm^2)	Current efficiency (%)
Z1	2.1	94.3
Z2	2.2	97.4
Z3	2.3	92
Z4	2.5	96
Z5	3.5	97
Z6	4.5	96.4
Z7	5.0	95.2
Z8	5.5	87.6
Z9	6.0	98

7.1.2 Effect of agitation on zinc electrodeposition

The use of bath agitation is often intended to improve the mass transport in the electrolyte and therefore enhance the rate of deposition. All investigations were carried out with the aim of producing a nominal thickness of 8 μm.

Table 7.3 Results of the effect of agitation on the deposit thickness of zinc electrodeposited from a bath containing 250 g/l $ZnSO_4.7H_2O$, 80 g/l Na_2SO_4 and pH 2.6.

Sample	Agitation (rpm)	Current density (A/dm^2)	Deposit Thickness (μm)
23	800	3	8.7
24	700	3	8.5
25	600	3	8.9
25.1	600	3	8.5
26	800	3	7.5
26.1	800	3	7.6
26.2	800	3	8
26.3	800	3	8

It is obvious from table 7.3 that bath agitation had barely any effect on the deposit thickness of electrodeposits produced from the acid bath. Electrodepositon with or without agitation gave similar deposit thicknesses at constant duration and current density as can be seen from table 7.4. However, in terms of cathode current efficiency, bath agitation was found to reduce the current efficiency slightly with increase in agitation. Figure 7.1 shows that current efficiency of the bath in question was better without or at lower rates of solution agitation at a constant current density of 5 A/dm^2. Practically, such insignificant variations in current efficiency may be ignored, as the difference in current efficiency observed within the range of agitation investigated was quite small and may have occurred possibly due to experimental errors in

course of weighing the samples. It is also noteworthy that agitation could depolarise the hydrogen evolution reaction. However, it is perceived that agitation is likely to have reduced the nucleation rate of zinc on the surface of the cathode. The applied current was shared between two processes: zinc deposition and hydrogen evolution [165,166]. Since the hydrogen overpotential and hence evolution in this bath was quite high as was observed during the electrodeposition process, the main cathode reaction would have been zinc deposition.

With the alkaline bath, agitation obviously had a positive effect on cathode current efficiency (see table 7.1). Current efficiency of the bath without agitation was obviously very low as huge concentration of hydrogen bubbles were observed in the region of the cathode during deposition. However, with agitation, the current efficiency was significantly improved. Similar observations have previously been reported [167]. They stated that in the current density range of 0.5-4 A/dm^2 zinc deposition in the electrolyte without additives is mass transport limited, and therefore increasing agitation rate could increase the current efficiency. Furthermore, as shown in Figure 7.2, increase in current density was met with a corresponding increase in the cell voltage. This could lead to increase in energy consumption. In essence, at higher current densities, a larger driving force was required to effect zinc deposition due to possible rise in both anode and cathode potentials with increase in current density [168]. A possible explanation to the improvement in current efficiency of the alkaline bath with agitation is that, agitation is thought to prevent the adsorption of evolved hydrogen, which usually sits on the surface of the cathode thereby preventing zinc reduction. It has been reported [165] that the formation of hydrogen bubbles destroyed periodically by stirring the diffuse layer makes it possible for zinc replenishment; as a consequence, zinc deposition potential was reached again. As the hydrogen bubbles are swept away, a larger surface area on the cathode becomes available periodically for the deposition of zinc. Consequently, zinc deposition potential is increased with a corresponding increase in current efficiency. Another reason for the improvement in current efficiency could be due to impoved mass transport.

7.1.3 Effect of current density and time on zinc electrodeposition

In an attempt to optimise conditions for the production of 8 μm thick zinc electrodeposits, a range of current densities were investigated. In each case, maintaining a constant quantity of electricity supplied was crucial to obtain uniform deposit thickness in all the samples. Visually acceptable coatings were obtained within the current density range of 2.0-5.0 A/dm^2.

Table 7.4 Results of the effect of current density and agitation on the deposit thickness and current efficiency of zinc electrodeposited from bath containing 250 g/l $ZnSO_4.7H_2O$, 80 g/l Na_2SO_4 and pH 2.6.

Sample	Agitation (rpm)	Current density (A/dm^2)	Deposit Thickness (μm)	CCE (%)	Time (min.)
27	800	2	7.8	97.5	14
27.1	None	2	7.8	97.5	14
28	800	2.5	7.6	97	11
28.1	None	2.5	8.0	102	11
29	800	3.5	8.0	99.6	8
29.1	None	3.5	8.0	99	8
30	800	4	8.0	101	7
30.1	None	4	8.0	99	7

The experimental results in table 7.4 show that current density is inversely proportional to time to obtain the same deposit thickness. Increase in current density is accompanied by a decrease in deposition time to obtain 8 μm and vice versa. This is consistent with expectations since at higher current densities, the rate of deposition and deposit build-up is faster. On the contrary, low deposition current densities are associated with small nucleation rates so the layer thickness has to be large enough in order to cover the whole surface of the substrate [14]. This invariably means that lower current densities require longer duration to obtain a particular deposit thickness whilst higher current densities are required to produce the same deposit thickness at shorter durations. Therefore, for each current density there is a corresponding time duration for the production of 8 μm thick electrodeposits. The only exceptions would be when either the bath chemistry or other electrodeposition parameters are

modified to either enhance or reduce the nucleation and hence deposition rate or reduce/remove reactions in the vicinity of the cathode that are detrimental to metal deposition to obtain either thicker or thinner deposits. As obvious from table 7.5 it was established that the time duration required for the production of 8 μm thick zinc electrodeposits at a current density of 3 A/dm^2 was 9.5 minutes even at different values of bath pH. The effect of current density on cathode current efficiency with the acid bath is presented in Figures 7.3 and 7.4 respectively. The current efficiency of the bath appears to be independent of current density with or without agitation. This is an indication that there was negligible mass transfer resistance or concentration overpotential for the range of current densities investigated. Although not really in our range, similar observations were reported by SCOTT et al [168] over a current density range of 100-650 A/m^2.

7.1.4 Effect of temperature and pH

Change in solution pH did not have any significant effect on the deposit thickness. This is shown in table 7.5. For all the pH values investigated ranging from 3.2-5.0, the deposit thickness remained the same at 8 μm. Figure 7.5 shows that for the range of pH between 2.5-5.0, the cathode current efficiency increased with increase in pH. Similar observations have been reported by other investigators [13,17]. It was confirmed [13] that a decrease of the pH leads to a decrease of the efficiency at constant current. Also in agreement with [13], it can be seen from figures 7.1, 7.3, 7.4 and 7.5 that majority of current efficiency results produced at pH< 4 shows current efficiencies of less than 100%. However, in Figure 7.5, at pH> 4 almost all current efficiencies were greater than 100%. The reason for such behaviour is not very clear. However, it appears, at higher pH values, the formation and consequent codeposition of ZnO and $Zn(OH)_2$ probably occurred due to hydrogen evolution with a resultant increase in pH within the vicinity of the cathode.

Influence of temperature on CCE shows an increasing linear relationship. This is obvious from Figure 7.6 as increase in bath temperature from 30 to 40 °C was accompanied by a corresponding increase in the CCE from 96.0% to 97.4%. Similarly, SCOTT et al reported [168] that current efficiency increased with increase in temperature from 94.0% at 25 °C to

97.7% at 50 °C with a resultant decrease in energy consumption. They attributed this decrease in energy consumption to the increase in current efficiency and the decrease in cell voltage as the temperature rises. At higher temperatures the rate constants of both cathodic reactions increase hence a lower driving force is required [168]. It has also been reported [24] that the conductivity of an electrolyte increases with increase in temperature and noted that the effect of temperature is more pronounced at the higher acid concentrations.

Table 7.5 Results of the effect of pH on zinc electrodeposition from a bath containing 250 g/l $ZnSO_4.7H_2O$, 80 g/l Na_2SO_4.

Sample	Agitation (rpm)	Current density (A/dm^2)	Thickness (μm)	Deposition time (min.)	pH
34	800	3	8	9.5	5.0
34.1	800	3	8	9.5	5.0
35	800	3	8	9.5	4
35.1	800	3	8	9.5	4
36	800	3	8	9.5	3.2

7.1.5 Morphological characteristics of zinc electrodeposits

A number of surface morphologies of zinc electrodeposits are presented in Figures 7.7-7.9 produced from an acid sulphate bath containing 250 g/l $ZnSO_4.7H_2O$ and 80 g/l Na_2SO_4. Since zinc occurs in only one (hexagonal) crystalline form, the morphological features usually observed (moss, sponge, platelets, boulders) must originate from different arrangements of hexagonal units [169]. The predominant crystallographic orientations reported on zinc electrodeposits produced from acid sulphate baths without additives are usually the randomly preferred crystallographic orientations. Deposit properties of zinc amongst other factors are largely dependent on the texture and surface morphology of the electrodeposits and therefore widely investigated. A typical surface morphology of zinc produced from an acid sulphate bath is shown in Figure 7.7. These morphologies can be tailored with changes in

electrodeposition parameters such as current density, temperature, pH, hydrodynamics of catholyte flow [36], impurities and the presence of certain additives. Effects of some of these parameters on zinc electrodeposition are presented in the following sections.

7.1.5.1 Morphological changes with pH

Effect of pH changes on the cathode current efficiency of the bath containing 250 g/l $ZnSO_4.7H_2O$ and 80 g/l Na_2SO_4 has earlier been discussed in section 7.1.5. Electrodeposits were produced with pH variation in the range of 2.6-5.0 at a current density of 3 A/dm^2. Such variations obviously had no significant effect on the thickness of the electrodeposits. However, pH changes seem to have some effect on the morphology and preferred orientation of the electrodeposits. As can be seen from Figure 7.7 deposits obtained from a solution of pH 2.6 generally consisted of zinc platelets with the traditional random orientations associated with zinc electrodeposits from acid sulphate baths. However, at a pH value of about 5, the morphological features changed slightly from those at lower pH values. The random orientation observed in Figure 7.7 seems to have transformed to more of a combination of lateral stacking sequence of zinc crystals and zinc platelets aligned almost perpendicular to the cathode in Figure 7.8.

7.1.5.2 Morphological changes with temperature

Increase in temperature was observed to have some effect on the crystal orientation of the deposit. With increasing temperature, the lateral stacking sequence of crystal orientation appears to have transformed from the usually random orientations (see Figure 7.7) to that with the edges of the crystals perpendicular to the surface of the substrate (see Figures 7.9 and 7.10). At about 35 °C, onset of white patches was noticed as dots on the edges of zinc crystal (see Figure 7.9). As the temperature increased to 40 °C, the white patches became conspicuous on the surface of the deposit. The observed improvement in cathode current efficiency with increase in temperature as earlier discussed in section 7.1.4 and shown in Figure 7.6 is probably as a result of such growths and consequent incorporation in the electrodeposits thereby increasing the weight gain and hence cathode current efficiency. The crystals also

seem to have transformed from the usual hexagonal randomly preferred orientation to that with their edges perpendicularly oriented to the surface of the substrate (see Figure 7.10).

7.2 Zinc-nickel electrodeposition

Three types of baths were selected for the investigations of zinc-nickel electrodeposition, two sulphate-based acid baths with different constituent concentrations and a chloride-based bath. All baths were used extensively to investigate the effects of current density, temperature, agitation, pH and metal ion concentration on the characteristics of electrodeposits obtained. As with the case of zinc electrodeposition, influence of electrodeposition parameters such as current density, pH, temperature, bath composition and deposition time are presented and discussed in this section.

7.2.1 Effect of current density on zinc-nickel electrodeposition

Initial investigations carried out with a Hull cell suggested an acceptable current density range of 3 to 6 A/dm^2 for bath 1(a) in section 6.4.1. Visually acceptable coatings were obtained within this range of current densities. However, further investigations were carried out in a slightly wider range between 1 to 5 A/dm^2 for bath 1 (a) to have a broader knowledge of the appearance of these deposits at both high and relatively lower current densities. Also investigated was the current density range of 0.3 to 0.6 A/dm^2 for a bath with almost twice the nickel sulphate concentration that was present in bath 1(a). Figures 7.11 and 7.12 also show the relationship between current density, and percentage of nickel in the deposit. In practically all cases, it was evident that the nickel content of the deposit decreases with increasing current density as higher percentages of nickel were observed at lower current densities, even though both sets of data were produced at different metal ion concentrations and current densities. The observation that nickel content decreases with increase in current density is in close agreement with the works of other investigators [59,82,170-171]. A reduction in nickel content with increasing current density reflects the faster kinetics of zinc deposition at greater electrode polarizations. This is an indication that at lower values of current density there is transition from anomalous to normal codeposition. For the sulphate-based baths, the widely reported range of 10-15 wt% nickel in the deposit for optimum corrosion resistance suggested

by previous authors [69,59] was obtained in the current density ranges of 2-4 A/dm^2 and 0.3-0.4 A/dm^2 respectively for the 1(a) and (b) baths utilised. The anomalous nature of codeposition has been widely described using the hydroxide suppression model of three regions of codeposition developed by Dahms and Croll [70]. Although not all investigators agree with this model, it is thought in this model that at lower current densities, normal deposition usually occurs, where the more noble metal deposits preferentially. When the current density is increased, the transition from normal to anomalous deposition occurs with the amount of the noble metal in the deposit falling below the concentration of the metal in the bath. This transition is said to result from the formation of a critical concentration of zinc hydroxide at the cathode surface [82]. At higher current densities, there is yet another transition, where the normal takes over from the anomalous type.

7.2.2 Effect of temperature

Fig.7.13 shows the influence of temperature on the weight percentage of nickel in the electrodeposit. These investigations were carried out using a chloride-based acid solution containing 62.5 g/l $ZnCl_2$, 60.7 g/l $NiCl_2.6H_2O$, 200 g/l and pH 3.5. For the given deposition conditions, it can be seen that as the temperature increased from 25 to 40 °C, the nickel content of the deposit increased from 8.4 to 13.4 wt%. This indicates that temperature increase favours nickel deposition. Such behaviour was attributed to the decrease in cathode polarisation and enhanced temperature-dependent kinetics parameters and specifically related to nickel deposition, such behaviour is primarily the result of the intrinsically slow nickel kinetics [170]. An acceptable nickel content for corrosion resistance (10-15 wt%) as reported by [75] was obtained in a temperature range of 25 to 40 °C. The results presented here are in close agreement with earlier investigations [59,65] on a chloride bath. It has been reported [59] that with an increase in temperature from 25 to 40 °C, the nickel content in the deposit increased from 12.5 to 28.8%. The difference in the range of nickel percentage increase in their report with that presented here (8.4-13.4 wt%) for a similar temperature range is probably due to slight differences in the bath concentrations of the individual investigations. All the data presented in Figure 7.13 were produced at a current density of 3 A/dm^2, which falls within the optimum range of current densities of 2 to 4 A/dm^2 to produce deposits containing

12 to 13 wt% nickel for a nickel bath composition with 5 to 10 g/l nickel [59]. For the sulphate bath as can be seen from Figure 7.14, the current efficiency was found to be generally stable at about 70% over a wide range of deposition time. This is an indication that deposition time does not have significant influence on the deposition behaviour of zinc-nickel for the conditions of deposition investigated here and therefore not an appropriate parameter to be considered while studying the properties of a zinc-nickel electrolytic bath.

7.2.3 Effect of bath concentration

The ultimate aim of studying the electrodeposition behaviour of the zinc-nickel system was to produce coatings with the desired concentration of nickel being 10 to 15 wt% for optimum corrosion resistance, morphology, microstructure and hence phase distribution of the electrodeposit. The need therefore, to optimise the concentrations of the different metal ions in the plating solution to obtain the said range and other characteristics as mentioned above was crucial. However, in this work, only the effect of $NiCl_2.6H_2O$ in 5 g/l increments was considered. An acid chloride bath was used to investigate the effect of nickel ion concentration in the bath and its concentration in the electrodeposit.

$NiCl_2.6H_2O$ concentration in the range of 65.7 to 80.7 g/l was considered to study the effect of nickel ion concentration in the bath on nickel content in the deposit as shown in Fig. 7.15. It is obvious from Figure 7.15 that changes in the nickel content of the deposit took a minimal increasing trend from about 10.4 wt% to about 13.3 wt% as the bath concentration of $NiCl_2.6H_2O$ was increased from 60.7g/l to 75.7g/l consequently maintaining an acceptable range of 10.4 to13.3 wt% nickel in the deposit for optimum corrosion resistance. However, beyond 75.7g/l increase in the nickel content of the deposit shows a sharp gradient. This is an indication that for the bath in question, up to a bath concentration of 75.7g/l $NiCl_2.6H_2O$, the deposition showed an anomalous behaviour. Beyond this concentration, normal deposition begins to take place where the more noble nickel is deposited in preference to the less noble zinc. The overall trend is consistent with previous works [58,65] in that increasing the Ni^{2+} ion in the bath results in an increase in the nickel content of the deposit and supports the theory that the reduction of nickel ions is controlled by diffusion [65].

7.2.4 Morphology of Zinc-Nickel elctrodeposits

The morphology of zinc–nickel electrodeposits was obviously affected by variables such as current density, temperature and metal ion concentration of the bath. Each of these parameters as earlier mentioned affects the alloy composition. Changes in morphology of zinc-nickel electrodeposits with nickel content in the deposit have been reported [56]. Since each of these parameters either increases or decreases the nickel content of the electrodeposit, morphological changes, which are largely a function of the elemental composition of the electrodeposits, are inevitable.

7.2.4.1 Influence of uneven current distribution

It is perceived that uneven current distribution at the cathode produces dissimilar surface morphologies. In an attempt to verify this, investigation on the percentage of nickel on both the edges and centres of a number of samples were carried out and the results are presented in table 7.9. It is obvious that in almost all the investigations, the percentage of nickel at the centres was higher than at the edges where the current is thought to be higher. These observations seem to compliment previous observations in section 7.1.2 that the percentage of nickel in the deposit increases with higher current densities. The influence of this uneven current distribution and hence the percentage of the codepositing elements on the surface of the cathode with more nickel at the centre than at the edges of the cathode is further illustrated in Figures 7.16a & b. As can be seen in Figure 7.16a, the morphology has hexagonal-based pyramidal crystals with each hexagonal crystal separated from it adjacent neighbour by intergrannular cracks. Such distinct pyramidal crystals are not prominent at the centre of the deposit (see Figure 7.16b), as they tend to form clusters of irregularly shaped crystals with obvious intergrannular cracked boundaries possibly due to stress in the process of nucleation and crystal growth typical of zinc-nickel electrodeposits.

Table 7.9 Results on the effect of uneven distribution of current on the surface composition of the cathode produced from a bath containing 62.5 g/l $ZnCl_2$, 60.7 g/l $NiCl_2.6H_2O$, 200 g/l NH_4Cl, pH 3.5 and T= 30 °C.

Sample Zn-Ni	Ni wt% (Edge of deposit)	Ni wt% (Centre of deposit)	Ni wt% (Edge + Centre)/2
19.1	9.6	10.8	10.2
20.1	10.1	10.8	10.4
21	10.6	10.6	10.6
22.1	11.7	12.3	12.0
22.2	12.2	13.0	12.6
23.1	12.6	13.8	13.2
24.1	12.4	14.1	13.2

7.2.4.2 Influence of temperature and nickel content on zinc-nickel morphology

As earlier mentioned, the morphological changes observed in zinc-nickel electrodeposits are largely a function of changes in the nickel content of the deposit associated with changes in the individual parameters. In section 7.2.2, it was found that increase in temperature was met with a corresponding increase in the nickel content of the deposit. These results are further complimented in Figure 7.17, which shows SEM micrographs of zinc-nickel electrodeposits produced from an acid chloride bath at different temperatures with different contents of nickel in the deposit. At 25 °C as can be seen in Figure 7.17(a) the alloy exhibits regularly shaped nodular grains with gaps between individual grains. This is an indication that such deposits could be porous and hence poorly corrosion resistant. Interestingly, the percentage of nickel in this deposit is 7.5 wt%, which is less than the widely reported range of 10 to 15 wt% nickel for optimum corrosion resistance. Apart from being porous and inhomogeneous, zinc-nickel electrodeposits with lower percentages of nickel than the optimum range of 10 to 15 wt% nickel, are capable of developing dendritic growths as can be seen in Figure 7.18. Similar morphologies have previously been reported [56,65]. As the temperature was increased from 25 to 30 °C, the nickel content of the deposit simultaneously increased to 11.7 wt% with

obvious morphological transformations from the predominantly regular grain shaped morphology observed in Figure 7.17(a) to a homogeneously compact morphology as can be seen Figure 7.17(b). Such homogeneously compact and crack-free morphologies probably account for the excellent corrosion resistance of zinc-nickel electrodeposits as it is less likely for corrosive species to migrate and penetrate these electrodeposits easily than those with some form of porosity. It has been suggested that the lower Zn-Ni alloy corrosion rates, when compared to Zn-Co and Zn-Fe, are due to the predominant presence in this layer of crystallographic planes with a higher packing density [172]. Further increase in temperature up to 40 ^{o}C was accompanied with a corresponding increase in the percentage of nickel in the deposit up to 13.4 wt%. However, as can be seen in Figure 7.17(c), initiation of microcracks or fissures in the coatings accompany the morphological changes probably as a result of increase in nickel content of the coatings at higher temperatures. This is an indication that at higher contents of nickel in the deposit, the deposits could become stressed and brittle. Other investigators [65,173] have made similar observations on changes in nickel content of the deposit with changes in temperature. According to ALFANTAZI et al [65] for deposits produced at 25 ^{o}C, a rough surface morphology was obtained and the structure contained a fine-grain matrix of γ-phase and coarse η-phase crystals. However, they noted that deposits produced at 40 ^{o}C were much smoother and the deposit consisted entirely of γ-phase with nodular fine-grain structure morphology with grain size in the range of 0.5-2 μm. The slight difference in morphological changes observed in this work and that of [65] at 40 ^{o}C is probably due to difference in individual bath formulations. Studying the effect of substrate type on Zn-Ni electrodeposition, ALFANTAZI et al [173] noted that the effect of copper and mild steel substrates are the same in that the Ni content increases as bath temperature was increased. It has also been shown previously that nickel content in the deposit is the major parameter controlling the morphology in pulse-plated Zn-Ni alloys [174].

CHAPTER EIGHT

8 ELECTRODEPOSITION OF ZINC/SILICA COMPOSITE COATINGS

The following sections, contain findings on an extensive study of the electrolytic codeposition characteristics of zinc/silica composite coatings.

8.1 Preliminary investigation on Zn/SiO_2 codeposition from an acid electrolyte

Prior to carrying out the production of zinc-silica composite electrodeposits, 20 nm and 2 μm size particles, were chosen and characterised to determine the average particle sizes. The 20 nm particles were received in the form of a colloidal suspension and the 2 μm particles in a dry powder form. The wide difference in particle size was chosen in order to investigate the effect of this parameter on the codeposition behaviour of particles, which will be discussed in section 8.2.5. SEM micrographs of the characterised particles are shown in Figure 8.1. It is obvious from these micrographs that the morphology and size distribution of 20 nm particles was relatively uniform and even whilst the larger 2 μm particles exhibited a high level of no-uniformity in size with irregular surface morphologies. However, the use of TEM may have better characterized these particles.

Preliminary investigations on Zn/SiO_2 electrodeposition were carried out to study the mechanism of codeposition and subsequent incorporation of the silica particles in the growing zinc metal matrix. To achieve this, an acid sulphate zinc bath with 13 g/l concentration of 20 nm silica particles from a 40% colloidal suspension of silica was prepared and left to agitate for 24 hrs with a mechanical stirrer. Such a low concentration of silica was used initially to ensure maximum suspension of the particles in the bath and avoid SiO_2 falling out of suspension. The resultant suspension was highly stable even without agitation. For purposes of comparison, two different bath formulations as can be found in subsections 1a & 1b of section 6.5.1, were prepared and utilised to produce the SEM micrographs in Figures 8.2 and 8.3

respectively. These micrographs give an indication of the possible mechanism of incorporation of the codepositing silica particles. In both cases, it is obvious that the particles tend to randomly incorporate onto the sidewalls of the hexagonal crystals. It has been reported [147] that zinc electrodeposits incorporate SiO_2 in two ways. The particles line up along the macrosteps grow laterally and sweep up the particles to the edges of the hexagonal crystals and eventually become incorporated into the macrostep sidewalls of the edges of these hexagonal crystals whilst the other SiO_2 particles are randomly dispersed on the surfaces of the hexagonal plane, remains adsorbed at these sites with their lower portions incorporated onto these planes [147]. There appears to be some similarities with the described mechanism in Figures 8.2 and 8.3 especially at the edges and macrosteps between neighbouring crystals. In Figure 8.2, it appears the randomly dispersed particles seem to have initially deposited on the edges of the crystals and then subsequently swept either onto or beneath the surfaces of the laterally stacking layers of hexagonal crystals probably due to the prevalent forces (hydrodynamic, electrophoretic, adsorption and electrostatic), which may be acting on the particles. As the particles remain adsorbed onto either the surfaces or edges of the hexagonal crystals, they become subsequently entrapped into the growing metal matrix.

8.1.1 Current efficiency of the Zn/SiO_2 bath

Cathode current efficiency continues to dominate as one of the most widely investigated parameters in assessing the properties of an electrolytic bath. The efficiency of a plating bath alleviates the problem of excessive energy consumption on side reactions and hence improves the effectiveness of the plating system. As earlier discussed in section 7.1.1, the bath without particles exhibited high current efficiency values. However, this does not appear to be the case when particles were added into the zinc bath. As was with the case of pure zinc and zinc-nickel baths, the influence of a number of parameters on the cathode current efficiency of the zinc-silica bath was investigated. Some of the findings are presented in the following sections 8.1.1.1-8.1.1.2.

8.1.1.1 Influence of current density

Influence of current density on cathode current efficiency was investigated using a bath with a relatively high concentration of 20 nm silica particles when compared to that utilised in the study of the codeposition mechanism discussed earlier in section 8.1. As can be seen from Figure 8.4, the cathode current efficiency of the bath investigated appears to decrease with increase in current density. Similarly, the effect of two current densities on the cathode current efficiency of a relatively lower bath concentration of 20 nm particles was investigated with increasing deposition time as shown in table 8.1

Table 8.1 Relationship between current density, time and current efficiency. SiO_2 (20 nm) concentration in bath 26 g/l.

Deposition time, Seconds	Current efficiency, %	
	30 A/dm^2	40 A/dm^2
60	70	69.7
75	84	82
90	76.4	60

Although not a huge difference, it is obvious from table 8.1 that the majority of the current efficiency values at 30 A/dm^2 were higher than the corresponding values at 40 A/dm^2. Thus complimenting the results in Figure 8.4. The general trend indicates that current efficiencies are higher at lower current densities for the experimental conditions utilised here. Such behaviour of an electrolytic bath could probably be attributed to polarisation at the surface of the cathode [131]. Similarly, GHORBANI et al [131] while studying a graphite-brass composite coating system reported that cathode current efficiency of the system declined with the increase of current density. Furthermore, Figure 8.4 shows that there was no significant change in the cathode current efficiency of the bath within a wide range of current density. This behaviour is probably due to the high bath concentration of particles. The starting and lowest current density of 10 A/dm^2 gave significantly high current efficiency of about 80 %. However, within the current density range of 15 A/dm^2 and 30 A/dm^2, the change in cathode

current efficiency was negligible. Apart from polarisation effects, as earlier mentioned, the sudden reduction in current efficiency from a current density of about 15 A/dm^2, is an indication that agglomeration of silica particles probably occurred. This was practically evident, as the viscosity of the solution was observed to increase. Agglomerated particles have a tendency to adsorb onto surfaces and therefore may have adsorbed onto the surface of the cathode thereby blocking off the surface of the cathode from reducible species and consequently causing the decrease in cathode current efficiency.

8.1.1.2 Influence of particle concentration in bath

The relationship between particle loading, weight percentage of particles in deposit and cathode current efficiency is shown in Figure 8.5. It is clear from the figure that cathode current efficiency decreases as the particle concentration increases. The trend appears to take a linear fashion for all bath concentrations investigated. This decrease in cathode current efficiency is probably due to an increase in solution resistance. Since silica particles in question are a non-conducting species in the composite electrolytic bath, it is not surprising that increasing their concentration in the bath could be met with a corresponding decrease in solution conductivity and hence cathode current efficiency. On the contrary, rate of particle incorporation appears to increase with increase in particle loading up to a maximum. Beyond the maximum point a decreasing trend is observed. This is an indication that up to the bath concentration of maximum particle incorporation, cathode current efficiency and particle loading were inversely proportional. However, beyond this bath concentration of particles, both particle incorporation and cathode current efficiency begin to decrease. The observed decrease in both phenomena may not only be attributed to poor solution conductivity but also to possible agglomeration as previously mentioned in the section 8.1.1.1. Similar observations have previously been reported on zinc-silica composite electro-galvanising [150]. According to them, solution resistance in an electro-galvanising bath could become unnecessarily high, resulting in a poorer current efficiency and increased consumption of electric power for electrogalvanising.

8.1.1.3 Relationship between current efficiency and deposit morphology

Cathode current efficiency appears to have an effect on the morphology of Zn/SiO_2 electrodeposits. This is shown in Figure 8.6. The cathode current efficiency of each of these deposits were calculated and found to be different from each other with an increasing order from Figures 8.6(a) to 8.6(b). On analysis with the SEM, it was found that the bright portions were zinc and the darker regions gave mainly silicon peaks. Critical observation of these deposits reveals that the regions showing zinc patches on the surfaces of these morphologies increased with increasing current efficiency. This is an indication that current efficiency has a dynamic relationship with the morphologies of zinc-silica electrodeposit. This appears to be an issue of available sites for the nucleation and hence reduction of zinc ions. The current efficiency was highest for the morphology (8.6b) with more 'islands' of zinc as white patches unevenly distributed in the dense mass of codeposited silica as the dark portions. Such islands of electrodeposited zinc on the surface of the morphology may have provided more active sites for the reduction of incoming zinc ions. On the other hand, it was obvious that the morphology (8.6a) with fewer of these white zinc patches exhibited the lowest cathode current efficiency. Also, because the dense mass of deposited silica is largely inert, rather than providing sites for the deposition of zinc, it covered up large areas for possible metal ion reduction, which may have contributed to the observed decrease in cathode current efficiency. Similar observations on the 'blocking' effect of particles thereby reducing the electrode surface area have been reported [133]. According to them, SiC particles that are being embedded in the growing metal layer cause an apparent decrease in the electrode surface area, probably due to the blocking effect on the surface by partly engulfed particles. They further noted that the presence of particles being embedded in the surface does not only increase the surface inhomogeneity but also makes the microscopic current distribution over the surface more uneven. Also, ASLANDIS et al [122] emphasised the importance to note that electrode blocking by titania modified particles could also result in an additional pH increase in the vicinity of the cathode which promotes hydroxide formation, the zinc adsorption onto the silica, and as a consequence the electrolytic codeposition.

8.2 Parameters affecting the rate of particle incorporation

As earlier mentioned, the rate of particle incorporation depends on a number of fundamental electrodeposition parameters. Findings on the influence of each of these parameters are therefore presented in the following sections.

8.2.1 Effect of current density

Current density is one of the most widely investigated parameters in composite electrodeposition. The influence of current density on the rate of particle incorporation appears to be associated with overpotentials. Overpotentials of metal deposition are higher with higher current densities. Therefore higher rates of metal deposition are expected at higher overpotentials.

The relationship between current density and rate of particle incorporation with different particles sizes is presented in Figure 8.7. Also presented is figure 8.8 showing the relationship between current density and particle incorporation, with the use of one particle type and different bath agitation techniques. Different particles sizes in Figure 8.7 were utilised on the assumption that they could have unique codeposition behaviour due to the possible difference in forces required for their effective migration to the surface of the cathode. Consequently this could lead to varying degree of incorporation. It has been suggested [129] that the dependence of the vol.% of particles incorporated in an electrodeposit on current density is related to the nature of the particles (size and morphology) and thus how they are caught in the deposit. As can be seen in Figure 8.7, for both particle sizes, a peak in particle incorporation was achieved at 15.0 A/dm^2. Further increase in current density resulted in initially lower rates of incorporation for both particle sizes. However, at higher current densities of about 30 A/dm^2 there was a further increase in particle incorporation for the 2 μm particles. Although produced at higher current densities, the trend is similar to other reported composite electrodeposition systems [115,128-129, 143]. It has been reported [115] that particle incorporation behaviour, as a function of current density, can be divided into several regions: initially a region where incorporation increases sharply reaching a maximum value, followed by a sharp decrease in incorporation, then a region where incorporation is fairly constant, and

then another decrease as mass transport-limited conditions are approached. Although no clear conclusive explanations on the trend of particle incorporation with changing current density appear in the literature, a number of arguments put forward appear to favour increased overpotentials of metal deposition which in turn lead to higher electric fields and consequently improved electrophoretic migration of the particles [82]. Based on existing theories on the adsorption and subsequent co-migration of particles and adsorbed metal ions towards the cathode, it might be reasonable to suggest that at higher overpotential, there is the tendency for more particles with adsorbed metal ions to be attracted by the electric field generated due to high current densities. This could lead to a high concentration of particles and metal ions within the vicinity of the cathode, which in turn could lead to faster rates of metal ion reduction. Alternatively, it is also reasoned [82] that since the zeta potential of the particles is inversely related to the ionic concentration of the solution, as more metal ions are been used up at higher current densities, there is likely to occur a corresponding increase in the zeta potential of the particles due to the reduction of viscocity of the bulk solution. Reduction of viscosity is thought to improve the mobility of the particles. As the viscous drag of particles reduces and their mobility increases, there is the tendency for more particles to reach the surface of the cathode and eventually become incorporated. Generally, particles in contact with a liquid tend to acquire an electrical charge on their surfaces. When subjected to an electric field, each particle and the ions closely associated with it move through the solution as a unit. The potential at the boundary between this unit and the surrounding medium, is known as the zeta potential.

Whilst current density appears to have a clear remarkable influence on the rate of particle incorporation, this influence does seem to be slightly different with particle type as is seen in Figure 8.7. It shows that larger particles incorporate better than their smaller counterparts with increasing current density. Also, it appears that the sharp increasing and decreasing trends are more pronounced with the larger particles. Similarly, it has been reported [115] that the regions where the amounts of incorporation sharply increase or decrease with current density are sensitive to particle size. Various explanations have been given for such deposition behaviour. In some cases it is considered that, up to the maximum current density where incorporation occurs, codeposition is controlled by mass transfer [175,176]. In other systems,

it is suggested that, before the maximum, the process is controlled by adsorption of the particles, while an increase in current density results in more rapid deposition of the metal matrix and fewer particles are embedded in the coating [129]. In Figure 8.7, therefore, the sharp increase for particle incorporation for each type of particle up to the maximum point could indicate a fast mechanism of SiO_2 incorporation and beyond the maximum, metal deposition could be the predominant codeposition process. Most previous studies on the effect of current density on rate of particle incorporation in composite electrolytic systems appear to have observed this sudden increase in particle incorporation up to a maximum value and often an inconsistent increasing or decreasing trend

Furthermore, effect of increasing current density was studied using different types of solution agitation as can be seen in Figure 8.8. The general trend appears to be an increasing one. Each type of agitation used was based on the optimum value for maximum particle incorporation. The increase in rate of particle incorporation is probably due mainly to mass transport effect and particle type. Since optimum rates of solution agitation were used in both cases, it was expected that, replenishment of metal ions rapidly used up at the cathode due to the high current density could be effective as a result of effective mass transport since it is assumed here that metal ions are adsorbed onto silica particles in the bath. This invariably means that the combination of optimum rates of agitation together with rapid reduction rates could lead to high rates of particles incorporation. As more metal ions are being used up, more particles together with the adsorbed ion are effectively transferred towards the vicinity of cathode with consequent incorporation as the metal ions become reduced.

8.2.2 Influence of deposition time on particle incorporation

The rate of particle incorporation with increasing deposition time at a constant current density of 30 A/dm^2 is shown in Figure 8.9. The trend of incorporation indicates that there is insignificant increase in the rate of particle incorporation with increase in deposition time. This indicates a relatively uniform rate of incorporation within the specified duration for approximately 1.0 μm depth from the surface of the coating (energy dispersive X-ray analysis approximate analysis volume). For each current density, there is probably a maximum

deposition time limit for maximum particle incorporation beyond which no further increase in the rate of particle incorporation takes place. This is possibly associated with increase in cathode surface pH and subsequent hydroxide formation. On the cathode, $Zn(OH)_2$ is formed due to hydrogen evolution and subsequent pH increase [121]. Since the isoelectric point shifts towards negative values at higher pH, it might be reasonable to suggest that the longer the plating time, the higher the pH at the cathode surface and therefore the possibility of a lower isoelectric point and more negative zeta potential. As the pH increases there is probably a corresponding decrease towards more negative values of the zeta potential, which could promote the agglomeration of particles giving rise to lower rates of particle incorporation. However, it has been reported by other investigators [152] that the codeposition of silica is negligible at low pH and increases with increasing pH of the electrolyte. The difference in observations with other investigators [152] is probably due to the particle type and bath formulation. However, it should be noted, that the high rates of particle incorporation at high pH values could be as a result of the analysis technique picking up large agglomerates and not an overall sum of evenly dispersed particles. This is a possibility because at high pH values, particles tend to agglomerate. The agglomerated particles could easily adsorb onto the surface of the cathode and become covered by the growing metal matrix. This is often deemed to be detrimental to the integrity of the coating.

8.2.3 Effect of bath agitation on particle incorporation

Understanding mass transport effects in composite electrodeposition is crucial towards developing an effective plating process. Amongst other parameters, metal reduction and particle incorporation rates are, to a large extent, dependent on how many reducible species or second phase particles to be incorporated arrive in the vicinity of the cathode. Whilst the in-situ mass transport of the electrolytic system is often effected by the electromotive force (EMF), electric field effects, electro-osmotic and electrophoretic forces during electrodeposition. These are often insufficient to obtain the desired electrodeposit, thus mass transport is often enhanced by solution agitation. Different types of solution agitation have been reported [124-125]. However, vibratory agitation was given particular attention here because it has one special virtue-it is particularly effective in composite electroplating where it

is necessary to maintain second phase particles in suspension in such a way that they can be systematically and quantitatively incorporated into the electrodeposit [161].

Figure 8.10 shows the relationship between rate of bath agitation and the level of particle incorporation for a fixed bath particle concentration of 13.0 g/l and particle size of 2 μm. Rate of particle incorporation visibly increased until it attained a maximum at amplitude of about 1.5 mm and then decreased gradually with further increase in agitation. In an attempt to avoid erroneous conclusions on the effect of agitation on particle incorporation, further investigations were carried out using 20 nm particles and 30 A/dm^2 (Figure 8.11). Similarly Figure 8.12 shows the effect of agitation using magnetic stirring and 20 nm particles in the bath on their rate of incorporation. From Figures 8.11 and 8.12 it appears there was a general tendency for the incorporation of particles to increase to a maximum and then began to decrease in all cases as the rate of bath agitation increases. Although at various magnitudes, this behaviour seems to be independent of particle size and bath concentration of particles. The decrease in incorporation rate has previously been attributed to the collision factor [119]. When the quantity of the transferred particles is too great to be completely entrapped by the growing matrix, the free particles at the electrode surface collide with the incoming particles. The impact of such collisions could result in repulsion of the incoming particles. Since particles need some degree of "residence time" on the surface of the cathode to be entrapped in the growing metal matrix, if the repelling action from the collision is greater than the forces attempting to hold particles on the surface of the cathode, the length of time each particle might remain per unit time on the surface of the cathode to become entrapped becomes shorter. This could lead to reduced rates of incorporation. Similarly other researchers [131] have noted that this collision factor results in a decrease in the rate of incorporation. MULLER et al [128] reported that at low rotation speeds the fluid flow induced by a RDE is not capable of transporting all the particles to the cathode and, when the rotation speed is too high, the rate of particle removal becomes greater than that of attachment at sites on the electrode surface [143]. KALANTARY and GABE [126] also reported that an increase in vibratory agitation should increase the degree of incorporation. However, excessive agitation reduces incorporation as particles are swept away from the surface before incorporation can take place. Similarly, GHORBANI et al [131] also reported that at high agitation rates, because of the

turbulent flow in the bath, graphite particles on the surface of the cathode are washed away leading to a decrease in incorporation of graphite in the composite coating. Other investigators [129-130] also reported a similar trend of particle incorporation. Although produced at widely different experimental conditions, the results presented in Figures 8.10, 8.11 and 8.12 seem to agree with these authors. In each of these figures, residence time of the particles on the cathode appears to be a major determinant factor on the rate of particle incorporation. In a RDE system, increasing the rotational speed effectively reduces the residence time of the particle at the electrode surface, further inhibiting incorporation [115]. Such behaviour appears to be similar for each system investigated. In each of the figures, it may be assumed that the increase in particle incorporation up to the maximum indicates a faster reduction of adsorbed zinc ions. In general if the agitation is too low, particles in the bath may not disperse completely, except when their density is low. On the other hand, if the agitation is too high, particles will not have sufficient time to get attached to the surface and this results in poor particle incorporation [109]. It has been suggested that the stirring speed should be optimised based on the size of the second phase particles to be incorporated [109].

For the purpose of comparison, two types of agitation are presented in Figure 8.8. It is obvious that the rate of particle incorporation was improved for the vibratory agitation as opposed to magnetic stirring over a significant range of current densities. A possible explanation is that there is a tendency for particles to remain longer on the cathode surface (high residence time) due to the reciprocal motion of the perforated plate causing a rotational motion with the commencement of eddy patterns at amplitudes up to 0.62 mm [126]. The fluid rotational motion is circular in a vertical plane thereby allowing particles to remain longer within the vicinity of the vertical cathode and consequently becoming occluded in the growing metal matrix. Magnetic stirring induces a horizontal flow which has the tendency to sweep away particles from the surface of the cathode consequently reducing their residence time, which could lead to poorer rates of incorporation. Mechanical agitation has been shown to result in lower incorporation due to its directional flow recently by other researchers [109].

8.2.4 Effect of N, N-dimethyldodecylamine on rate of particle incorporation

Surface-active agents otherwise known as surfactants are widely utilised to modify the characteristics of surfaces and interfaces. This is because surfactants are known to have an ability to adsorb onto surfaces. The action of surfactants is based on their ability to reduce the surface tension of these surfaces and interfaces. Adsorption of a cationic surfactant develops a net positive charge on a particle surface, which prevents the particle from being agglomerated, and hence, increases the stability of the particle suspension in the bath [144]. In an aqueous composite electrolytic system where migration of both the metal ion species and second phase materials towards the cathode for deposition is essential, the use of surfactants has found extensive favour amongst researchers. Depending on the characteristics of the second phase material, the surface to be deposited and the composition of the bath amongst others, either a non-ionic or cationic surfactant can be used.

According to [100], alteration of the surface, via the adsorption of surfactant species, markedly promotes the incorporation of particles. Illustrations to confirm this was based on their findings that in nickel-diamond composite electrodeposition, the zeta potential was negative in the absence of surfactant but became less negative as the level of cationic surfactant was increased. At a solution level of approximately 8 mg of surfactant per gram of diamond the zeta potential was zero and hence there was no net charge on the particle. At higher surfactant levels, the zeta potential became increasingly positive, allowing the amount of diamond powder incorporated into the deposit to be enhanced due to the increasing positive charge on the particles.

A similar trend of improved incorporation to that described above was observed in Figure 8.13, which shows that increasing the bath concentration of NND improves the rate of particle incorporation for 2 μm particles. There was no significant increase in the incorporation of 20 nm particles, rather a slight decreasing trend was observed. The increase in particle incorporation of the 2 μm particles attained a maximum value at 2.5 ml/l NND. It has been reported [177] that the optimal surfactant concentration for maximum codeposition is the concentration, where the adsorption of the surfactant on the particle is maximal. This suggests that 2.5 ml/l of NND is the optimum concentration for maximum silica incorporation. Beyond

this concentration, a sharp decrease in incorporation was observed with further increase in the bath concentration of NND. This behaviour can be attributed to a number of reasons. At low concentrations of NND, the silica particles may not have acquired sufficient positive charge to prevent their agglomeration [178]. On the other hand, at an optimum concentration (2.5 ml/l) of NND, the particles may have acquired sufficient positive charge that could stabilise them in the solution due to electrostatic repulsion. Similar observations have previously been reported [107] with cetyl trimethyl ammonium bromide (CTAB). ZHITOMIRSKY [117] also attempted to give an explanation for the codeposition enhancement behaviour of cationic surfactants. He stated that cationic surfactants act as electrolytes in compressing the double layer of ceramic particles, resulting in particle flocculation and increasing the deposition process efficiency. Several investigators have addressed a number of reasons for the selective improvement of incorporation rates for the larger against the smaller sized particles, although a clear theory is not apparent. However, it might be reasonable to consider the surface area to volume ratio of the different sizes of particles. For the same volume and bath loading of the separate types of particles, the surface area available for possible adsorption of NND will be larger for smaller particles than for larger ones. This could lead to excessive amounts of NND on the smaller particles due to the larger area of adsorption consequently causing electrostatic repulsion and therefore reduced rate of incorporation. It could also be associated with the hydrophilic characteristics of SiO_2 and difference in momentum of the particles. NOWAK et al [133] reported that for both flotation and codeposition processes a solid particle approaches an interface and rupture of the aqueous film between the particle and the interface must occur to allow the capturing of the particle.

ZHITOMIRSKY [117] also noted that surfaces of oxide particles dispersed in water tend to coordinate water molecules to form hydroxylated surfaces with the surfaces becoming positively or negatively charged depending on the pH. The momentum acquired from the prevalent (electrophoretic, electroosmotic and hydrodynamic) forces in the bath, may not be large enough for the 20 nm particles to penetrate and hence rupture the aqueous film between the particle and the interface for them to be captured at the interface. FRANSAER et al [179] proposed hydration forces as the adhesion force governing particle incorporation. This repulsion force arises from the work required to remove the ordered hydration layers at the

solid-liquid interfaces for solids coming into close contact. Hence it was argued [143] that the hydrophobic nature of the adsorbed cetylpyridium chloride dimers diminishes the hydration forces and enhances polystyrene codeposition.

Based on the proposals elsewhere [133,179,], it might be reasonable to consider that for incorporation of particles to occur, they must have sufficient terminal momentum (greater than all other opposing forces) to either overcome the ordered hydration forces or rupture the aqueous film between the particle and the interface. Since this momentum is largely a function of particle mass and velocity just before incorporation, particles with larger momentum will be able to rupture the aforementioned forces much more easily than their smaller counterparts and hence incorporate better. It is also noteworthy, as obvious in Figure 8.14 that at optimum conditions of 2.5 ml/l NND, 50 g/l of 2 μm particles, the rate of particle incorporation was slightly over twice the rate of incorporation without NND. Improved rates of particle incorporation were also observed in the presence of NND at higher bath concentration of particles as can be seen in Figure 8.15 .Similar observations have been made by other researchers [99] using a Ni/SiC system in the presence of sodium dodecylsulfate as bath additive. According to them, before the addition of sodium dodecylsulfate to the nickel electrolyte, the amount of SiC particles in the coating was very small, 1 wt % in agglomerated distribution dispersion. However, they found that addition of sodium dodecylsulfate was beneficial for improving the amount and uniformity of the dispersed particles in the nanostructured layer.

8.2.5 Effect of particle size on rate of incorporation

Although already mentioned quite a bit in the previous section, effect of particle size would be discussed more broadly in this section. From Figures 8.13 and 8.16, it is obvious that rate of incorporation is largely dependent on the particle size. The presence of NND did not cause any significant increase in the rate of incorporation for 20 nm particles since the maximum incorporation observed was approximately 5 wt% for deposition with or without NND in the bath. Whilst for the same conditions for 2.0 μm particles, up to approximately 21 and 16 wt% of silica was deposited with or without NND in the bath respectively. At optimum conditions,

the rate of particle incorporation was even higher as seen in Figure 8.14. The larger particles were found to produce higher silica content in the coatings under all experimental conditions. These observations seem to agree with previous works [132,142,180,] on the Ni/SiC system, which suggest that codeposition of particles decreases with decrease in particle size. In aqueous plating electrolytes particles easily agglomerate due to compression of the diffuse double layer surrounding the particles through the high ionic strength. This could lead to flocculation and consequently agglomeration of particles. This effect is more pronounced for particles of submicron size as the shearing forces on the agglomerates, created by agitation of the plating bath, decreases with particle size [142]. Such behaviour may have contributed to the low rate of incorporation of the 20 nm-sized particles. Similarly, it has been reported [140] that the agglomeration of SiC particles in the electrolyte would result in enhanced amount of agglomerated layer of SiC particles in the codeposited layer. The agglomeration of graphite particles has also been reported [181]. However, in this work, considering the large difference in particle size ratio of 20 nm: 2 μm being 1:100, the number of 20 nm-sized particles codeposited must be greater but their overall mass deposited less. Recently, GARCIA et al [135] examined the number density of particles in an electroplating solution for three different SiC particle sizes, namely 5, 0.7, and 0.3 μm. According to them, the number density of particles rather than volume fraction of SiC in the coating increases with decreasing particle size. However, HOU et al [140] argues that the assumption of the mono-dispersed particles in the plating solution is not realistic since the agglomeration of SiC particles must occur significantly to decrease the free energy in the system.

FEGSEM micrographs as shown in Figures 8.1 (a) and (b) reveal that the 2 μm particles had fairly irregular geometries whilst the 20 nm particles were round shaped. The geometry of irregularly shaped particles tends to provide better interlocking with other codepositing species and with the metal matrix and hence could become readily incorporated into the growing metal matrix. It has been reported that angular shaped particles will have a greater tendency to adhere to the surface upon impingement than round ones [109]. However, APACHITEI et al [182-183] have shown that spherically shaped alumina particles resulted in better incorporation than irregular ones. In addition, Figure 8.1(b) shows a range of particle sizes many nowhere near 2 μm. The use of such uneven particle size distribution could lead to

the production of inhomogeneous composite electrodeposits. Non-uniform size distribution in such deposits could affect the anticipated properties and performance, which may be desired but may not be achieved.

8.2.6 Effect of particle loading on particle incorporation

The effect of bath concentration of SiO_2 particles is shown in Figure 8.17. There are obviously two distinct trends of incorporation. Up to the bath concentration of approximately 100 g/l of silica particles, there is an obvious increasing trend. However, beyond this concentration, the incorporation behaviour takes an increasing trend with a sinusoidal response. This is probably due to the fact that beyond 100 g/l, the effective saturation particle concentration of the bath would have been exceeded and agglomeration begins to occur which could lead to uneven distribution of particles in the coatings. Consequently, the analytical probe may have picked either pockets of agglomerates giving high peaks or regions of low incorporation with lower peaks for coatings produced beyond 100 g/l SiO_2, hence the sinusoidal response beyond this concentration. The trend of incorporation indicates an overall increase with increasing bath concentration for the 2 μm particles. The observations seem to agree with other investigators [121] that SiO_2 contents in the composite electrodeposits increase with an increase in its concentration in the bath. However, too high a concentration of silica particles in the electro-galvanising bath may affect its stability, causes cohesion or precipitation of silica particles, and generally reduce the service life. In addition, solution resistance in the electro-galvanising bath could become unnecessarily high, resulting in a poorer current efficiency and increased consumption of electric power for electrogalvanising [150] as discussed earlier in section 8.1.1.2. Although the overall trend of incorporation appears to be an increasing one, it is obvious from Figure 8.17 that the points below the line are more than those above beyond a bath loading of 100 g/l of SiO_2. This shows that a decrease rather than increase in incorporation is favoured beyond the effective bath concentration of particles, which appears to be 100 g/l in this case suggesting that the trend line is not representative of the overall trend. A better description of the trend would be that of an increase to a maximum and then a decrease with further increase in the bath concentration of particles [127-130,134].

The agglomeration of SiO_2 particles at high bath concentration was observed with the 20 nm particles. Figure 8.18 shows EDX analysis, SEM micrographs of surface and cross-sectional views of a zinc-silica electrodeposit from a bath concentration of 104 g/l of 20 nm-sized particles deposited at 30 A/dm^2. Analysis using the SEM revealed two distinctly deposited layers. An under layer of dendritic zinc matrix and a top layer of SiO_2. Dendritic growth behaviour in composite electrodeposition has been reported [131]. The surface morphology (see Figure 8.18b) was also analysed and the white patches were identified as zinc and the darker portions gave strong silicon peaks (see Figure 8.18a). The high overpotential may have increased the rate of Zn^{2+} reduction on the cathode, which could cause an increase in pH of the cathode. Increase in pH is thought to cause the agglomeration of particles. Consequently, the agglomerated particles may have become adsorbed as a top layer preventing further zinc deposition. This indicates that excessive addition of nano-sized silica particles in an aqueous bath could results in an adsorbed layer of silica rather than codeposition. Although, the properties of such deposits were not investigated here, such electrodeposits are likely to behaviour in a number of ways when subjected to a corrosive medium. Firstly, they could exhibit high porosity if there is insufficient metal matrix in the top layer to provide the desired metal-particle bonding. In that case it would be expected that ingress of corrosive species could easily attack poorly bonded agglomerates and penetrate the coating quite easily consequently reducing its life. Or, secondly, due to the relatively thick layer of no-conducting inert particles, ingress of corrosive species may be hindered if there is sufficient metal-particle interfacial bonding holding the particles in place. Since the particles are inert, they could act as insulating sites in the coating for the propagation of corrosion current. As a consequence, the corrosion resistance could be improved over that of ordinary zinc coatings.

8.3 Cathodic polarisation studies

Cathodic polarisation studies were carried out on mild steel to aid a mechanistic understanding of the separate influences of NND and SiO_2 on zinc electrodeposition. Mild steel panels were polarised from their open circuit potential. Both dilute and concentrated baths were used for studying the effect of SiO_2, whilst only a dilute bath was used in the case of NND. Dilute electrolytes were employed in order to achieve well-defined deposition behaviour in the

polarisation curves as opposed to solutions with high zinc levels where metal reduction peaks are less clear [82]. As can be seen from Figure 8.19, both dilute and concentrated electrolytes had similar behaviours in the presence of SiO_2 particles. The results from Figure 8.19 indicate that there are two main reduction reactions H^+ and Zn^{2+} forming H_2 and Zn respectively. The zinc appears to deposit at potentials below –1000 mV vs SCE. Activity prior to this is attributed to oxygen reduction and possibly hydrogen evolution off the steel. Increased activity following zinc reduction is due to concurrent hydrogen evolution. Figure 8.19 also indicates that there was an increase in the zinc deposition current densities for the baths with silica particles. This trend could support the assumption that when silica particles are added into a zinc bath, the zinc ions tends to adsorb onto the surface of the SiO_2 particles [122], migrate to the cathode and consequently increase the zinc deposition current density due to the now higher concentration of zinc ions in the vicinity of the cathode. The adsorption of zinc ions onto SiO_2 has also been reported by other researchers [184]. The authors attributed the mechanism of cation adsorption to proton release and noted that adsorption of zinc ions on silica increases with increase in pH of the solution up to 7 and then decreases. However, these observations may not be the same with other composite electrodeposition systems as it has been reported that SiC powder would not significantly affect the electrochemical reduction of nickel ions in a Watts bath [119]. This is probably due to the effect of particle type and possible differences in surface characteristics between SiO_2 and SiC. Such differences could be sufficient for the systems to exhibit dissimilar electrochemical behaviours. SIMMONS [82] reported a slightly different trend with zinc/PTFE baths. He stated that upon addition of PTFE to the zinc electrolyte, the whole polarisation curves appeared to shift to more cathodic potentials (i.e for a given potential the current density became slightly lower). A similar trend to Simmons [82] was observed in the present investigations when NND was added to the zinc baths (Figure 8.20). NND also causes a reduction in the zinc deposition signal, which appears to be approximately proportional to its bath concentration. A possible explanation for such behaviour is that NND present in the solution competes with zinc cations for active sites on the electrode and particle surfaces. When there is sufficient NND adsorbed onto these surfaces, the zinc deposition current density decreases. Alternatively, the NND could become adsorbed onto the electrode surface thereby blocking off and consequently preventing further

deposition of zinc hence the diminishing current densities as the concentration of NND in the bath increases.

Mass transport behaviour of the zinc-silica composite system was also studied and the results presented in Figures 8.21 and 8.22. It is obvious from both figures that current density increased for all the investigations carried out in the presence of bath agitation. In all the figures, it appears zinc deposition did not occur until the potential was about –1130 mV vs SCE. A gradual increase, depending on the concentration of Zn^{2+}, with steep activation is then observed in a short range of potential and then diffusion control appears to take over at higher potential values. However, for the investigations without agitation, the zinc deposition current appears to be very low. This is an indication that for the bath compositions and deposition conditions utilised here, agitation was favourable for the zinc deposition reaction due to enhanced mass transport. Similar improvements in mass transport and hence zinc deposition current densities have previously been reported [12].

8.4 Morphological studies of zinc/silica electrodeposits

The morphology of a zinc-silica electrodeposit produced with 20 nm sized particles is presented in Figures 8.2 and 8.3. As can be seen, the electrodeposit consists of crystals with distinct sequential layer-by-layer stacking of hexagonal platelets with their bases parallel to each other and to the surface of the substrate thereby forming short columns of crystals. The parallel alignment of hexagonal plane crystals to the surface of the substrate have been reported by other investigators [147].

Figures 8.23 and 8.24 are surface morphologies of zinc-silica electrodeposits with 24 wt% and 16.8 wt% of 2 μm silica particles produced from baths containing 2.5 ml/l and 1.0 ml/l of NND respectively. Figures 8.23, and 8.25(a) indicate that NND does not only enhance the codeposition of 2 μm silica particles but also exhibits an acceptable levelling effect of the electrodeposits. Figure 8.24 shows acicular morphology for the zinc/silica electrodeposits. Similar acicular zinc/silica morphologies have been reported elsewhere, produced when surfactants have been added to the electroplating bath [178]. The formation of such

morphogies is attributed to preferential adsorption of the surfactants on (0002) planes leading to the preferential growth of (1010) zinc planes perpendicular to the (0002) plane. In addition, these deposits could provide sufficient anchor on application of polymer paints [178]. However, it is noteworthy that excessive addition of surfactants to the electrolytic bath could be detrimental to the process. Apart from reduced rates of particle incorporation with NND beyond the optimum concentration as previous discussed and seen in Figure 8.13, NND appears to promote stress in the electrodeposits. This is obvious from Figure 8.27 produced from a bath containing about 5 ml/l of NND. However, it could also be blistering due to hydrogen evolution. At such high concentrations of the surfactant, the zinc crystal may have been stressed to limit with the consequent initiation of cracks in the deposits. Such cracks were visually evident especially at the edges of the samples were current density is presumably higher. Generally, it has been reported [100] that free surfactants can be incorporated into an electrodeposited layer and can cause adverse changes in the mechanical properties of the electrodeposits such as high stress and brittleness.

The highly uniform distribution of particles in Figures 8.23 and 8.25 is an indication of the de-aggregation and the enhanced mono-dispersion effect of NND. Minimal agglomeration is observed in these deposits. Being dense and compact, these deposits could exhibit enhanced corrosion resistance if the interfacial bonding between the particles and the metal is strong. However, the effect of a non-uniform size distribution of particles in the deposit is obvious in Figure 8.26 due to the uneven size distribution of 2 μm particles used as earlier characterised in Figure 8.1(b). There appears to be poor contacts at the interfaces between the larger particles and the metal matrix in Figure 8.26 resulting in porosity. These porous sites are probably due to stress exacted on the metal matrix due to the size of the larger particles and could provide suitable sites for the ingress of corrosive species thereby enhancing a quicker mechanism of dissolution. In contrast, there are reasonably compact deposits at the sites where smaller particles are deposited. Such locations on the deposit should exhibit better corrosion resistance. Similar results have been reported [185] in a SiC/Ni system. Acccording to these authors, ultra fine particles, although more difficult to codeposit, produce composite electrodeposits with smoother and better bonding characteristics between SiC and Ni than that

in coarse SiC/Ni composites. In many applications, it is therefore recommended that a codeposition of ultra-fine particles with metal is preferable to coarse particles [185].

8.5 Evaluation of the level of adsorbed particles following electrodeposition

Because of the possibility of particle adsorption on the surfaces of the electrodeposits during removal of samples from the electrolytic bath which could lead to erroneous results, evaluations of the strength of this adsorption on the electrodeposits were carried out.

Table 8.2 Evaluation of the level of adsorbed particles on the electrodeposits

Serial Number	SiO_2 in deposit, wt%	
	Ultrasonic cleaning	Without ultrasonic cleaning
1	7.62	6.7
2	8.2	12.4
3	10.6	16.0
4	17.0	16.8
5	11.0	10.3

The results in table 8.2 shows the weight percent of SiO_2 in the deposit for a number of samples produced under the similar experimental conditions with one analysed without ultrasonic cleaning and the other after ultrasonic cleaning. The variation of particle incorporation for each pair of results (with and without ultrasonic cleaning) appears to fluctuate only slightly, suggesting few particles are adsorbed on removal of freshly deposited coating from the electrolyte.

CHAPTER NINE

9 ELECTRODEPOSITION OF ZINC-NICKEL/SILICA COMPOSITE COATINGS

The results and discussions presented in this section are findings on the electrolytic codeposition behaviour of Zn-Ni/SiO_2 from an acid sulphate bath. This was chosen because of its advantages when compared to alkaline bath as earlier enumerated in section 7.1.1. As was with the case of Zn/SiO_2, the Zn-Ni/SiO_2 was quite compatible and suspension stability was good especially with the 20 nm particles. However, suspension stability for 2 μm particles was an issue due to the relatively large particle size and was therefore regularly kept in suspension by bath agitation.

9.1 Parameters influencing the deposition process

As with the case of Zn/SiO_2 the parameters determining the codeposition behaviour of the ternary Zn-Ni/SiO_2 system such as current density, solution agitation, particle loading, particle size and bath composition were investigated and are presented in the following sections.

9.1.1 Influence of current density on deposit composition

The influence of current density on the rate of SiO_2 incorporation for a Zn-Ni/SiO_2 system with 2 μm particles is shown Figure 9.1. The incorporation behaviour appears to be similar to that of Zn/SiO_2. The general trend seems to be that of an increasing one to a maximum, a decrease and then an increase although more data points would have confirmed these trends more fully. Some investigators have reasoned that the region before the current density where the maximum rate of incorporation is observed could be due to the increasing tendency for the adsorbed ions/particles to arrive at the cathode [129], whilst in other investigators [128,175-176] it is considered that up to the current density maximum, codeposition is controlled by

charge transfer, and beyond this point the process changes to mass transport control. Furthermore, other models [179] have attributed the particle incorporation behaviour to the strength of solvation forces governing the particles. They reported that the point where maximum incorporation occurs is a result of minimum solvation forces existing between water molecules and the particles at the point of zero charge (p.z.c). However, the validity of such claims could not be proven in this work as point of zero charge measurements were not carried out.

The energy required for the deposition of metal ions that are solvated as well as adsorbed on to the surface of a particle is larger than that of a freely solvated metal ion. As a result of this difference in activation energy the initial low codeposition is probably due to the deposition of free metal ions. As the current density increases, this energy difference criterion becomes less important and the codeposition of particles increases up to a maximum as suggested from Figure 9.1. Beyond the current density for maximum particle incorporation, the rate of incorporation decreases. Although this trend is not a likely conclusive deposition behaviour for all composite electrodeposition processes due to the influence of other parameter under specific deposition conditions, a possible explanation for such behaviour is that at higher current densities, the loose adsorption of particles at the surface of the cathode becomes rate controlling and because this is always slower than the metal deposition rate, particle incorporation tends to decrease with increase in current density [186]. Also, it is noteworthy that the Coulombic force transports both particles and metal ions simultaneously onto the cathode. SiO_2 particles become adsorbed onto the cathode and are subsequently covered in the metal matrix as the current density increases. However, at current densities above 3 A/dm^2, transportation of metal ions to the cathode may have been faster than the SiO_2 particles, which could result in rapid metal deposition and reduced rates of particle incorporation as earlier mentioned. Other investigators [127-128,132] have made similar observations. In the case of Zn-Ni/SiO_2 composite electrodepositon, an alternative explanation for the decrease in SiO_2 incorporation could be as a result of change in the actual concentration SiO_2 in the vicinity of the cathode with increase in current density as compared to the number of possible intermediate reactive species such as $ZnOH^+$ and $NiOH^+$.

Figures 9.2 and 9.3 show the influence of current density on nickel deposition in the presence and absence of SiO_2 in the Zn-Ni bath with different particle sizes. As can be seen from Figure 9.2, the rate of nickel deposition appears to decrease with increase in current density for the bath without SiO_2. However, this does not seem to be the case with the bath containing 20 nm SiO_2 particles. It is obvious from this figure that for the bath containing SiO_2 particles, increase in current density beyond 4 A/dm^2 tends to show a transition from the anomalous behaviour to that of normal deposition as more nickel begins to deposit. It has been reported [121] that the SiO_2 colloid accelerates the electrodeposition of Fe group metals. These authors further stated that in anomalous codeposition, where the electrochemically less noble metal tends to deposit preferentially to the more noble metal, SiO_2 colloids act to shift the anomalous codeposition to the normal. Similarly, NOWAK et al [133] reported that a decrease in the charge transfer resistance takes place on addition of silica in a Watt's nickel bath accompanied by an increase in current. A possible explanation to this behaviour is that in the electrolyte, Fe group metals tend to adsorb onto SiO_2. During the process of electrodeposition, the pH of the electrolyte in the vicinity of the cathode is generally thought to be higher than that of the bulk solution. In this region of increased pH, SiO_2 particles tend to agglomerate. It has been reported [187] that SiO_2 colloids start to agglomerate at neutral pH. The agglomerated colloid may then suppress the formation of $Zn(OH)_2$ which could result in blocking the diffusion of zinc ions to the cathode and realising the normal codeposition process.

Further investigations were carried out to ascertain how the presence of SiO_2 particles in the zinc-nickel bath acts to shift the anomalous behaviour by slightly modifying the bath chemistry and changing the particle size to a larger one as shown in figure 9.3. Although not a very wide difference in the nickel deposition rate, it is obvious that for each of the current densities investigated, the bath containing SiO_2 colloids showed a slightly higher level of nickel deposition. These results appear to be in agreement with other investigators [121], who reported that, preferential adsorption and colloid agglomeration causes an induced codeposition. Similarly, SUROWKA et al [188] investigated the codeposition behaviour of Co-P/TiO_2 and reported that the weight percentage of the alloying element phosporus was higher with the bath containing TiO_2 particles than that without TiO_2 for all the range of current densities investigated. Not only was the weight percentage of phosphorus higher, but

also the amount of TiO_2 was reported to have increased with increase in current density. The amount of SiO_2 incorporated points to the fact that at lower current densities only a small amount of SiO_2 incorporation takes place. An increase in the current density intensifies this process, thus the electrodeposits produced at higher current densities exhibit a higher percentage of SiO_2. A number of reasons such as particle type, size and surface characteristics, and the difference in elemental composition of the two systems could be responsible for the wide variation in the rate of particle incorporation. Furthermore, the results presented in Figure 9.3 also appear similar to those reported by WU et al [186] for a Co-Ni/Al_2O_3 system. They noted that Al_2O_3 particles in the electrolyte promote the codeposition of cobalt and hence make the cobalt content in the deposit higher than Al_2O_3 particles were not present. Not only was cobalt deposition improved but also the incorporation of Al_2O_3. This behaviour was attributed to the adsorption of Co^{2+} on the surface of Al_2O_3, which increased its surface charge. As can be seen from Figure 9.3, the nickel content of the deposit was higher with the bath containing SiO_2 particles for all the current densities investigated. This shows that the presence of SiO_2 in the bath enhances the deposition rate of nickel.

9.1.2 Effect of particle size on the deposit composition

The effect of particle size on the deposition behaviour of Zn-Ni/SiO_2 was also investigated as shown in Figure 9.4. The effect of particle size is clear. For nearly all the current densities investigated, it is obvious that the amount of SiO_2 incorporated was higher with the 2 μm particles than with the 20 nm particles investigated under similar experimental conditions. Although at slightly different deposition conditions, a similar trend was observed with the Zn/SiO_2 electrodeposition already discussed in section 8.2.5. Although, the overall amount of silica incorporation appears to be higher for the larger particles for the deposition conditions investigated here, as shown in Figure 9.4, the trend of incorporation for the individual particles seems different. This is obvious from Figures 9.4 and 9.5. From Figure 9.4, it is obvious that for the range of current density investigated, the rate of incorporation of 2 μm particles tends to decrease with increase in current density. On the contrary, it can be seen from Figure 9.5 that 20 nm particles show an increasing trend with increase in current density. Similarly, MAURIN and LAVANT [180] reported in their studies on a Ni/SiC system, the mean fraction

of incorporated SiC particles against current density for four kinds of Lonza SiC powders. According to them, the rate of incorporation of the biggest particles decreased with current density. For smaller particles, the weight percent of incorporation was smaller but tended to increase with increase in current density. This is in agreement with the findings here when 20 nm particles were utilised, although the range of current densities investigated was different and there was no alloying element such as nickel in their baths. Also, SIMMONS [82] in his Zn-Co/PTFE composite system reported a similar trend to the results presented in Figure 9.5. According to him, current density appears to be the most influential parameter in enhancing the rate of PTFE incorporation. However, in the present work with the 2 μm particles, the trend of particle incorporation was quite different as shown in Figure 9.1. The system where 2 μm particles were used was closely similar to that of Zn/SiO_2 baths without nickel. Although the overall amount of particles incorporated for the 20 nm bath was relatively smaller than in the baths where 2 μm particles were utilised, the gradient of particle incorporation for the smaller particles appears higher see Figures 9.1 and 9.5. This is an indication that when an alloying element such as nickel is added into the Zn/SiO_2 bath, not only does the rate of particle incorporation differs with different particle sizes, but also the trend of particle incorporation with increasing current density. The trend of incorporation of the 20 nm and 2 μm particles was quite similar for most of the investigation in the Zn/SiO_2 system already discussed in the previous chapter even though incorporation rates were significantly smaller for the 20 nm particles in nearly all the investigations. The effect of particle size on the rate of particle incorporation is widely reported in the literature [132, 142, 180]. Each of these investigators noted that particle incorporation decreases with decrease in particle size. It was therefore concluded that rate of particle incorporation is largely dependent on particle size.

The results in Figure 9.5 further underline the effect of current density and current density distribution on the rate of particle incorporation. It is generally accepted that current distribution during electrodeposition is unequal especially on flat panels due to electric field effects and are believed to be higher at the edges. Based on that, analysis for rate of particle incorporation was carried out on both the centre and edges of samples in baths containing 20 nm particles. It is obvious in Figure 9.5 that for the range of current densities investigated, the rate of particle incorporation was found to be higher at the edges. There is also an increasing

trend with increase in applied current density. This is an indication that higher current densities favour the rate of incorporation of 20 nm SiO_2 particles. It has been reported [190] that at more cathodic deposition potentials, the rate of deposition of nickel and iron increases which might result in a larger fraction of adsorbed SiO_2 particles being incorporated. Although the results indicate that the amount of particle incorporation is higher for the 2 μm particles than the 20 nm particles, it is not yet very clear why the smaller sized particles are more difficult to codeposit.

9.1.3 Effect of particle loading and bath agitation

In order to study the effect of bath concentration of particles on the codeposition behaviour of Zn-Ni/SiO_2, the content of SiO_2 in the bath was varied from 13 to 52 g/l for different current densities with 20 nm particles. The different effects of particle loading, with and without bath agitation are shown in Figures 9.6 and 9.7. Figure 9.6 shows the trend of SiO_2 incorporation with increase in SiO_2 content of the bath in the absence of agitation. The results indicate that rate of SiO_2 incorporation for all the current densities investigated increases until it attained an optimum value for each current density at 40 g/l of SiO_2 in the bath. Further increase in the bath content of SiO_2 shows a decreasing trend for the current densities investigated. Similarly, Figure 9.7 was produced from the same bath but with agitation. The trend of SiO_2 incorporation was quite similar to that without agitation. The obvious difference was that in this case the optimum bath concentration of 40 g/l observed for the bath without agitation for maximum particle incorporation was continues to increase. Optimum bath content of SiO_2 could not be established here, as particle loadings higher than 52 g/l were not investigated. The increase in SiO_2 content of the deposit in each case is probably due to the adsorption of SiO_2 particles on to the surface of the cathode aided by effective agitation. As these particles remains adsorbed onto the surface of the cathode, the depositing metal starts to build around and consequently encapsulate them. Increase in the deposit content of SiO_2 with increase in SiO_2 concentration in the bath has been reported [189-190]. TAKAHASHI et al [189] found that the SiO_2 content of the plated layers increased rapidly with an increase in the SiO_2 concentration in the bath, showing that the Guglielmi's two-step deposition model did not hold in their case. Other investigators have also reported a similar trend [128-129,186,].

RAMASUBRAMANIAN et al [190] also reported that at a fixed deposition potential, the amount of SiO_2 included increases as the concentration of SiO_2 in the solution increases. According to them, the phenomenon is probably due to the increased availability of SiO_2 particles in the solution in a colloidal form. In the present work for the bath without agitation, any further addition of particles beyond the optimum bath concentration of 40 g/l, results in reduced incorporation. A number of reasons are thought to be responsible for this reduction in particle incorporation. Firstly, the phenomenon of effective saturation particle concentration [181] of the bath begins to play a significant role. For the experimental conditions utilised to produce Figure 9.6, the effective saturation particle concentration of the bath appears to be attained at a SiO_2 concentration of 40 g/l. Secondly, beyond this concentration, particles tend to agglomerate and a decreasing trend is observed. Agglomeration of particles in electrolytic baths is widely reported [134,150,181] in the literature. The observed decreasing trend is probably due to agglomeration with consequent sedimentation of the agglomerates. When particles agglomerate, they tend to increase in size. As the diameter of the agglomerate increases, the higher its tendency to settle out of suspension due to the gravitational force being greater than the combined forces enhancing buoyancy. KIM and YOO [132] reported that large particles have a tendency to sink due to their weight after impact, which decreased the amount of co-deposition. Settling out of suspension of the larger agglomerates leads to a reduction of the effective saturation particle concentration of the bath, consequently leading to reduced rates of particle incorporation. GER [141] concluded in his investigation that the amount of SiC particles in the deposited layer is dominated by the well-dispersed particles. According to him, as long as the amount of effective particles in the plating bath is increased, more embedded amount of SiC can be achieved. Similarly, HAMID [134] investigated the thermodynamic parameters influencing the electrodeposition of Zn-Co/TiO_2 and reported that TiO_2 incorporation increases sharply and attained an optimum value of 16.6 vol. % at 30 g/l of TiO_2 suspension in the electrolyte. The difference in optimum bath concentration of particles for maximum incorporation with this present work is probably due to the nature of particle, particle size or bath composition.

Improvement in the rate of particle incorporation at higher bath concentrations of SiO_2 was observed when bath agitation was applied as can be seen in Figure 9.7. Also in Figure 9.8 the

influence of bath agitation for two bath concentrations of SiO_2 is quite obvious. Not only is the effect of bath agitation obvious, effect of bath concentration can also be seen. For nearly all the current densities investigated in Figure 9.8, the overall rate of particle incorporation was higher for the baths containing the higher concentration of particles with or without agitation. This is probably due to the frequency of particles reaching the surface of the cathode. However, for the same bath concentration of particles, the effect of bath agitation appears to show a slightly different trend for the two types of particle concentration in the bath. It appears the rate of particle incorporation is better in the absence of bath agitation for the bath with a lower concentration of particles. On the contrary bath agitation appears to favour the rate of particle incorporation for the bath with higher concentration of particles. This is an indication that bath agitation and mass transport plays a significant role in particle incorporation for composite electrodeposition systems and its effectiveness depends on the bath concentration of particles. There appears to be a number of reasons linked to this incorporation behaviour. Recently, FRANSAER et al [179] developed a model of particle codeposition based on detailed analysis of particle trajectory by taking into account all particle-electrode interaction and hydrodynamic forces. Forces of friction F_{fric}, adhesion F_{Adh}, shear F_{shear}, and stagnation F_{stagn} were identified as possible hydrodynamic forces responsible for such incorporation behaviour. The main factor governing particle incorporation for the bath with 26 g/l of SiO_2 is probably adsorption and surface coverage of the cathode. Due to the low bath concentration of particles, adsorption and particle-electrode interaction is likely to be higher in the absence of agitation. On application of current, the adsorbed particles become gradually covered in the growing metal matrix. However, with bath agitation, the loosely adsorbed particles could be washed away and their residence time on the surface of the cathode becomes reduced for incorporation to take place. It is necessary to take into account the effect of the shear force F_{shear} exerted by fluid flow parallel to the wall on the attached particles, which tends to remove them before they become definitely entrapped in the metal layer [180]. It is pertinent to note that the highest rates of incorporation for both 26 g/l and 52 g/l of SiO_2 were obtained at the least current density and without bath agitation. On the contrary, although maximum incorporation was observed at the lowest current density and in the absence of agitation, the overall trend of particle incorporation for the bath with 52 g/l shows an improvement with bath agitation. As earlier discussed, the phenomenon of effective bath concentration and

agglomeration of particles appears to be playing an important role here again. Apart from the fact that at higher current densities, more metal deposition takes place and with consequent reduction in rates of particle incorporation, the progressive decreasing trend observed without bath agitation is an indication that particles agglomerate and settle out of solution thereby reducing the effective bath concentration of the particles. However, with the bath agitation, the rate of agglomeration may be lower with better particle dispersion. This is probably because in the presence of bath agitation, particle-particle attractive forces which are likely to cause the agglomeration of particles is reduced, consequently enhancing the effective dispersion of particles in the bath and hence better incorporation. It is also noteworthy that the overall difference in the rate of particle incorporation, for the range of current densities investigated, is quite minimal which is an indication that similar amount of particles reaches the surface of the cathode per unit time as the suspension exceeds its effective saturation particle concentration in the bath. Also, beyond 40 g/l of SiO_2 in the bath, the rate of particle incorporation shows that incorporation rates decrease with increase in current density as can be seen in Figure 9.6.

Figure 9.9 shows the effect of SiO_2 content in the zinc-nickel electrolyte on the nickel content in the deposit. The level of nickel deposition indicates a decreasing trend as the bath concentration of SiO_2 increases for all the current densities investigated. It has been reported [133] that the introduction of particles to the solution may be accompanied by the introduction of impurities, which influences the coverage of the electrode by adsorbed intermediates. Influence of impurities and additives on the codeposition behaviour will be discussed in more detail in the next section. Since electrodeposition generally involves adsorbate intermediates such as $Zn(OH)^+$ and $Ni(OH)^+$ in the present investigations, it is obvious from Figure 9.9 that the increasing participation of SiO_2 in bath inhibits the alloy deposition. The mechanism of inhibition is probably due to the increasing adsorption of SiO_2 particles on the surface of the cathode which could lead to reducing the surface coverage of $Zn(OH)^+$ and $Ni(OH)^+$ by decreasing the active surface area for the reduction these species. This inhibitive effect could be more on the $Ni(OH)^+$ than the $Zn(OH)^+$.

9.1.4 Influence of bath additives

The effect of bath additives in composite electrodeposition has been widely investigated. Bath additives are usually utilised with the aim of improving the deposition process. However, the wrong choice or inappropriate concentrations of these additives could adversely affect the deposition process.

Figures 9.10 and 9.11 shows the influence of N,N-dimethyldodecylamine (NND) on the deposition behaviour of nickel and silica respectively from a Zn-Ni/SiO_2 composite bath. The results presented in Figure 9.10 shows that for all the current densities investigated, the amount of nickel deposition was higher in the absence of NND in the bath. This is an indication that the presence of NND in the bath was detrimental to the deposition of nickel. Also, Figure 9.11 shows the silica incorporation behaviour with and without NND in the Zn-Ni bath. For the range of current densities investigated, it is clear that the rate of silica incorporation was significantly lower in almost all cases for the baths with NND. The reasons for such behaviour are not very clear. However, it is probably due to possible adsorption of NND onto the surface of the cathode. Visually, the deposits appeared dark and burnt, a further indication of a major change in the deposition/growth process.

The influence of this surfactant on the codeposition behaviour of Zn/SiO_2 was investigated and has earlier been discussed in section 8.2.4. It was found that the presence of NND in the composite bath greatly enhanced the rate of incorporation of 2 μm silica particles.

9.2 Cathodic polarisation studies of Zn-Ni/SiO_2

As with the other systems examined, cathodic polarisation studies were conducted for Zn-Ni/SiO_2 baths in order to understand the deposition kinetics of the composite coatings. The cathodic polarisation investigations were conducted with the same solution formulations as those used in the production of Zn-Ni and Zn-Ni/SiO_2 coatings.

The cathodic polarisation behaviour of Zn-Ni electrolytes with and without SiO_2 under different hydrodynamic conditions is shown in Figures 9.12-9.13. Although the different metal

ions reduction peaks are not very distinct, the curves generally represent two consecutive reductions, in which H^+ and Zn^{2+}/Ni^{2+} are reduced to H_2 and Zn-Ni alloy respectively.

The results presented in Figure 9.12 show that the addition of SiO_2 into the Zn-Ni baths significantly affected the electrochemical behaviour of the codeposition kinetics. It appears that for all the conditions investigated, on addition of SiO_2 in the bath, the deposition potential was shifted to more cathodic potentials, consequently increasing the cathodic polarisation. Furthermore, this behaviour was obviously independent of the prevalent hydrodynamic conditions as it can be seen that the same trend was observed with or without bath agitation. The shift to lower potentials on the addition of particles could be attributed to a decrease in the active surface area of the cathode, owing to the adsorption of particles. Increase in the cathodic polarisation on the addition of inert particles into an electrolytic bath has been reported by other authors [186, 191]. In their study, WU et al [186] reported that cathodic polarisation increases with increase in Al_2O_3 concentration in the bath and cobalt ions in the electrolyte causes a reduction of polarisation whilst nickel ions do not change the polarisation behaviour. Similarly, SHI et al [191] reported that the cathodic polarisation potential of the composite electrolyte increased with increasing Si_3N_4 concentration in the plating bath and attributed it to a decrease in active sites on the cathode due to the adsorption of Si_3N_4 on the surface of the cathode. Furthermore, SHI et al [192] also reported that the cathodic polarisation potential of the composite electrolyte in a Ni-Co/SiC increased with increasing SiC concentration in the plating bath. In all these cases, the cathode current density was shown to decrease as cathodic polarisation occurred with the addition/increase in particle concentration in the bath.

Slightly different observations were made in the previous chapter when 20 nm-sized SiO_2 particles were added to a pure zinc bath. It was observed that as the potential increased to more cathodic regions, the cathode current density simultaneously increased for the baths with SiO_2 both with low and high concentrations of zinc ions. The reasons for such discrepancies are not very clear. However, a number of reasons might be responsible for such behaviour. Firstly, it could be due to particle size and its surface characteristics. In the case of Zn/SiO_2 cathodic polarisation, 20 nm particles were used whilst in that of $Zn\text{-}Ni/SiO_2$, 2 μm particles

were used. It has been argued [133] that in the case of micron-sized particles, negligibly small amount of ions are adsorbed on the surface in comparison to the amount of ions present in the layer of electrolyte of the same thickness as the particle diameter, adjacent to the electrode surface. So it is rather doubtful that the current connected with the reaction of such small amounts contributes to a measurable extent to the electrode reaction. Also, due to the larger particle size of the 2 μm particles, they could provide substantial coverage of the surface of the cathode, large enough to prevent the deposition of metal ions. This could have lead to the decrease in cathode current density when 2 μm particles were added to the Zn-Ni bath. On the contrary, because of the very small nature of the 20 nm particles, metal deposition could still take place with less hindrance. Also, since the surface energy of smaller particles is generally higher than that of larger particles, adsorption of metal ions may be more effective on smaller particles than larger ones. This could lead to an increase in the metal ion concentration on the surface of the cathode due to adsorption of metal ions onto the surface of the 20 nm particles with susbsequent migration to and incorporation in, the electrodeposit. This may have been responsible for the increase in the cathode current density as 20 nm particles were added to the zinc baths. Secondly, the presence of nickel and associated difference in bath composition could also be a possible reason for the difference in polarisation behaviour for the two systems.

Figure 9.13 shows the deposition kinetics of the Zn-Ni baths with particles and at different rates of agitation. Contrary to expectations that the cathodic polarisation would shift to more negative values with increase in bath agitation due to improvement in mass transport of the system, the deposition behaviour appears to be slightly different. As can be seen from Figure 9.13, 300 rpm instead 900 rpm shows the lowest cathode current densities. Although the reasons for such behaviour are not very clear, it is probably associated with the residence time of particles and particle surface coverage per unit time. It is obvious from this figure that shifts towards more cathodic regions increased with decrease in the rate of agitation in the order between 900 rpm, 600 rpm and 0 rpm. However, the highest rate of increase towards more cathodic potential regions was observed at 300 rpm. This is an indication that high adsorption of particles and frequency of particles reaching and remaining on the surface of the cathode was favoured in the absence of agitation and was even greater at 300 rpm. At 300 rpm the

process of transport to the cathode, adsorption and residence time of particles may have been better, consequently providing large surface coverage and reducing the number of active sites on the surface of the cathode and hence decreasing the rate of reduction the of metal ions. This could probably be the optimum rate of agitation for maximum particle incorporation for this system. The higher the amount of particles reaching the surface of the cathode and remaining adsorbed, the higher the tendency for more particles to be incorporated. At very high rates of bath agitation such as 900 rpm, particles are generally thought to be swept away from the surface of the cathode. This may have lead to the increase in the metal iron reduction as a result of lower surface coverage by particles.

9.3 Morphology and microstructure of Zn-Ni/SiO_2 coatings

Figure 9.14 shows the morphology of Zn-Ni/SiO_2 electrodeposits containing 13 wt% nickel and different amounts of SiO_2. A close inspection of Figure 9.14(a) reveals the presence of microcracks in the deposit with a particle content of 2.4 wt%. However, when the SiO_2 content in the coating increased to 11.3 wt% as can be seen in Figure 9.14(b), the microcracks seem to have disappeared. Similarly, Figure 9.15 shows micrographs containing 13.4 wt% of nickel but with slightly different SiO_2 contents in the coatings. Also as can be seen from these micrographs, Figure 9.15(a) with a lower content of SiO_2, shows the clear propagation of microcracks while there were no such features obvious in Figure 9.15(b) with a higher content of SiO_2 in the deposit. These microstructural characteristics show that varying the content of SiO_2 in the zinc-nickel matrix is capable of changing the morphology and hence the microstructure of these coatings. Cracks generally originate from points of weaknesses. The observed changes in the microstructure of these coatings are an indication that at lower content of particles in the deposits, there is possibly a poor dispersion of particles. Therefore dispersion-strenghtening effect by the particles may not have been achieved. As a consequence, incorporated particles could have caused localised stress, which eventually lead to the initiation of cracks due to possible interfacial weaknesses at these points between the particles and the alloy matrix. The occurrence of microcracks after annealing of a Ni-Fe/Si_3N_4 has been reported [193]. However, at relatively higher contents of SiO_2 in the coatings as can be seen in the Figures 9.14(b) and 9.15(b), there appears to be an even distribution of particles

with clearly no cracks in the coatings. Such coatings are likely to exhibit higher corrosion resistance as will be discussed in the next chapter.

CHAPTER TEN

10 EVALUATION OF THE CORROSION PERFORMANCE OF ZINC AND ZINC-NICKEL/SILICA COMPOSITE COATINGS

Evaluation of the corrosion performance of the coatings was mainly carried out using methods based on the neutral salt spray test ASTM B117 and electrochemical linear polarisation resistance measurements.

10.1 Neutral salt spray performance

10.1.1 Conventional Zinc-based coating

Apart from the literature review where properties of other conventional zinc-based coatings such as Zn-Co, Zn-Mn, Zn-Fe and Zn-Sn were investigated, conventional coatings experimentally investigated in the present work were limited to zinc and zinc nickel alloys. Summary of the neutral salt spray performance of nominally 8 μm zinc and zinc-nickel coatings at different electrodeposition conditions are given in table 10.1 below.

Table 10.1 Summary of corrosion performance of zinc and zinc-nickel in a neutral salt spray chamber

Coating system	Current density (A/dm^2)	Agitation type		Alloy element, nickel (wt.%)	Average time to 5 % red rust (hours)
		Vibratory Amplitude (mm)	Magnetic stirring (rpm)		
Acid zinc (2)	2		300		40
	5		300		40
	5		500		45
Acid zinc(3)	2		300		42
	5		300		50
	5		500		53
Acid zinc-nickel (1)	2	0.6		81	21
	2			91	21
	5	0.6		11.7	502
	5			11.4	451

The formulations of acid zinc baths (2) and (3) are given in section 6.3.1

From the results, it can be seen that the corrosion protection properties of samples produced from acid bath (3) were slightly better than those from acid bath (2). All the samples produced from bath (2) showed approximately 40 hours time to 5% red rust whilst for samples from bath (3), the time to 5% red rust was approximately 50 hours. The reasons for such discrepancies are not very clear. However, it is probably due to the differences in bath formulations of the two baths. Acid bath (3) contains $Al_2(SO_4)_3$. The use of $Al_2(SO_4)_3$ along with other additives have been reported [30] to improve the bright and smoothness of zinc electrodeposits. Another reason for the slight difference in corrosion resistance of samples produced from these separate acid zinc baths could be due to possible differences in the morphology and microstructure of these coatings.

Figure 10.1 shows SEM micrographs of the surface morphologies of electrodeposits from the separate baths. As can be seen, Figure 10.1(a) exhibits the usual random crystallographic orientations characteristic of acid zinc baths. However, it is evident from Figure 10.1(b), which was produced from a different bath composition as labelled in the figure caption that the crystallographic orientation appears to have slightly changed from that of random orientation to more of basal orientation. It has been reported [71] that coatings, which have no basal texture, exhibit the highest corrosion current. According to them, as the intensity of the basal texture increases the corresponding corrosion current decreases significantly, and thereby the corrosion resistance of the coatings improves. The slight improvement in corrosion resistance observed between the two acid baths could therefore be attributed to possible changes in crystallographic orientation of electrodeposits produced from the individual baths. And also, visual observation of the coatings showed those, which exhibited higher corrosion rates from the two baths, were brighter and more coherent.

The results in Table 10.1 also show the corrosion performance of zinc-nickel alloys. Obviously, the corrosion performance of zinc-nickel alloys was better than that of ordinary zinc coatings. The poorer corrosion resistance behaviour of zinc coatings to their alloy counterparts has been attributed to its poor barrier protection properties [194]. Other investigators [71] have attributed the corrosion resistance behaviour of zinc to its deposit texture and surface morphology as mentioned earlier, which in turn depends on the range of current densities at which samples were produced. Furthermore, it was noted that coatings with hexagonal basal platelets exhibits better corrosion behaviour than their pyramidal counterparts due to their higher binding energy [71].

Zinc-nickel – As mentioned earlier in previous chapters, zinc alloys could provide good protective properties if it has either low porosity with a high zinc content (which is known to be less noble than steel surface) or, a high content of a more noble component (Co, Ni, Fe) which has a tendency to passivate in certain corrosive media [195]. The corrosion stability depends greatly upon the alloy composition and its homogeneity, which in turn depends on certain deposition parameters [195]. Changes in the composition of zinc-nickel alloys with

changes in parameters such as current density, bath pH, temperature and bath composition have been reported [59, 65, 75].

It can be seen from table 10.1 that the level of corrosion protection of zinc-nickel alloy is significantly higher than that of ordinary zinc and is largely a function of the alloy composition. Zinc-nickel alloy compositions with predominantly nickel in the deposit were found to be less resistant to corrosion than pure zinc. The bath formulation and deposition conditions in such cases appear to have favoured a normal deposition process where the nobler nickel was preferentially deposited. However, at a higher current density of 5 A/dm^2, the deposition process appears to have shifted to an anomalous type and the less noble zinc becomes preferentially deposited. With an average nickel content of about 11.5 wt% in the deposits, the corrosion resistance of the zinc-nickel alloy was substantially improved to a magnitude of over ten times that of pure zinc.

Also, Figure 10.2 shows the relationship between the nickel content of the deposit and the corrosion resistance of the coatings. It is evident that as the nickel content increases from 8.6 wt% to higher values, the corrosion resistance of the coatings also increases simultaneously. At a value of approximately 12 wt% of nickel in the coatings, the corrosion resistance seems to attain a maximum value. From this Figure, it appears that the optimum nickel content in zinc-nickel coatings for maximum corrosion resistance is in the range of about 11 to 13 wt%. This observation is in good agreement with other researchers [71]. PARK and SZPUNAR [71] found that zinc-nickel coatings that have a low (approximately 13 wt%) nickel content show the lowest corrosion current whereas coatings with higher than 15% nickel show a high corrosion current .

It has also been reported [71] that the corrosion behaviour of zinc-based alloys is influenced by the texture, stress in the coatings, phase composition and chemical composition. Although each of these microstructural characteristics is affected by changes in process parameters and it is difficult to separate the role each of them plays in the corrosion resistance of zinc-based alloys, the influence of chemical composition and phase distribution of these coatings on the corrosion behaviour appears to be closely interrelated. In the case of zinc-nickel, it seems that

the ratio of the different types of phases present in the coatings is directly related to the current density and the nickel content of the deposit and hence the rate of dissolution of these coatings. PARK and SZPUNAR [71] reported the presence of η and γ phases in zinc-nickel coatings. They observed that the η phase dominates when the nickel content is about 13 wt% whereas the coatings have both the η and γ phase at 15 wt%, the latter only begins to form at this compositon. As the nickel content of the coatings increases, the γ phase also simultaneously increases leading to higher rates of corrosion. It was concluded that zinc-nickel coatings consisting of the η single phase at the lower nickel content of 13 to 15 wt% have better corrosion resistance than the coatings consisting of the γ secondary phase that has higher than 15 wt% nickel content. The γ phase is thought to be electrochemically nobler than the η phase. This difference in nobility could lead to unequal rates of dissolution due to the possible existence of a local cell between the two phases. Although, X-ray diffraction analysis were not carried out to determine the different phases present in the coatings studied here, morphological differences with changes in nickel content of the deposit seem to give a clue to differences in corrosion rates at various nickel contents in the coatings.

Figure 10.3 shows surface morphologies of zinc-nickel coatings containing different amount of nickel. Comparing the trend of morphological evolution seen in Figure 10.3 as the nickel content of the deposit increases between 8.6 and 13.8 wt% to the trend of corrosion rate shown in Figure 10.2, it is obvious that the nickel content of the deposit is a determining factor in the corrosion behaviour of zinc-nickel coatings. Figure 10.3(a), which was produced at room temperature (25 ^{o}C) with a nickel content of 8.6 wt% showing morphology made of incoherent nodular grains with large gaps between individual grains. Such morphologies could exhibit a high level of porosity, which could lead to unhindered migration of corrosive species such as chloride ions through the coating and enhance galvanic interaction with the underlying steel substrate, consequently becoming poorly corrosion resistant. This may have accounted for its relatively lower corrosion rate compared to others as shown in Figure 10.2. However, as the nickel content of the deposit increased from 8.6 to 11.7 wt% (produced at 30 ^{o}C), it appears there was significant grain refinement resulting in relatively compact and coherent coatings. With further increase in temperature, which was accompanied with a corresponding increase in the nickel content of the deposit to 13.8 wt %, there is the tendency for the grain size even

becoming larger as obvious in Figure 10.3(c). Close observation of these morphologies shows that Figure 10.3(b) appears more compact, smoother and coherent than Figure 10.3a&c. This probably contributed to the better corrosion resistance of these coating with 11.7 wt% nickel as obvious in Figure 10.2. The incoherent nodular morphology of Figure 10.3(c) is likely to account for the poorer corrosion behaviour of the zinc-nickel coatings with nickel content higher than 13 wt% as evident in Figure 10.3.

10.1.2 Corrosion performance of Zn/SiO_2 composite coatings

In this section, findings on the corrosion resistance behaviour of Zn/SiO_2 composite coatings in a neutral salt spray chamber are presented. Most of the results presented here are based on the time to 5 wt% red rust as time to white rust were not recorded since the electrodeposits were in the unpassivated state.

Figure 10.4 shows the corrosion resistance behaviour of zinc-silica composite coatings with different silica contents in the coatings. For the purpose of comparison, pure zinc coating without silica particles produced from a similar sulphate bath without particles were also tested. From this figure, it can be seen that ordinary zinc coatings corroded at about 40 hours. However, with the incorporation of silica particles in the zinc matrix, the hours to 5% red rust obviously increased to higher values. The trend appears to be that of an increasing one as it was evident that increasing the content of silica in the coating simultaneously increased the hours to 5% red rust becoming even more obvious from about 5 wt% SiO_2. Although the method of corrosion measurement was dissimilar to the salt spray method utilised here, HAMID and GHAYAD [120] reported a similar improvement in corrosion resistance when polyethylene (PE) particles were electrolytically incorporated into a nickel matrix. According to them, the corrosion rate of Ni-PE composites was decreased with increase in PE volume percent up to 0.03 m/year with 30 vol.% PE. The decrease was attributed to the presence of PE particles in nickel deposit, which lead to a decrease in its porosity. SURVILIENE et al [196] also reported that SiC particles enhance the corrosion resistance of chromium coating as a result of the structural characteristics of the coatings obtained; namely the size and number of pores.

Figure 10.5 shows the surface morphology and cross-sectional views of Zn/SiO_2 electrodeposits produced from a sulphate bath containing 2 μm particles and NND. As can be seen from this figure, the distribution of silica particles incorporated is quite even on both the surface and the cross-sectional views of the coating. Although, several investigators have reported [149] on the improvement of corrosion resistance when silica particles are incorporated in a zinc electrodeposit, there is no clear explanation on the mechanism of improvement. However, the general tendency could be that of support of corrosion products. The corrosion products of zinc especially in a salt spray environment are generally known to consist of zinc oxide, zinc hydroxide and zinc hydroxychloride. SAKODA et al [197] reported that the corrosion resistance of zinc coated steel is due to the low corrosion current density caused by the formation of insulating zinc hydroxychloride which is a protective corrosion product. According to them, the composite coating has a high corrosion resistance because of the low corrosion current density, which may be affected by the microstructure of the protective corrosion products. It has been proposed that the corrosion products, which are supported by SiO_2 particles, act as a barrier film for the corrosion reaction of the Zn/SiO_2 composite and that the consumption rate of zinc is very low [198-199]. This is probably because, apart from providing support for the corrosion products of zinc, the presence of silica in the coating appears to provide sites for possible interruption of the corrosion current due to their inert characteristics. Furthermore, the presence of silica particles in the zinc coatings could enhance the process of passivation and deactivation of active sites on the coatings probably by providing a physical barrier consequently enhancing the corrosion resistance behaviour.

In Figure 10.4, it was found that the corrosion resistance of the coatings increased with increase in particle content of the coating. Based on this observation, it might be reasonable to suggest that the higher the content of inert particles in the coating, the higher the number of interruption sites for the propagation of corrosion current and hence lower conductivity and dissolution rates. However, this may not be the case at excessively high contents of silica in the coating. Although not investigated in the present work, if the particle content of the coatings continued to increase, there is likely to be an optimum ratio of metal-particle bonding

for maximum corrosion performance. Also, conductivity and capacitance measurements were not carried out on the composite coatings in this work. However, NOWAK et al [133] calculated the dependence of the capacitance of SiC/Ni on the SiC content in the composite coating. According to them, despite the large scatter in the results, the correlation between the capacitance and the SiC content in the composite reveals a decrease in capacitance at increasing content of SiC in the composite coating. Relating this to Figure 10.4, it implies that the presence of more inert particles in the composite coating could lead to lower rates of the coating capacitance and hence increase in the corrosion resistance of the coatings.

Not only does the corrosion performance of Zn/SiO_2 composite electrodeposits depend on the particle content of the coating, it also appears to depend on changes in the microstructure of the coatings due to the presence of these particles. KIMOTO et al [152] stated that the corrosion resistance of zinc plated steel sheets is improved by the dispersion of oxide particles such as SiO_2, Al_2O_3, TiO_2 and is affected by not only codeposition ratio but also by the characteristics of the oxide particles themselves and the microstructure of the codeposit. It has also been reported [200-201] that the presence of particles in the electrolyte leads to extensive modifications of the texture and microstructure of the metal matrix even if they are not incorporated into the deposit.

10.1.2.1 Effect of nitrates on the corrosion resistance of Zn/SiO_2

Figure 10.6 shows the influence of sodium nitrate and vibratory agitation amplitude on the corrosion resistance behaviour of Zn/SiO_2 coatings. Pairs of samples produced at the same rates of solution agitation, one from a bath containing sodium nitrate and the other from a bath without sodium nitrate were subjected to a neutral salt spray test. These investigations were carried out to confirm claims by other researchers [150] that the dispersion of nitrogen compounds at low concentrations together with silica particles into a zinc plating layer stabilises and largely improves its corrosion resistance. The chances of $NaNO_3$ in the ionised form as Na^{2+} and NO_3^{2-} becoming deposited in the zinc layer were quite slim because of their positions in the electrochemical series compared to their Zn^{2+} and SO_4^{2-} counterparts in the bath and therefore not a very significant influence on the Zn/SiO_2 coatings was expected.

However, contrary to expectations, as evident from Figure 10.6, for nearly all the conditions investigated, it is evident that samples produced from the bath containing small amounts of $NaNO_3$ exhibited small, but significantly higher corrosion resistance behaviour. The reasons for this improvement are not fully known [150]. However, it was reasoned [150] that these nitrogen containing compounds may well act on the surface of the zinc plating layer on the surface of the steel sheet during electrogalvanising. Their oxidising action could activate the entire surface of the plating layer so as to permit easy adsorption of silica particles in the electrogalvanising bath. Consequently, silica particles are precipitated and uniformly dispersed and incorporated in the growing zinc matrix. This would then eliminate the instability of corrosion resistance of the coating caused by non-uniform dispersion of silica particles.

Influence of nitrate ions on the morphology of zinc electrodeposit has also been reported by other investigators [169]. According to them, addition of nitrate to an acid zinc electrolyte exerts a marked effect on the morphology of the electrodeposited zinc. Of the several possible explanations of the phenomena the most plausible one seems to be the incorporation of oxide in the deposit as the result of the oxidative power of the nitrate ions, or the modification of the reaction kinetics.

Based on the findings in Figure 10.6 and investigations reported elsewhere [150,169], it might be reasonable to suggest that the presence of nitrogen containing compounds in either a zinc bath or incorporated into a zinc deposits seems to influence the corrosion behaviour of these coatings probably due to their oxidative characteristics or as a 'filler' of possible porosity between the zinc matrix and incorporated particles [150].

10.1.3 Corrosion performance of Zn-Ni/SiO_2 coatings

Figures 10.7 and 10.8 are salt spray results of Zn-Ni/SiO_2 coatings produced from similar baths and electrodeposition conditions with and without bath agitation respectively. In both figures, the results indicate that the trend of corrosion resistance was similar for the baths without silica particles with or without bath agitation. However, for the baths containing 26 g/l silica particles, the corrosion resistance behaviours were slightly dissimilar. For the bath

without agitation as evident from Figure 10.7, there was no obvious trend in the time to 5% red rust for all the current densities investigated with the bath containing silica particles. However, for a similar bath with agitation, as can be seen in Figure 10.8, the time to 5% red rust seems to be decreasing as the current density increases from 3 to 7 A/dm^2.

Furthermore, in an attempt to confirm the influence of particles in the bath on the corrosion resistance of electrodeposits produced from such baths as already shown in Figures 10.7 and 10.8, influence of a higher bath concentration of particles in the baths was investigated using 52 g/l of SiO_2 with similar electrodeposition conditions as those in Figures 10.7 and 10.8. The results in Figures 10.9 and 10.10 also show that samples produced from baths containing silica particles exhibited higher corrosion behaviour than those without particles. Although the conditions of his investigations are slightly different from the present work, BECH-NIELSEN [151] reported that the rate of corrosion of electrodeposited zinc in near-neutral chloride solutions can be lowered by as much as 75% by adding fine, inert particles of substances such as MnO_2 , Fe_3O_4, SiC and TiN to a well stirred solution by stopping the spread of local areas of etching. The corrosion of zinc in neutral to weakly acid chloride solutions takes place via a local attack. There is also spreading of the attack, so that new areas become sites of dissolution. Based on the work of BECH-NIELSEN [151], it might be reasonable to consider that if an ordinary suspension of particles in a well-stirred solution is capable of conferring some amount of corrosion resistance on the zinc electrodeposit, this effect might even be greater if such particles are embedded in the zinc coating itself. This could account for the observed improvement in corrosion behaviour from Figures 10.7-10.10. In this case it was considered that the corrosion resistance was not just as a result of particles in suspension but as incorporated particles in the zinc-nickel matrix as will be seen later.

The overall trend of corrosion resistance shows that in all the electrodeposition conditions investigated, the corrosion resistance of samples produced from the baths containing silica particles were higher than those without silica particles in the baths. As mentioned earlier, this may have been due to texture and microstructural changes, which could occur on the electrodeposits from the baths with particles even when such particles are not incorporated in these coatings.

Table 10.2 Relationship between nickel and silica contents in deposit with time to 5% red rust for Zn-Ni and Zn-Ni/SiO_2 composite coatings.

Type of Coating	Time to 5% red rust (hours)
Zn	40
Zn-11 % Ni	284
Zn-11 % Ni - 1 % SiO_2	408
Zn-11 % Ni – 2 % SiO_2	571
Zn-12 % Ni	502
Zn-12 % Ni - 3.3 % SiO_2	685
Zn-12 % Ni - 4.2 % SiO_2	716
Zn-12 % Ni – 5.0 % SiO_2	740

In order to confirm the influence of silica particles on the corrosion resistance behaviour of Zn-Ni/SiO_2 composite electrodeposits, coatings containing different amount of nickel and silica were prepared and subjected to the neutral salt spray test. Table 10.2 shows the corrosion resistance data of the Zn-Ni/SiO_2 coatings with different contents of nickel and silica particles. Conventional zinc and zinc-nickel alloy data are also included. Two alloy contents with 11 wt% and 12 wt% Ni were chosen as they fall within the widely reported range of 10 to 15% Ni for best sacrificial protection and for ease of comparability as the content of silica changes in the coating. It is obvious from table 10.2 that for both the zinc-nickel coating with either 11% Ni or 12% Ni, the corrosion resistance appears to increase with increase in the particle content of the coating. This trend is quite similar to the trends previously discussed for the Zn/SiO_2 in section 10.1.1.2. Here again, it is considered that the possible enhancement of the corrosion resistance behaviour of these coatings is probably due to support of the corrosion products in the presence of these particles. Similarly, HAMID [134] investigated the salt spray corrosion behaviour of Zn-Co-TiO_2 and found that the corrosion performance of these coatings increased with increase in the volume percent of TiO_2 particles in the coatings. According to them, the high corrosion resistance of Zn-Co-TiO_2 has

been suggested to be due to the formation of $ZnCl_2$, $Zn(OH)_2$ in a network form and to support of the corrosion products by the dispersed TiO_2 particles.

10.2 Linear polarisation resistance studies

The linear polarisation resistance method is one of the most widely utilised electrochemical techniques to produced supplementary data on the corrosion resistance of coatings due to the limited information obtainable from neutral salt spray methods. SHORT et al [72] noted that although the salt spray test is widely employed, it is recognised that only a limited amount of information can be obtained and electrochemical techniques are useful in providing supplementary data. Apart from that, linear polarisation resistance methods do not require large polarisation of the sample being investigated as it is with the case of other techniques such as Tafel extrapolation, which requires polarisation over a large potential range to obtain corrosion data. Often, such data are not representative of the corrosion behaviour particularly during anodic polarisation, which could allow surface changes to occur due to corrosion and/or passivation of the metal. And also, the possibility of excess adsorption of hydrogen or build up of hydroxyl ions at the metal/solution interface during cathodic polarisation could lead to the modification of surface chemistry, making it no longer representative of the actual surface undergoing corrosion [202]. For these reasons, linear polarisation resistance method was chosen and utilised to study the corrosion behaviour of these coatings. Table 10.3 below shows some data.

Two coating systems are represented in table 10.3. Those produced from baths with and without NND. For the purposes of consistency, samples, which were, produced under similar experimental conditions and hence current density of 30 A/dm^2 were chosen to produce Figure 10.11. The results in table 10.3 and Figure 10.11 shows that as the particle content of the deposit increases the linear polarisation resistance value also increases. Similarly for the system produced with NND present in the bath, the linear polarisation resistances of coatings were also found to increase as the particle content increased. This is an indication that the content of silica in the coating has a substantial influence on the corrosion resistance behaviour of these coatings. Moreover, these results appear to be consistent with the results

obtained from the salt spray test discussed earlier and outlined in Figure 10.4. Also, for the purposes of comparison, the average open circuit potential values of the Zn/SiO_2 coatings produced from an NND-free bath are presented in Figure 10.12 as a function of particle content in the deposit. Although, there doesn't seem to be any consistent trend, it appears there is tendency for the rest potential of coatings with higher contents of silica particles to shift towards more cathodic values than those with lower contents of particles. If this is true, the corrosion resistance of coatings with higher particle content of silica should be lower than those with lower particle contents. Thus, contradicting the linear polarisation resistance values. However, assessment of the corrosion resistance of coatings based on rest potentials is not a very reliable standard and therefore could be ignored. Moreover, the number of samples investigated was relatively few. Also, it is noteworthy that even though more negative potentials suggest more active coatings, porosity can follow activity. At very high silica contents, the coatings could exhibit some amount of porosity, which could result in higher activity and thus more negative potentials.

Table 10.3 Rest potential and linear polarisation resistance data for 8 μm Zn/SiO_2 composite coatings in 5 % NaCl solution. Surface area of polarisation was $1cm^2$.

Coating system	Current density (A/dm^2)	SiO_2 in deposit (wt%), 2 μm	Average polarisation resistance (Ω)	Average potential (mV vs SCE)
Zn/SiO_2	30	9.7	624.8	-1048
Zn/SiO_2	30	12.0	436.4	-1040
Zn/SiO_2	30	17.8	891.0	-1076
Zn/SiO_2	30	21.3	1130.6	-1068
Zn/SiO_2 + NND	30	4.1	411.4	-1046
Zn/SiO_2+ NND	30	12.0	540.5	-1069
Zn/SiO_2+ NND	30	17.1	614.8	-1062

The results presented in table 10.4 shows values of the rest potential and linear polarisation resistance data for Zn-Ni/SiO_2 composite coatings containing 12 wt% nickel. The trend of linear polarisation resistance is quite similar to that of Zn/SiO_2 earlier discussed above in the previous paragraph. It is evident from table 10.4 that there is a tendency for the linear polarisation resistance to increase as the particle content of the coating increases. Although not a very large difference, there is also the tendency for the rest potential of the coatings to shift towards more anodic values as the content of SiO_2 in the coatings increases thus making it consistent with the linear polarisation data. According to STERN AND GEARY'S [203] equation the corrosion current of a coating during linear polarisation resistance is inversely proportional to the linear polarisation resistance. Based on this equation and the data presented in tables 10.3 and 10.4, it might be reasonable to suggest that since the linear polarisation resistance appears to increase with increase in particle content of the deposits, the corrosion current will decrease simultaneously. Obviously, the higher the amount of inert components in the composite system, the less reactive such a system could become which could lead to lower dissolution rates and consequently better corrosion resistance. However, this may not always be the case as earlier suggested if the interfacial bonding between the particles and the metal matrix are weak and incapable of holding the particles in place. Also, an implication for the cathodic protection of the underlying steel at excessively higher particle contents and hence LPR values is that the sacrificial protective ability could be lost due to less sacrificial matrix metal. This could hasten the corrosion of the underlying steel substrate. Although investigated in a slightly different electrolyte from that utilised in the present work, typical linear polarisation resistance value for zinc of about 0.1167 KΩ has been reported [9].

Table 10.4 Rest potential and linear polarisation resistance data for Zn-Ni/SiO_2 composite coatings with 12% nickel in 5% NaCl solution.

Serial number	Current density (A/dm^2)	SiO_2 in deposit (wt%), 20 nm	Average polarisation resistance (Ω)	Average potential (mV vs. SCE)
1	3	1.2	809.5	-996
2	3	3.5	873	-983
3	4	5.5	1100	-949
4	5	6.0	961.6	-984

10.3 Anodic polarisation studies

In order to obtain further information on the corrosion resistance of the coatings in question, anodic polarisation studies were carried out on Zn, Zn-Ni, Zn/SiO_2 and Zn/Ni-SiO_2 coatings. Table 10.5 shows the corrosion potentials of Zn/SiO_2 with different contents of 20 nm silica particles in the deposits. Although the values here are pretty close the general tendency is that the corrosion potential increases in the anodic direction as the particle content of the deposit increases. As mentioned earlier, corrosion potentials are not a very reliable parameter for the assessment of corrosion rates of coatings. However, the results in table 10.5 is an indication that the presence and subsequent increase in the particle content of the deposit improves the corrosion resistance of Zn/SiO_2 coatings, thus complimenting the salt spray results discussed earlier in section 10.1.1.2.

Table 10.5 Rest Potential data of Zn/SiO_2 composite coatings during anodic polarisation in 5% NaCl solution.

Serial number	SiO_2 in deposit (wt. %), 20 nm	Average rest Potential (mV vs. SCE)
1	3.2	-1067
2	4.0	-1061
3	5.3	-1058

The anodic polarisation behaviour of Zn, Zn-Ni, Zn/SiO_2 and $Zn\text{-}Ni/SiO_2$ coatings are shown in Figures 10.13-10.19.

10.3.1 Anodic polarisation behaviour zinc and zinc-nickel coatings

Curve A in Figures 10.13 shows the anodic polarisation behaviour of a zinc coating in 5% NaCl solution. On increasing the applied potential above the corrosion potential hereafter abbreviated as E_{corr}, the coating begins to dissolve rapidly as evident from the rapid increase in the current density until it reaches a potential of about -712 mV where a peak in the dissolution current density is attained. With further increase in the applied potential, the current density starts to decrease. The decrease in current density with further increase in potential is probably due to a simultaneous exposure of some portion of the underlying steel substrate in this range of potential. GIRIDHAR and VAN OOIJ [204] reported that reduction of dissolved oxygen to OH^- ions at these localised cathodic sites will not only consume a fraction of the total number of electrons generated from the anodic dissolution of the remaining zinc but also will lead to a steady increase in the pH at the surface of the working electrode. According to them the former effect accelerates the corrosion rates of the remaining zinc and thus increases the fractional cathodic area of exposed steel. It is noteworthy that the net current appearing in the external circuit is the difference between currents due to the anodic and cathodic reactions occurring at the surface of the working electrode exposed to the electrolyte [204].

It has been reported [205] that increase in pH at the cathodic sites due to OH^- generation could lead to the precipitation of zinc corrosion products (oxide, hydroxide and/or hydroxy chlorides of zinc) at these sites. When the remaining zinc has completely dissolved off at a potential of about –600 mV, the whole surface of the working electrode is probably covered by a "passive" film of zinc corrosion products. The constant current density observed within the applied potential range of –600 mV to 400 mV (SCE) is an indication that such a passive film of zinc corrosion products is probably present in this potential region. Further increase in the applied potential above –400 mV appears to have resulted in the destruction of the passive film and consequently rapid anodic dissolution of the steel substrate. Although the formation of such a passive film could not be confirmed in the present work, other investigators [82,204] carried out further investigations on the anodic dissolution behaviour of pure zinc for purposes of comparison and found that such a decrease in current density and passivation does not occur when bulk pure zinc is tested under identical conditions. According to them, in the absence of cathodic sites of exposed steel, the appropriate pH conditions necessary to form the passivating film of corrosion products cannot arise. Evidence given for the possible formation of a passive film was that the potential where rapid dissolution of steel occurred was higher than the rest potential of bare steel. Similarly, as evident from Figure 10.13, the potential at which rapid dissolution of steel occurred was approximately –300 mV (SCE) based on the results elsewhere [204] the rest potential of bare steel is –568 mV (SCE).

In the case of Zn-Ni labelled as sample B in Figure 10.13, the anodic dissolution current density gradually increased up to a critical point and then starts to decrease without exhibiting any obvious passivation behaviour. The peak current densities in these curves show complete dissolution of the coatings and the potential at which, passivation if any, starts to take place. However, it is noteworthy that the dissolution potentials for the Zn-Ni alloy were relatively higher than the pure zinc coatings up to the critical dissolution current density. Also, the critical current density for the Zn-Ni coating was slightly lower than that of pure zinc, which are all indications that the Zn-Ni alloy coatings are likely to be more corrosion resistant than the pure zinc coatings on steel. Neutral salt spray test results in section 10.1.1 seem to support this claim.

10.3.2 Anodic polarisation of Zn/SiO_2

Figure 10.14 show the anodic polarisation behaviour of Zn/SiO_2 coatings containing different amounts of SiO_2 in the deposits. From this figure, it is obvious that the amount of SiO_2 in the coating significantly affects the anodic polarisation behaviour of these coatings. As the SiO_2 in the deposit increased from 5.4 wt% to 22 wt%, there is obviously a corresponding decrease in the peak dissolution current density. Within similar applied potential ranges, the coatings with the highest amount of SiO_2 of about 22 wt% showed the least dissolution current density whilst coatings with the lowest amount of SiO_2 of about 5.4 wt% in the coating showed the highest dissolution current density peak.

The influence of NND in the baths on the anodic dissolution behaviour of Zn/SiO_2 coatings was also investigated and the findings are presented in Figures 10.15 and 10.16. Figure 10.15 shows the anodic polarisation curves of Zn, Zn-8.5 wt% SiO_2 and Zn-8.5 wt% SiO_2 from a bath containing NND. It is also obvious from this figure that the peak anodic current density was highest for pure zinc followed by that with 8.5 wt% SiO_2 whilst the lowest anodic current density was exhibited by the coating with 8.5 wt% SiO_2 which was produced from a bath containing NND. Similarly, Figure 10.16 shows the anodic polarisation curves for Zn/SiO_2 coatings both with 19.6 wt% of SiO_2 and one produced from a bath containing NND. The results, as was with the case for Figure 10.15 show that the peak anodic current density of the coatings from baths containing NND was the lowest. Although anodic polarisation is not the best method for the assessment of the corrosion resistance of coatings as earlier mentioned, it can give useful information. The results in Figures 10.14-10.16 are an indication that the corrosion resistance of these coatings are likely to increase with the presence and/or increase in particles content of the coatings. If that is true, the results also appear to support previous finding on linear polarisation resistance tests presented in section 10.2 that the corrosion resistance of Zn/SiO_2 coatings seems to improve with increase in the SiO_2 content of the coatings.

10.3.3 Anodic polarisation of Zn-Ni/SiO_2 composite coatings

Figure 10.17 shows the anodic polarisation studies of Zn, Zn-Ni and Zn-Ni/SiO_2 labelled samples A, B and C respectively. Zinc and zinc-nickel polarisation curves are included here principally for the purpose of comparison with the Zn-Ni/SiO_2 composite coatings. It is obvious from Figure 10.17 that the corrosion potentials of Zn-Ni and Zn-Ni/SiO_2 are both higher than that of zinc. It can also been seen from this figure that up to the maximum dissolution current densities of each of the coatings, the potentials of Zn-Ni and Zn-Ni/SiO_2 coatings were higher. This is an indication that the corrosion resistance of Zn-Ni and Zn-Ni/SiO_2 are likely to be better than that of pure zinc. However, at a potential of about -500 mV (SCE), it appears the corrosion rate of zinc seems to be lower than the others probably due to the evident passivation behaviour. The dissolution behaviour of Zn-Ni and Zn-Ni/SiO_2 shows that the rest potentials of these coatings are quite close initially but as the applied potential is increased; the dissolution potential of Zn-Ni/SiO_2 appears to shift slightly towards more anodic potentials. It is also obvious that the rapid dissolution of steel occurred at a much higher potential. This is an indication that the presence of SiO_2 particles appears to enhance shifting of the dissolution potential of the Zn-Ni/SiO_2 coatings towards more anodic potential than the Zn-Ni coatings without particles. Although, this is no conclusive evidence that Zn-Ni coatings produced from a bath containing silica particles are more resistant to corrosion than those produced from baths without particles, a number of reasons could be responsible for such behaviour. Firstly, apart from being incorporated in the deposit, presence of SiO_2 in the bath probably changed the deposition behaviour of Zn-Ni leading to changes in deposit texture, morphology and microstructure. As mentioned earlier in this chapter, it has been reported [151] that the presence of particles in the bath could affect the microstructure of the coating and therefore its corrosion resistance. Another possible reason for the observed difference in the anodic dissolution potentials and current densities of Zn-Ni and Zn-Ni/SiO_2 could be as a result of (i) coating thickness, (ii) coating porosity, (iii) uniformity of the coating thickness, (iv) scan rate of the applied potential and (v) composition and conditions (pH, temperature, aeration and stirring) of the electrolyte [204]. SHI et al [192] investigated the corrosion resistance properties of Ni-Co/SiC nanocomposite coatings using the Tafel slope method and found that the nanocomposite coatings exhibited smaller corrosion current densities than the Ni-Co alloy coatings. They attributed the improvement in electrochemical

performance of these coatings to the reduction in defect size of the nanocomposite coatings due to the incorporation of the nanoparticles. Improvements in the microstructure with increase in nano silica contents in the Zn-Ni/SiO_2 composite coatings were also observed in the present work (see Figures 9.15 and 9.16). Furthermore, it has been stated that the deposition of the SiC nano-particles in a composite coating could help to prevent corrosion pits from growing and also accelerate the passivation process of the metal matrix [192].

Figure 10.18 shows the influence of NND on the anodic polarisation behaviour of coatings produced from a Zn-Ni/SiO_2 composite bath with and without NND. From this figure it is obvious that NND in the bath significantly affected the anodic polarisation behaviour of the Zn-Ni/SiO_2 coatings. A unique feature of this figure is that the corrosion potential tends to decrease with increase in the amount of NND in the bath. Furthermore, it is evident from Figure 10.18 that up to the first peak of dissolution current density, the dissolution potential for all the current densities for the coating from the NND-free bath was higher than for those coatings from baths containing NND. Also, whilst in the case of the coating from an NND-free bath which had only a maximum current density peak before the bare steel starts to dissolve at an applied potential of about –165 mV (SCE), coatings from the NND-containing baths showed a second current density peak at an applied potential of about – 415 mV. The current then decreases with slight increase in potential up to –377 mV when the steel substrate probably starts to dissolve. The general trend of dissolution behaviour exhibited by coatings produced from baths containing NND shows that on polarisation from the rest potential of about – 1077 mV (SCE), the coatings rapidly dissolve until a maximum current density at a potential of about – 750 mV is attained. At this potential, as earlier discussed for pure zinc coatings, all the sacrificial coatings would have been dissolved consequently exposing areas of the underlying steel substrate. With further increase in potential, the anodic dissolution current density simultaneously decreases due to the exposure of larger area of the substrate until it reaches a potential of about – 484 mV. A further small potential increase up to – 415 mV produces a further increase in current and then a decrease until – 377 mV when the steel substrate starts to dissolve. A number of reasons could be responsible for this additional peak. Firstly, the presence of NND in the bath probably affected the alloy deposition behaviour and hence the phase distribution in the coatings. Within the potential range of – 484 mV and – 415

mV where a slight increase in the anodic dissolution current density was observed, the presence of a less protective alloy phase appears to be a possibility. A further drop in current density beyond – 415 mV indicates the presence of additional protective film just before steel begins to dissolve at – 377 mV. Apart from the possibility of the presence of less protective alloy phases, another possible explanation to the existence of this additional peak in the "passive" region is that small amounts of NND may have become incorporated in the deposit. The general trend of anodic polarisation behaviour of these coatings investigated in Figure 10.18 shows that the critical dissolution current densities of the coatings produced from the baths containing various amounts of amounts of NND in all cases appears to be lower that that without NND. This is an indication that the presence of NND in the bath could enhance the corrosion resistance of the coatings obtained. The incorporation of surface additives in an electrodeposit is thought to change the properties of the coating. This could either be an improvement of a specific property or a detrimental effect on the coating. It has been reported [206] that the addition of a number of additives showed good response of the passivated deposits, even better than that obtained with some zinc-alloys. It has also been reported [143] that the effect of surfactants can be related to changes in surface roughness of zinc due to surfactant adsorbed on the electrode.

CHAPTER ELEVEN

11 EVALUATION OF THE WEAR RESISTANCE BEHAVIOUR OF ZINC/SILICA AND ZINC-NICKEL/SILICA COMPOSITE COATINGS

During contact of two surfaces in relative motion, wear is the damage of a solid surface involving progressive loss of materials. Occurrence of wear between two unlubricated surfaces in relative motion one against the other presents several interactions both on the macroscale and nanoscale [207]. Zinc and its alloys are relatively soft and ductile; and are highly prone to such wear and degradation when in contact with, and in sliding motion relative to another surface. One possibility to increase the durability and performance of zinc-based coatings for different applications is to deposit them as composite coatings. In this section, results of wear resistance behaviour, when SiO_2 particles are incorporated electrolytically into zinc and zinc-nickel matrices, are presented and attempts to explain the wear mechanism are made.

11.1 Wear characteristics of Zn and Zn/SiO_2 coatings

Figure 11.1 shows the wear rate of zinc coatings without SiO_2 particles under two different loads of 0.8 N and 2.9 N with increasing number of wear cycles. The results show that the weight loss of zinc electrodeposits was lower for a load of 0.8 N than that of 2.9 N in all cases. This is an indication that the wear resistance of pure zinc coatings are likely to decrease with increasing load. Not only is the weight loss higher with a larger applied load, the weight loss values for each of these loads tends to increase with increasing number of cycles. The gradient of weight loss seemingly higher with a larger load than a smaller one which is an indication that the wear rate of pure zinc coatings is likely to be higher with larger loads than smaller loads. This is reasonable because zinc is quite a soft and ductile metal such that on the

application of a large load, the penetration dept of the counter steel ball could generally be greater thus having a larger contact surface area with the coating, a sliding motion of which could lead to substantial removal of the coating.

Similarly, results in Figure 11.2 show the wear behaviour of Zn/SiO_2 composite coatings containing approximately 5 wt% of 20 nm SiO_2 particles in terms of weight loss, investigated under similar experimental conditions as Figure 11.1. The only difference being that in this case, the coating was a composite of zinc and silica. Also evident here is the fact that weight loss values for the larger load of 2.9 N were much higher than those of 0.8 N further underlining the influence of normal load on the level of wear. However, it should be noted here that, the general increasing trend, which was observed in the case of pure zinc with the different loads, was not so obvious in this case as the weight loss values were relatively constant with the increasing wear cycle especially with the larger load of 2.9 N. The reasons for such behaviour is not at first very clear. However, it is assumed here since there were no SEM micrographs taken to show that the wear scar of Zn/SiO_2 could be much larger than the pure zinc such that even at the lowest cycle of 500, the entire coating on the track of the counter steel ball was probably worn out with no further contacts between the diameter of the counter steel ball and the coating. As a result any further increase in the number of cycles beyond 500 cycles would have no significant wear on the coating as the counter steel ball may not have any contact with the rest of the coating out of its wear track consequently normalising the weight loss values. Lower cycles would therefore have been more appropriate for these investigations. Also, although the amount of different loads investigated here are quite small, the consistent higher weight losses observed with the larger load of 2.9 N shows that the wear resistance of these coatings are likely to be better with smaller loads. Although the metal matrix in this case is zinc, it has been reported [208] that reinforcement of SiC particles in an alloy matrix offered improved wear resistance under less severe conditions such as low applied loads, wherein the dispersoid particles could be retained by the matrix due to low cutting depths made by the abrasive particles. The range of loads applied in his investigations was 1, 3, 5 and 7 N. According to these reported investigations, the dispersoid particles deteriorated the wear response of the matrix under more severe conditions of abrasion, such as

at high loads, because of larger cutting depths causing fracturing and partial removal of the reinforcement particles.

Possible explanations to the poorer wear resistance behaviour of the Zn/SiO_2 as compared to its pure zinc counterpart as evident from Figures 11.1 and 11.2 could be as result of abrasive wear due to the presence of SiO_2 particles dispersed in the metal matrix, which in turn depends on the content and nature of the particles in the coating [135,186]. Also, due to the soft and ductile nature of pure zinc, the type of metal-particle bonding in the composite coating may not be strong enough to resist the amount of applied external force aimed at causing wear to take place. Consequently, the harder ceramic SiO_2 particles would have pulled out of the metal matrix and also contributed to further wear of the coating along the wear track as an abrasive component of the composite coating. It has been reported [135] that a competition takes place between the beneficial increase in hardness due to the reinforcing SiC particles codeposited in a nickel coating, and their adverse effect. According to them, although increase in the number density of codeposited particles produces higher hardness and mechanical strength, it could also increase abrasive wear when reinforcing particles are pulled out of the composite coatings during sliding wear.

Similar findings to the present work have been made in other coating systems by other investigators [106,209]. By using depth of worn scars as a measure of the wear performance of Ni and some Ni-based composite coatings, SHRESTHA et al [106] reported that the anti-wear performance of pure Ni was better than that of coating type labelled as $1\text{-}Ni/Al_2O_3$ and 1-Ni/BN respectively. The better wear performance of pure Ni to 1-Ni/BN was attributed to the higher ductility of 1-Ni/BN than the Ni coating [210]. LEVIN et al [208] investigated the erosion resistance of $Ni\text{-}Al_2O_3$ metal-matrix composites produced via hot isostatic pressing (HIP) and electrodeposition techniques and found that for both composites, an increase in Al_2O_3 content led to an increase in erosion rate of the composites and that pure Ni showed the best erosion resistance.

11.2 Wear characteristics of Zn-Ni/SiO_2 coatings

Figure 11.3 shows the wear resistance behaviour in terms of weight loss versus number of wear cycles on Zn-Ni and Zn-Ni/SiO_2 coatings containing 1 wt % and 11 wt % of 20 nm silica particles respectively. As can be seen from this figure, weight loss of the coatings without silica and those with 11 wt% SiO_2 appears to take an increasing trend whilst coatings with only 1 wt% SiO_2 shows a mixed response with increase in the number of wear cycles. However, a unique trend in this figure is the magnitude of weight loss for each of the three types of coatings. It is obvious that for all the number of wear cycles investigated, the weight loss values for the coatings with 1 wt % SiO_2 were lower than those of the Zn-Ni alloy and the alloy with 11 wt% SiO_2. Similarly, weight loss values for the Zn-Ni alloy were lower than coatings with 11 wt% SiO_2. This shows that the wear resistance of Zn-Ni alloy is improved in the presence of approximately 1 wt% SiO_2 but decreases at 11 wt% SiO_2. The effect of silicon content on the mechanical and tribological properties of zinc-aluminium-silicon alloy has been reported [211]. However, it should be noted that the third component in the aforementioned alloy system is silicon and not silica as is in the present work. The authors found that friction coefficient and wear rate of the alloys decreases with increasing silicon content up to 2 wt% Si, but above this level they increased as the silicon content increased further. On analysis of the microstructure and chemical composition of the alloy they found that the addition of silicon had no effect on the dendritic structure of the alloy but formed silicon particles. The increase in wear rate above 2 wt% silicon was attributed to the fact that silicon particles became coarser and formed groups by gathering in certain places consequently leading to the formation of silicon free areas in the matrix and therefore reduction of the reinforcement effect of silicon. The uneven distribution of silicon particles in the alloy was also thought to be responsible for the cracking behaviour of the alloys. This behaviour can be related to that of agglomeration in composite electrodeposition known to be detrimental to the intergrity of the coatings. Similarly, it has been reported [212] that addition of 1% silicon into zinc-based alloys increases their tensile strength, hardness and wear resistance but reduces ductility.

The results presented in Figure 11.3 are in agreement with the other investigators [209]. For both powder processed methods and electrodeposited methods, they found that coatings with the highest amount of particles exhibited the highest erosion rates. Similarly, Figure 11.4(a-c)

shows the surface morphology of Zn-11%Ni, Zn-11%Ni-1%SiO_2 and Zn-11%Ni-11%SiO_2 coatings respectively. The presence of cracks is quite obvious in the coatings containing the highest amount of SiO_2 particles (see Figure 11.4c). Occurrence of such huge cracks is probably due to the presence of a relatively high amount of SiO_2 in the coatings, 11 wt% in this case. Generally, cracks are points of weakness in coatings and could lead to the negative influence of brittle fragmentation caused by increasing microcracking tendency due to the reinforcement phase [208]. It is therefore not surprising that a coating with such cracks showed the weakest resistance to wear.

As further evidence of the poorer wear resistance behaviour of coatings with the highest amount of SiO_2 particles, Figure 11.5 shows the width of each worn groove as a function of increasing load for Zn-11% Ni and Zn-11% Ni-11%SiO_2. It can be seen that for all the applied range of loads, the width of the coatings with 11%SiO_2 was much larger than those without particles in the coating. This is an indication that coatings with 11%SiO_2 were less resistant to wear than those without particles for the prevalent experimental conditions. Also, the lower rate of scatter for the Zn-11% Ni-11%SiO_2 coatings shows the similarity in the behaviour of these coatings. Additionally, Figure 11.6 shows the surface morphologies of typical worn grooves of (a) Zn-11% Ni and (b) Zn-11% Ni-11%SiO_2. It is evident from this figure that the severity of the damage and the size of the worn surface of the coating with 11% SiO_2 was greater than that without particles. This appears to be a confirmation that the wear resistance of Zn-11%Ni-11%SiO_2 is much lower than the same alloy without particles in the coating. Furthermore, the morphologies of the worn surfaces show the presence of material waves [213-214] for the coatings with 11% SiO_2, whilst such features were less obvious for the coatings without particles. Material waves tend to occur when coatings with cracks are subjected to wear.

Reasons for the improvement in wear behaviour of the particles with 1 wt%SiO_2 and reduction with 11 wt% SiO_2 as shown in Figure 11.3 are not very clear. However, a possible explanation is that under lower particle content, the dispersion of the particles in the alloy matrix was relatively even. However, as earlier discussed in previous chapters, at excessively high contents of particles in the bath, agglomeration of particles occur leading to the incorporation

of agglomerates in the deposit. Incorporation of such pockets of agglomerates could lead to localised stress, which possibly contributed to the huge crack propagation obvious in Figure 11.4 (c). This could have caused the high rate of wear observed for coatings containing 11% SiO_2 probably due to the 'ploughing' effect of agglomerated particles. Figure 11.7 shows the influence of increasing load on the wear behaviour of Zn-11%Ni, Zn-11%Ni-1%SiO_2 and Zn-11%Ni-11%SiO_2 at 100 cycles. For the range of loads investigated, the weight loss tends to increase with increasing normal load. It is also noticeable in the same figure that at a lower normal load of 10 N, the weight loss is lower for the coating without particles and increases with increase in amount of particles in the coatings. At slightly higher loads of 15 and 20 N, weight loss of all three types of coatings tends to normalise. However, at the highest load of 25 N, reverse is the case where the weight loss becomes higher for the coatings without particles and decreases with increasing amount of particles for the present conditions of investigation. Similarly, it has been reported [215] that zinc-based matrix alloy exhibited lower wear rate than that of the composite prior to seizure and the trend reversed during seizure. This behaviour has been attributed [215] to the difference in lubricity, thermal stability and load bearing characteristics of microconstituents of the individual coatings. According to them, the low melting characteristics of various microconstituents in the (zinc-based) matrix alloy enabled it to perform better than the composite at low operating temperatures (generated at low speed/pressure) only. On the contrary, higher thermal stability imparted by the dispersoid SiC particles caused the composite to exhibit better wear properties at higher operating temperatures generated at high speed/pressure. This was probably the case with the present work as obvious in Figure 11.7 where the weight loss for the coating without SiO_2 particle was lower than those of the composites with SiO_2 and increased with increasing amount of particles in the coatings at a load of 10 N. On the contrary, the weight loss was highest for the coating without particles and decreases with increase in particle content of the coating at 25 N. A possible explanation of this phenomenon is that at a lower load of 10 N, the major microconstituent (i.e zinc-rich phase η) of the zinc-alloy matrix, reported to have a lubricating nature [3, 216] probably acted as a solid lubricant, which could lead to a lower coefficient of friction, and therefore better wear resistance. However, the microconstituent of the (zinc-based) alloy system being a low melting material is restricted in its positive role to lower operating temperatures [217-218]. Generally frictional heating is likely to be higher at

more severe conditions (i.e higher loads). It has been reported [219] that increasing frictional heating causes larger adhesion of the sample material to the disc making the occurrence of wear more probable. The presence of particles is thought to reduce such frictional heating in case of the composite than the alloy by reducing the effective area fraction of the matrix part of the sample in contact with the counterface [215]. Accordingly, (excessive) adhering tendency of the composite with the counterface reduces over the matrix alloy under identical test conditions, thereby decreasing the extent of frictional heating [215]. This behaviour probably accounted for the observed increase in the wear rate of the alloy without SiO_2 particles at a higher load of 25 N as compared to its composite counterparts in Figure 11.7. It is obvious that at 25 N the weight loss decreases with increase in SiO_2 content of the coatings.

CHAPTER TWELVE

12 CONCLUSIONS AND FUTURE WORK

12.1 Zinc and zinc-nickel electrodeposition

12.1.1 Zinc electrodeposition

Two broad types of baths were studied. Properties of the acid sulphate and alkaline non-cyanide baths were investigated. It was established that;

- Cathode current efficiency of the acid sulphate baths was much higher than that of the alkaline non-cyanide baths practically for all the current densities investigated.
- Solution agitation was slightly detrimental to the current efficiency of the acid sulphate bath. However, cathode current efficiency of the alkaline bath was significantly improved in the presence of solution agitation.
- Electrodeposits from the acid sulphate baths were more coherent and visually more acceptable than the alkaline baths.

12.1.2 Zinc-nickel electrodeposition

For zinc-nickel electrodeposition, a chloride-based acid bath and two sulphate-based acid baths with different compositions were studied under similar experimental conditions and the following conclusions reached;

- Zinc-nickel electrodeposition was found to be anomalous as the less noble zinc was preferentially deposited in the majority of investigations carried out.
- Nickel content of the electrodeposits decreased with increasing current density in practically all cases even though sets of data were produced at different metal ion concentrations and current densities.

- The pH range between 3.5-5.5 was found to be suitable for the production of electrodeposits with a nickel content in the range of 10-15 wt% for optimum corrosion resistance.
- Increase in temperature was found to improve the rate of nickel deposition.
- Increase in nickel ion concentration in the bath was also found to improve the rate of nickel deposition.
- Morphological changes of zinc-nickel electrodeposits were identified to be a function of the nickel content of the deposit, which appears to change with changing deposition parameters.
- Compositional dissimilarities were found on the zinc-nickel samples especially between the centres and edges of the samples. This is attributed to uneven current distribution effects on the sample during electrodeposition.

12.2 Zinc/SiO_2 composite electrodeposition

Zinc/SiO_2 composite electrodeposits have been successfully produced from sulphate baths and the following conclusions reached:

- Increase in bath concentration of particles was found to reduce the CCE of the composite bath. This behaviour is attributed to increase in solution resistance with increasing particle content of the bath. To the contrary, particle incorporation appears to increase with increase in particle loading.
- The rate of particle incorporation was found to be dependent not only on the magnitude, but also, on the type of agitation. Vibratory agitation was more effective than magnetic stirring for the conditions of deposition investigated in the present work.
- Addition of N, N Dimethyldodecylamine cationic surfactant significantly improved the rate of particle incorporation for 2 μm particles. The optimum bath concentration of NND for maximum particle incorporation of 2 μm particles was found to be 2.5 ml/l. Improvement in particle incorporation was not observed with the 20 nm SiO_2 particles. Rather, an inhibitive trend was observed.
- It was found that the level (wt%) of larger particles (2 μm) in the deposits was higher than that of smaller particles (20 nm) in practically all investigations. However,

excessive addition (104 g/l) of 20 nm particles, lead to the incorporation of thick layers of agglomerated SiO_2 particles.

- Cathodic polarisation studies revealed that addition of SiO_2 to the zinc bath increased the zinc deposition current densities. To the contrary, addition of NND to the bath seemed to inhibit the rate of zinc deposition.

12.3 Zinc-nickel/SiO_2 composite electrodeposition

As with its Zn/SiO_2 counterparts, Zn-Ni/SiO_2 electrodeposits were produced from acid sulphate baths with the following findings:

- Influence of current density on the rate of particle incorporation seems to be that of an increasing one to a maximum, a decrease and then an increase although more data points would have confirmed these trends more fully. Also, nickel deposition was favoured in the presence of particles with increasing current density for the experimental conditions investigated in the present work. Effect of current density distribution on the samples show that particle incorporation was higher at the edges where current densities are generally thought to be higher.
- Influence of particle size on the rate of incorporation shows that the amount of larger (2 μm) particles incorporated was higher than that of the 20 nm particles for the entire range of current densities investigated.
- The rate of particle incorporation as a function of particle loading in the bath was similar to that of Zn/SiO_2. The trend appears to be that of an increasing one up to a maximum and then a general tendency to decrease. Optimum particle loading for maximum incorporation for 20 nm SiO_2 particles was established at approximately 40 g/l for the range of current densities studied without agitation. The rate of particles incorporation was significantly increased at higher bath loading beyond 40 g/l in the presence of agitation.
- Nickel deposition appears to decrease with increase in bath concentration of 20 nm SiO_2 particles. This is an indication that there should be an optimum bath concentration of particles for maximum nickel deposition.

- Cathodic polarisation studies show that addition of SiO_2 particles in a Zn-Ni bath shifted the deposition potential to more cathodic values with a corresponding decrease in cathode current density. Rate of bath agitation was also found to have significant influence on the cathodic polarisation behaviour of Zn-Ni/SiO_2 composite bath.
- Morphological and microstructural changes seem to accompany changes in the SiO_2 content of the composite coatings.

12.4 Corrosion performance

Neutral salt spray tests and linear polarisation resistance methods were utilised to assess the corrosion performance of the coatings.

12.4.1 Neutral salt spray

12.4.1.1 Zinc and zinc-nickel coatings

- Time to 5% red rust of ordinary zinc coatings appears to be in the range of 40-50 hours.
- Difference in corrosion behaviour of zinc coatings seems to depend on the texture, morphology and crystallographic orientations of the coatings.
- Corrosion performance of zinc-nickel alloys was significantly better than ordinary zinc coatings. Maximum corrosion resistance of the deposits appears to lie within the range of 11-13 wt% nickel in the deposit. Changes in morphology of zinc-nickel coatings were found to be a function of nickel content in the deposit.

12.4.1.2 Zinc/SiO_2 composite coatings

- SiO_2 particles incorporated in a zinc matrix were found to improve the corrosion performance of zinc coatings. This effect was more obvious from about 5 wt% SiO_2 in the Zn/SiO_2 coatings. The general trend appears to be that of an increasing one with increasing content of SiO_2 in the deposit.
- The mechanism of improvement is considered to be that of support of corrosion products of zinc such as zinc oxide, zinc hydroxide and zinc hydroxychloride by the SiO_2 particles. It is also reasoned that the presence of SiO_2 particles in the zinc matrix

provides sites of possible diversion/or interruption of the corrosion current due to their inert characteristics.

- Presence of nitrates in low concentrations in the Zn/SiO_2 bath was found to improve the corrosion resistance of the Zn/SiO_2 coatings. The improvement was probably due to the oxidising action of nitrate ions and the incorporation of oxides as 'fillers' of possible porosity between the zinc matrix and incorporated particles.

12.4.1.3 Zinc-nickel/SiO_2 composite coatings

- Similar to the of Zn/SiO_2 system, the electrolytic incorporation of SiO_2 particles in a zinc-nickel matrix was found to improve the corrosion resistance of these coatings. Although optimum particle concentration in the deposit for maximum corrosion performance was not established, the corrosion resistance tends to increase with increasing particle content of the deposit from approximately 5 wt % SiO_2.
- For all the deposition condition investigated in the present work, the overall trend shows that the corrosion resistance of samples produced from the baths containing SiO_2 particles were higher than those without particles in the bath.

12.4.2 Linear polarisation resistance

- Electrochemical studies show that the content of SiO_2 particles has a significant influence on the linear polarisation resistance and tends to increase with increase in particle content.
- The polarisation resistance values for Zn/SiO_2 coatings were found to be lower than those of Zn-Ni/SiO_2. However, the trends were similar as each was found to increase with increase in particle content of the coatings.

12.4.3 Anodic polarisation

12.4.3.1 Zinc and zinc-nickel coatings

- Although there was no obvious passivation region for the zinc-nickel coating, the dissolution potential for zinc-nickel alloy was higher than that of pure zinc coating.

Also, the critical dissolution current density was slightly lower than that of zinc coating. Thus indicating better protective tendencies.

12.4.3.2 Zinc/SiO_2 coatings

- Average rest potential values for Zn/SiO_2 coatings tend to increase in the anodic direction with increase in particle content.
- Anodic dissolution current densities appear to decrease with increase in SiO_2 content of the coatings.
- Critical anodic dissolution and passivation current densities were substantially lower for Zn/SiO_2 coatings produced from bath containing NND than their counterparts.

12.4.3.3 Zinc-nickel/SiO_2 coatings

- The anodic dissolution potential of Zn-Ni/SiO_2 appears to shift towards more positive values than Zn-Ni coatings. Also, it was found that the rapid dissolution of steel coated with Zn-Ni/SiO_2 occurred at much higher potentials than those coated with Zn-Ni.
- Prior to the start of steel dissolution, significant decrease in current density was observed for coatings from baths containing NND, whilst this decrease was insignificant for the coating from baths without NND. The decrease appears to be proportional to the concentration of NND in the bath.
- Peak current densities of the coatings from baths containing NND were slightly lower than that without NND in the bath.

12.5 Wear behaviour

- Weight loss of ordinary zinc was lower than that of Zn/SiO_2 and appears to increase with increase in load and number of cycles for the conditions of investigation.
- Wear resistance behaviour of Zn-Ni and Zn-Ni/SiO_2 coatings with different amounts of SiO_2 particles shows that weight loss of Zn-Ni-1 wt %SiO_2 was lower than those of ordinary Zn-Ni and Zn-Ni-11 wt % SiO_2. The wear performance of these coatings took

the following order of 1 wt %SiO_2 > 0 wt %SiO_2 > 11 wt %SiO_2 with increasing number of cycles.

- It was also found that the morphology of the worn grooves were dissimilar with changes in SiO_2 content of the coatings as worn grooves of Zn-11%Ni-11 wt % SiO_2 exhibited re-occurrent wave forms in contrast with that without particles and with 1wt% SiO_2 indicating the presence of a high density of cracks due to the large amount of particles incorporated.
- Wear behaviour of Zn-Ni and Zn-Ni/SiO_2 composites appears to change with the magnitude of load used in the investigations. It was found that the wear resistance decreased in the order of 11 wt % SiO_2 < 1 wt % SiO_2 < 0 wt % SiO_2 at lower loads of 10 N. However, at 25 N the reverse was the case where the wear resistance took the following order of 11 wt % SiO_2 > 1 wt % SiO_2 > 0 wt % SiO_2. This behaviour is attributed to possible differences in thermal stability and hence lubricity of major microconstituents (i.e zinc-rich η phase) due to frictional heating.

12.6 General conclusions

The successful incorporation of SiO_2 particles into zinc and zinc-nickel electrodeposited matrices largely depends on the current density, bath agitation, bath additives, pH, temperature, size and nature of particles. When incorporated, the corrosion and wear behaviour of the composite coatings are largely dependent on the content of SiO_2 particles in the coatings. Finally, the corrosion resistance of zinc and zinc-nickel alloys appears to improve when SiO_2 particles are electrolytically incorporated. However, the mode of wear behaviour of the aforementioned coatings appears to change with changes in wear testing parameters and conditions.

12.7 Future work

Usually most projects based on scientific research are ended with the identification of more problems and new challenges. Also, due to time constraints, all the set goals are usually not met. This project is no exception. It is therefore suggested that the following uncompleted tasks and new challenges identified be investigated in the future:

- It might be useful to investigate other forms of bath agitation such as air sparging. Sedimentary deposition techniques may also be worth investigating for improvement in particle incorporation.
- As an alternative method to the DC method utilised in the present work, pulse plating may be worth investigating to determine its effect on incorporation.
- To have a better understanding of the electrophoretic behaviour of SiO_2 particles in aqueous solution, it might be worth carrying out zeta potential studies.
- Corrosion and wear performance of coatings containing the same weight percent of 2 μm and 20 nm particles should be investigated.
- Further investigations on the corrosion performance of coatings containing the same amount of SiO_2 particles produced with and without NND should be carried out using method such as Electrochemical impedance spectroscopy (EIS), anodic and cathodic polarisation of coatings and deducing the corrosion rates by Tafel extrapolation. Also, XRD analysis of these coatings is necessary to assess their chemical compositions and phase distributions as there were consistent unique peaks identified during the anodic polarisation of coatings produced from Zn-Ni/SiO_2 baths containing NND.
- Friction coefficients and hardness are vital properties closely related to the wear resistance of materials. It is therefore recommended that these be investigated for each of the coatings with different particle contents of 20 nm and 2 μm to determine effects of particle size and optimum contents of particles for maximum friction coefficient, hardness and wear resistance.
- Studies on the wear behaviour under lubricated conditions is also recommended.
- Tribocorrosion studies may also be relevant for a better understanding of the composite tribobological system when subjected to wear.
- Bonding and adhesion strength between organic coatings and these composite coatings may be investigated to study their improvement in the presence of particles which could provide better interlocking between the underlying inorganic composite coating and the top organic coatings possibly due to surface roughness or interfacial gaps between the particles and the matrix.

REFERENCES

[1] G.D. Wilcox and D.R. Gabe, Corr. Sci., **35**, 1251 (1993).

[2] A. Hovestad, L.J.J. Janssen, J. Appl. Eletrochem., **25,** 519 (1995).

[3] S.W.K Morgan, Zinc and its Alloys and Compounds. Ellis Horwood limited. (1985).

[4] C.J. Slunder and W.K Boyd, "Zinc: Its corrosion resistance". Zinc Development Association (1971).

[5] K.R. Trethewey and J. Chamberlin, Corrosion for Science and Engineering, 2nd ed., Longman Group Limited, (1995).

[6] S. Oesch and M. Faller," Environmental effects on materials: The effect of the air pollutants SO_2, NO_2, NO, and O_3 on the corrosion of copper, zinc and aluminium. A short literature survey and results of laboratory Exposure:" Corr. Sci., **39** (9) 1505 (1997).

[7] J.F. Henrikson and A. Rode, in 10th Scandinavian Corrosion Congress, Stokholm. 39 (1986).

[8] J.E. Svensson and L.G. Johansson, J. Electrochem. Soc., **140**, 2210(1993).

[9] M. M. Abou-Krisha, Appl. Surf. Sci., **252** 1035 (2005).

[10] J.H Lindsay, R.F. Paluch, H.D. Nine, Plat. Surf. Finish., **76**, 107 (1989).

[11] Yu. S. Gerasimenko, M.V Nechai, N.A Belousova, Mater. Sci., **35**, 273 (1999).

[12] I. Zouari, F. Lapicque, Electrochim. Acta, **37**, 439 (1992).

[13] X. Ye , J.P Celis, M. De Bonte, J.R.Roos, J. Electrohem. Soc., **141**, 2698 (1994).

[14] D. Vasilakopoulos, M. Bouroushian, N. Spyrellis, Trans. Inst. Met. Finish., **79,** 107 (2001).

[15] A.E. Alvarez, D.R. Salinas, J. Electroanal. Chem., **566** 393 (2004).

[16] G.D. Wilcox and P.J. Mitchell, Trans. Inst. Met. Finish., **65**, 76 (1987).

[17] E. Epelboin, M. Ksouri and R. Wiart, J. Electrochem. Soc., **122**, 1206 (1975).

[18] Kh.M.S. Youssef, C.C. Koch, P.S. Fedkiw, Corr. Sci., **46** 51 (2004).

[19] M.V. Simicic, K.I Popov, N.V. Krstajic, J. Electroanal. Chem., **484** 18 (2000).

[20] V. Velinov, E.Beltowska-Lehman and A. Riesenkampf, Surf. Coat. Technol., **29** (2) 77 (1986).

[21] G.L.M.K.S Kahanda and Tomkiewicz, J. Electrochem. Soc., **136**, 1497(1989).

[22] J.T Kim and J. Jorne, J. Electrochem. Soc., **127**, 8 (1980).

[23] E. Epelboin, Lejay and R. Wiart, Electrochimica Acta **20** 603 (1975).

[24] A.M Alfantanzi and D.B Dreisniger, J. Appl. Electrochem., **31,** 641 (2001).

[25] D.S Baik and D.J. Fray, J. Appl. Electrochem., **31,** 1141 (2001).

[26] B.K Thomas and D. J. Fray, Trans. Inst. Min. Met. Sect., **C 91**, C 105(1982).

[27] D.J. Mackinnon, J.M. Brannen, J. Appl. Electrochem., **9,** 55 (1979).

[28] R. Ichino, C. Cachet, and R. Wiart, Electrochimica Acta, **41** 1031 (1996).

[29] B.C. Tripathy, S.C. Das, P. Singh, G.T. Hefter, V.N. Misra, J. Electroanal. Chem., **565** 49 (2004).

[30] L. Muresan, G. Maurin, L. Oniciu, S. Avram, Hydrometallurgy **40** 335 (1996).

[31] N.M. Martyak, Materials Characterisation **50** 269 (2003).

[32] E.A Kalinnovskii and V.V Sfender, Uhr. Khim. Zh., 23(1995).

[33] J. Bressan and R. Wiart, J. Appl. Electrochem., **9,** 43 (1979).

[34] J.W. Diggle and A. Damjanovic, J. Electrochem. Soc., **119** 1649 (1972).

[35] D.J Mackinnon; J.M. Brannen, V.I Lakshmanan, J. Appl. Electrochem., **9** 603(1979).

[36] J. McBreen (Principal investigator), 'Investigation of the zinc electrode reaction', Annual Report, Brookhaven National Laboratory, October, 1979-september, 1980 Report BNL-51370 as reported in ref. 38.

[37] J. Mcbreen and G. Gannon, Annual Report on subcontract P.O. Box 451 6210, Lawrence Berkeley Laboratory, April. 1983.

[38] V. Jiricny, H.Choi, J.W. Evans, J. Appl. Electrochem., **17**, 91 (1987).

[39] J.L Faltemier and C.W. Tobias, "The effect of hydrodynamic flow in the morphology of electrodeposited zinc" Lawrence Berkeley Laboratory, Report LBL-16485 (September, 1983) as reported in ref. 38.

[40] V. Rangarajan, N.M. Giallourakis, D.K Matlock, G. Krauss, J. Mat. Shaping Technology, **6**, 217(1989).

[41] H.C Rogers, in Ductility, p 31. American society for metals, Metal Park,OH (1968).

[42] D.R Fasnacht and T.J O'Keefe, J. Appl. Electrochem., **10,** 495 (1980).

[43] D.R Fasnacht and T.J. O'Keele, Met. Trans., **B 14B,** 645 (1983) as reported in ref. 38.

[44] M. Maja and Spinelli, J. Electrochem. Soc.,**118,** 1538 (1981).

[45] H. Fubayashi, Ph.D Thesis, University of Missouri Rolla (1972), as reported in ref. 38.

[46] M. M. Jaksic, Surf. Coat. Technol., **28,** 113 (1986).

[47] M.M Jaksic, Surf. Technol., **24,** 193 (1985).

[48] R.D Naybour, Electrochim Acta. **13,** 763(1968).

[49] M. Maja and P. Spinelli, J. Electrochem. Soc.,**118** 1538 (1971).

[50] A.J Gay and F. Bergsma, Electrochim. Acta. **23,** 1067 (1978).

[51] A.F Sammells, Electrolyte stoichiometric considerations for zinc deposition in the zinc-chlorine battery. In J.B Bertowitz and H.P Silverman (eds), Energy storage, Electrochemical society, Pennington NJ 121-129 (1976) as reported in ref. 46

[52] A. Brenner, "Electrodeposition of Alloys" vol. I and II, Academic press, New York and London (1963).

[53] D. Landolt, Electrochim. Acta. **39,** 1075 (1994).

[54] R.B Waterhouse and A.Niku-Lari, Metal Treatment Against Wear, Corrosion, Fretting and Fatigue, Pergamon Press, pp. 195-211 (1988).

[55] M.F. Mathias and T.W. Chapman, J. Electrochem. Soc., **137,** 102 (1990).

[56] M. Benballa, L. Nils, M. Sarret, C. Muller, Surf. Coat. Technol., **123,** 55 (2000).

[57] M. Gavrila, J.P. Millet, H. Mazille, D. Marchandise, J.M. Cuntz, Surf. Coat. Technol., **123,** 164 (2000).

[58] G. Roventi, R. Fratesi, R.A. Della Guardia and G. Barucca, J. Appl. Electrochem., **30,** I73 (2000).

[59] A. Abibsi, J.K Dennis and N.R Short, Trans. Inst. Met. Finish., **69,** 145 (1991).

[60] J.B Bajat, M.D. Maksimovic, V.B. Miskovic-Stankovic, S. Zec, J. Appl. Electrochem., **31,** 355 (2001).

[61] S.S Abd El Rehim, E.E Fouad, S.M.A. El Wahab and H.H Hassan, Electrochim. Acta **41,** 1413 (1996).

[62] F.J. Fabri Miranda; O.E Barica, O.R. Mattos and R. Wiart, J. Electrochem. Soc., **144,** 3441 (1997).

[63] E. Chassaing and R.Wiart, Electrochim. Acta **37,** 545 (1992).

[64] R. Fratesi, G. Roventi, J. Appl. Electrochem., **22,** 657 (1992).

[65] A.M Alfantazi, J. Page, U.Erb, J. Appl. Electrochem., **26,** 1225 (1996).

[66] V.A Knodler, C.J. Raub and E. Raub, Metalloberflacho, **39,** 21(1985) as reported by Ref. 60.

[67] C.Q Jessen. Danish Ph.D Thesis, Publication P.I 89-10-A AP.89-10, Technical University of Denmark (1989) as reported by Ref. 60.

[68] E. Beltowska-Lehman, P. Ozga, Z. Swiatek, C. Lupi, Surf. Coat. Technol., **151-152** 444 (2002).

[69] W. Zhongda, L. Fedrizzi, P.L Bonora, Surf. Coat. Technol. **85,** 170 (1996).

[70] H. Dahms and I.M Croll. J. Electrochem. Soc., **112,** 771 (1965).

[71] H. Park and J.A Szpunar, Corr.sci., **40,** 525 (1998).

[72] N. R. Short, A. Abibsi and J.K. Dennis, Trans. Inst. Met. Finish., **67** 73 (1991).

[73] M. Heydarzadeh Sohi, M. Jalali, Journal of Materials Processing Technology **138** 63 (2003).

[74] A.M Alfantazi, A study on the synthesis, characterisation and properties of pulse-plated ultrafine-grained Zn-Ni Alloy coatings. Ph.D Thesis, Queen's University, Kingston Ontario, 1994 as reported in ref. 71.

[75] S. Rajendran, S. Bharathi, T. Vasudevan, Trans. Inst. Met. Finish.; **78,** 129 (2000).

[76] J.A Wharton, G.D. Wilcox and K.R. Baldwin, Trans. Inst. Met. Finish.; **77** (4) 152 (1999).

[77] G. Chawa, G.D. Wilcox and D.R. Gabe, Trans. Inst. Met. Finish.; **76** (3) 117 (1998).

[78] J.D. Jensen, G.W. Critchlow and D.R. Gabe, Trans. Inst. Met. Finish., **76** (5) 187 (1998).

[79] J.D. Jensen, D.R. Gabe, G.D.Wilcox. Surf. Coat. Technol., **105,** 240 (1998).

[80] S.S. Abd El Rehim, E. Emad, M. Khaled, M. Fettouhi and J. Shirokoff, Trans. Inst. Met. Finish.; **79** (3) 95 (2001).

[81] E. Gomez, E. Pelaez, E. Valles, J. Electroanal. Chem., **469** 139 (1999).

[82] M. Simmons, Ph.D Thesis, Loughborough University, 2001.

[83] V. Narasimhamurthy and B.S Sheshadri, Trans. Inst. Met. Finish., **77,** 29 (1999).

[84] S. M. Rashwan, A. E. Mohamed, S. M. Abdel-Wahaab and M. M. Kamel, J. Appl. Electrochem., **33** 1035 (2003).

[85] S.S Abd El Rehim, M.A.M. Ibrahim, S.M. Abd El Wahaab and M.M Dankeria, Trans. Inst. Met. Finish., **77,** 31 (1999).

[86] Z. Tu, Z. Yang, M. An, W. Li, and J. Zhang, Trans. Inst. Met. Finish., **77,** 246 (1999).

[87] G. D. Wilcox and B. Petersen, Trans. Inst. Met. Finish.; **74,** 115 (1996).

[88] D. Sylla, J. Creus, C. Savall, O. Roggy, M. Gadouleau, Ph. Refait, Thin Solid Films **424** 171 (2003).

[89] N. Boshkov, Surf. Coat. Technol. **172** 217 (2003).

[90] C. Muller, M. Sarret, T. Andreu, Electrochim. Acta, **48** 2397 (2003).

[91] B. Bozzini, E. Grikonis, A. Fanigliulo, A. Sulcius, Surf. Coat. Technol., **154,** 294 (2002).

[92] K. N. Srinivasan, M. Selvam, S. Venkata Krishna Iyer, J. Appl. Electrochem., **23,** 358 (1993).

[93] A. Sulcius, G. Buineviciene B. Stulpinas, Soviet Electrochem., pp. 1172-1174 (1988) as reported in ref 87.

[94] St. Vitkova, V. Ivanova, G Raichevsky, Surf. Coat. Technol., **82,** 226 (1996).

[95] P.M. Vjatchslav, Electrolititcheskoe osajddenie splavov, mash, Leningrad, 1977.

[96] O.A Ashiru, J. Shirofoff, Appl. Surf. Sci., **103** 159 (1996).

[97] K. Wang, H.W. Pickering, K.G. Weil, Electrochim. Acta **46** 3835 (2001).

[98] E. Guaus, J. Torrent-Burgues, J. Electroanal. Chem., **549** 25 (2003).

[99] L. Benea, P.L. Bonora, A.Borello, S. Martelli, F. Wenger, P. Ponthiaux and J. Galland, J. Electrochem. Soc., **148 (7)** C461 (2001).

[100] K. Helle and F. Walsh. Trans. Inst. Met. Finish., **75,** 53 (1997).

[101] J.P. Celis and J.R. Roos, J. Electrochem. Soc., **124** 1508 (1977).

[102] N. Guglielmi, J. Electrochem. Soc., **119** 1009 (1972).

[103] A.M.J. Kariapper, J. Foster, Trans. Inst. Met. Finish., **52** 87 (1974).

[104] J.P. Celis, J.R. Roos and C. Buelens, J. Electrochem. Soc., **134** 1402 (1987).

[105] B. Bozzini, Trans. Inst. Met. Finish., **77** 135 (1999).

[106] N.B. Shrestha, K. Sakurada, M. Masuko, T Saji, Surf. Coat. Technol., **140** 175 (2001)

[107] C. Filiatre, C. Pignolet, A. Foissy, M. Zembala, P. Warszynski, Colloid and Surfaces A: Physiochem. Eng. Aspects **222** 55 (2003).

[108] H. Matsuda, Y. Kiyono, M. Nishira and O. Takano, Trans. Inst. Met. Finish., **72(2)** 55 (1994).

[109] J.N. Balaraju, T.S.N. Sankara Narayanan and S.K. Seshadri, J. Appl. Electrochem. **33** 807 (2003).

[110] I. Rajagopal, *in* T.S. Sudarshan (Ed.) 'Surface Modification Technologies: An Engineering Guide' (Marcel Dekker, New York, 1989).

[111] N. Felstein, T. Lancsek, D. Lindsay, and L. Salerno, Met. Finish., **81**, 35 (1983).

[112] M.D. Feldstein. Plat. Surf. Finish., **85,** 248 (1998).

[113] M. Nishira and O. Takano, Plat. Surf. Finish., **81**, 48 (1994).

[114] C. Kentepozidou, C. Kiparissides, F. Kotzia, C. Kollia, N.J. Spyrellis, Mat. Sci., **31,** 1175 (1996).

[115] J.L. Stojak and J.B. Talbot. J. Electrochem. Soc., **146,** 4504 (1999).

[116] J.P Celis and J.R. Roos, 'Electrolytic and Electroless Composite Coatings'. Review in coatings and corrosion **5**, 1(1982).

[117] I. Zhitomirsky, Advances in Colloids and Interface Science **97** 279 (2002).

[118] S Wang, W J. Wei, Material Chemistry and Physics **78** 574 (2003).

[119] S.H Yeh and C.C. Wan, Plat. Surf. Finish., **84** 54 (1997).

[120] Z. Abdel Hamid, I.M Ghayad, Materials Letters **53** 238 (2002).

[121] A. Takahashi, Y. Miyoshi and T. Hada, J. Electrochem. Soc., **141** (4), 954 (1994).

[122] D. Aslandis, J. Fransaer, and J.P Celis, J. Electrochem. Soc., **144** (7), 2352 (1997).

[123] S.H Yeh and C.C. Wan, J. Appl. Electrochem., **24**, 993 (1994).

[124] D.R. Gabe, Trans. Inst. Met. Finish., **81** (1) 7 (2003).

[125] C.P.S. Johal, M.R Kalantary and D.R. Gabe, Trans. Inst. Met. Finish., **67** 31 (1989).

[126] M.R Kalantary and D.R. Gabe, Trans. Inst. Met. Finish., **67** 28 (1989).

[127] J. Zhu, L. Liu, G. Hu, B. Shen, W. Hu, W. Ding, Materials Letters **58** 1634 (2004).

[128] C. Muller, M. Sarret, M. Benballa, Surf. Coat. Technol., **162** 49 (2002).

[129] Y. L Wang, Y.Z. Wan, Sh.M. Zhao, H.M. Tao, X.H. Dong, Surf. Coat. Technol., **106** 162 (1998).

[130] P.A. Gay, P. Bercot, J. Pagetti, Surf. Coat. Technol., **140** 147 (2001).

[131] M. Ghorbani, M. Mazaheri, K. Khangoli, Y. Kharazi, Surf. Coat. Technol., **148** 71 (2001).

[132] S.K. Kim, H.J. Yoo, Surf. Coat. Technol., **108-109** 564 (1998).

[133] P. Nowak, R.P. Socha, M. Kaisheva, J. Fransaer, J.P. Celis and Z. Stoinov, J. Appl. Electrochem., **30** 429 (2000).

[134] Z. Abdel Hamid, Anti-corrosion Methods and Materials **48** 235 (2001).

[135] I. Garcia, J. Fransaer, J. P. Celis, Surf. Coat. Technol., **148** 171 (2001).

[136] M.R. Porter, Handbook of Surfactants, Second ed., Blackie Academic & Professional, 1994.

[137] B. Jonsson, B. Lindman, K. Holmberg and B. Kronberg, Surfactants and Polymers in Aqueous Solutions, John Wiley (1998).

[138] D.C. Cullum, Introduction to Surfactant analysis, First ed., Blackie Academic & Professional, (1994).

[139] A.B. Vidrine and E.J. Podlaha, J. Appl. Electrochem., **31** 461 (2001).

[140] K.H. Hou, M.D. Ger, L.M. Wang, S.T. Ke, Wear **253** 994 (2002).

[141] M.D. Ger, Materials Chemistry and Physics **87** 67 (2004).

[142] J. Fransaer, E. Leunis, T. Hirato and J.P. Celis, J. Appl. Eletrochem., **32,** 123 (2002).

[143] A. Hovestad, R.J.C.H.L. Heesen, L.J.J. Janssen, J. Appl. Eletrochem., **29,** 331 (1999)

[144] N.K. Shrestha, M. Masuko, T. Saji, Wear **254** 555 (2003).

[145] Z. A. Hamid and A.M.A. Omar, Anticorrosion Methods and Materials **46** (3) 212 (1999).

[146] I.Zhitomirsky,http://www.tms.org/pubs/journals/JOM/0001/Zhitomirsky/Zhitomirsky-0001.html 09/01/2003.

[147] K. Kondo, A. Ohgishi and Z. Tanaka, J. Electrochem. Soc., **147** (7), 2611 (2000).

[148] M. Hiramatsu and H. Kawasaki, *Hyomen-gijitu'* **40,** 406 (1989).

[149] S. Hashimoto and M. Abe, Corr. Sci., **36** (12) 2125 (1994).

[150] M. Abe, S. Yukimitsu, A. Takeshi and N. Hiroshi, United States Patent, 4,839,241 June, (1989).

[151] G. Bech-Nielsen, Corr. Sci., **38** (8) 1385 (1996).

[152] M. Kimoto, A. Yakawa, T. Tsuda, R. Kammel, Metal **44** (12) 1148 (1990).

[153] S. Rossi, F. Chini, G. Straffelini, P.L. Bonora, R. Moschini, A. Stampali, Surf. Coat. Technol., **173** 235 (2003).

[154] Q. Zhao, Y. Liu, H. Mueller-Steinhagen, G. Liu, Surf. Coat. Technol., **155** 279 (2002).

[155] S. Rossi, F. Deflorian, L. Fedrizzi, Proceedings of Eurocorr' 97, Trondheim N, 22/09/97; p. 57, NTNU, 1997.

[156] D. Weng, P. Jokiel, A. Uebleis, H. Boehni, Surf. Coat. Technol., **88** 147 (1996).

[157] Z. Guo and X. Zhu, Materials Science and Engineering **A363** 325 (2003).

[158] C. Donnet and A. Erdemir, Surf. Coat. Technol., **180-181** 76 (2004).

[159] K. Holmberg and A. Matthews, in: D. Dowson (Ed.), Coating Tribology, Elsevier, 1 (1994).

[160] M. Ward, B.Eng. Loughborough University of Technology, Loughborough, UK. (1995).

[161] M.R. Kalantary, S.A. Amadi and D.R. Gabe, Circuit World, **5**, 42 (1989).

[162] R.O. Hull. J. Am. Electroplat. Soc.,. **27**, 52 (1939).

[163] M. Wery, J.C. Catonne and J.Y. Hihn. J. Applied Electrochem., **30**, 165 (2000).

[164] N.M. Martyak, A. Jones, R. Wormuth. High speed zinc galvanising from methanesulfonate solution. Zinc-based steel coating systems: production and performance. Warrendale (PA): The Minerals, Metals and Materials Society; 1998. p. 293-301 as reported in ref. 31.

[165] D.R. Gabe, Trans. Inst. Met. Finish., **79** B78 (2001).

[166] T.D McColm and J.W. Evans. J. Appl. Electrochem., **31**: 411 (2001).

[167] I. Mirkova, M. Monev, I. Krastev, S. Raskov. Trans. Inst. Met. Finish. **73(3)** 107 (1995).

[168] A.C. Scott, R.M. Pitblado, G.W. Barton and A.R. Ault. J. Appl. Electrochem., **18** 120 (1988).

[169] A.J. Gay and F. Bergsma, Electrochim. Acta **23** 1067 (1978).

[170] H. Ashassi-Sorkhabi, A. Hagrah, N. Parvini-Ahmadi, J. Manzoori, Surf. Coat. Technol., **140** 278 (2001).

[171] F. Elkhatabi, M. Benballa, M. Sarret, C. Muller, Electrochim. Acta **44** 1645 (1999).

[172] R. Ramanauskas, P. Quintana, L. Maldonado, R. Pomes, M.A. Pech-Canul, Surf. Coat. Technol., **92** 16 (1997).

[173] A.M Alfantazi, G. Brehaut, U.Erb, Surf. Coat. Technol., **89** 239 (1997).

[174] A.M Alfantazi, A.M El-sherik, U.Erb, Scripta Metallurgica et Materialia **30** 1245 (1994) as reported in ref 65.

[175] K. Shrestha, I. Miwa, T. Saji, J. Electrochem. Soc., **48**, 85 (2001).

[176] C. Kerr, Barker, F. Walsh, J. Archer, Trans. Inst. Met. Finish., **78**, 171 (2000).

[177] K. Helle, Report AKZO research, Arnhem (1993) as reported in ref. 143.

[178] M. Hiramatsu, H. Kawasaki, Y. Nakayama and T. Omi, Plat. Surf. Finish., **74(7)**, 48 (1987).

[179] J.P. Fransaer, J.P Celis and J.R. Roos , J. Electrochem. Soc., **139**, 413 (1992).

[180] G. Maurin, A. Lavanant, J. Appl. Electrochem., **25**, 1113 (1995).

[181] A. Afshar, M. Ghorbani, M. Mazaheri, Surf. Coat. Technol., **187** 293 (2004).

[182] Apachitei, J. Duszcyzyk, L. Katgerman and P.J.B. Overkamp, Scripta Materiala, **38**, 1347 (1998).

[183] Apachitei, J. Duszcyzyk, L. Katgerman and P.J.B. Overkamp, Scripta Materiala, **38**, 1383 (1998).

[184] A. Cabot and A. Foissy, J. Materials Science **33** 3945 (1998).

[185] S. Wang and W. J. Wei, Materials Chemistry and Physics **78** 574 (2003).

[186] G. Wu, N. Li, D. Zhou, K. Mitsuo, Surf. Coat. Technol., **176** 157 (2004).

[187] K. Nishimura, Y. Miyoshi, T. Hada, J. Met. Finish. Jpn., **38** 217 (1987).

[188] J. Surowka, A. Budniok, B. Bzowski, J. Warczewski, Thin Solid Films **307** 233 (1997).

[189] A. Takahashi, Y. Miyoshi and T. Hada, Surf. Technol. **44 (11)** 977 (1993).

[190] M. Ramasubramanian, S.N. Popova, B.N. Popov and R.E. White, J. Electrochem. Soc., **143(7)**, 2164 (1996).

[191] L. Shi, C.F. Sun, F. Zhou, W.M. Liu, Materials Science and Engineering **A 397** 190 (2005).

[192] L. Shi, C.F. Sun, F. Zhou, W.M. Liu, Appl. Surf. Sci., Article in press (2005).

[193] X. Li, Z. Li, Materials Science and Engineering **A 358,** 107 (2003).

[194] K.R. Baldwin and C.J.E Smith, Trans. Inst. Met. Finish., **74(6)**, 202 (1996).

[195] J.B. Bajat, V.B. Miskovic-Stankovic, Progress in organic coatings **49,**183 (2004).

[196] S. Surviliene, A. Lisowska-Oleksiak, V. Jasulaitiene and A. Cesuniene, Trans. Inst. Met. Finish., **83(3)**, 130 (2005).

[197] A. Sakoda, N. Usuki, S. Wakano and M. Nishihara, J. Surf. Finish. Soc., Jpn. **40**, 164 (1989).

[198] M. Abe, Y. Shiohara and A. Okado, Zinc-based coating systems. The Minerals, Metals& Materials Society, 171 (1989).

[199] M. Abe, S. Hashimoto, T. Nishimura and Y. Shiohara, Automotive Corrosion and Prevention conference & Exposition, SAE 932356 (1993).

[200] J.P Bonino, S. Loubiere and A. Rousset, J. Appl. Electrochem., **28,** 1227 (1998).

[201] R.P. Socha, P. Nowak, K. Laajalehto and J. Vayrynen, Colloids and Surfaces A: Physicochem. Eng. Aspects, **235,** 45 (2004).

[202] J.R. Scully and D.W. "Taylor. Laboratory testing - Electrochemical Methods of Corrosion Testing." *ASM Handbook*, 9th Ed. '*Corrosion*' ASM International. **13,** (1987).

[203] M. Stern and A.L Geary, J. Electrochem. Soc., **104**(1) 56 (1957).

[204] J. Giridhar and W.J. Van Ooij, Surf. Coat. Technol., **53** 35 (1992).

[205] I. Suzuki, Corr. Sci., **25** 1029 (1985).

[206] G. Barcelo, M. Sarret, C. Muller and J. Pregonas, Electrochimica Acta, **43 (1-2)** 13 (1998).

[207] M.D. Acunto, Nanotechnology, **15** 795 (2004).

[208] B.K. Prasad, Wear **252** 250(2002).

[209] B.F. Levin, J.N. DuPont and A.R. Marder, Wear **238** 160 (2000).

[210] O.A. Leon, M.H. Staia, H.E. Hintermann, Surf. Coat. Technol., **120-121 641 (1999).**

[211] T. Savaskan and A. Aydiner, Wear **257** 377 (2004).

[212] G. Purcek, T. Savaskan, T. Kucukomeroglu, S. Murphy, Wear **252** 894 (2002).

[213] J.M. Durand, M. Vardavoulias, M. Jeandin, Wear **181-183** 833 (1995).

[214] X.S. Xing and R.K.Y. Li, Wear **256** 21 (2004).

[215] B.K. Prasad, Wear **254** 35 (2003).

[216] R.J. Barnhurst, J.C. Farge, in: G.P. Lewis, R.J. Barnhurst, C.A Loong (Eds.), Proceeding of the International Symposium on Zinc-Aluminium (ZA) Alloys, 25th Annual Conference of Metallurgists, Metallurgical Society of Canadian Institute of Metals, 17-20 August 1986, pp. 85-105.

[217] B.K. Prasad, Metall. Mater. Trans. **A 28A** 809 (1997).

[218] B.K. Prasad, A.K. Patwardhan, A.H. Yegneswaran, Metall. Mater. Trans., **A 27A** 3513 (1996).

[219] B.K. Prasad, Wear **240** 100 (2000).

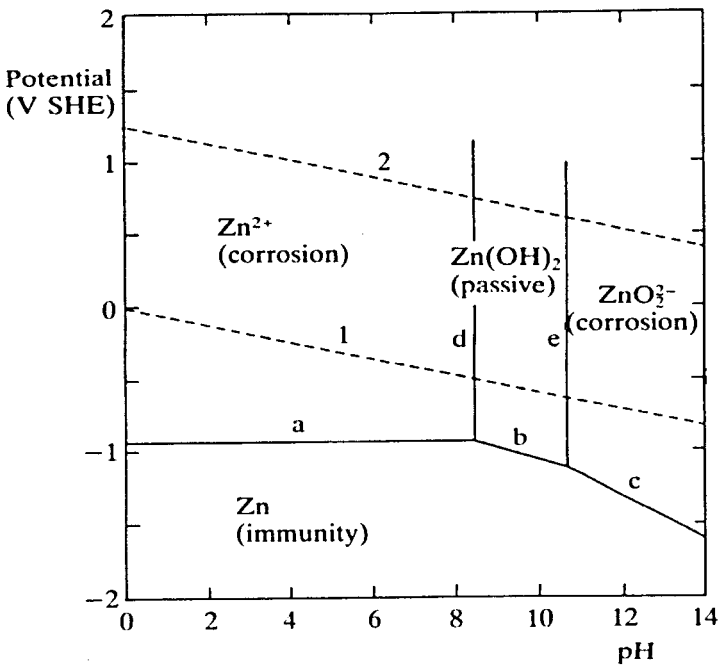

*Figure 2.1 E/*pH diagram of zinc in water (adapted from ref. 5)

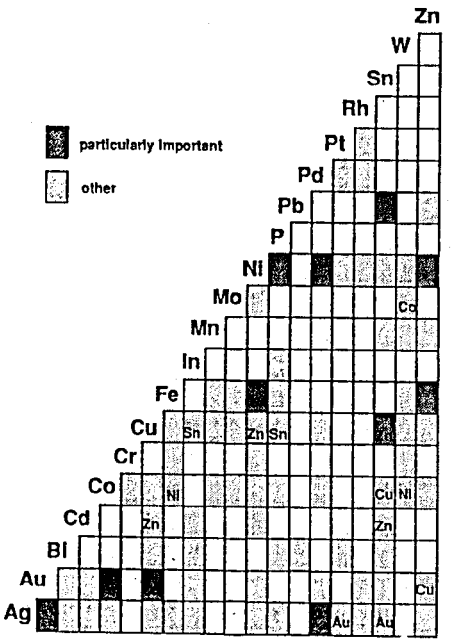

Figure 4.1 **Electrodeposited binary and ternary alloys. The dark grey areas denote alloys of particular importance. The chemical formulae indicate a third alloy element added to form ternary alloys [52].**

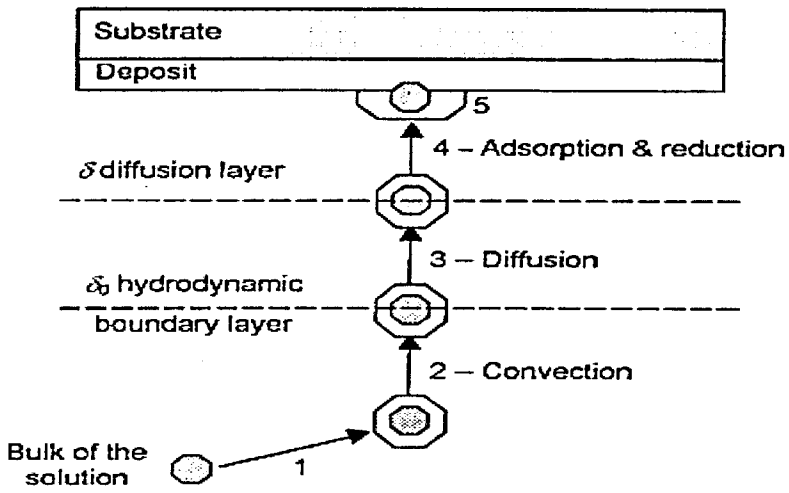

Figure 5.1 **Stages in the incorporation of an inert particle in an electrodeposit**

1. Formation of ionic cloud around the particle. 2. Convection of the particle towards the electrode surface. 3. Diffusion of the particle through a hydrodynamic boundary. 4. Diffusion through a concentration boundary layer. 5. Adsorption and reduction of the particle into the growing deposit [104].

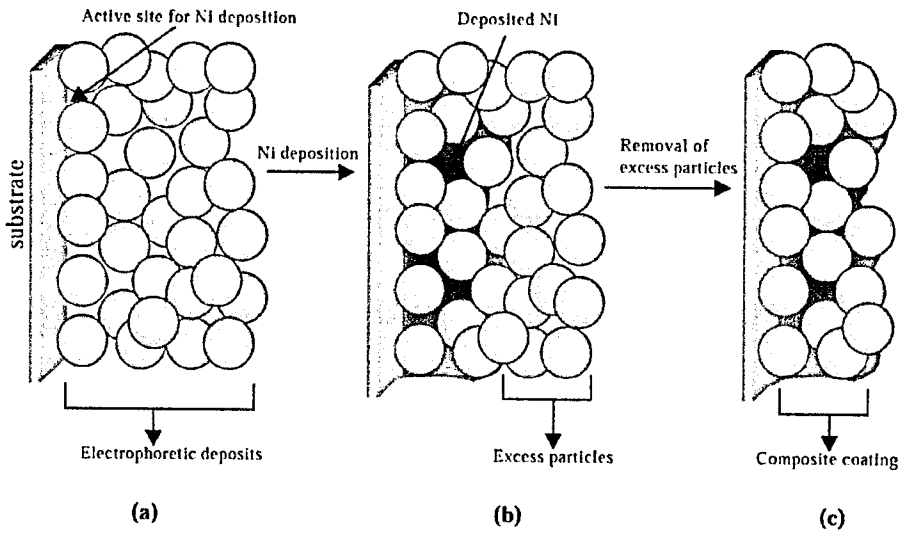

Figure 5.2 **Scheme showing the two-step method of composite coating (adapted from Ref 106). (a) Electrophoretic deposits by the first step; (b) Composite after nickel deposition in the second step; and (c) Composite after removing the excess particles that are loosely adsorbed to the surface.**

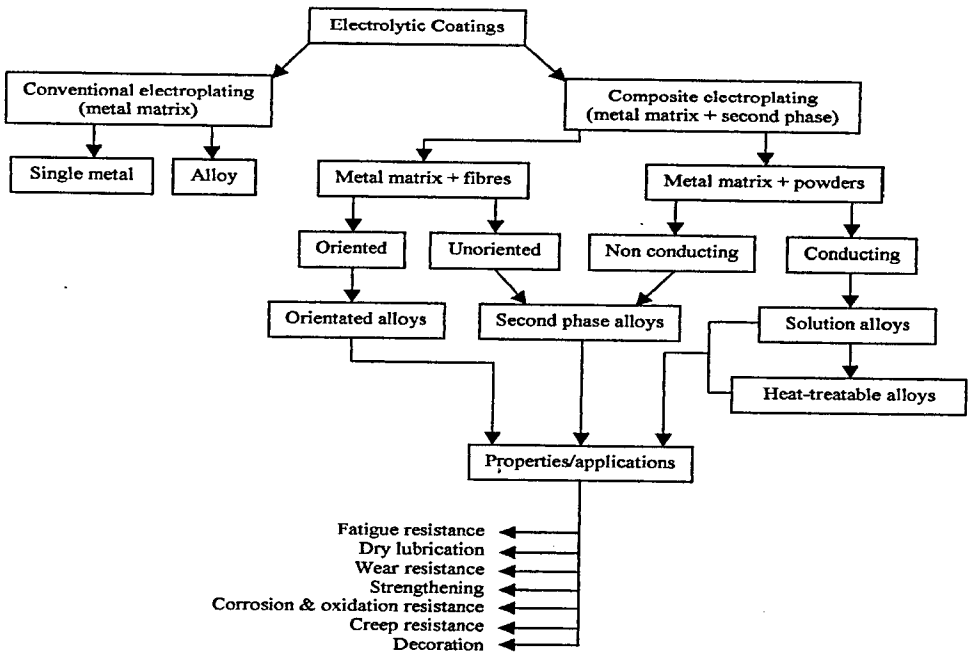

Figure 5.3 **Types of materials obtained by electrodeposition (Adapted from Ref. 116)**

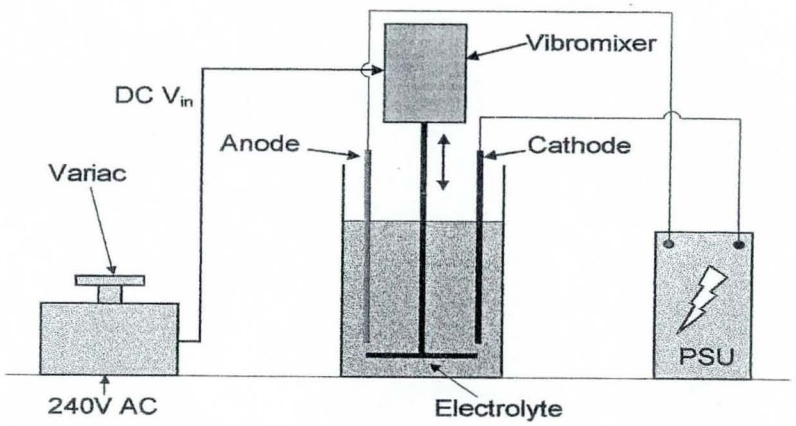

Figure 6.1 **Vibromixer Apparatus (adapted from Ref. 82)**

Figure 6.2 **Photograph of the experimental apparatus showing (A) Vibromixer (B) Power supply unit (C) Variac motor (D) Water bath (E) Electrolyte with submerged agitator disc.**

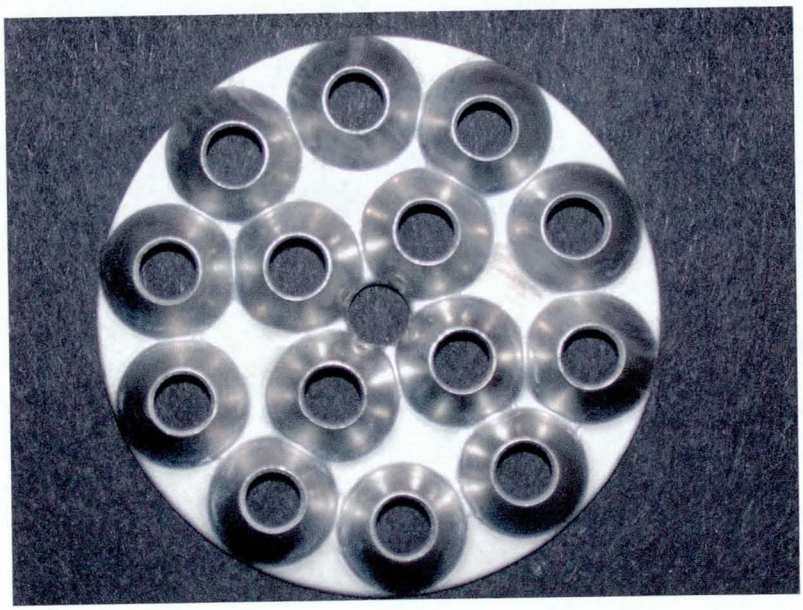

Figure 6.3 **Photograph of the top view of the agitator disc showing perforated conical discs.**

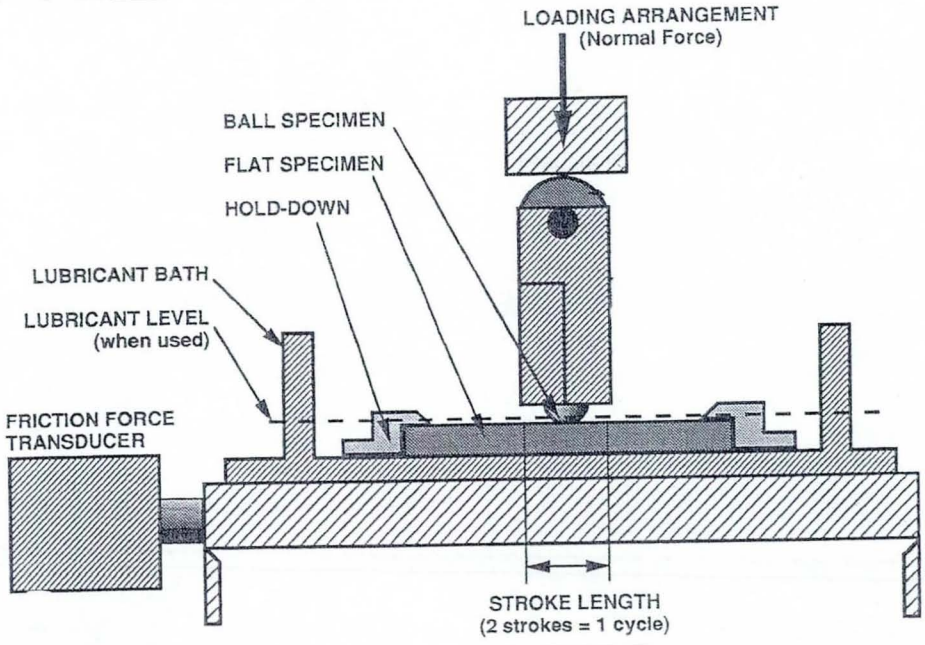

Figure 6.4 **Schematic diagram of the reciprocating wear test (Adapted from Ref. 158 with slight modifications).**

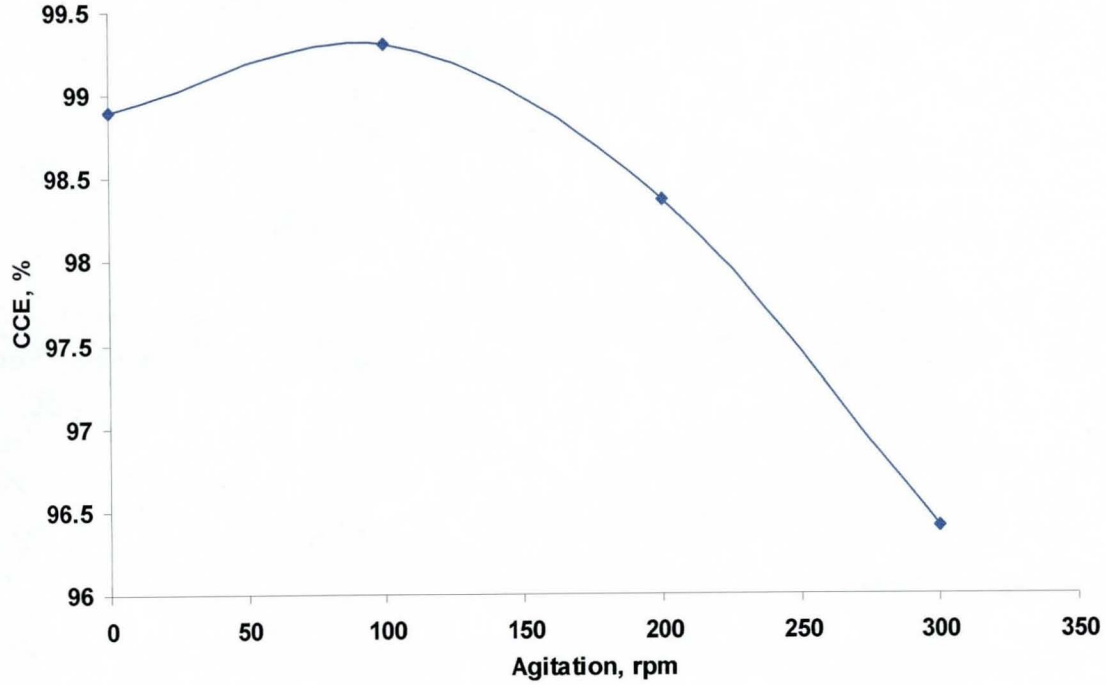

Figure 7.1 **Effect of bath agitation on the cathode current efficiency of the bath containing 250 g/l $ZnSO_4.7H_2O$, 80 g/l Na_2SO_4. Current density 5 A/dm^2, pH 2.8, T= 22 ^oC.**

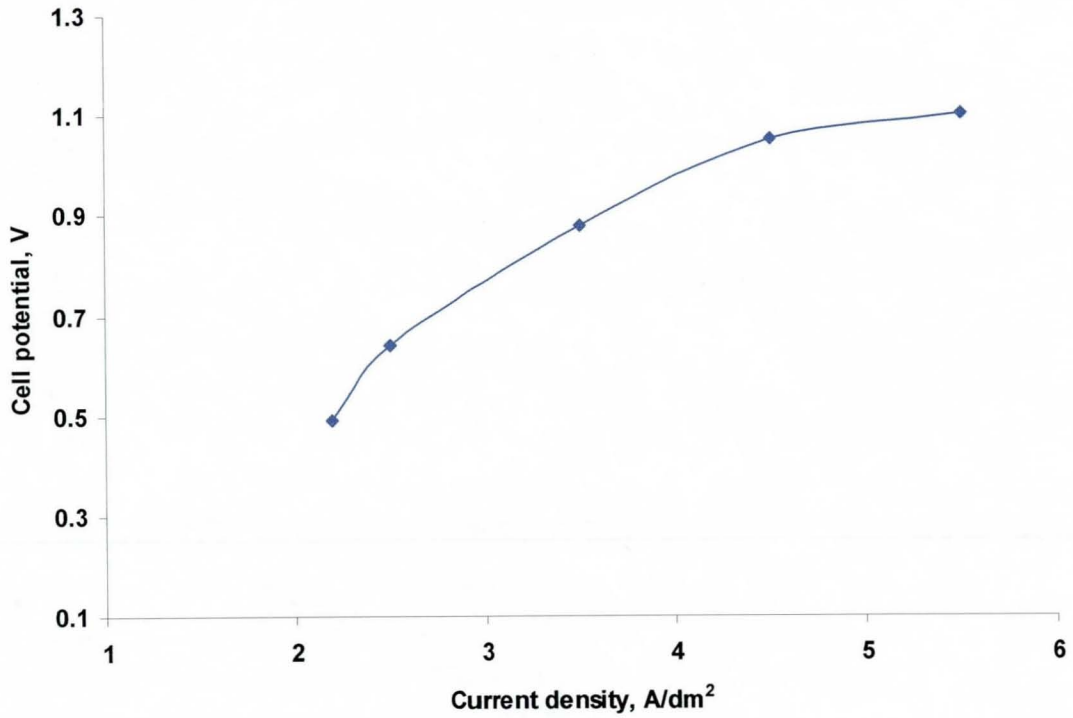

Figure 7.2 **Effect of increasing current density on the cell voltage of the alkaline bath. Agitation 300 rpm, pH 13.8, T= 22 ^0C.**

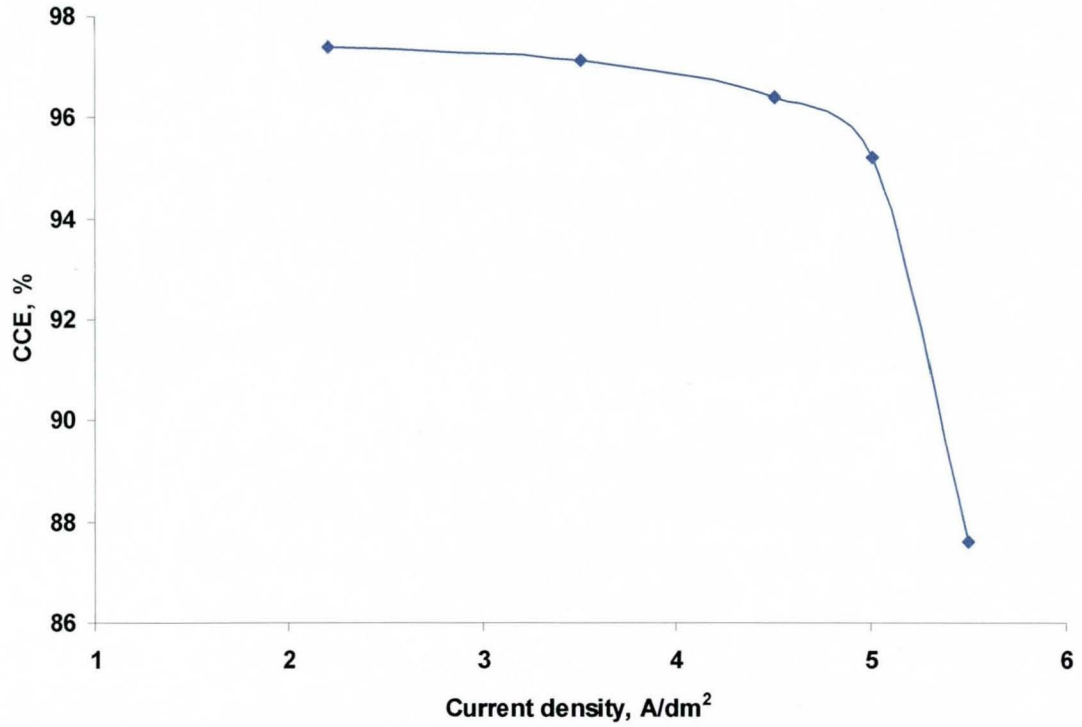

Figure 7.3 **Effect of current density on the CCE of zinc electrodeposition. Agitation 300 rpm, pH 2, deposition time 10 min, T= 22 °C.**

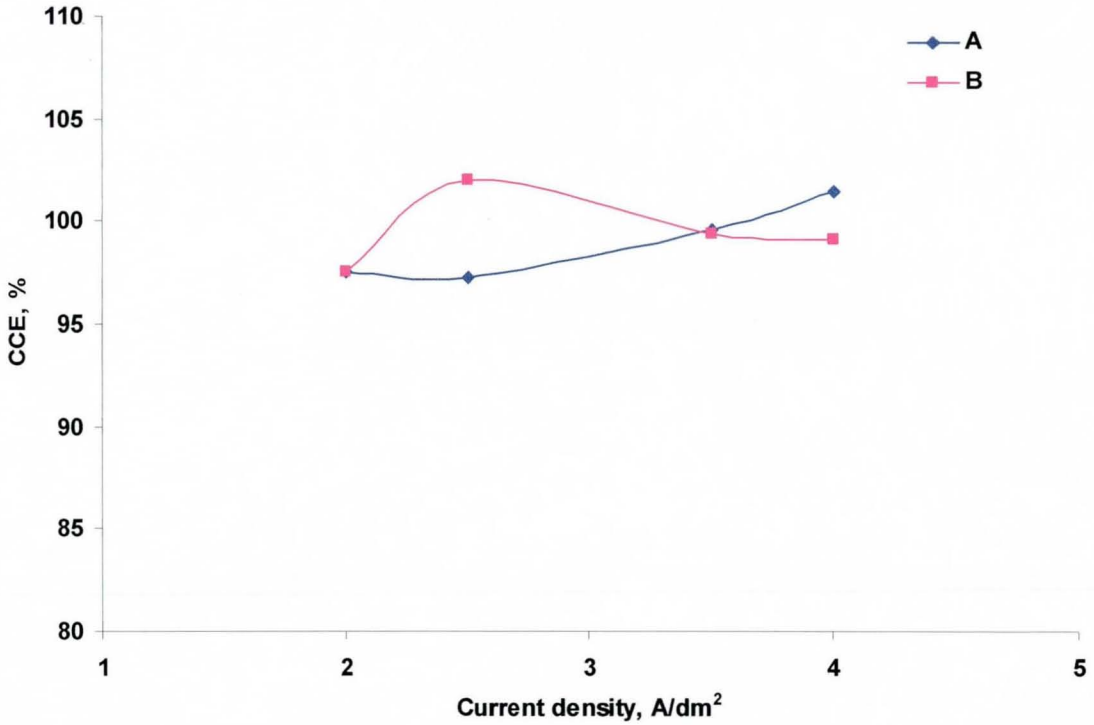

Figure 7.4 **Influence of current density on CCE of the acid zinc bath showing (A) with agitation and (B) without agitation.**

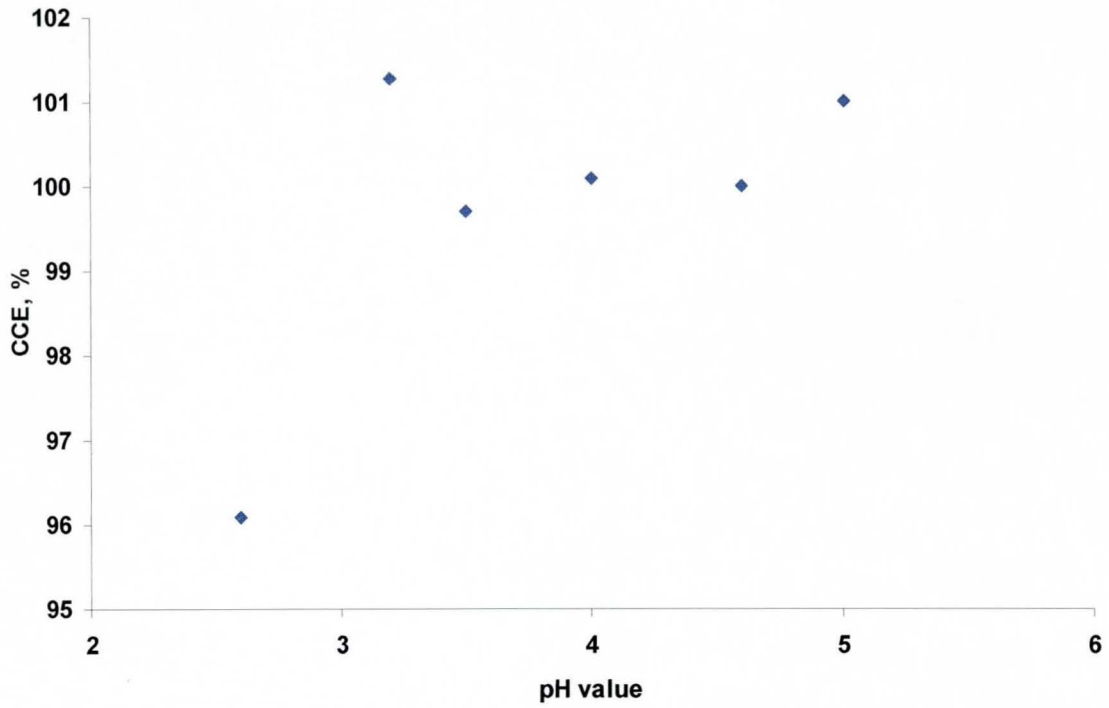

Figure 7.5 **Effect of pH on the CCE of zinc electrodeposition from the acid bath. Current density 5 A/dm^2, agitation 400 rpm, deposition time 6 min., T = 22 °C.**

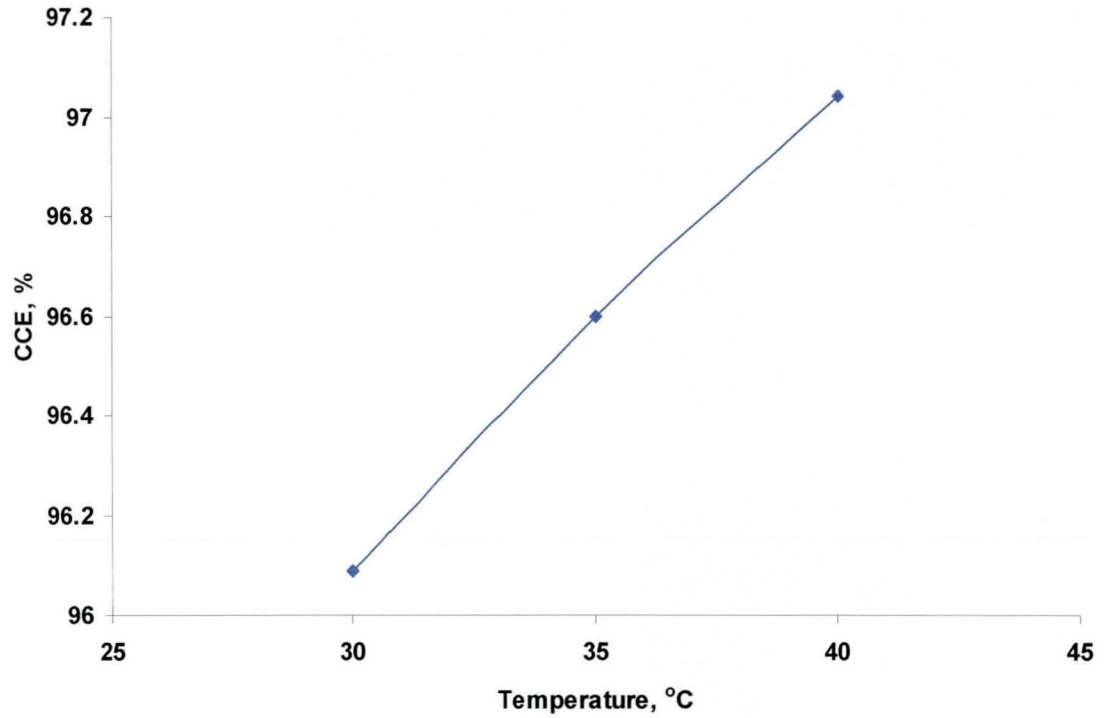

Figure 7.6 **Influence of bath temperature on the CCE of zinc electrodeposition from the acid bath. Current density 3 A/dm^2, agitation 800 rpm, pH 2.6.**

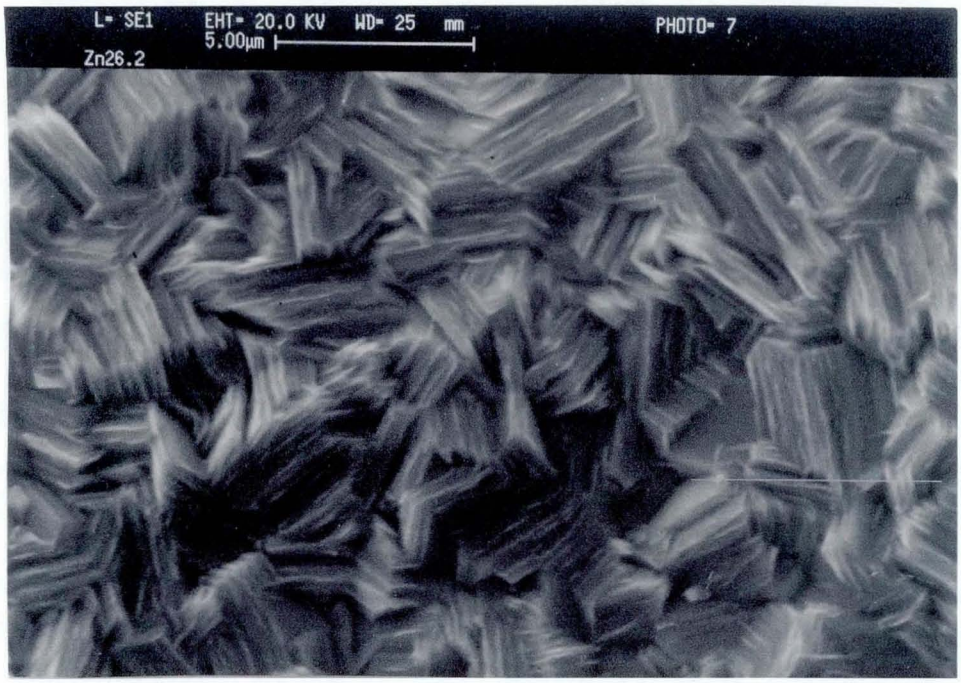

Figure 7.7 **SEM micrograph of zinc electrodeposit from the acid bath. Current density 3 A/dm^2, agitation 800 rpm and pH 2.6.**

Figure 7.8 **SEM micrograph of zinc electrodeposit from the acid bath. Current density 3 A/dm^2, agitation 800 rpm and pH 5.**

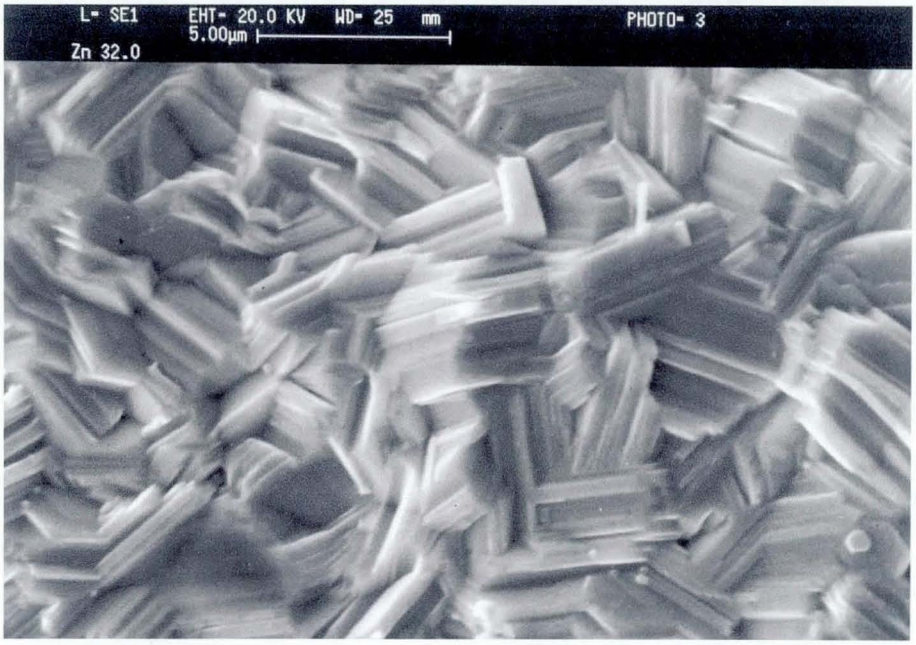

Figure 7.9 **SEM micrograph of zinc electrodeposit from the acid bath. Current density 3 A/dm^2, agitation 800 rpm, pH 2, T = 35 ^{o}C.**

Figure 7.10 **SEM micrograph of zinc electrodeposit from the acid bath. Current density 3 A/dm^2, agitation 800 rpm, pH 2, T = 40 ^{o}C.**

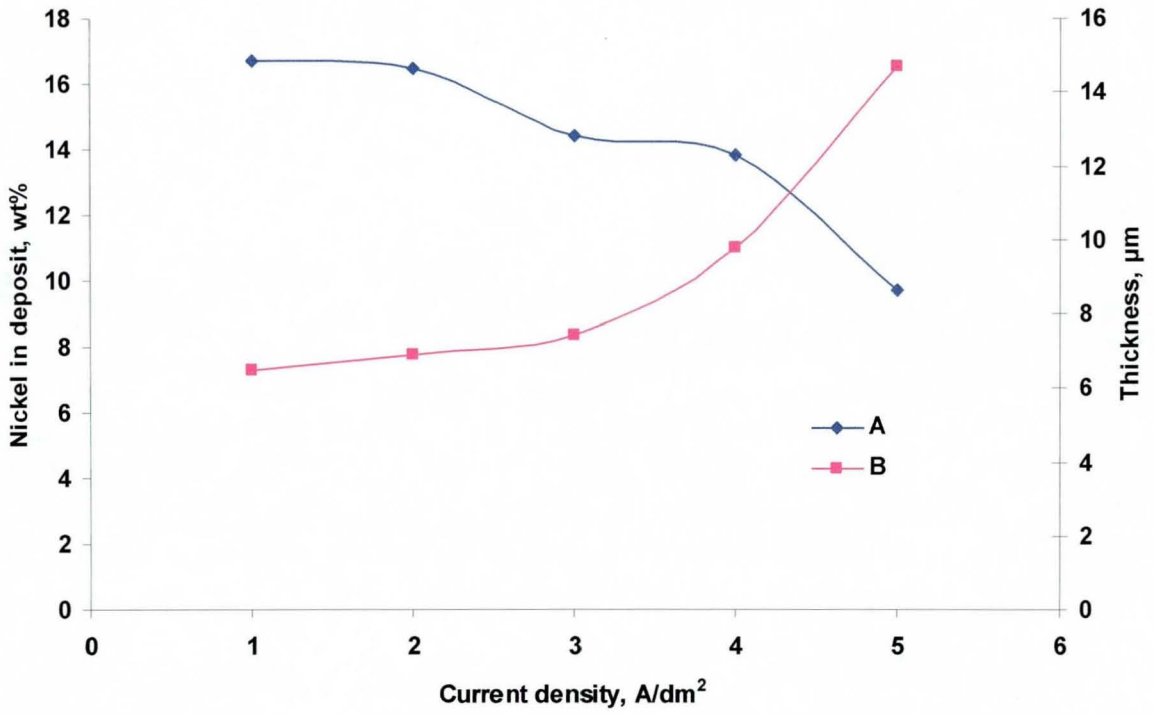

Figure 7.11 **Influence of current density on (A) nickel deposition (B) deposit thickness from a sulphate bath containing 264.5 g/l $ZnSO_4.7H_2O$, 350 g/l $NiSO_4.6H_2O$ and pH 3.5-4, T = 25 °C.**

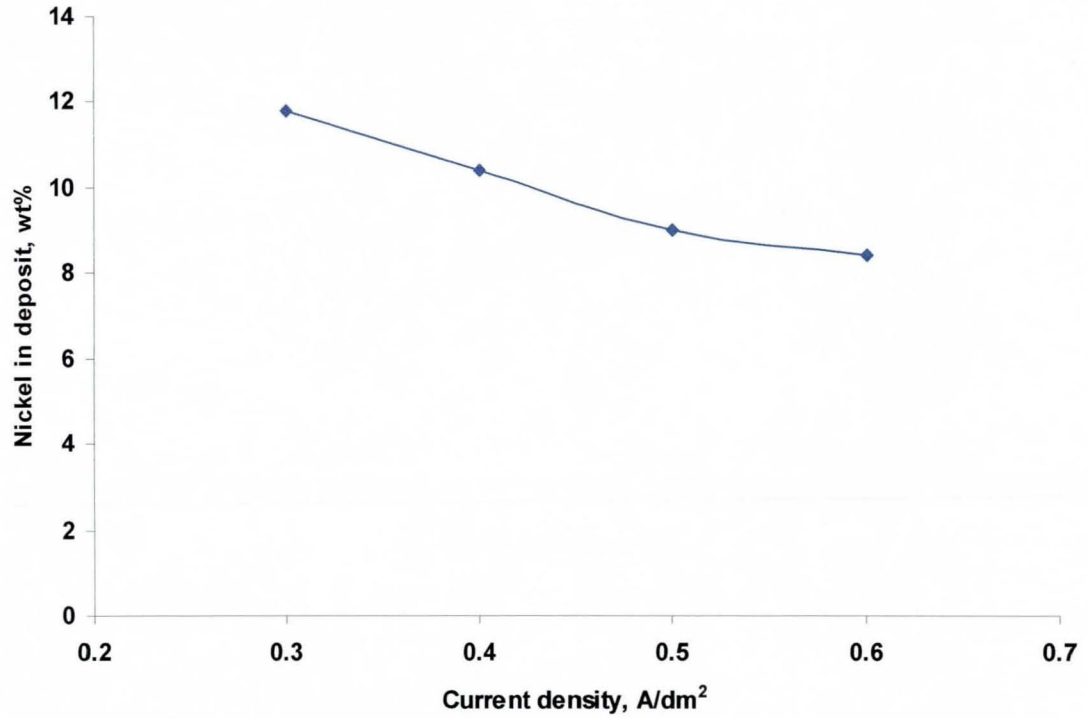

Figure 7.12 **Influence of current density on nickel deposition from a bath containing 288 g/l $ZnSO_4.7H_2O$, 184 g/l $NiSO_4.6H_2O$, pH 3.8 and T = 32 °C.**

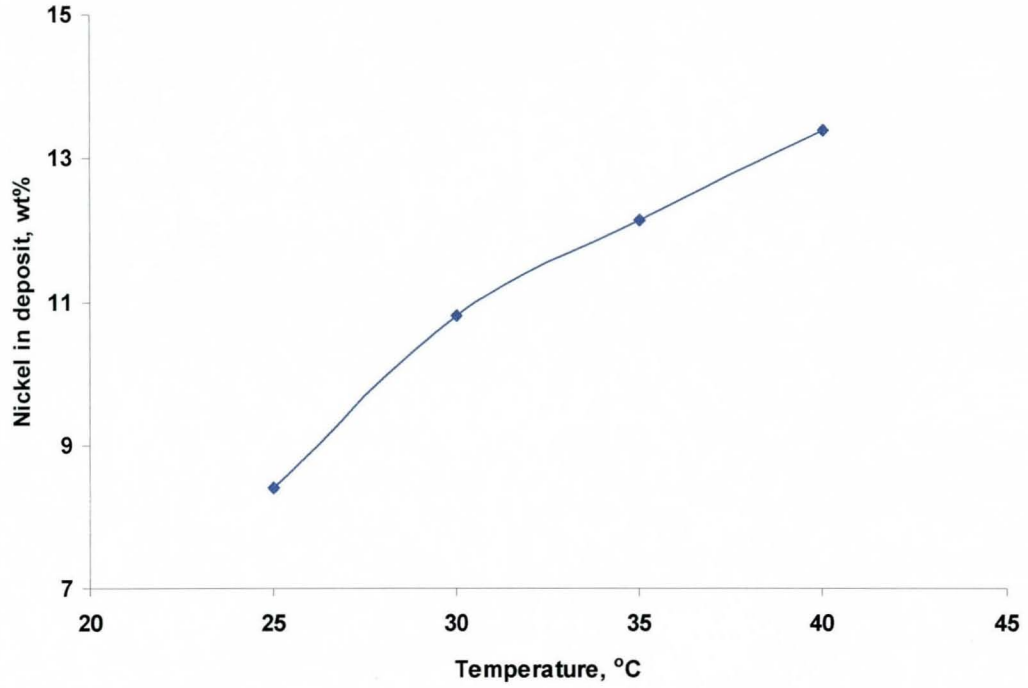

Figure 7.13 **Effect of temperature on the weight percentage of nickel in the Zn-Ni electrodeposit produced from a solution containing 62.5 g/l $ZnCl_2$, 60.7 g/l $NiCl_2.6H_2O$, 200 g/l NH_4Cl, pH 3.5.**

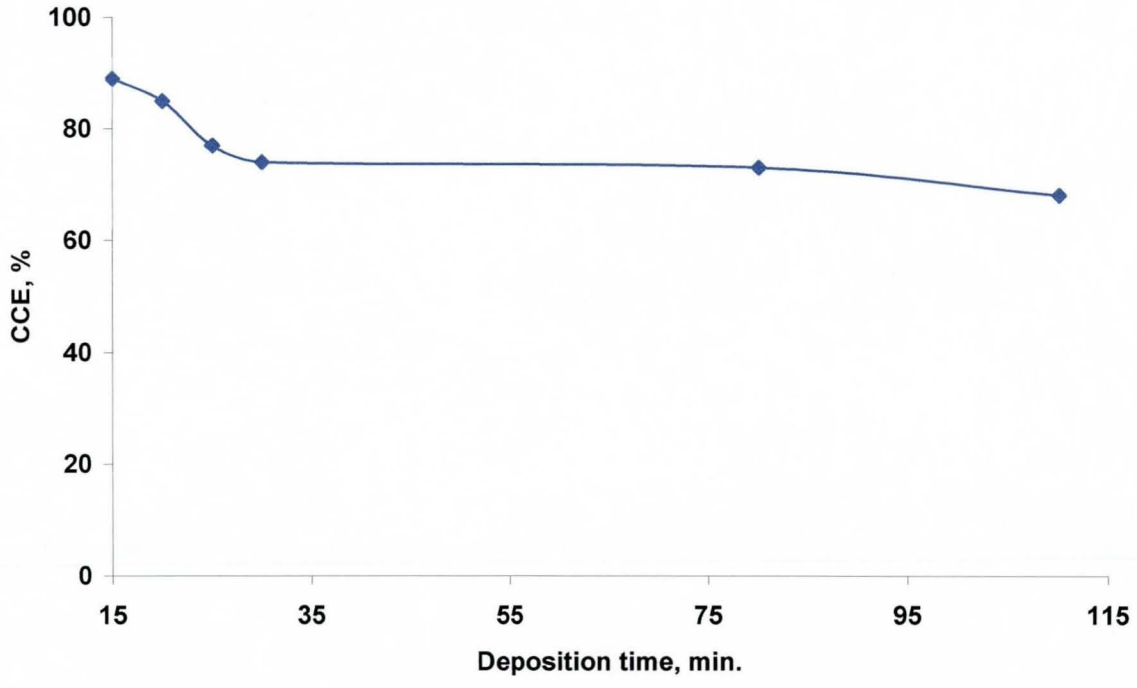

Figure 7.14 **Effect of deposition time on CCE of Zn-Ni electrodeposition from a bath containing 288 g/l $ZnSO_4.7H_2O$, 184 g/l $NiSO_4.6H_2O$. Current density 0.3 A/dm^2, pH 3.8, T 32°C.**

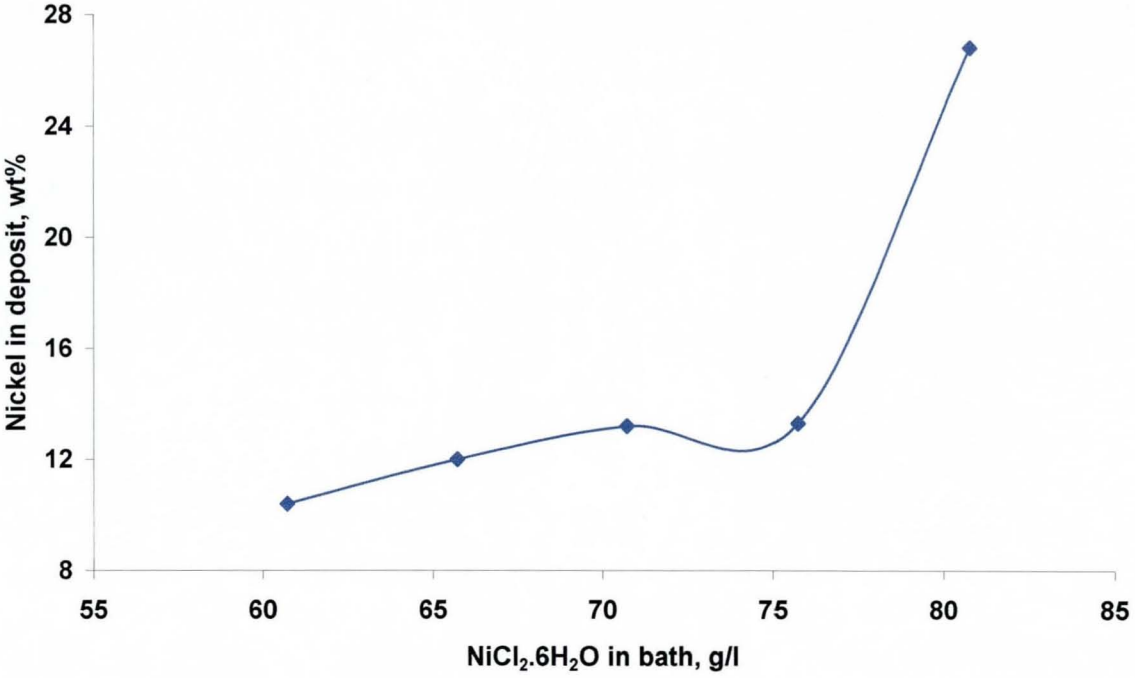

Figure 7.15 **Effect of $NiCl_2.6H_2O$ concentration in the bath on percentage of nickel in the electrodeposit. Current density of 3 A/dm^2, pH 4.5-5.5 , T = 30 ^oC.**

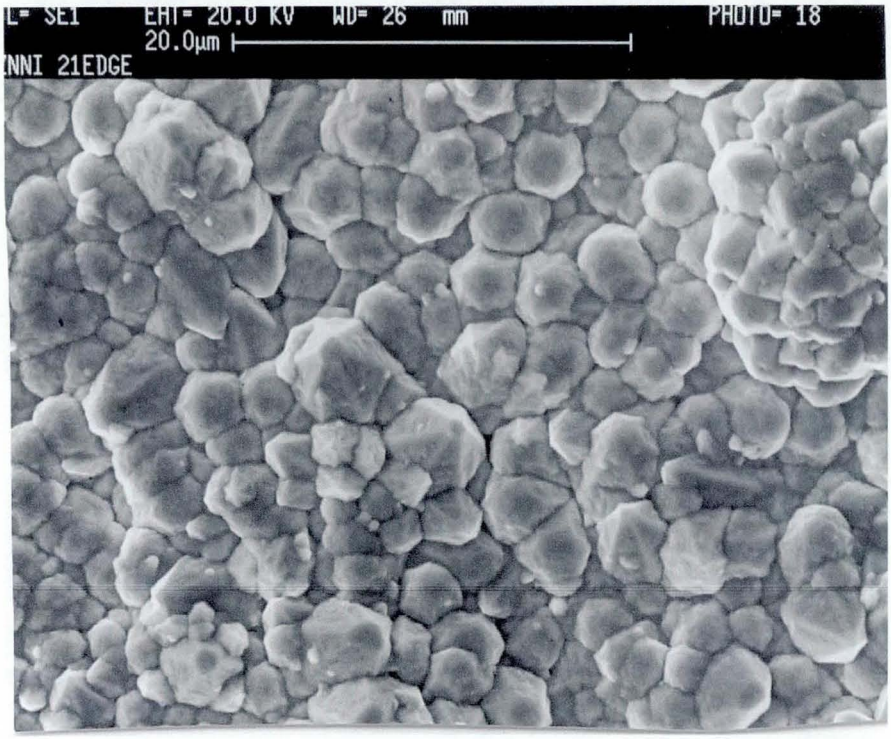

(a)

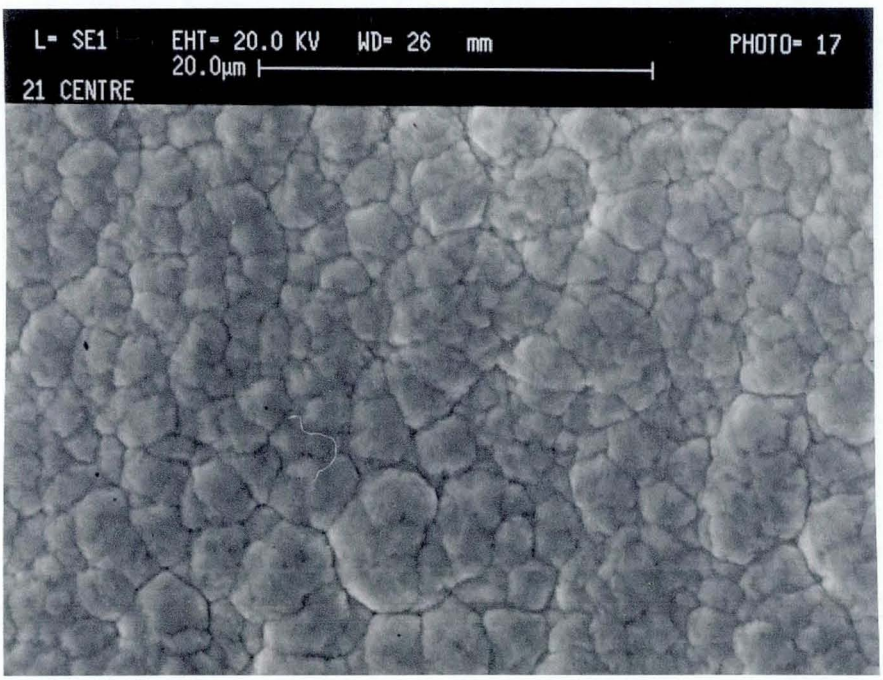

(b)

Figure 7.16 **SEM Micrographs of zinc-nickel electrodeposit with 10.6 wt% of nickel in the deposit showing (a) edge (b) centre of sample from a bath containing 62.5 g/l $ZnCl_2$, 60.7 g/l $NiCl_2.6H_2O$, 200 g/l NH_4Cl. Current density of 3 A/dm^2, pH of 4.5, T = 30^{o}C.**

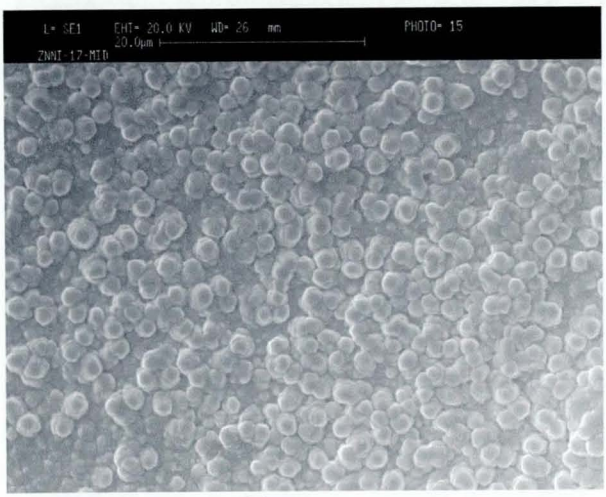

(a)

(b)

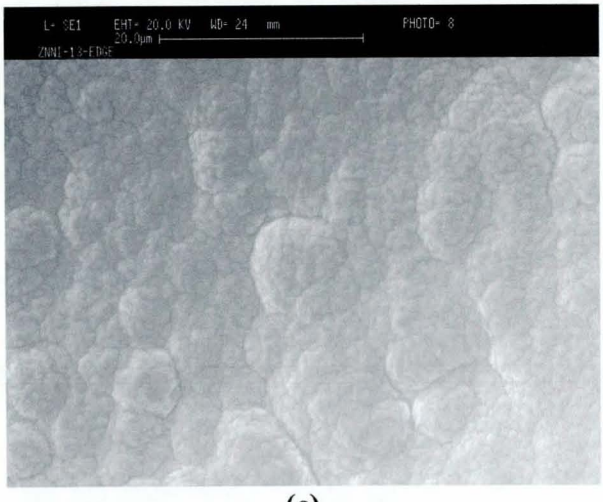

(c)

Figure 7.17 **SEM micrographs of zinc-nickel electrodeposits produced from a bath containing 62.5 g/l $ZnCl_2$, 60.7g/l $NiCl_2.6H_2O$, 200 g/l NH_4Cl, pH 3.5 at different temperatures. (a) T = 25 ^oC, Ni 7.5 wt%, (b) T = 30 ^oC, Ni 11.7 wt%, (c) T = 40 ^oC, Ni 13.4 wt%.**

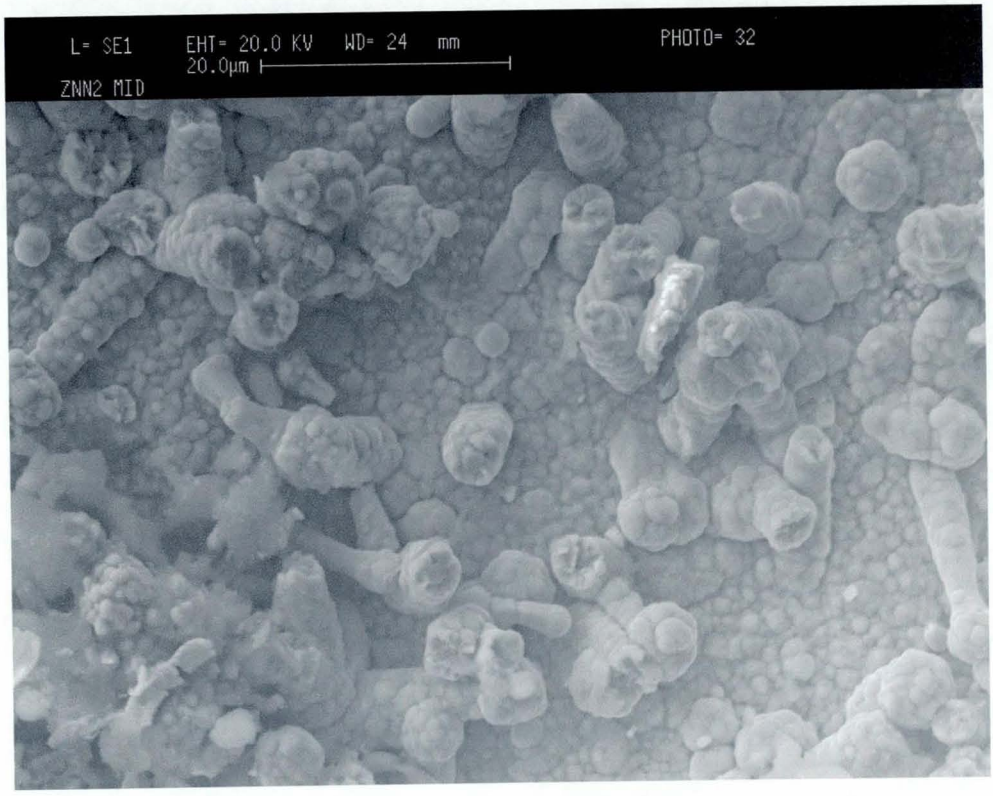

Figure 7.18 **SEM micrographs of zinc-nickel electrodeposits with 9.5 wt% Ni. produced from a bath containing 264.5 g/l $ZnSO_4.7H_2O$, 350 g/l $NiSO_4.6H_2O$, pH 3.5, T= 22 °C.**

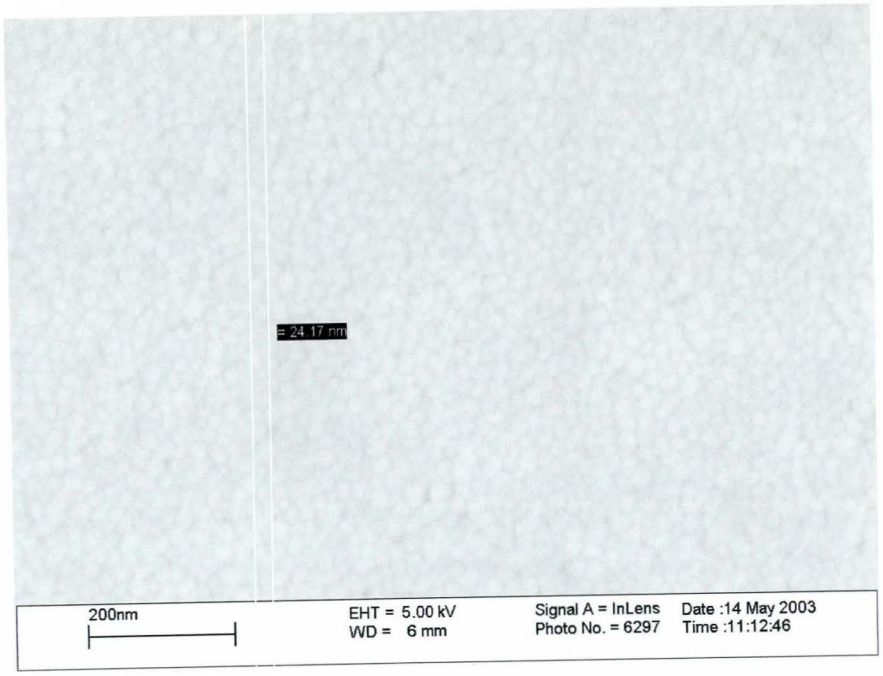

(a)

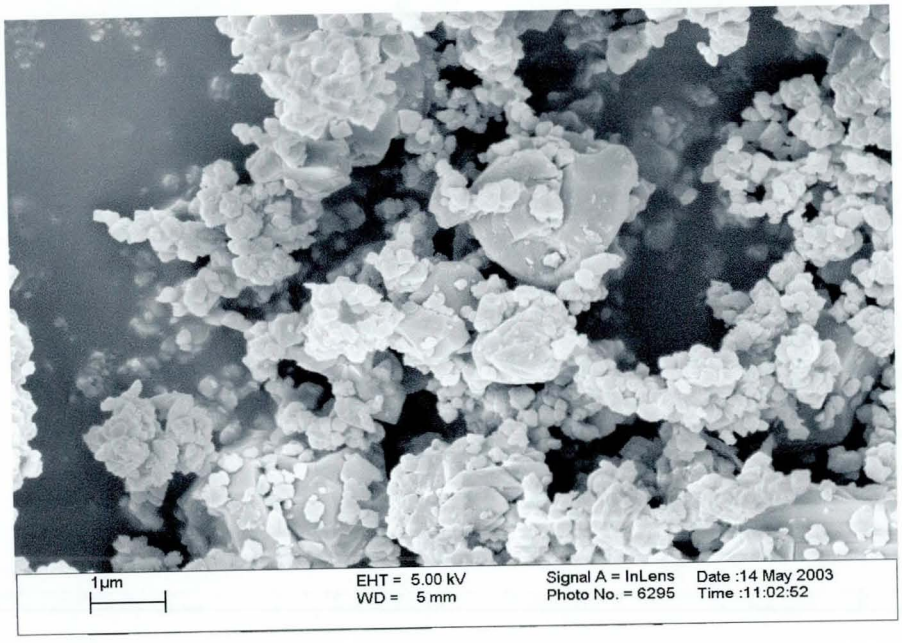

(b)

Figure 8.1 **SEM micrographs of (a) 20 nm and (b) 2 µm particles of silica.**

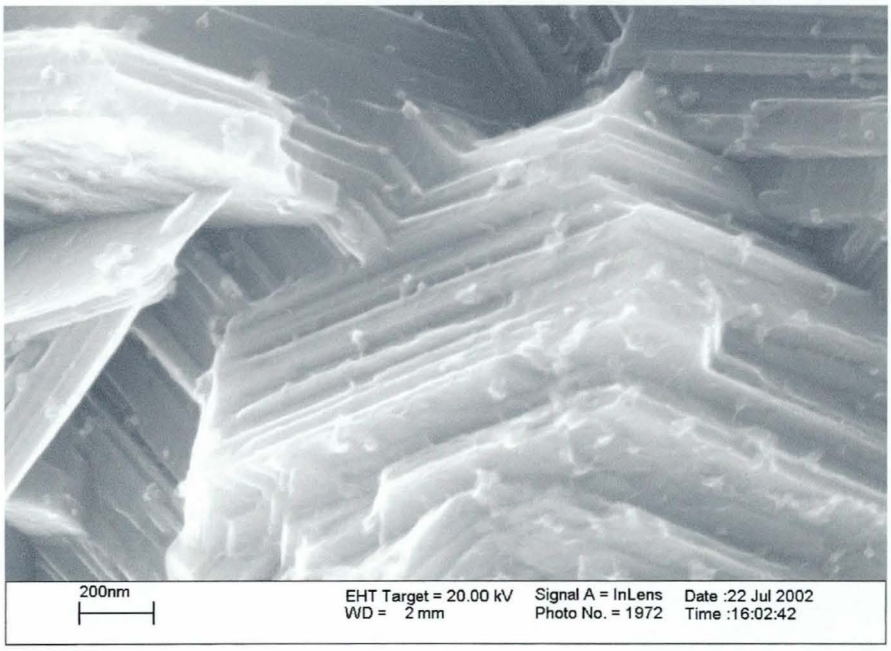

Figure 8.2 **SEM of Zn/SiO_2 electrodeposited at a current density of 30 A/dm^2, pH 2.6, and agitation 800 rpm, SiO_2(20 nm) 13g/l.**

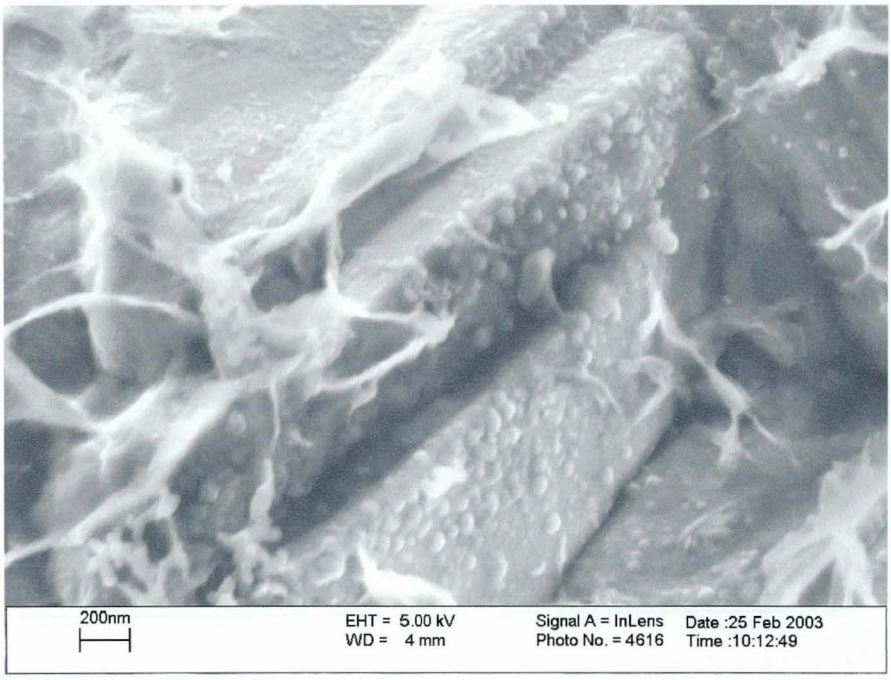

Figure 8.3 SEM of Zn/SiO_2 electrodeposited at a current density of 30 A/dm^2 SiO_2(20 nm).

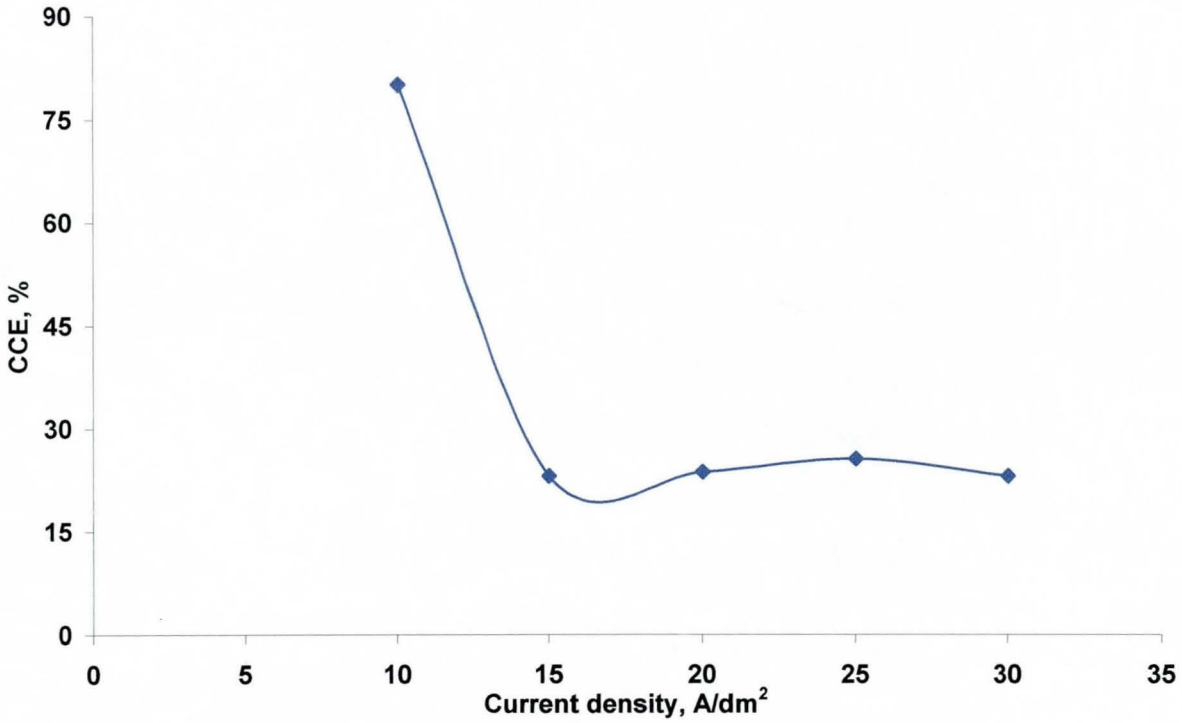

Figure 8.4 **Influence of current density on CCE of a Zn/SiO_2 bath containing 104 g/l SiO_2, and amplitude of vibration 0.55 mm.**

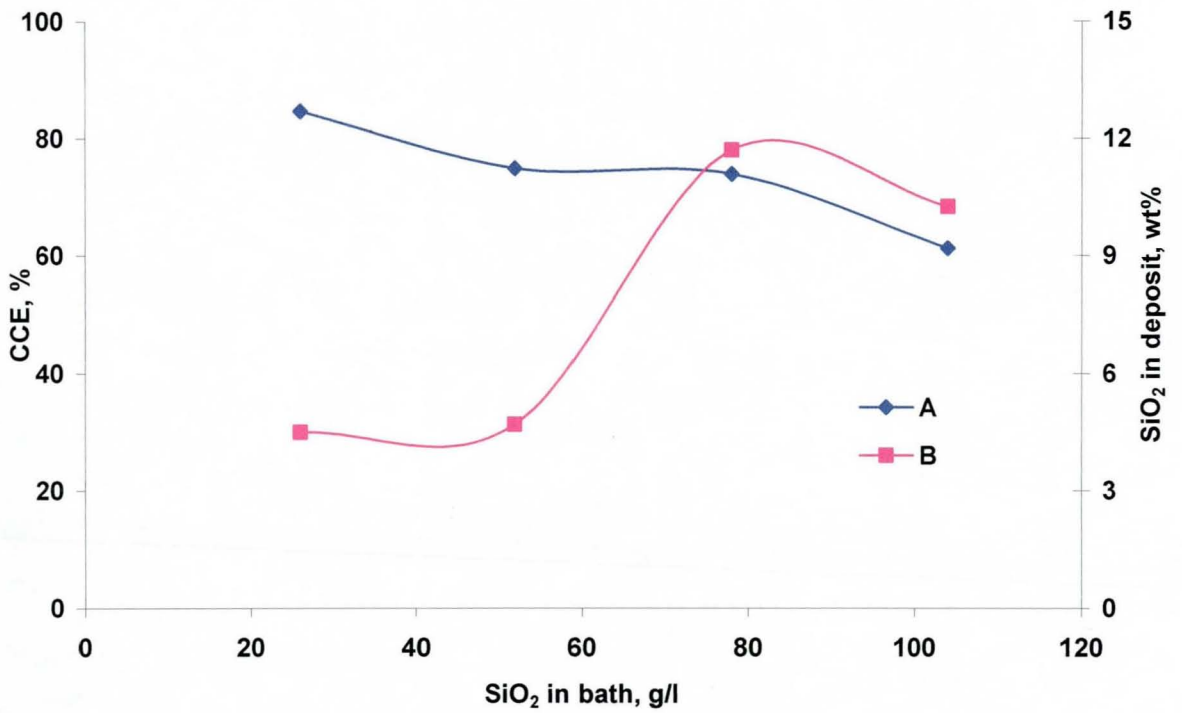

Figure 8.5 **Effect of particle loading on (A) CCE and (B) rate of particle incorporation in the deposit. SiO_2 20 nm, 500 rpm, pH 2 and 30 A/dm^2.**

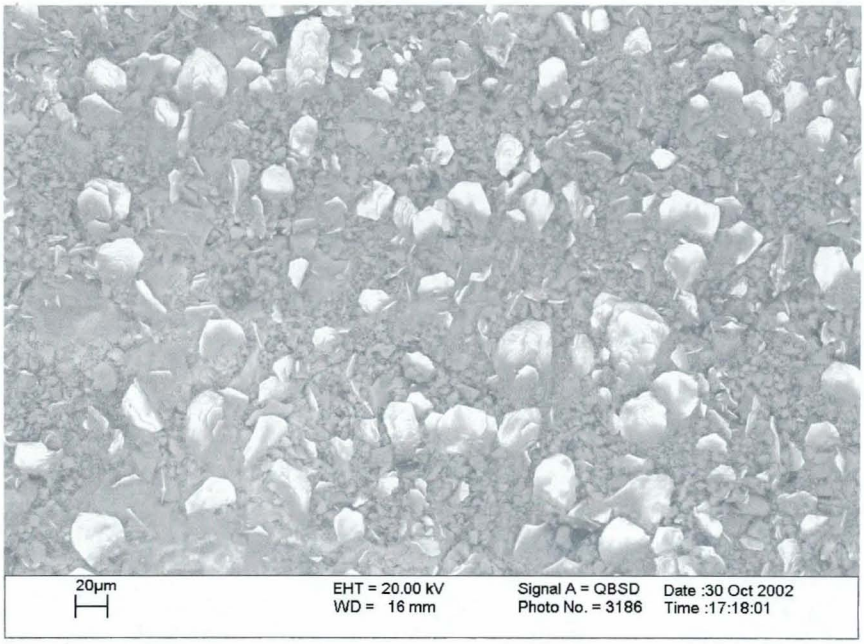

(a)

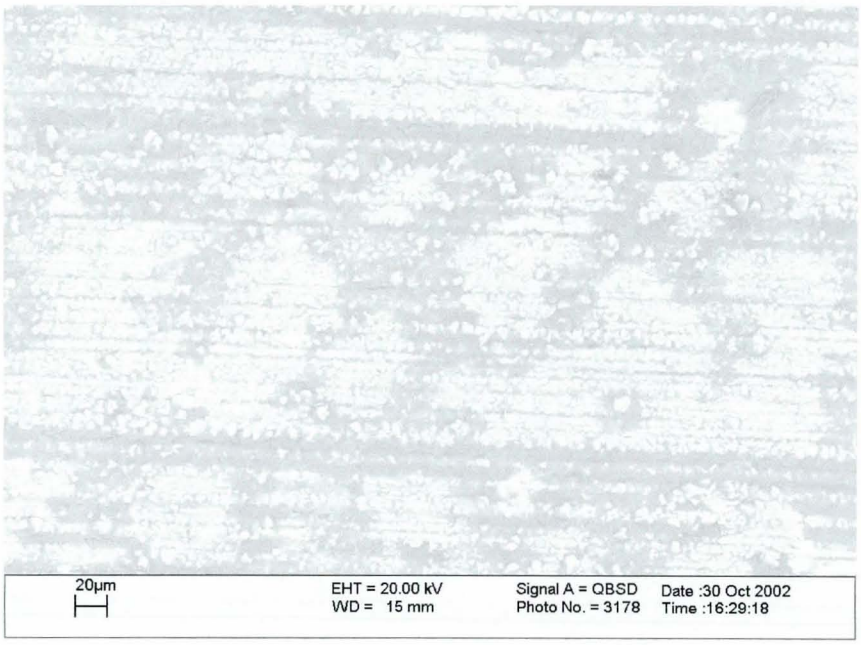

(b)

Figure 8.6 **Relationship between cathode current efficiency and deposit morphology of Zn/SiO_2 electrodeposits with cathode current efficiencies of (a) 8 % and (b) 23.5 %.**

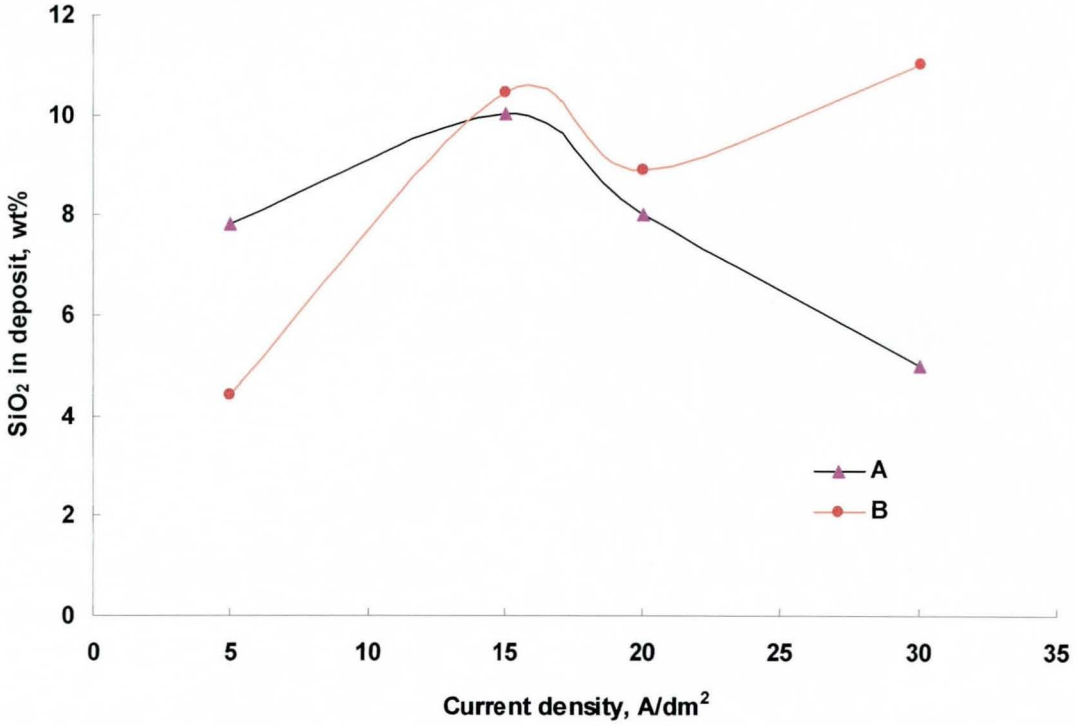

Figure 8.7. **Relationship between cathode current density and rate of particle incorporation for (A) 20 nm and (B) 2 μm particles with each of the baths containing 13 g/l SiO_2 and vibratory agitation amplitude of agitation 0.55 mm.**

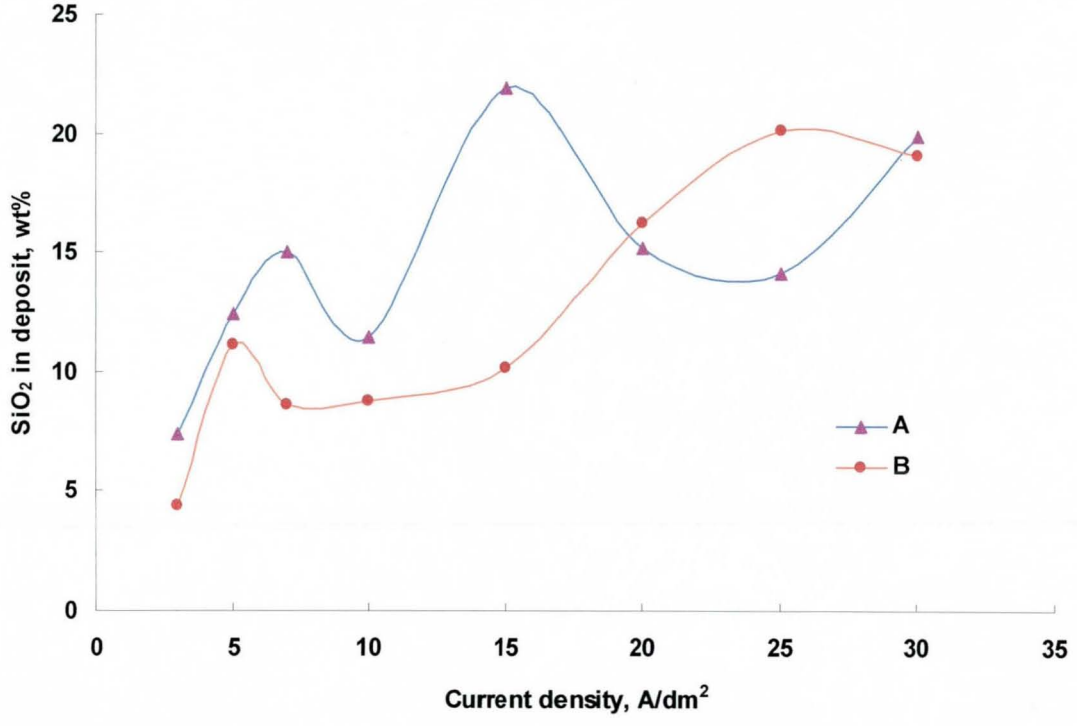

Figure 8.8. **Rate of particle incorporation vs current density for (A) vibratory agitation and (B) magnetic stirring. SiO2 (2 μm) 60 g/l bath loading.**

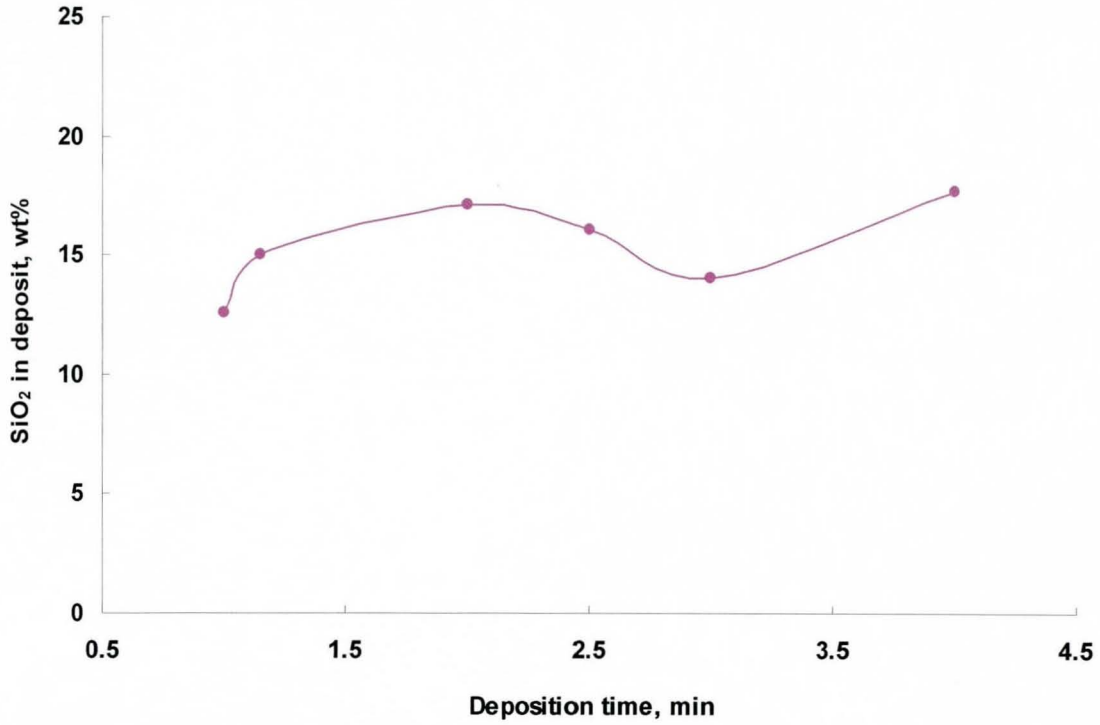

Figure 8.9. **Effect of increasing deposition time on rate of particle incorporation from a bath containing SiO_2 (2 μm) 80 g/l, Amplitude of vibration 1.8 mm, current density 30 A/dm^2.**

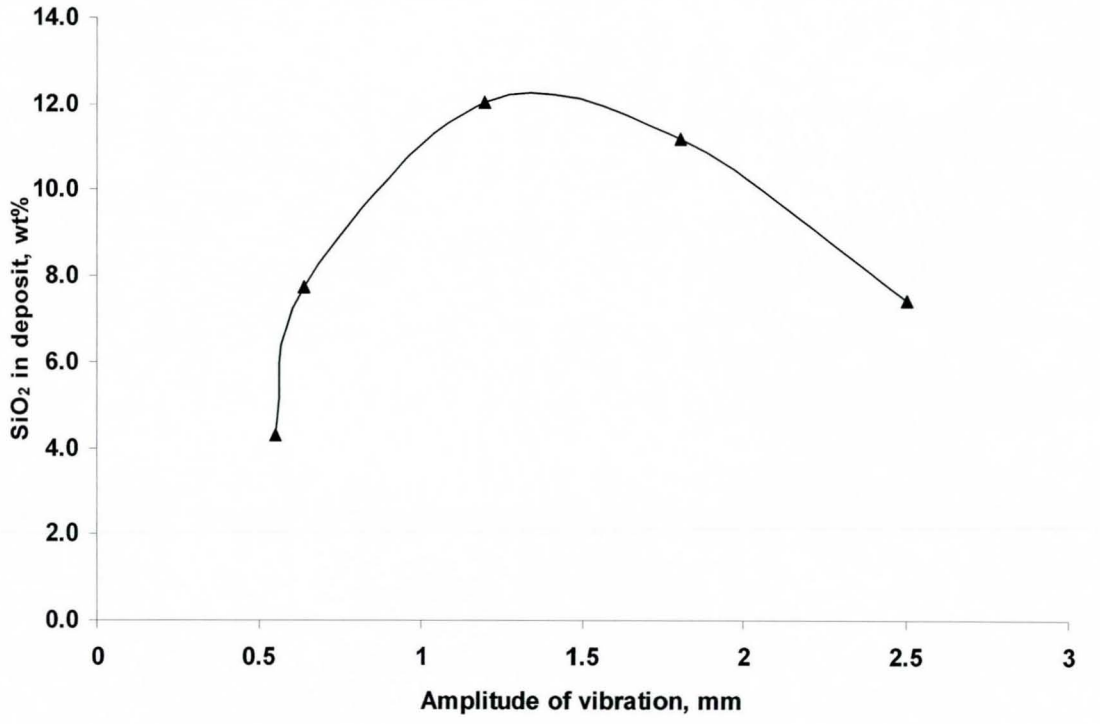

Figure 8.10. **Effect of vibratory agitation amplitude on the rate of particle incorporation. Current density 5 A/dm^2, SiO_2 (2 μm) concentration in bath, 13 g/l, pH 2, T = 50 ^{o}C.**

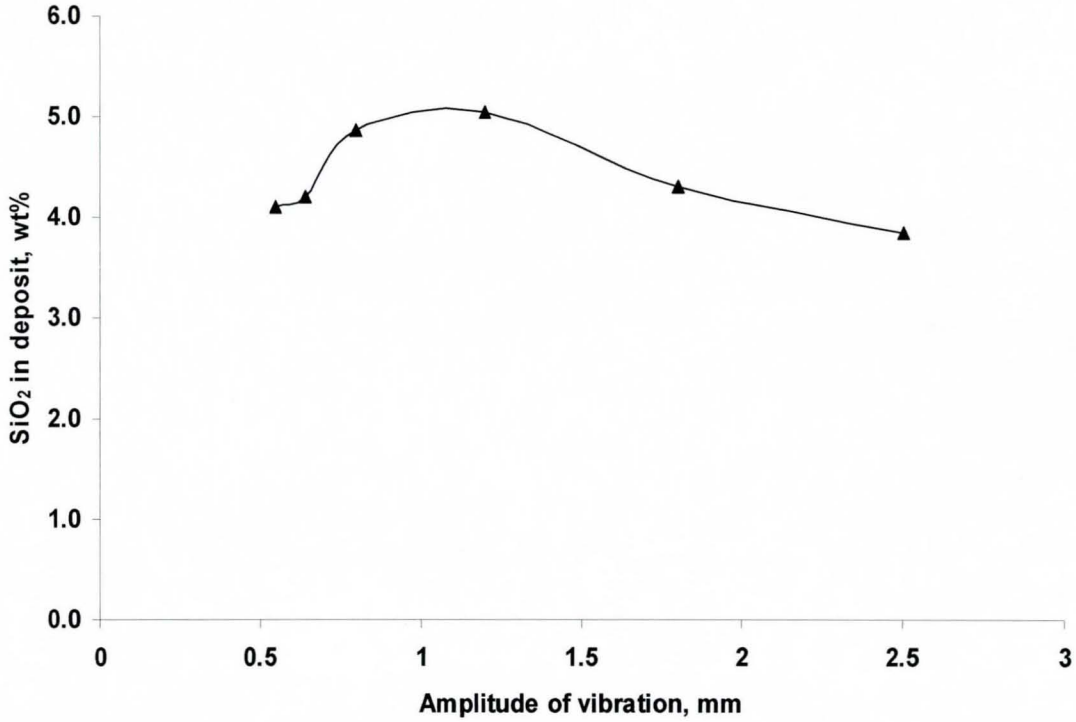

Figure 8.11. **Effect of vibratory agitation amplitude on the rate of particle incorporation. Current density 30 A/dm^2, SiO_2 (20 nm) 50 g/l, pH 2, T = 50 °C.**

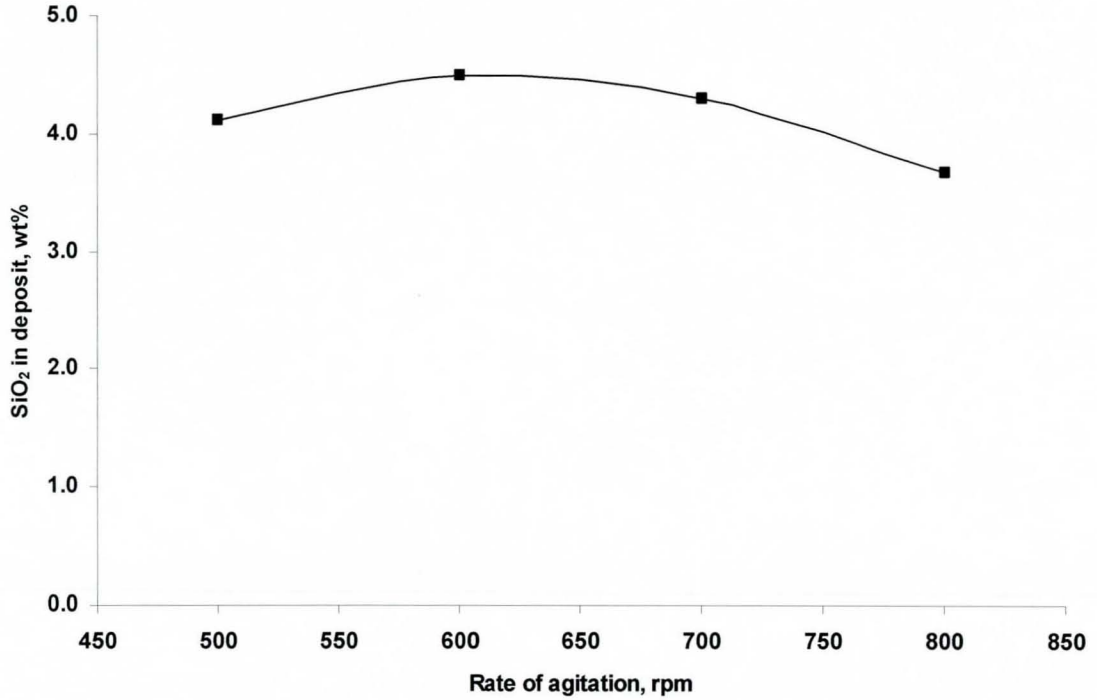

Figure 8.12 **Effect of agitation with a magnetic stirrer on the rate of particle incorporation. Current density 30 A/dm^2, SiO_2 (20 nm) 26 g/l bath loading.**

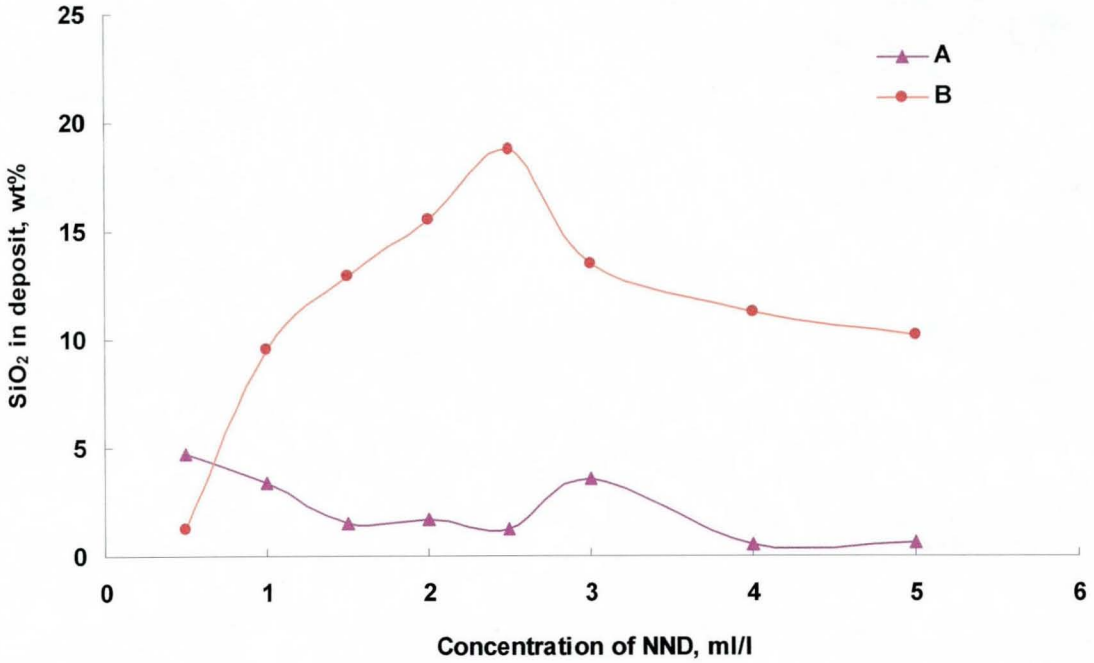

Figure 8.13. **Effect of N,N-dimethyldodecylamine (NND) on the rate of particle incorporation for (A) 20 nm and (B) 2 µm SiO_2 particles. Current density, 30 A/dm^2, SiO_2 50 g/l and amplitude of vibration 1.8 mm.**

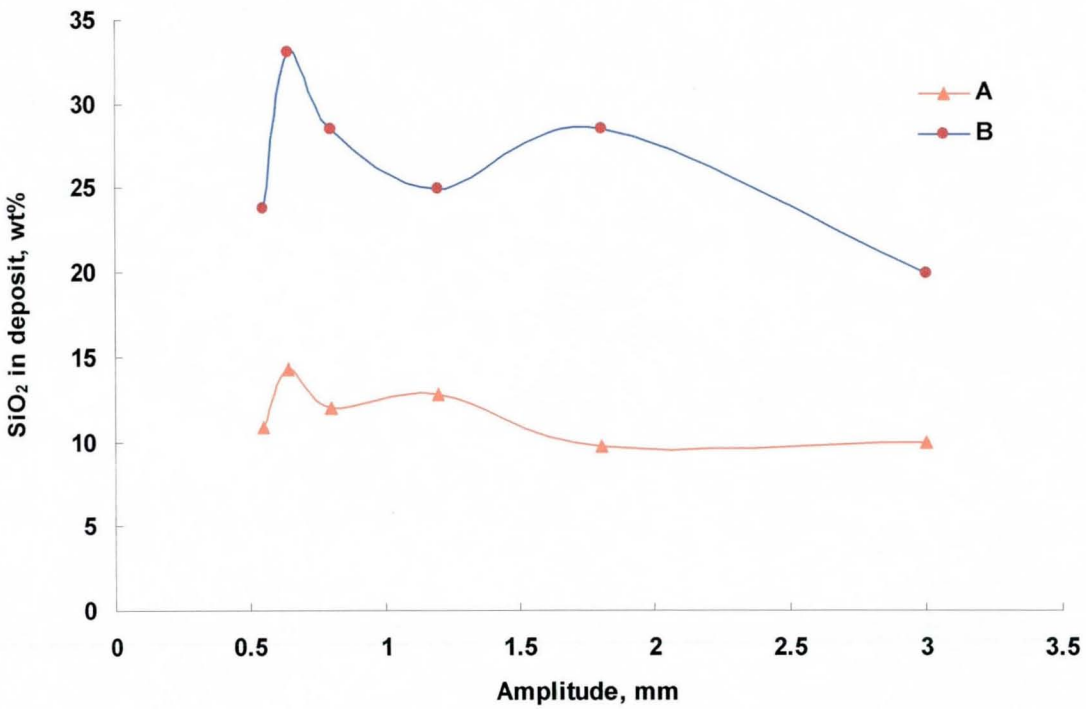

Figure 8.14. **Effect of N, N-dimethyldodecylamine (NND) on rate of particle incorporation from a bath containing (A) 0 ml/l NND (B) 2.5 ml/l NND. Current density 30 A/dm^2, SiO_2 (2 µm) 50 g/l.**

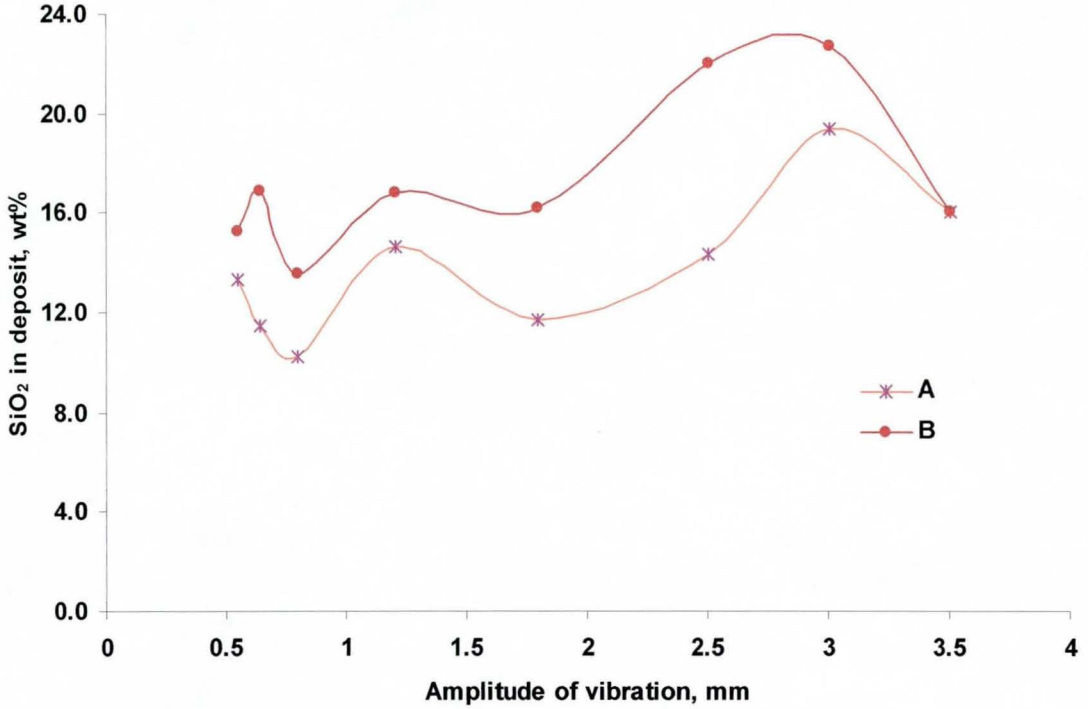

Figure 8.15 **Effect of vibratory agitation on the rate of particle incorporation from a bath containing (A) 0 ml/l NND and (B) 2.5 ml/l NND. Current density 30 A/dm^2, SiO_2 (2 µm) 80 g/l.**

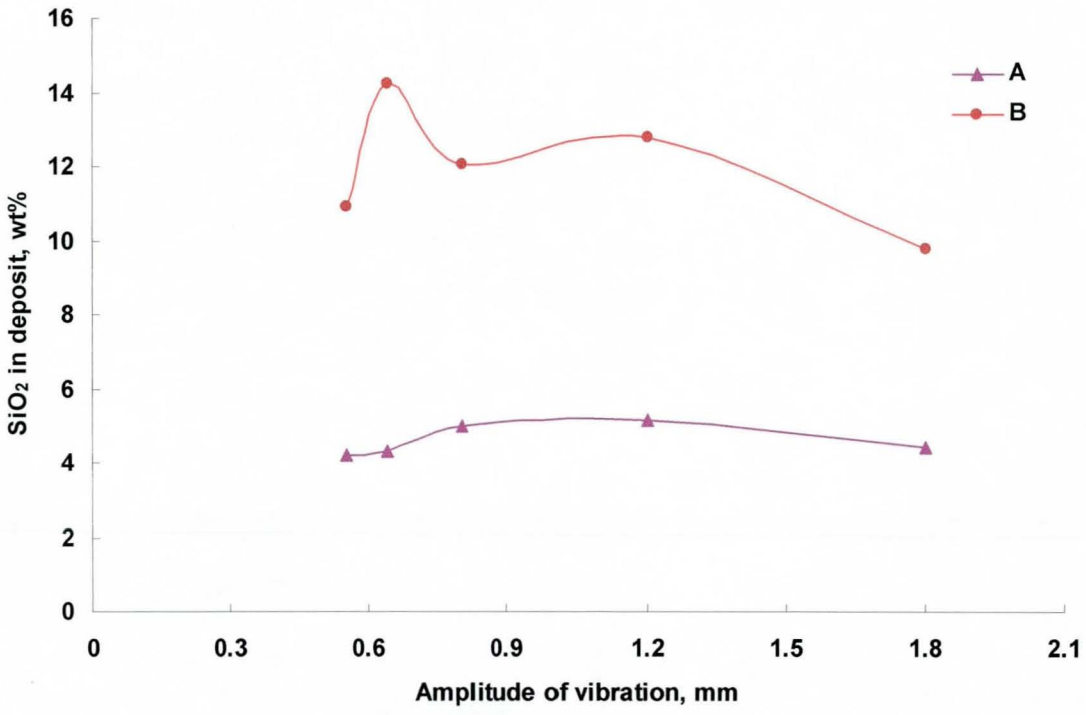

Figure 8.16 **Effect of vibratory agitation on the rate of particle incorporation for (A) 20 nm (B) 2 µm SiO_2 particles without NND. Current density 30 A/dm^2, SiO_2 50 g/l bath loading.**

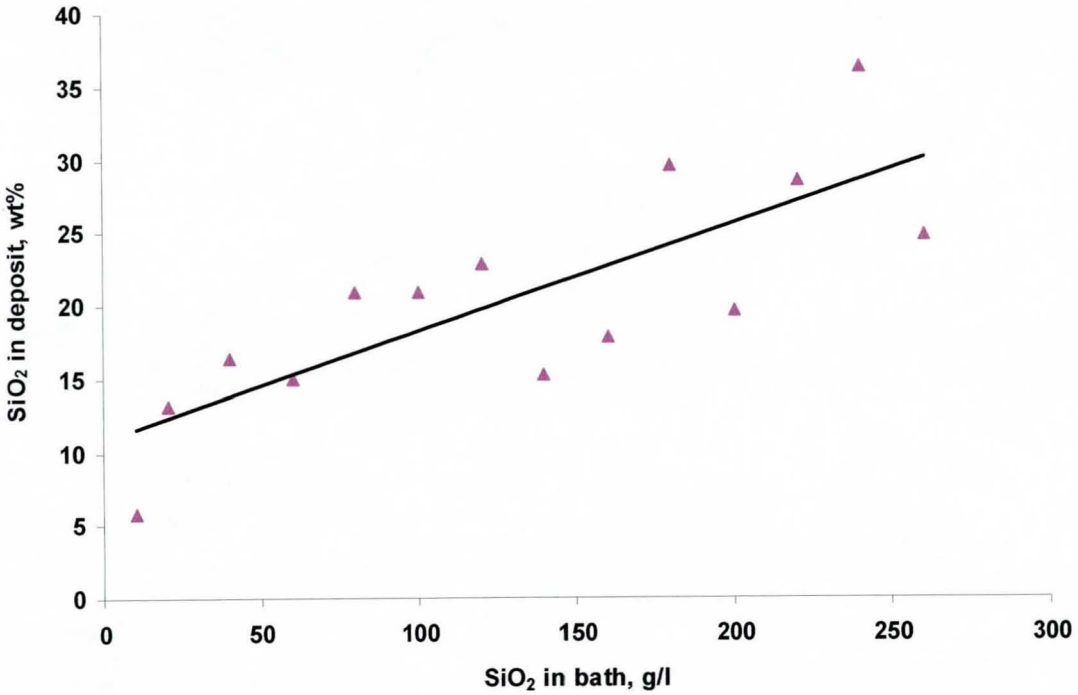

Figure 8.17 **Relationship between bath concentration of SiO_2 and weight percentage of SiO_2 in deposit. Particle size 2 μm and current density 30 A/dm^2.**

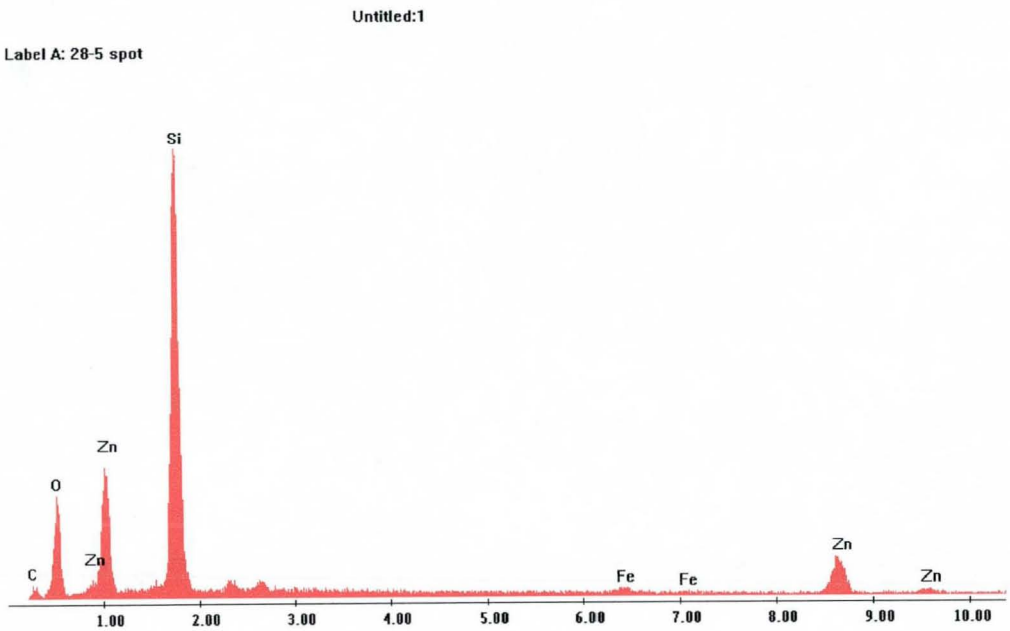

(a)

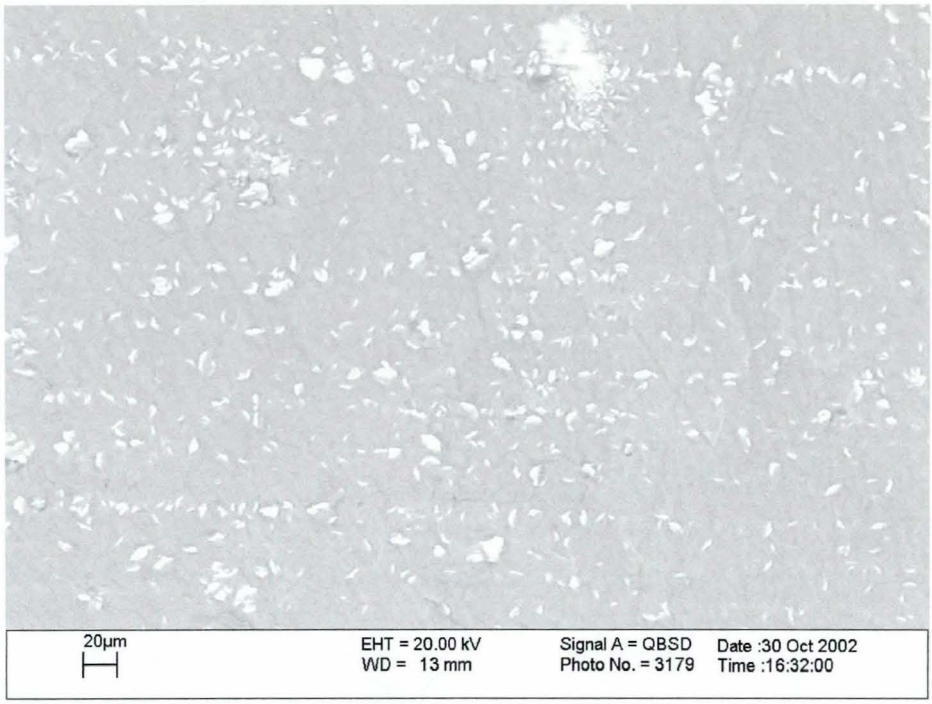

(b)

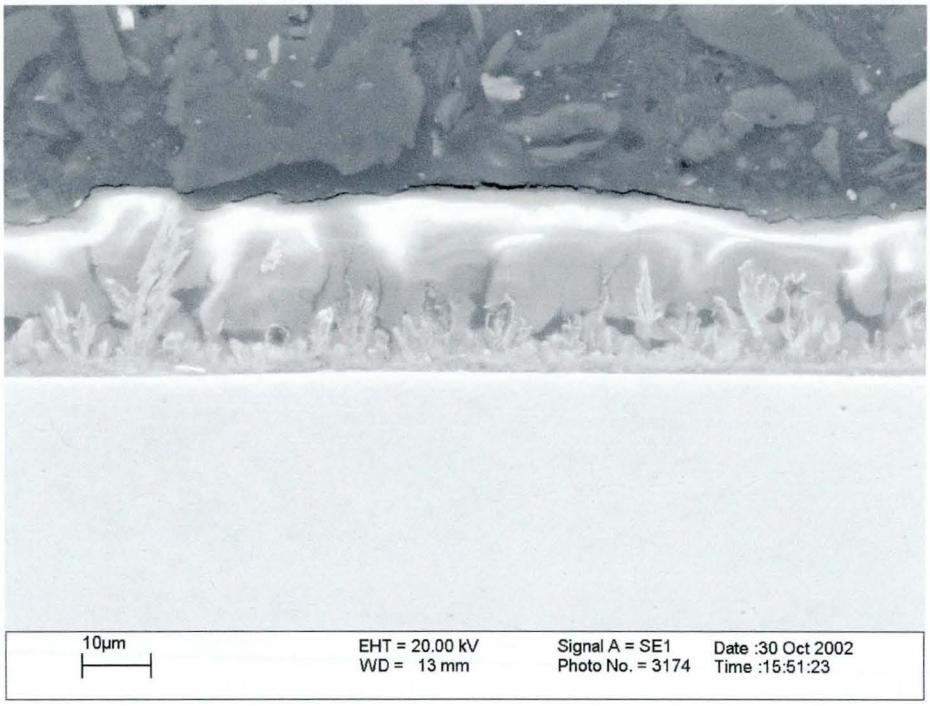

(c)

Figure 8.18 **SEM analysis of (a) EDX elemental analysis of dark areas on the surface of the composite electrodeposit (b) surface morphology and (c) cross sectional view of Zn/SiO_2 electrodeposit. SiO_2 (20 nm) 104 g/l, current density 30 A/dm^2, agitation 500 rpm and pH 2.**

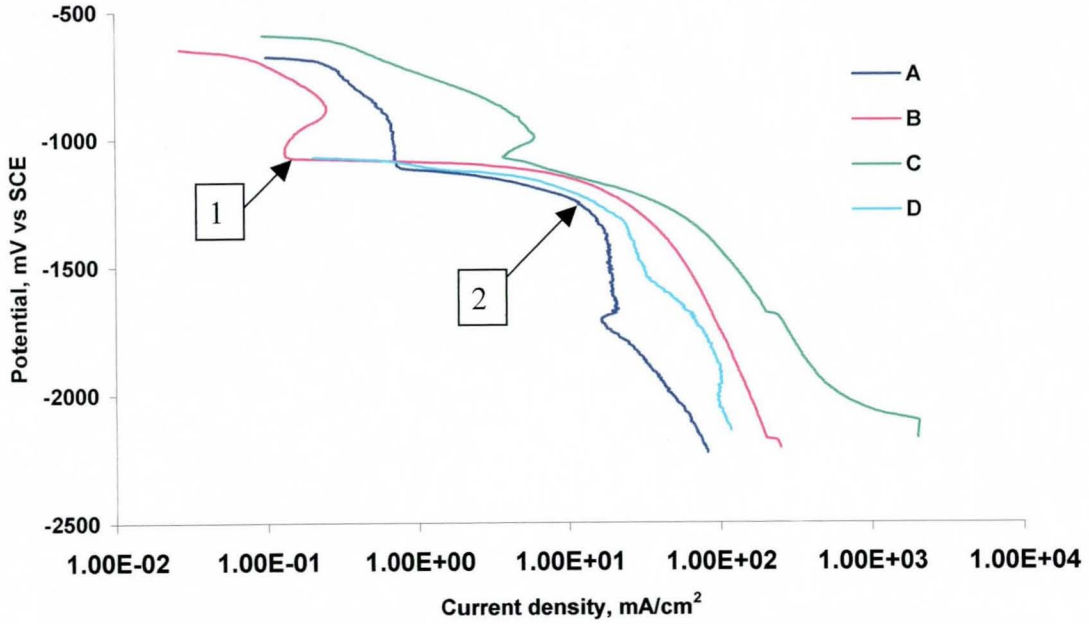

Figure 8.19 **Cathodic polarisation for mild steel in zinc, and zinc-silica electroplating solutions containing (A) 10 g/l $ZnSO_4.7H_2O$ (B) 250 g/l $ZnSO_4.7H_2O$ (C) 250 g/l $ZnSO_4.7H_2O$ +13 g/l SiO_2 (D) 10 g/l $ZnSO_4.7H_2O$ +13 g/l SiO_2. Region 1 nucleation and crystal growth, region 2 peak current density.**

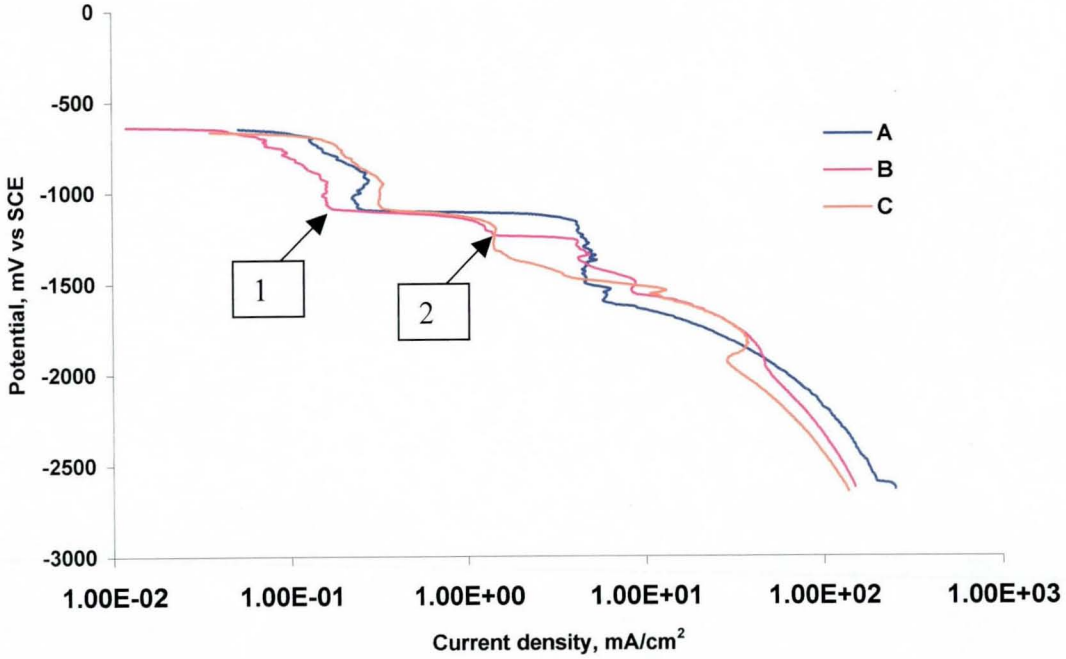

Figure 8.20. **Cathodic polarisation curves obtained for mild steel in zinc and NND-containing electroplating solutions. 10 g/l $ZnSO_4.7H_2O$, 80g/l Na_2SO_4. (A) 0 ml/l NND; (B) 0.04 ml/l NND; (C) 0.02 ml/l NND. Region 1 nucleation and crystal growth, region 2 peak current density.**

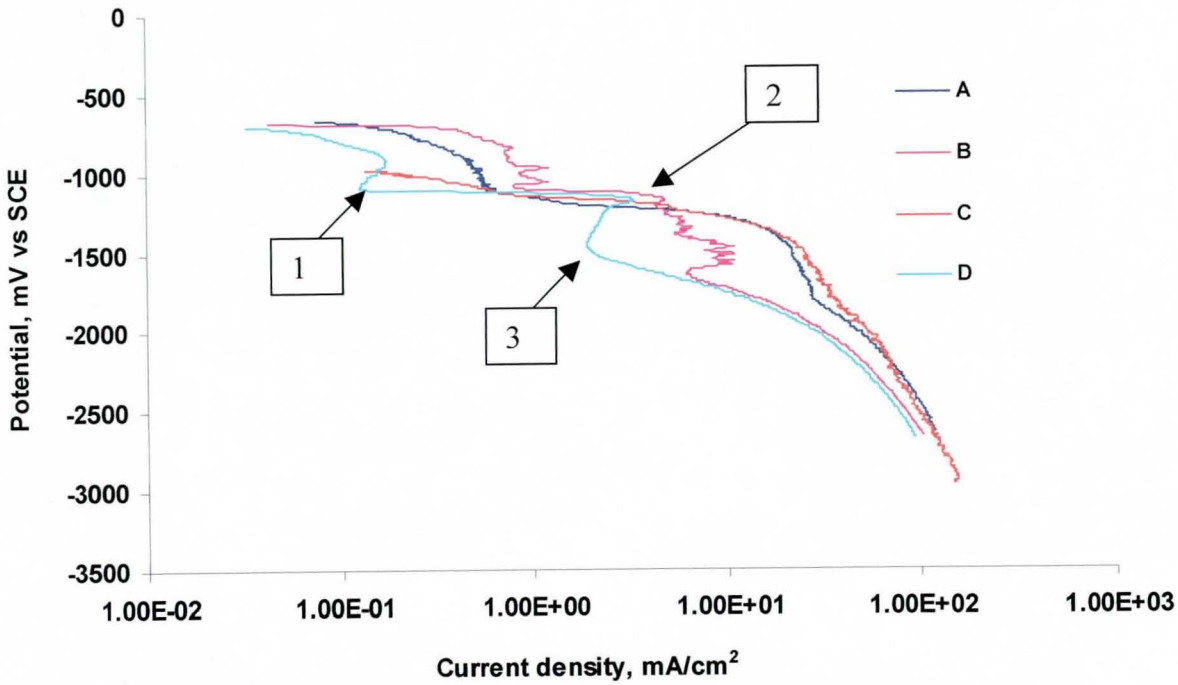

Figure 8.21 **Cathodic polarisation curves obtained for two baths of zinc/silica containing 250 g/l $ZnSO_4.7H_2O$ + 13 g/l SiO_2 (A) without agitation (C) agitation and a bath with 10 g/l $ZnSO_4.7H_2O$ + 13 g/l SiO_2 (B) agitation (D) without agitation. Region 1 nucleation and crystal growth, region 2 peak current density, region 3 limiting current density.**

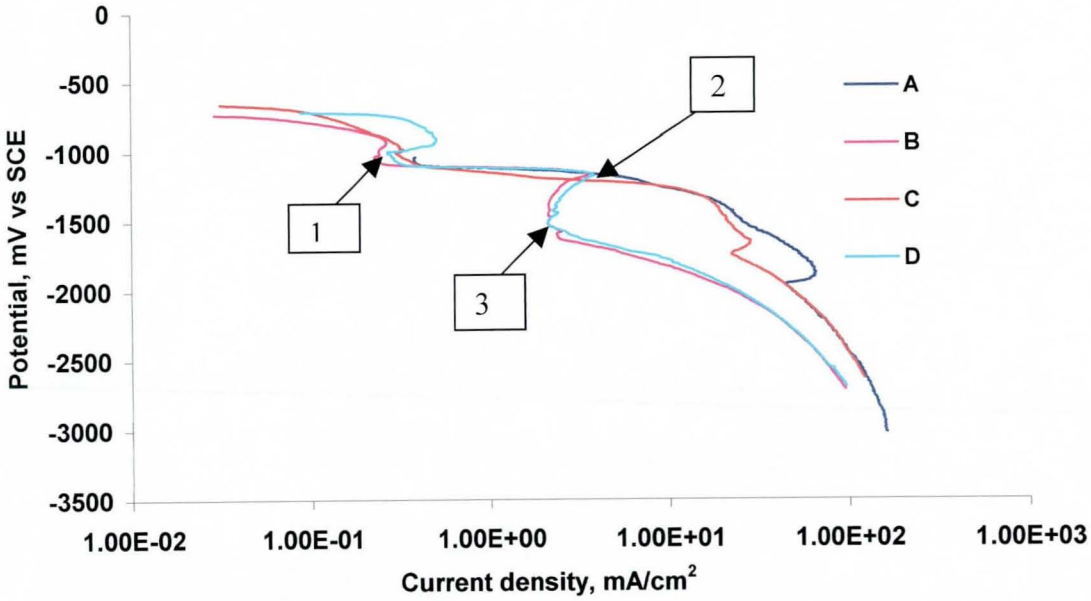

Figure 8.22 **Cathodic polarisation of zinc bath with low and high concentrations of zinc with and without agitation. Region 1 nucleation and crystal growth, region 2 peak current density, region 3 limiting current density.**

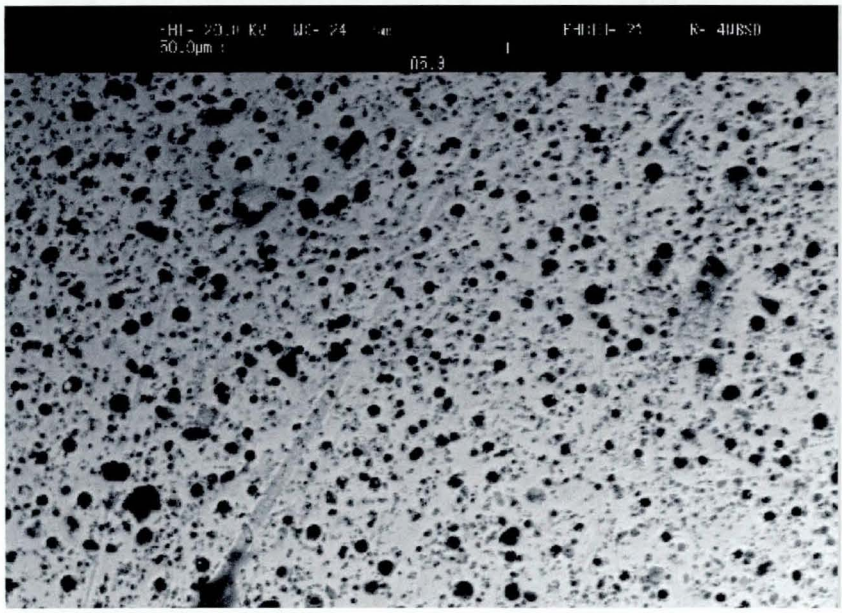

Figure 8.23 **SEM Micrograph of Zn/SiO_2 electrodeposit with 24 wt% SiO_2 from a solution containing 250 g/l $ZnSO_4.7H_2O$, 80 g/l Na_2SO_4, 50 g/l SiO_2 (2 µm), current density 30 A/dm^2, amplitude of vibration 1.8 mm, pH 2 and NND 2.5 ml/l.**

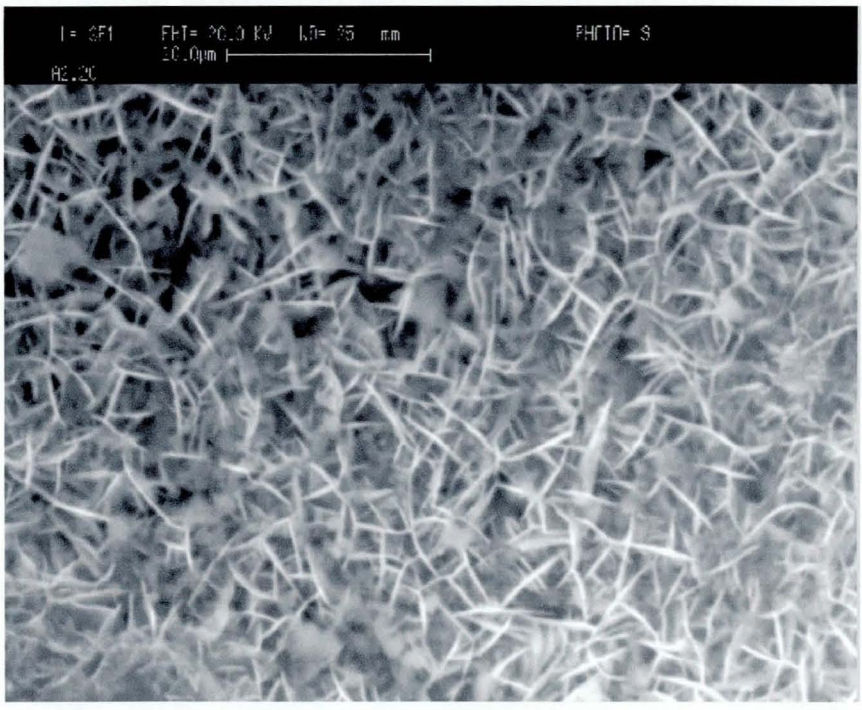

Figure 8.24 **SEM Micrograph of Zn/SiO_2 electrodeposit with 16.8 wt% SiO_2 from a solution containing 250 g/l $ZnSO_4.7H_2O$, 80 g/l Na_2SO_4, 50 g/l SiO_2 (2 µm), current density 30 A/dm^2, amplitude of vibration 1.8 mm, pH 2 and NND 1.0 ml/l.**

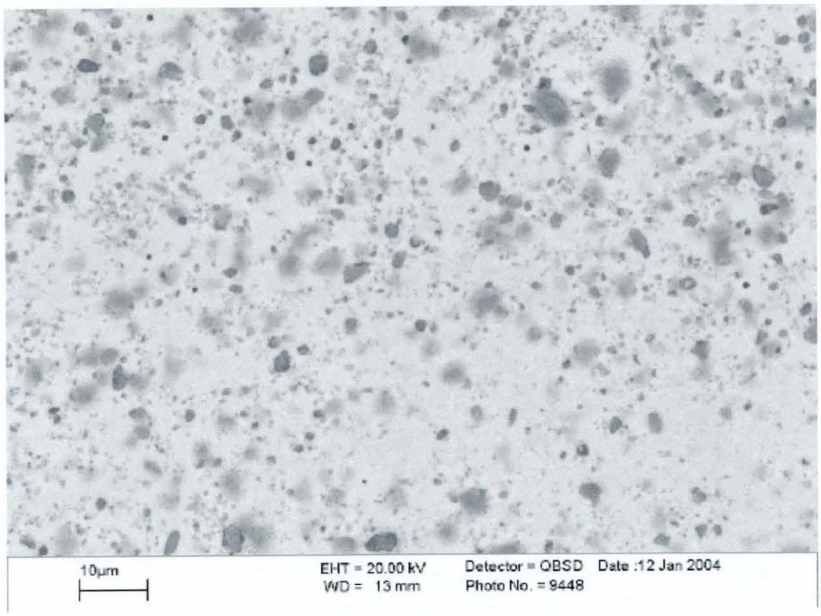

(a)

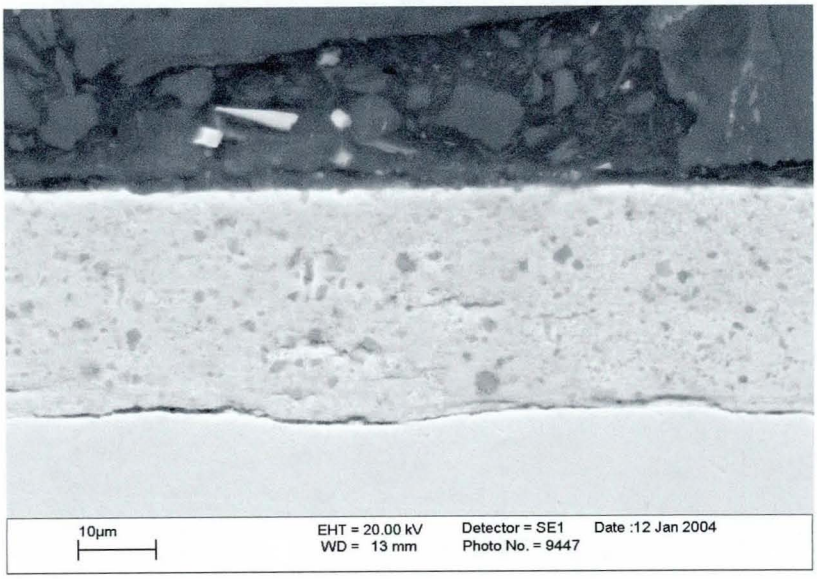

(b)

Figure 8.25. SEM Micrographs of Zn/SiO_2 electrodeposited with 26 wt% SiO_2 from a solution containing 250 g/l $ZnSO_4.7H_2O$, 80 g/l Na_2SO_4, 50 g/l SiO_2 (2.0 µm), current density 30 A/dm^2, amplitude of agitation 1.8 mm, pH 2.0 and NND 2.5 ml/l. (a) surface morphology (b) cross-sectional view.

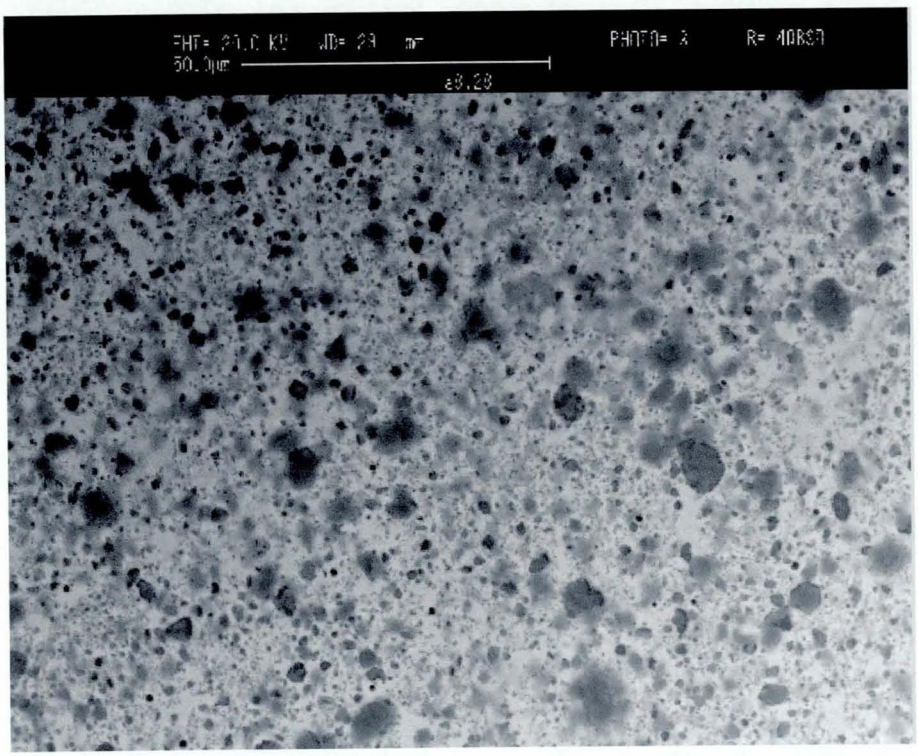

Figure 8.26. **Zn/SiO_2 electrodeposit (33 wt% of 2 μm SiO_2) obtained with 2.5 ml/l of NND in the bath.**

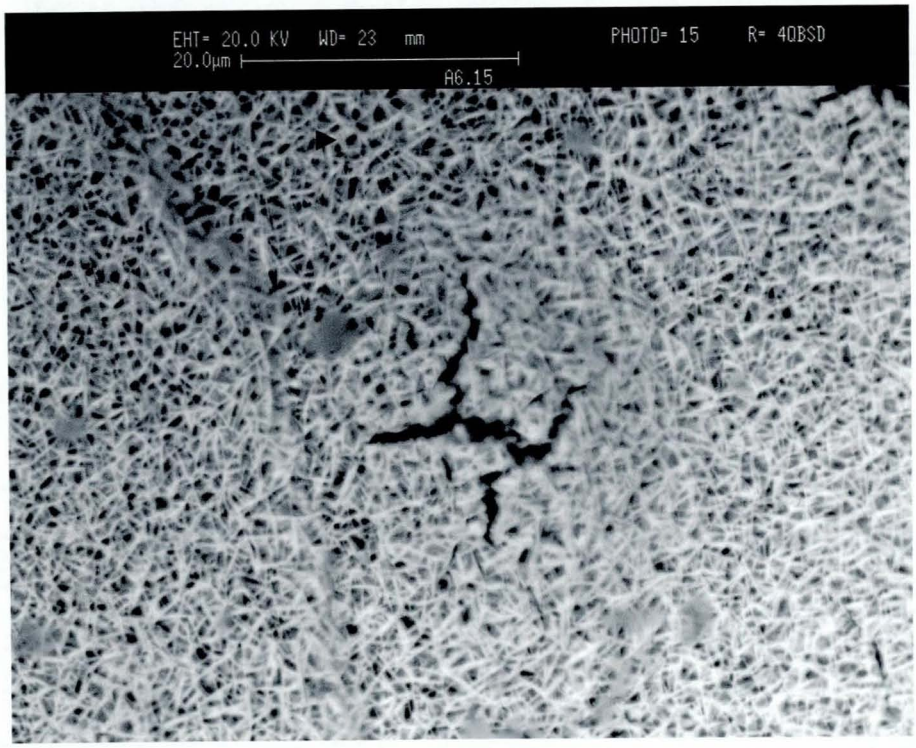

Figure 8.27. **Zn/SiO_2 electrodeposit obtained with 5 ml/l of NND in the bath.**

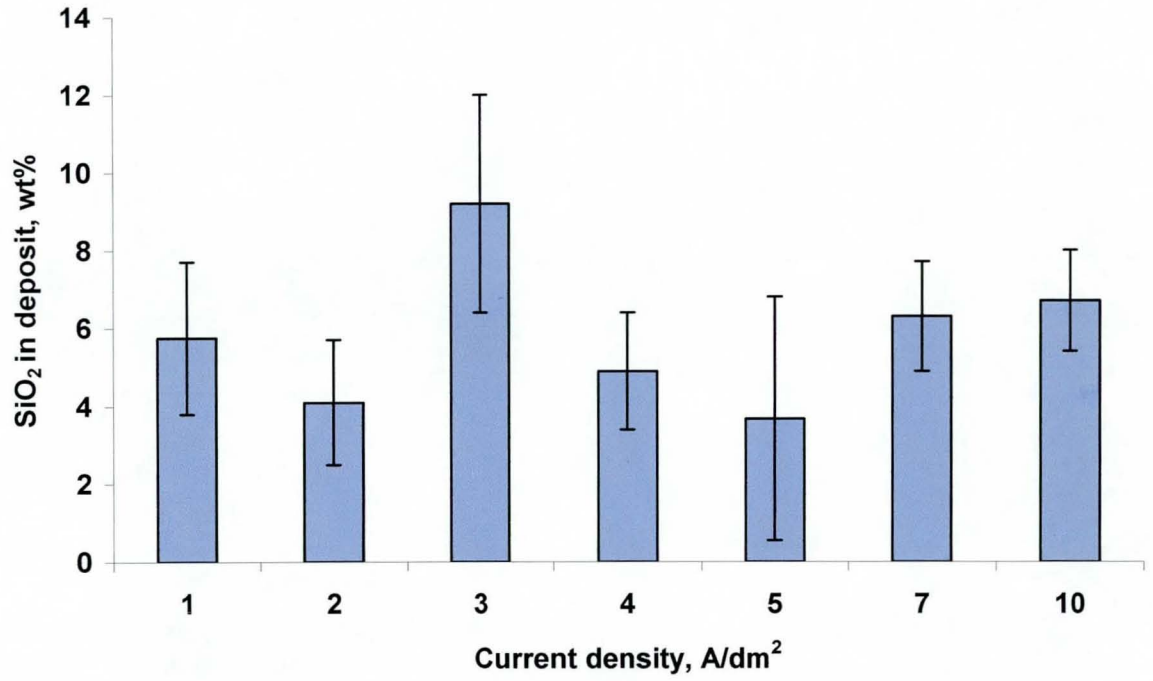

Figure 9.1 **Effect of current density on SiO_2 incorporation into zinc-nickel electrodeposits. Without NND, SiO_2 (2 µm) 20 g/l.**

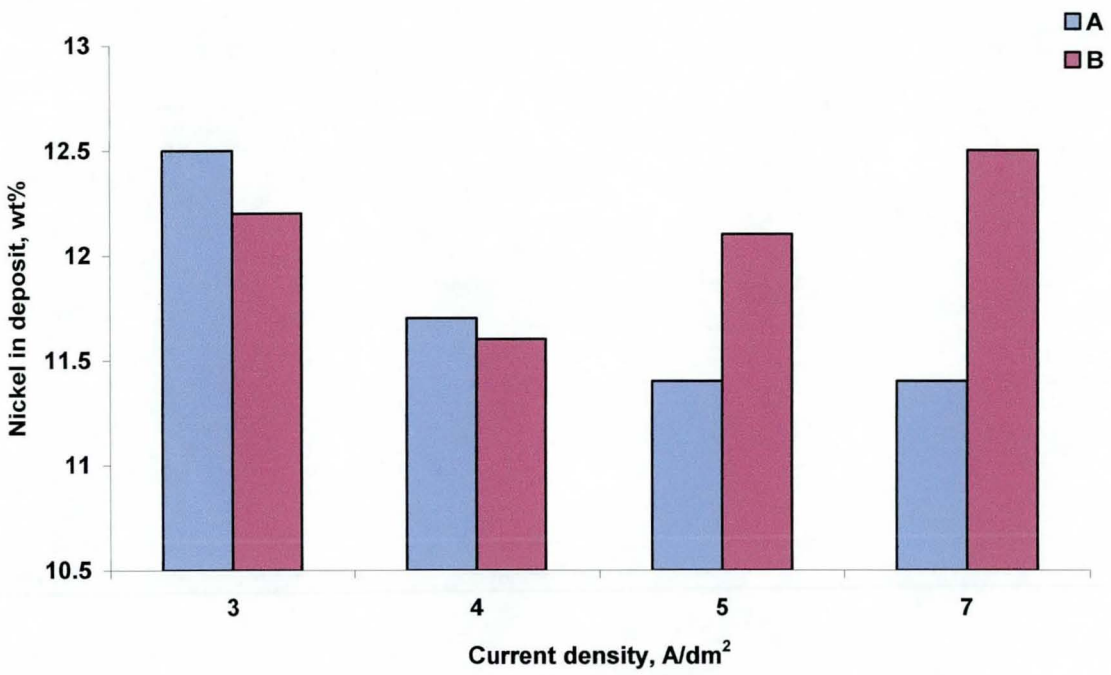

Figure 9.2 **Effect of current density on nickel content in zinc-nickel electrodeposits (A) without SiO_2 and (B) with 26 g/l SiO_2 (20 nm). Without bath agitation.**

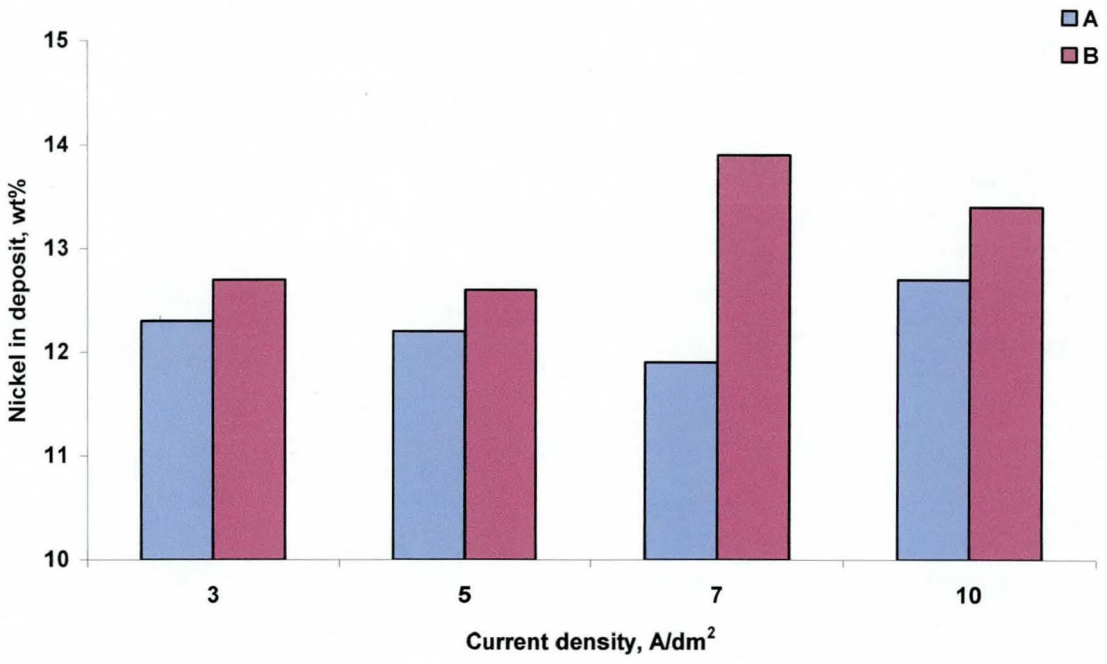

Figure 9.3 **Influence of current density on nickel content in zinc-nickel electrodeposits. (A) Without SiO_2 (B) with 20 g/l SiO_2 (2 µm) in the presence of bath agitation.**

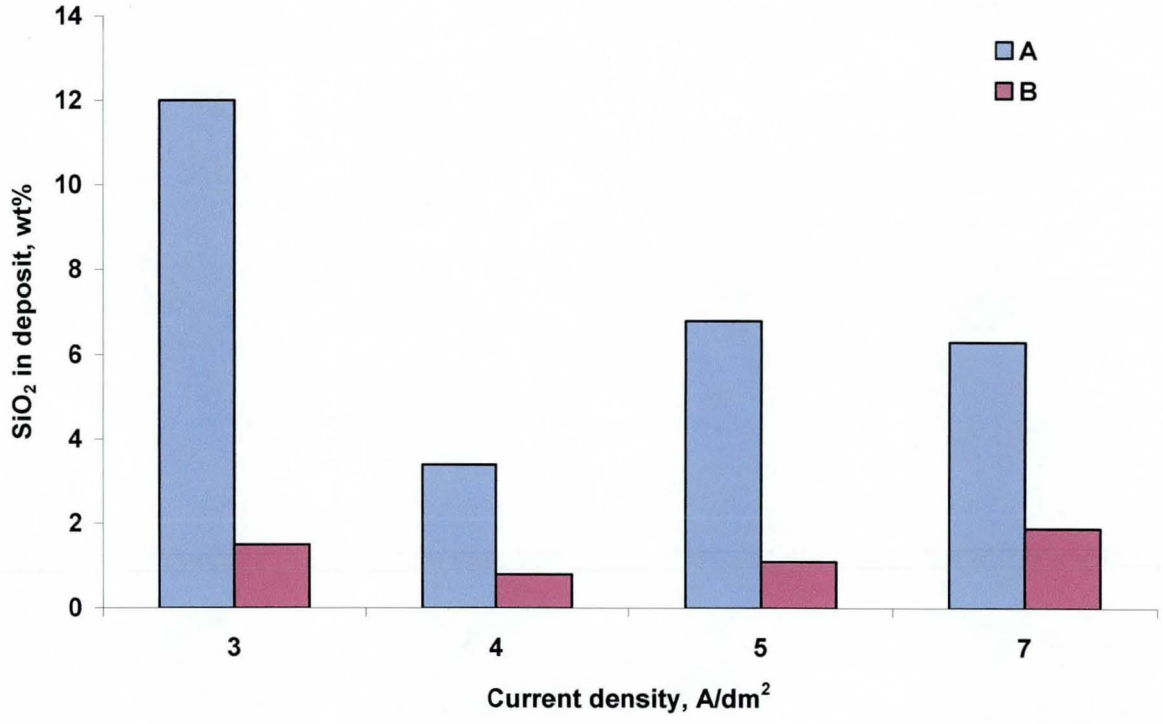

Figure 9.4 **Effect of particle size on particle incorporation during Zn-Ni/SiO_2 electrodepostion with (A) 2 µm (B) 20 nm.**

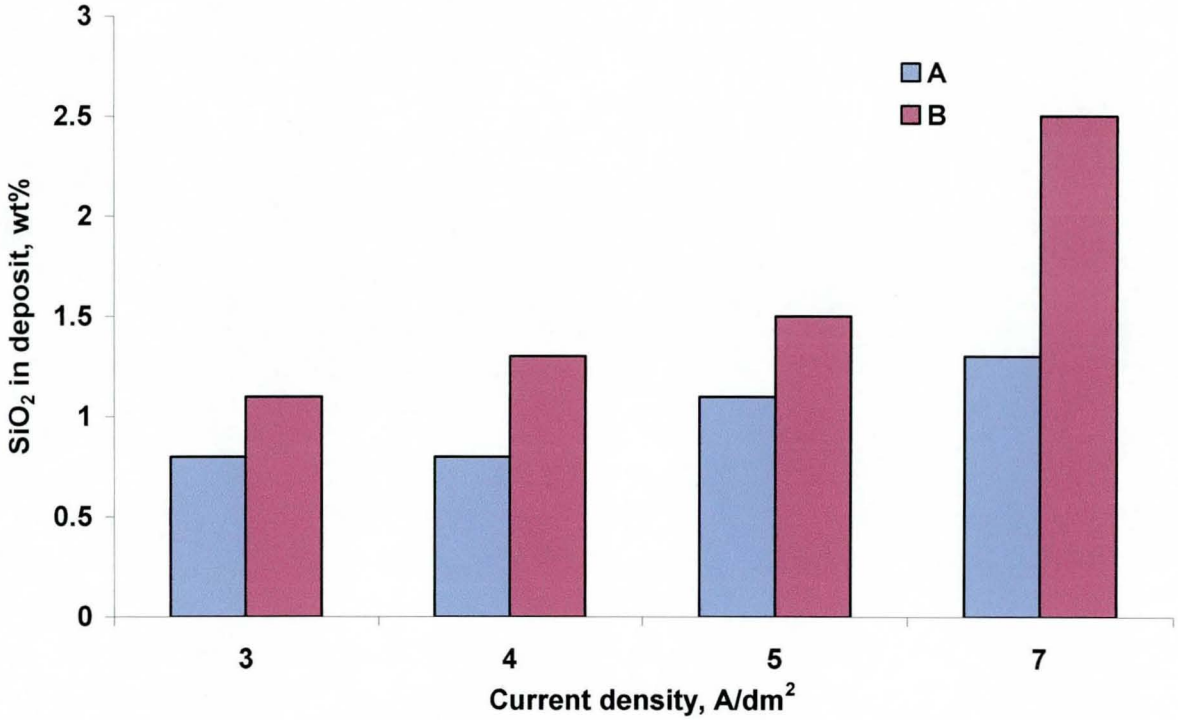

Figure 9.5 **Effect of current density on particle incorporation for 20 nm particles in zinc-nickel electrodeposit showing incorporation rates at (A) centre and (B) edges of each sample.**

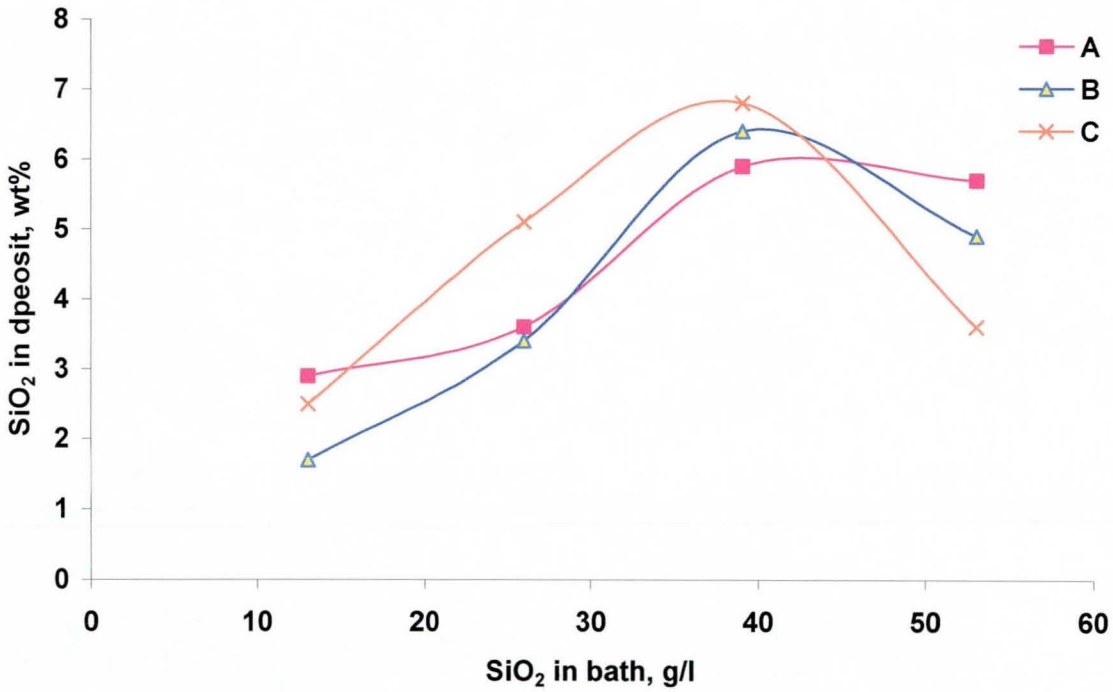

Figure 9.6 **Effect of particle loading on particle incorporation without bath agitation in the presence of SiO_2 (20 nm) at (A) 4 A/dm^2 (B) 5 A/dm^2 (C) 7 A/dm^2.**

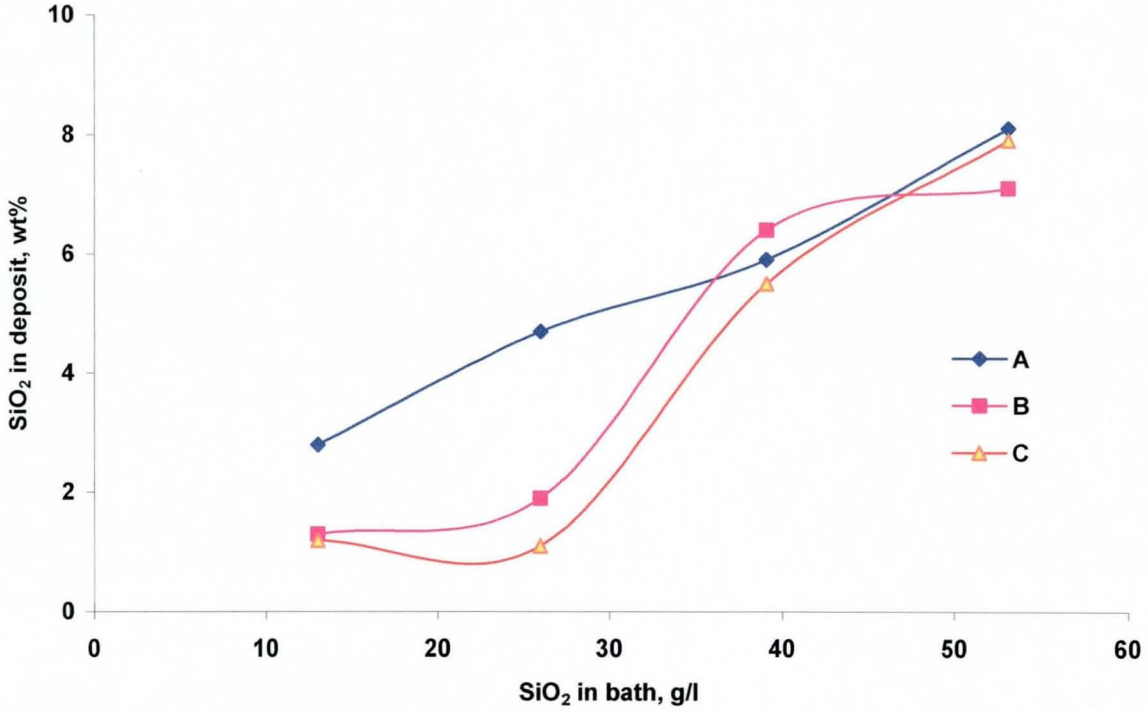

Figure 9.7 **Effect of particle loading on particle incorporation at (A) 4 A/dm^2 (B) 5 A/dm^2 (C) 7 A/dm^2 with bath agitation. SiO_2 (20 nm).**

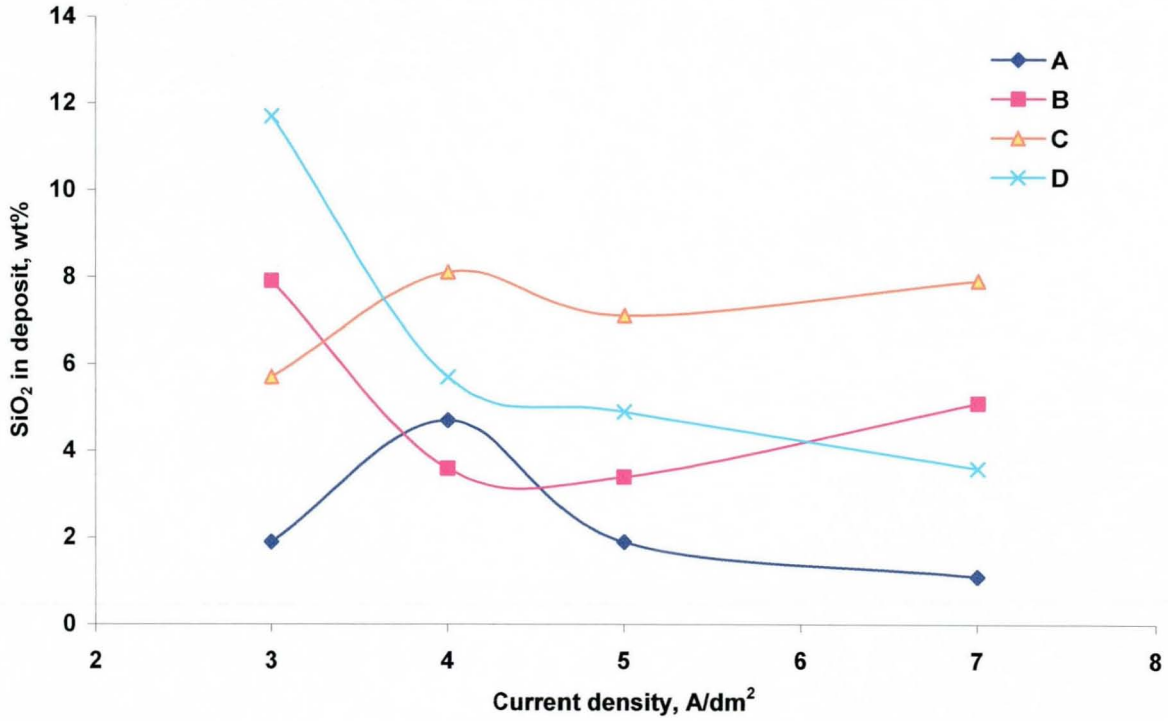

Figure 9.8 **Influence of current density and bath agitation on particle incorporation for baths with (A) 26 g/l SiO_2 and agitation (B) 26 g/l SiO_2 without agitation (C) 52 g/l SiO_2 and agitation (D) 52 g/l without agitation. Particle size 20 nm.**

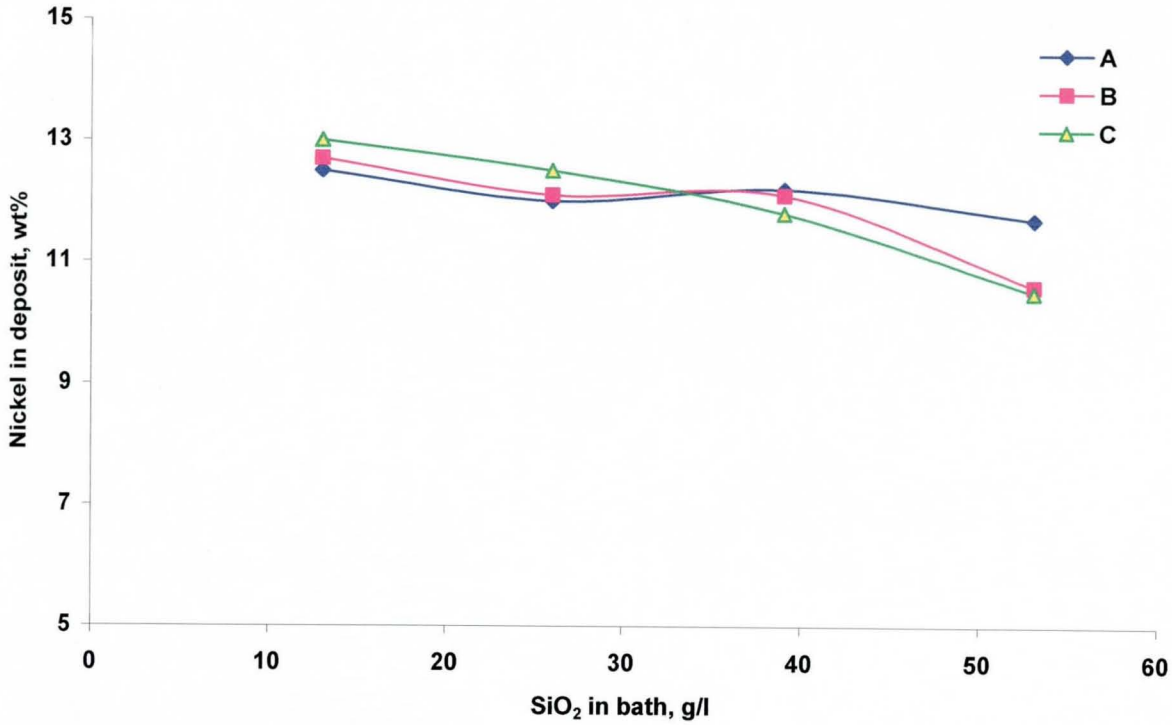

Figure 9.9 **Effect of SiO_2 content in zinc-nickel bath on nickel deposition at (A) 4 A/dm^2 (B) 5 A/dm^2 (C) 7 A/dm^2.**

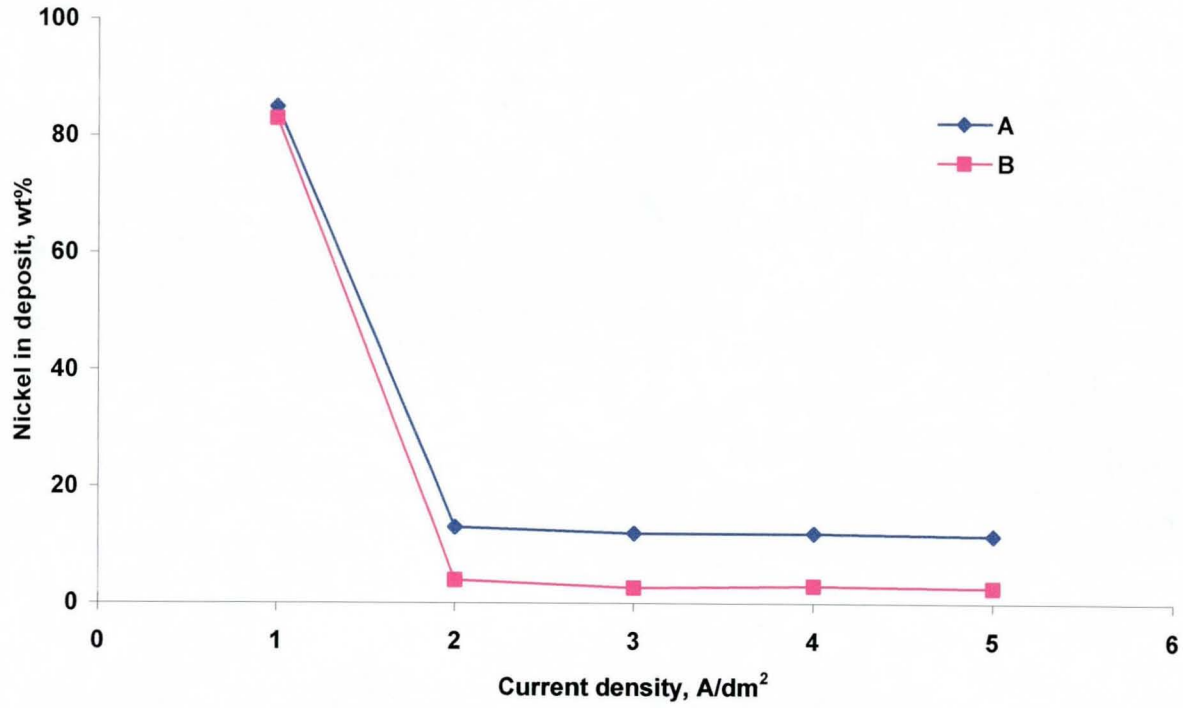

Figure 9.10 **Effect of current density on nickel deposition in the presence of SiO_2 (2 µm) 20 g/l (A) without NND (B) with NND.**

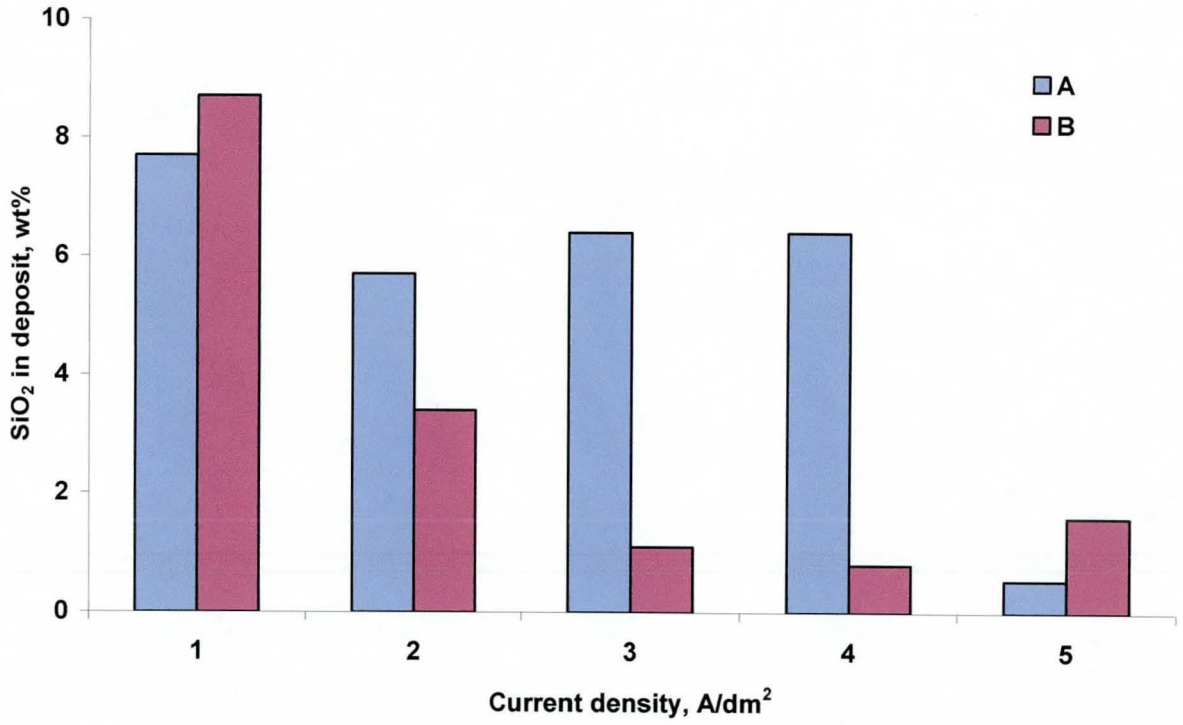

Figure 9.11 **Effect of current density on SiO_2 deposition from a zinc-nickel bath (A)without NND and (B) with NND, SiO_2 (2 µm) 20 g/l.**

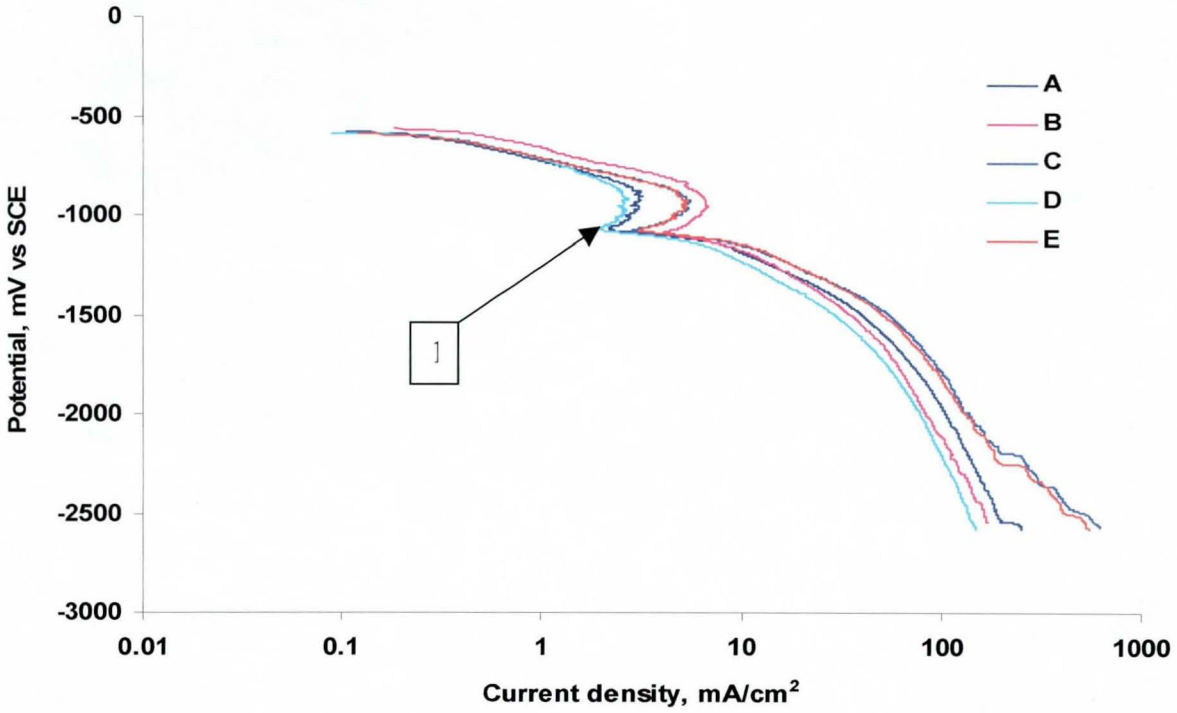

Figure 9.12 **Cathodic polarisation curves for Zn-Ni/SiO_2 with (A) 20 g/l SiO_2, 600 rpm (B) 20 g/l SiO_2, 0 rpm (C) 0 g/l, 300 rpm (D) 20 g/l SiO_2, 300 rpm (E) 0 g/l, 600 rpm. Region 1 nucleation and crystal growth.**

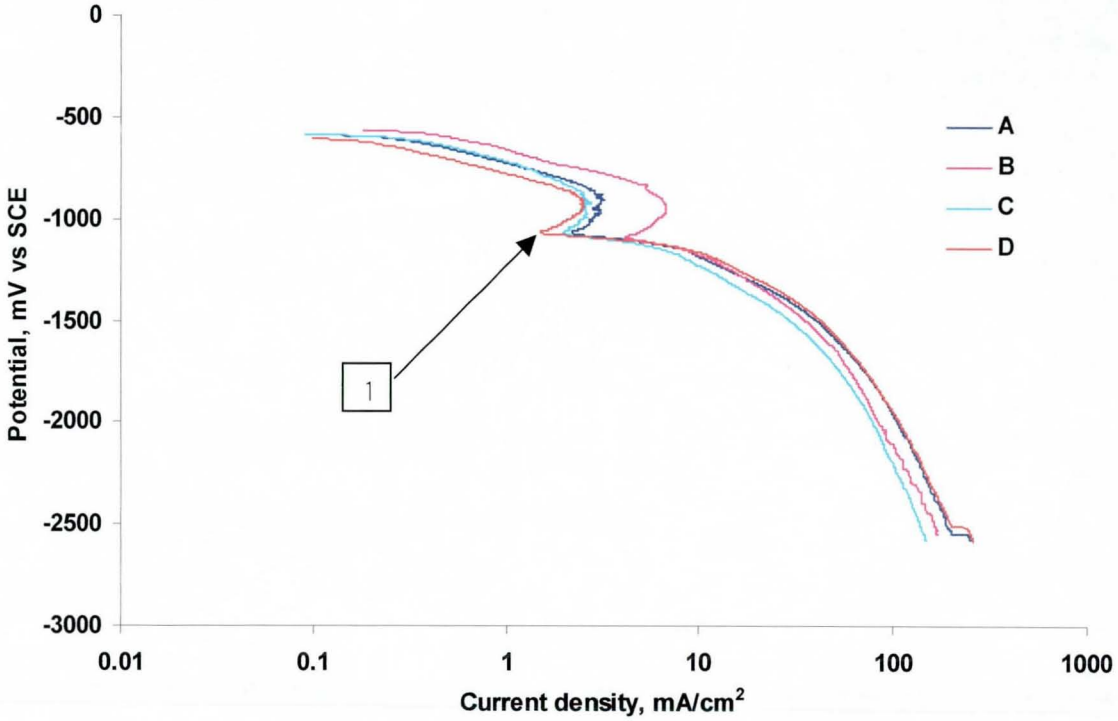

Figure 9.13 **Cathodic polarisation curves for Zn-Ni with 20 g/l of 2 µm SiO_2 in the bath with agitation at (A) 600 rpm (B) 0 rpm (C) 300 rpm (D) 900 rpm. Region 1 nucleation and crystal growth.**

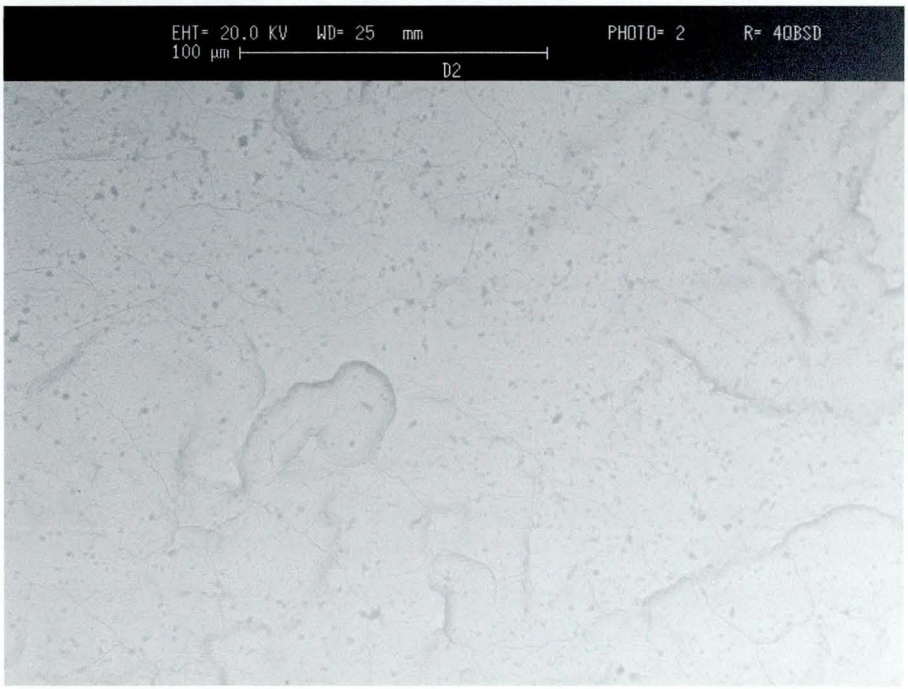

(a)

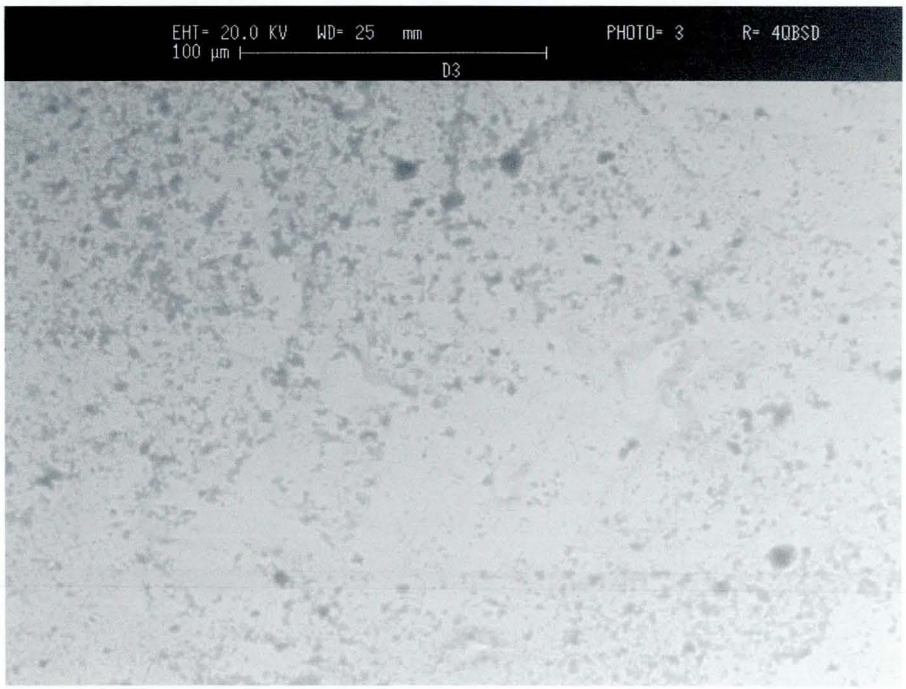

(b)

Figure 9.14 **SEM micrograph of Zn-Ni/SiO_2 electrodeposit with 13 wt% nickel and (a) 2.4 wt% SiO_2 (b) 11.3 wt% SiO_2.**

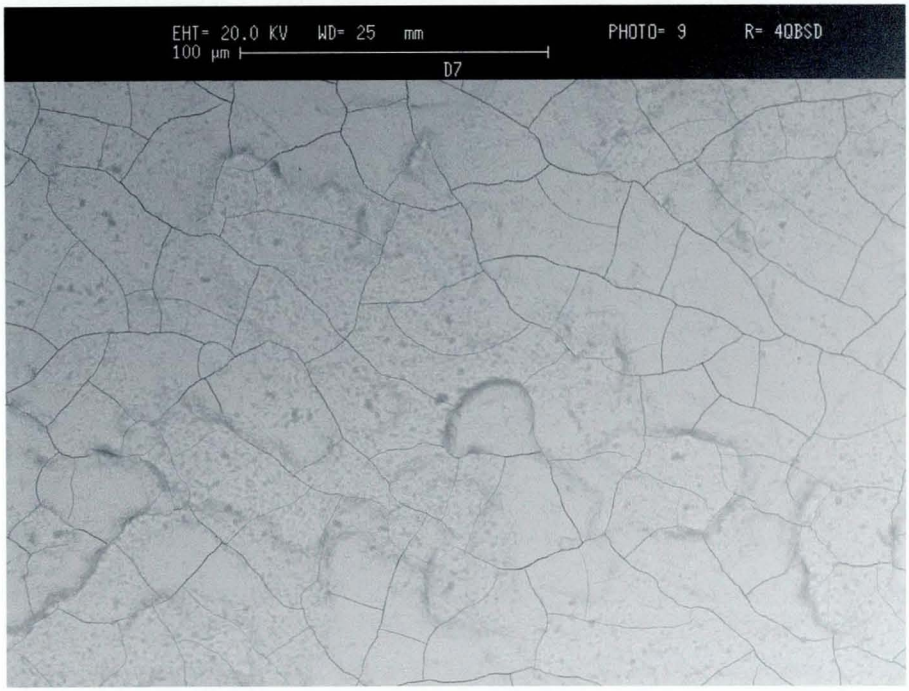

(a)

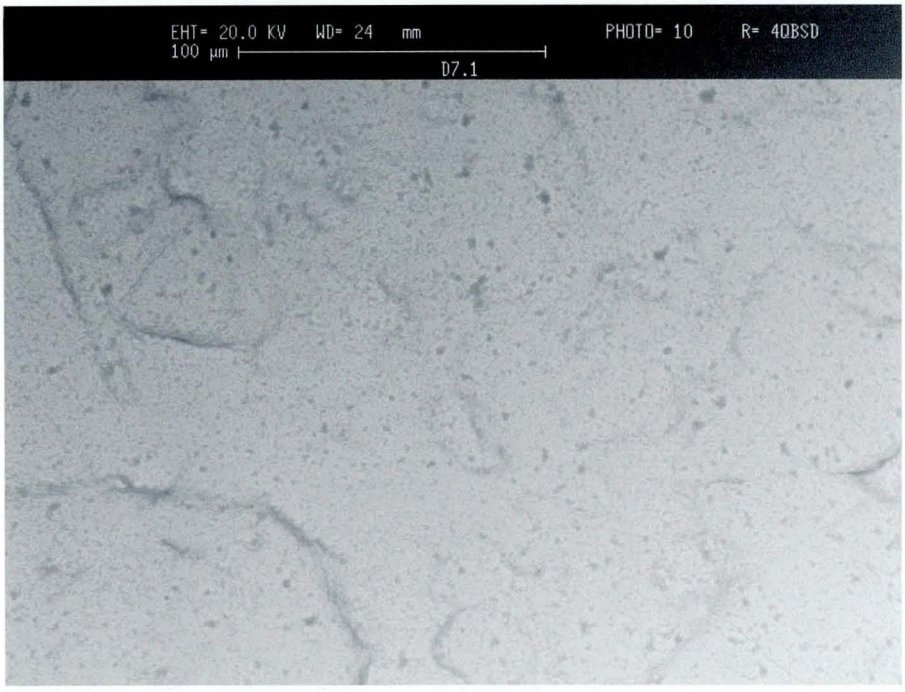

(b)

Figure 9.15 **SEM micrograph of Zn-Ni/SiO_2 electrodeposit with 13.4 wt% nickel and (a) 5.4 wt% SiO_2 (b) 7.5 wt% SiO_2.**

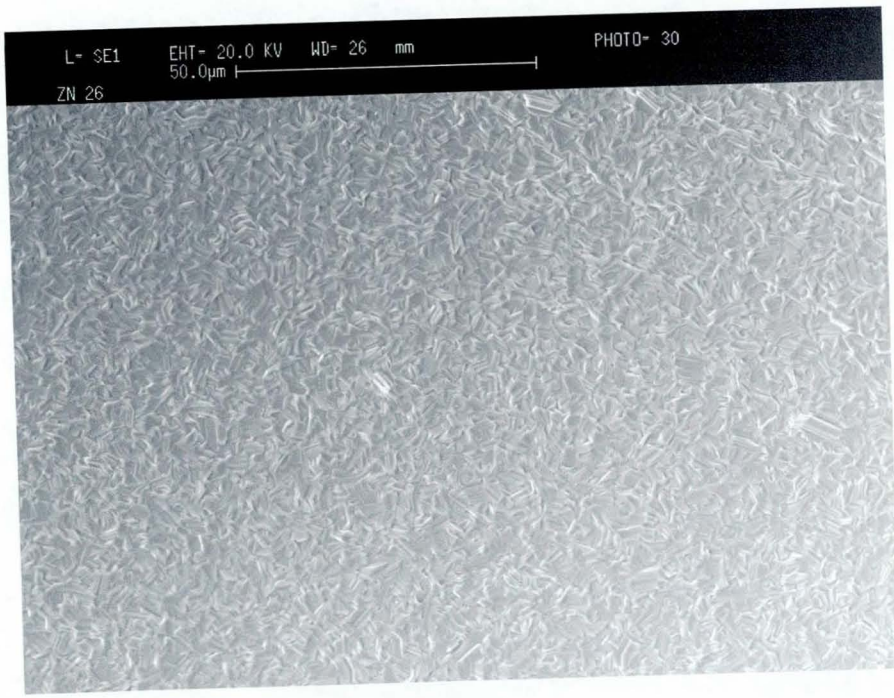

(a)

(b)

Figure 10.1 **SEM micrographs of zinc from baths containing (a) 250 g/l $ZnSO_4.7H_2O$, 80 g/l Na_2SO_4, pH 2.3 (b) 350 g/l $ZnSO_4.7H_2O$, 30 g/l $Al_2(SO_4)_3$, 30 g/l H_3BO_3, pH 2.3.**

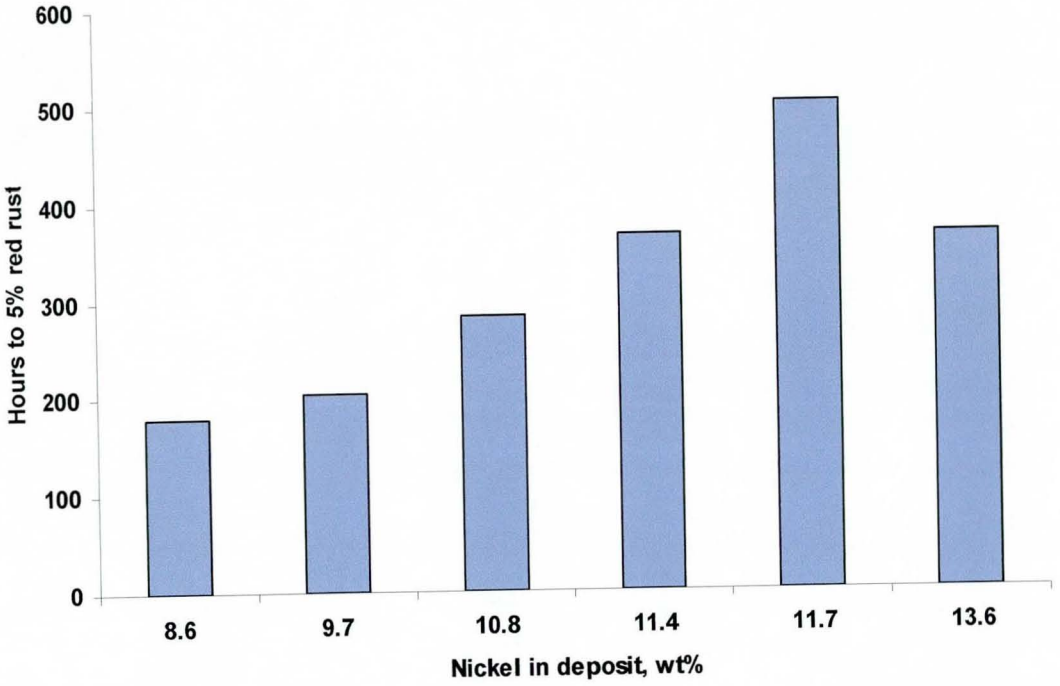

Figure 10.2 **Dependence of Hours to 5% red rust on nickel percentage in the deposit**

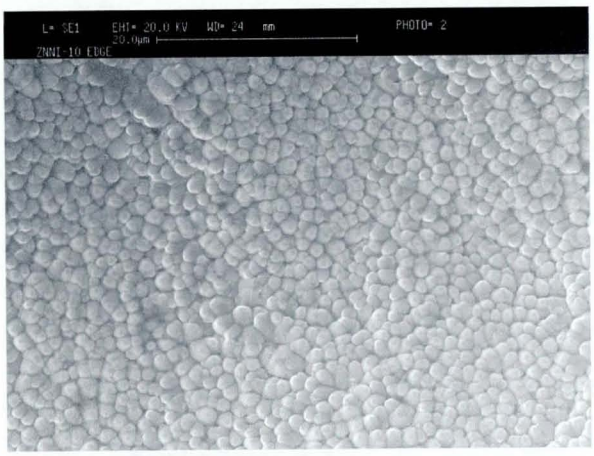

(a)

(b)

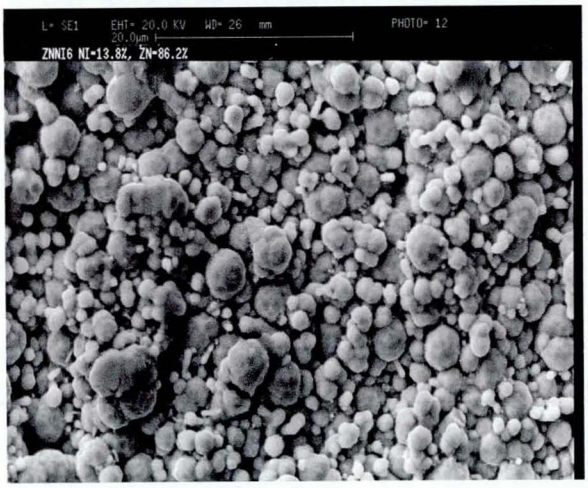

(c)

Figure 10.3 **SEM micrographs showing the surface morphologies of zinc-nickel electrodeposits containing (a) 8.6 wt% Ni (b) 11.7 wt% Ni and (c) 13.8 wt% Ni.**

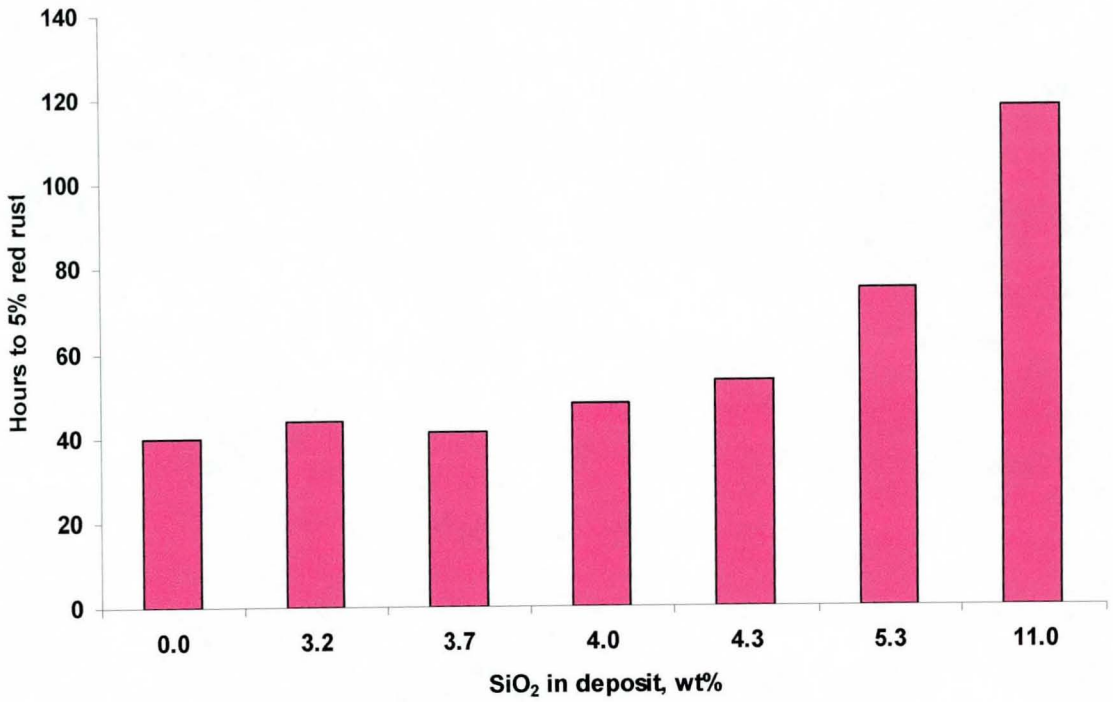

Figure 10.4 **Corrosion resistance of Zn/SiO_2 coatings with different contents of SiO_2 in the deposits.**

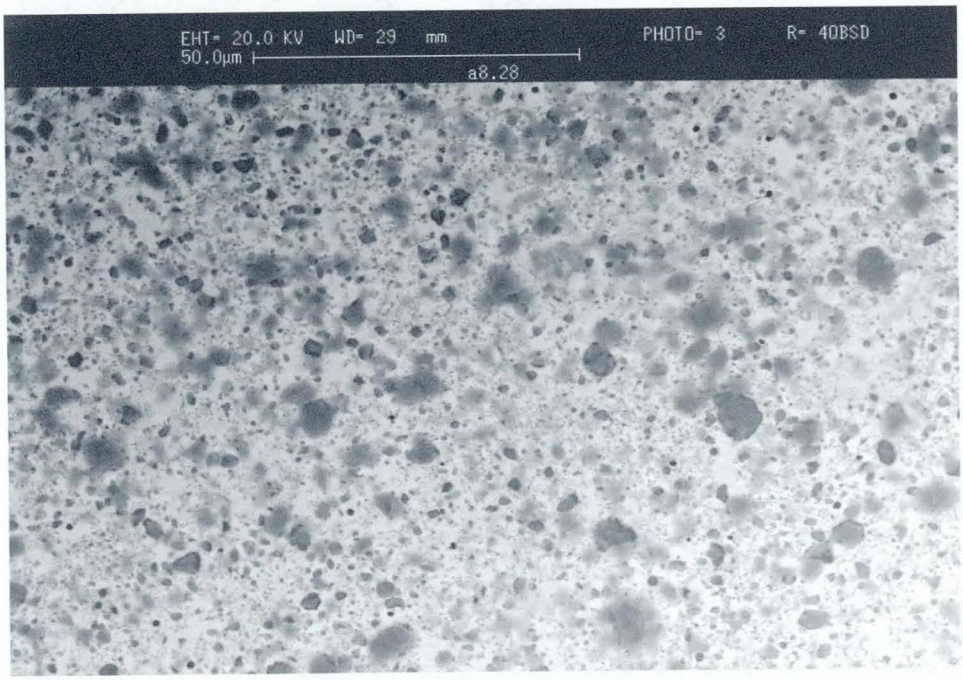

(a)

(b)

Figure 10.5 **SEM micrographs showing (a) surface (b) cross-sectional views of Zn-SiO_2 electrodeposits from a bath containing NND.**

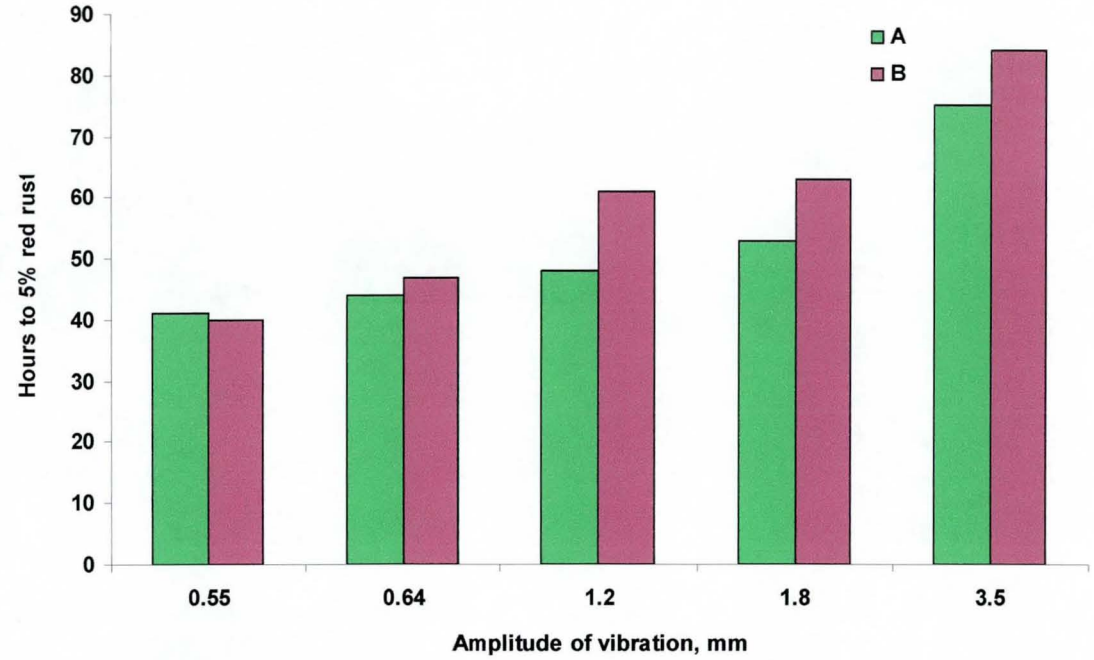

Figure 10.6 **Influence of $NaNO_3$ on the corrosion resistance of Zn/SiO_2 coatings from baths containing (A) 0 ppm $NaNO_3$ and (B) 1000 ppm $NaNO_3$ at different rates of solution agitation.**

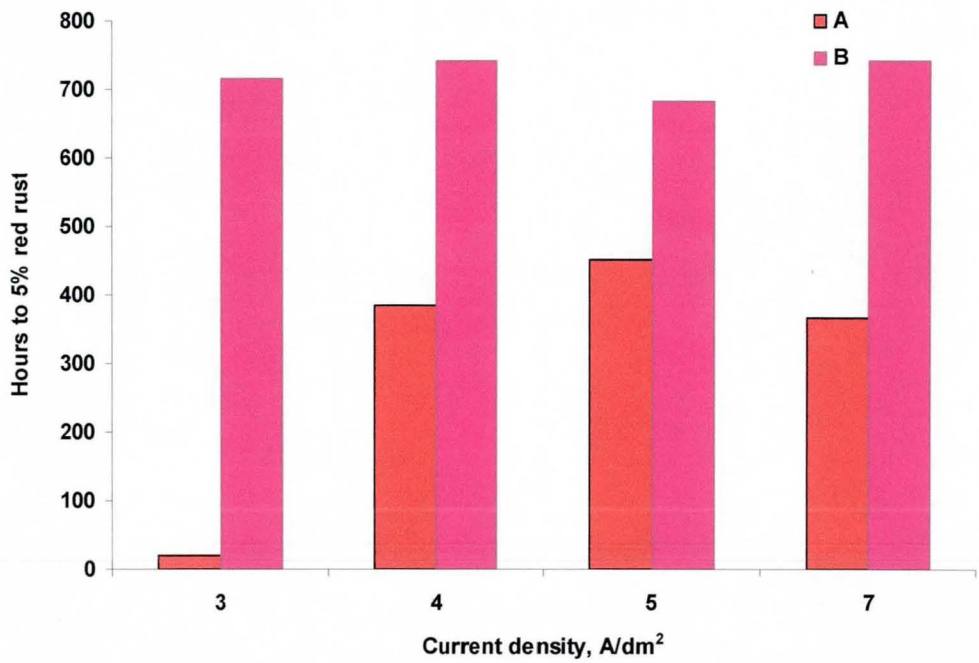

Figure 10.7 **Influence of current density on the corrosion resistance of Zn-Ni and $Zn\text{-}Ni/SiO_2$ electrodeposits without agitation from a bath containing (A) 0 g/l SiO_2 and (B) 26 g/l SiO_2.**

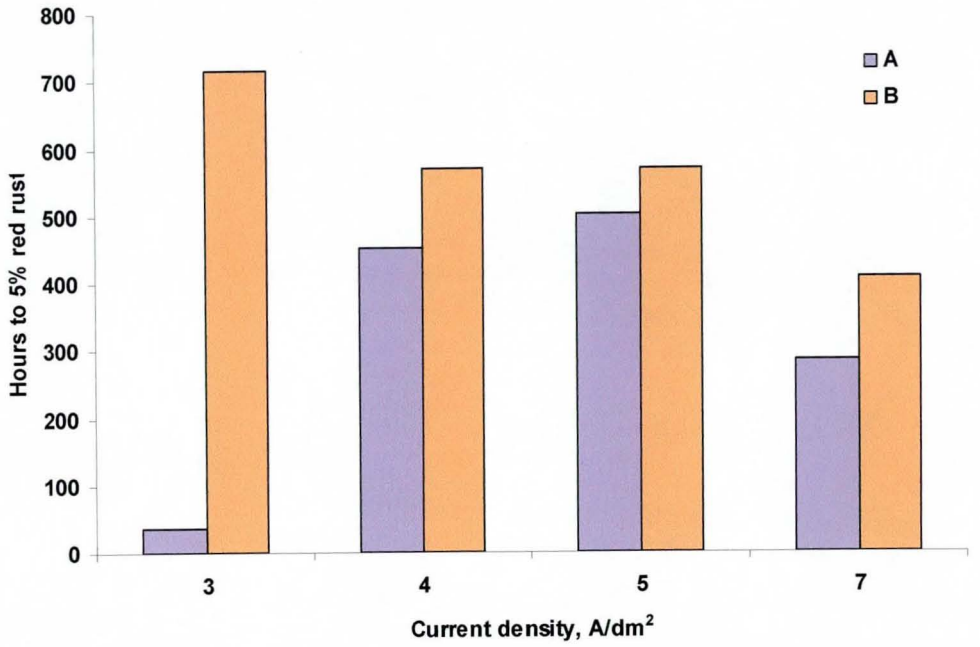

Figure 10.8 **Influence of current density on the corrosion resistance of Zn-Ni and Zn-Ni/SiO_2 electrodeposits in the presence of agitation from a bath containing (A) 0 g/l SiO_2 and (B) 26 g/l SiO_2. Vibratory agitation amplitude 0.64 mm.**

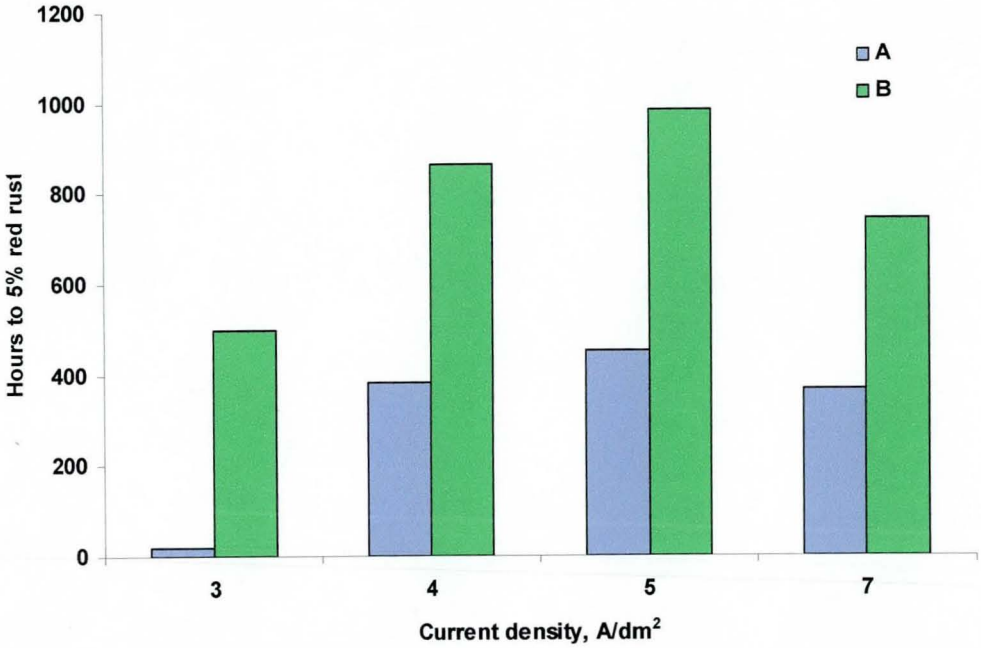

Figure 10.9 **Influence of current density on the corrosion resistance of Zn-Ni and Zn-Ni/SiO_2 electrodeposits without agitation from a bath containing (A) 0 g/l SiO_2 and (B) 52 g/l SiO_2.**

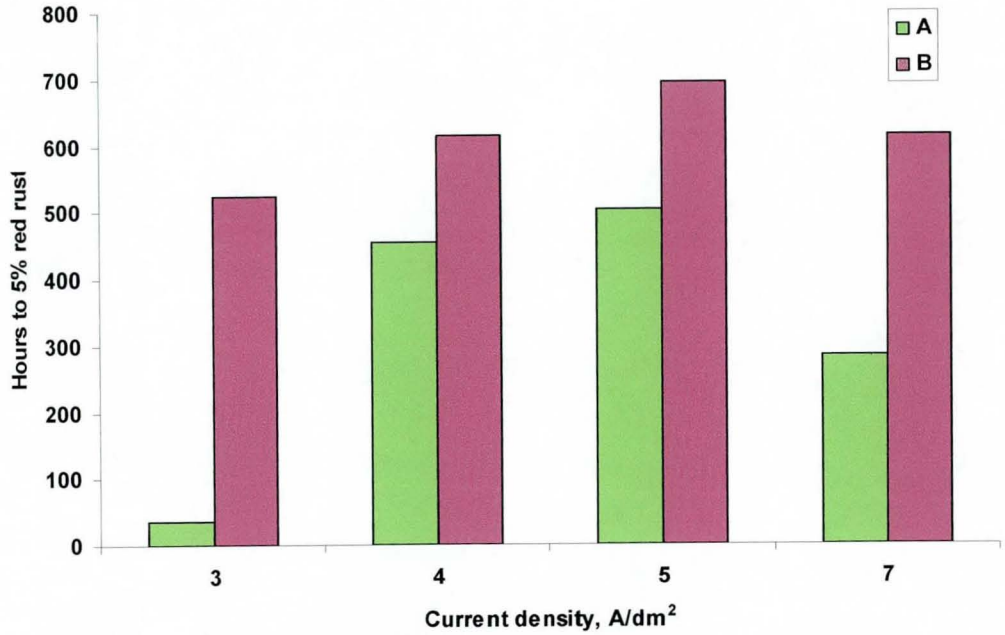

Figure 10.10 **Influence of current density on the corrosion resistance of Zn-Ni and Zn-Ni/SiO_2 electrodeposits in the presence of agitation from a bath containing (A) 0 g/l SiO_2 and (B) 52 g/l SiO_2. Vibratory agitation amplitude 0.64 mm.**

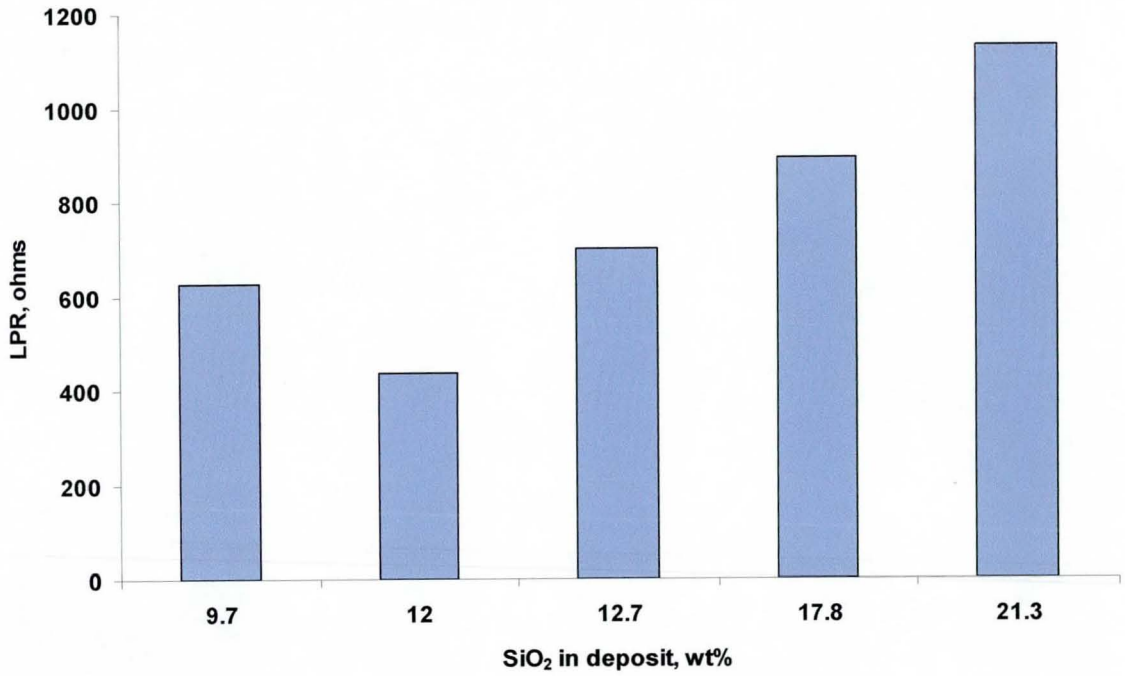

Figure 10.11 **LPR of Zn/SiO_2 composite coatings containing 2 μm particles without NND.**

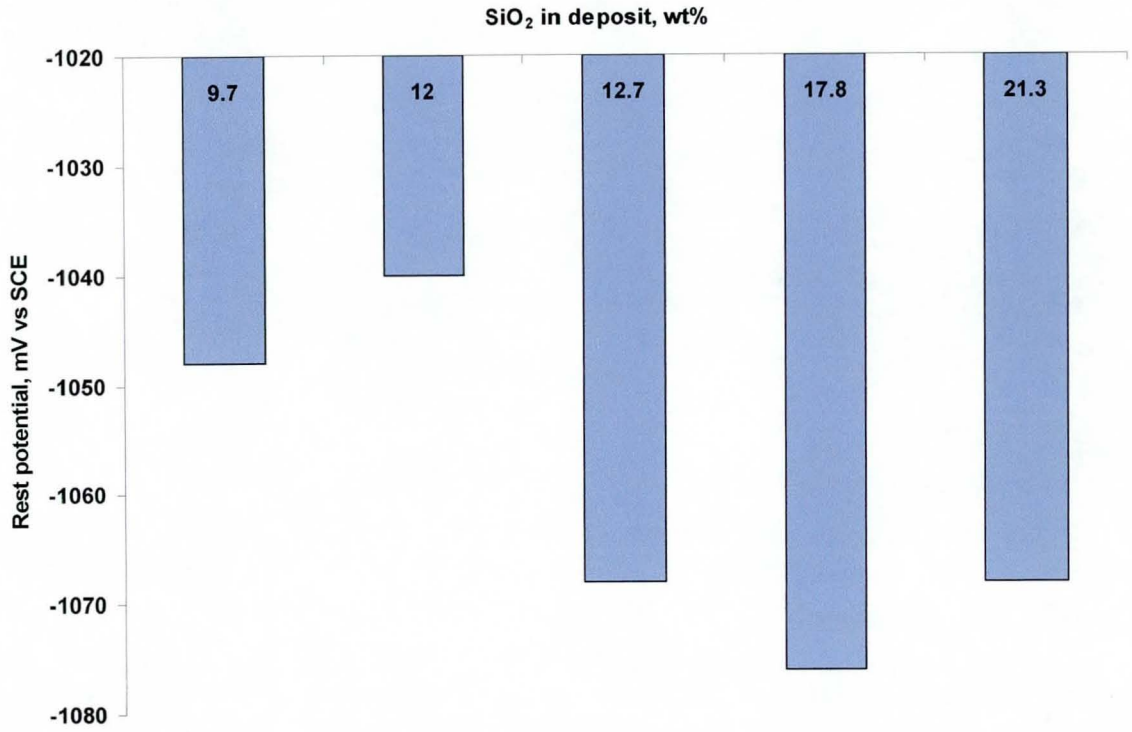

Figure 10.12 **Comparison of rest potential data for Zn/SiO_2 composite electrodeposit in 5% NaCl solution.**

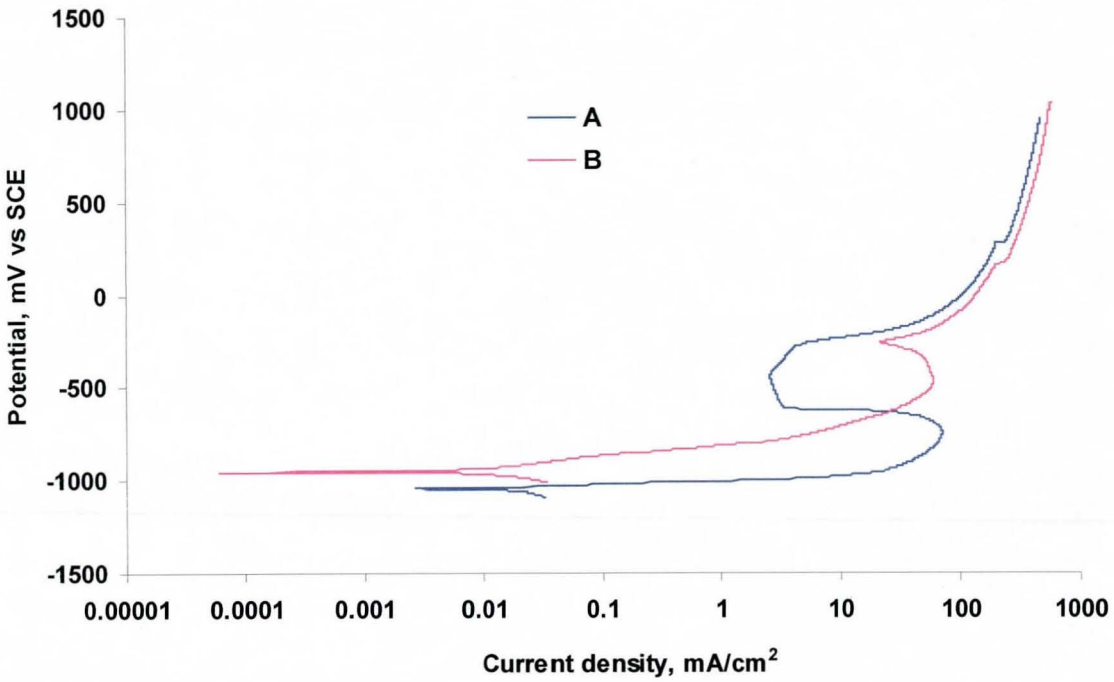

Figure 10.13 **Anodic polarization curves for (A) Zn (B) Zn-Ni in 5% NaCl solution.**

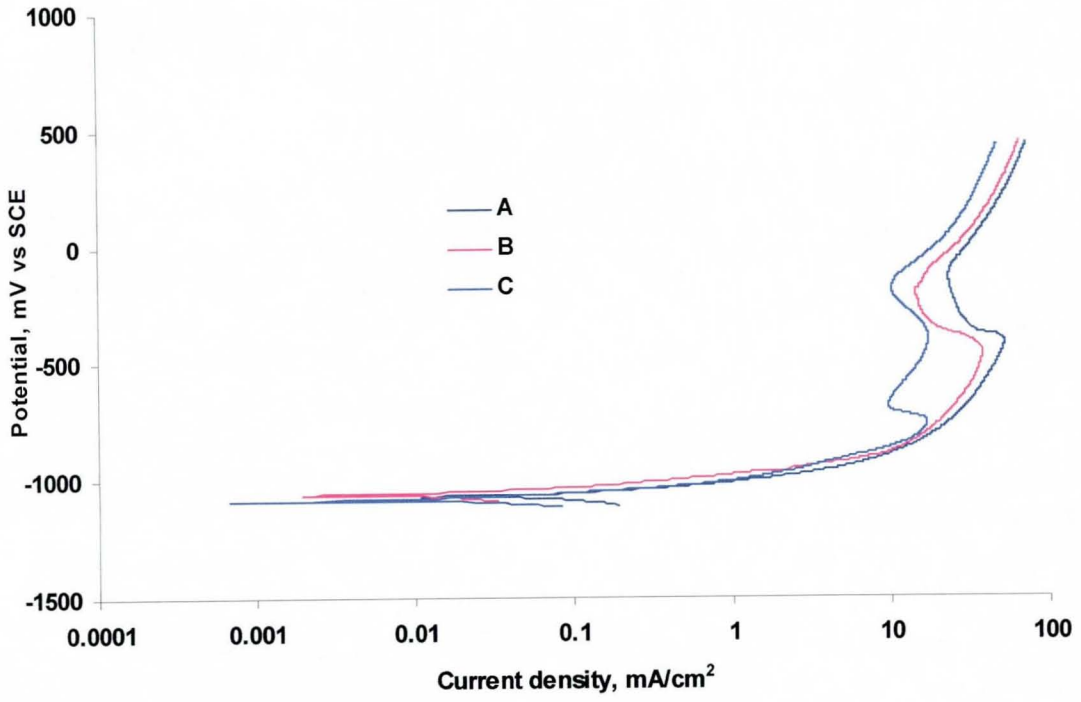

Figure 10.14 **Anodic polarization curves for Zn/SiO_2 coatings containing (A) 5.4% SiO_2 (B) 8.5% SiO_2 (C) 22 % SiO_2.**

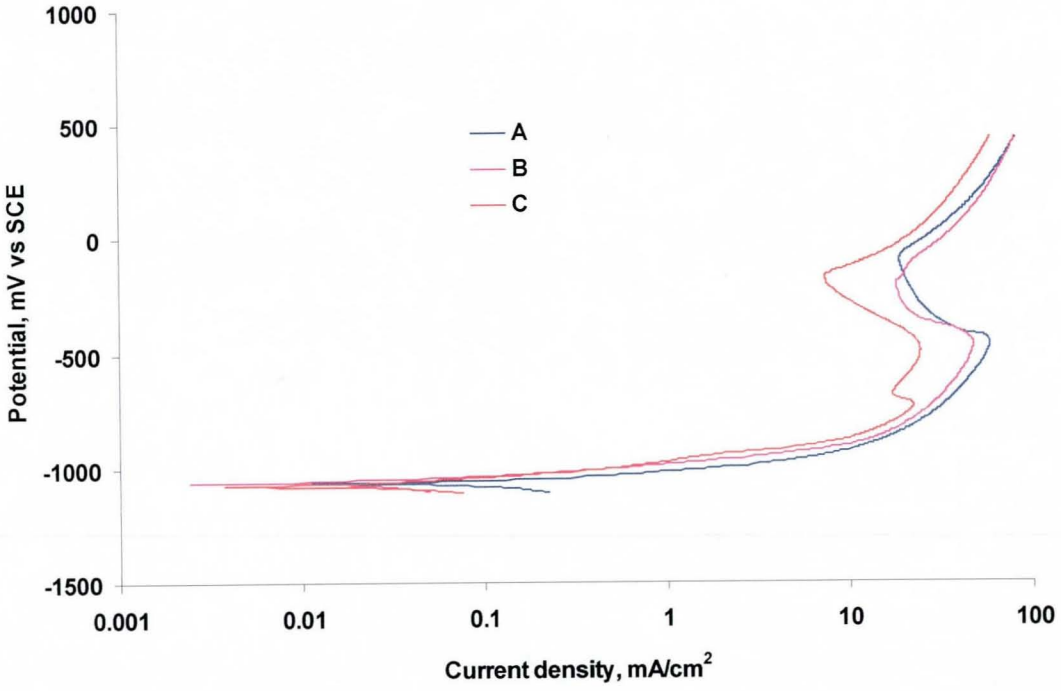

Figure 10.15 **Anodic polarization curves for Zn and Zn-SiO_2 coatings containing (A) 0 % SiO_2 (B) 8.5% SiO_2 (C) 8.5 % SiO_2 from a bath containing NND.**

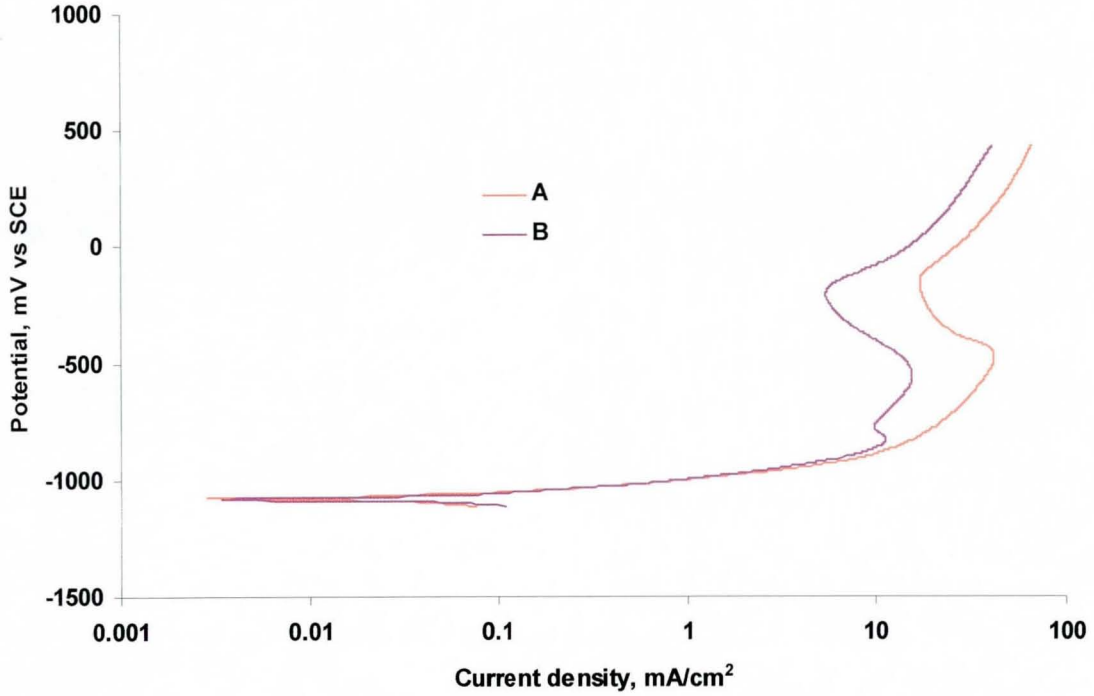

Figure 10.16 **Anodic polarization curves for Zn/SiO_2 coatings containing (A) 19.6 % SiO_2 (B) 19.6 % SiO_2 from a bath containing NND.**

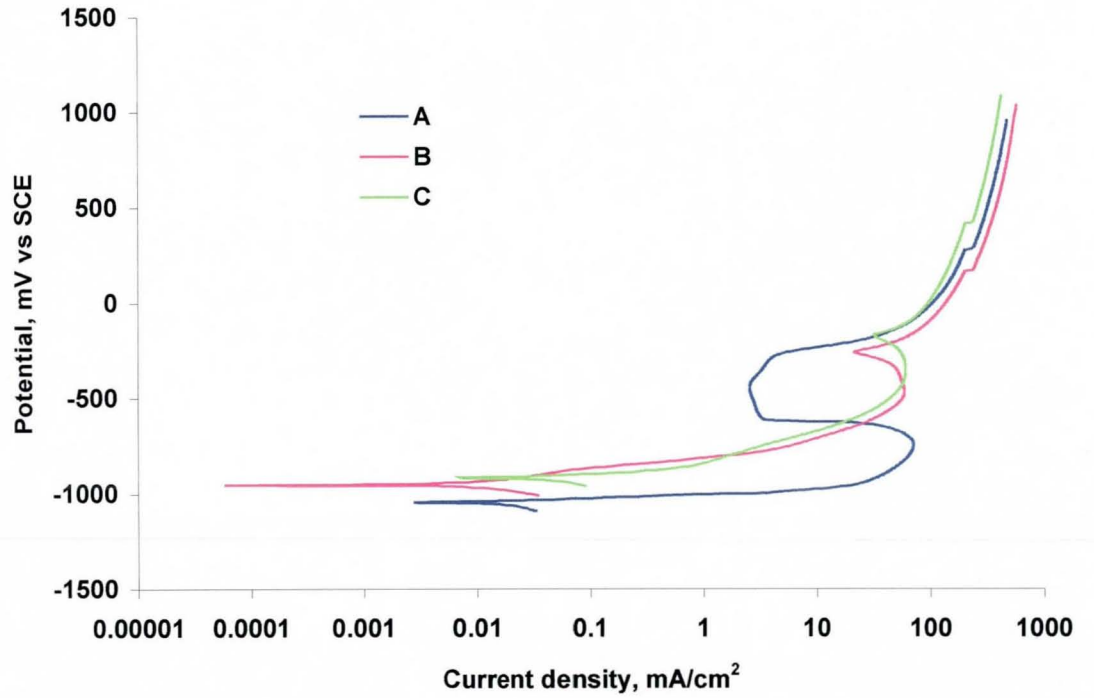

Figure 10.17 **Anodic polarization curves for zinc, zinc-nickel and zinc-nickel/silica coatings produced from (A) Zn (B) Zn-Ni and (C) $Zn-Ni/SiO_2$ baths.**

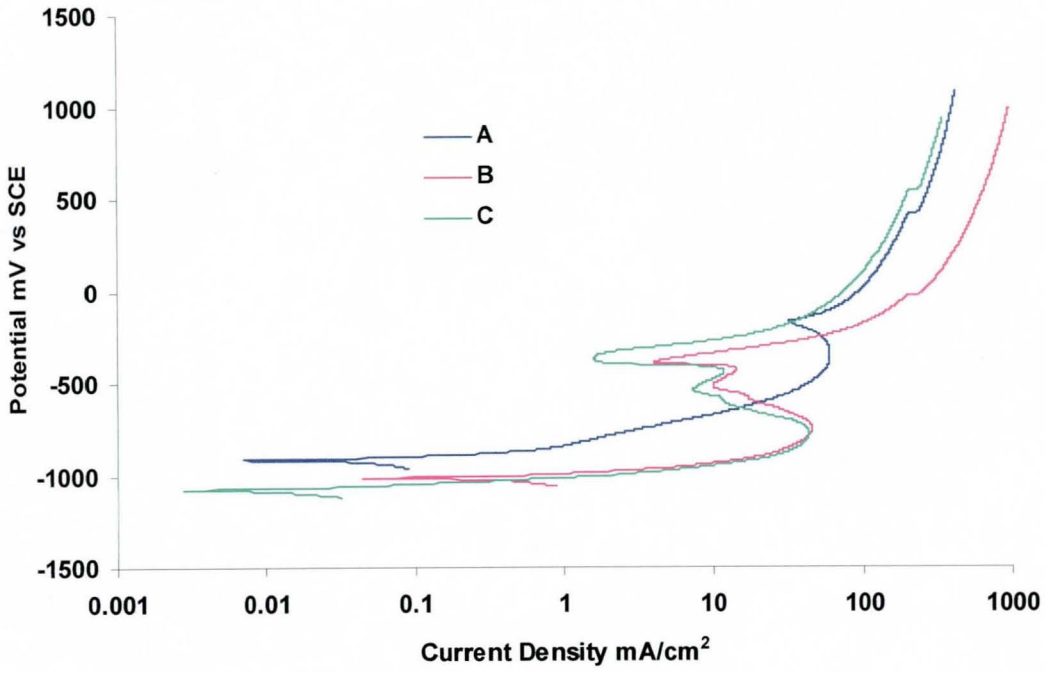

Figure 10.18 **Anodic polarization curves for Zn-Ni/SiO_2 coatings produced from baths containing (A) 0 ml/l (B) 0.25 ml/l (C) 5 ml/l NND.**

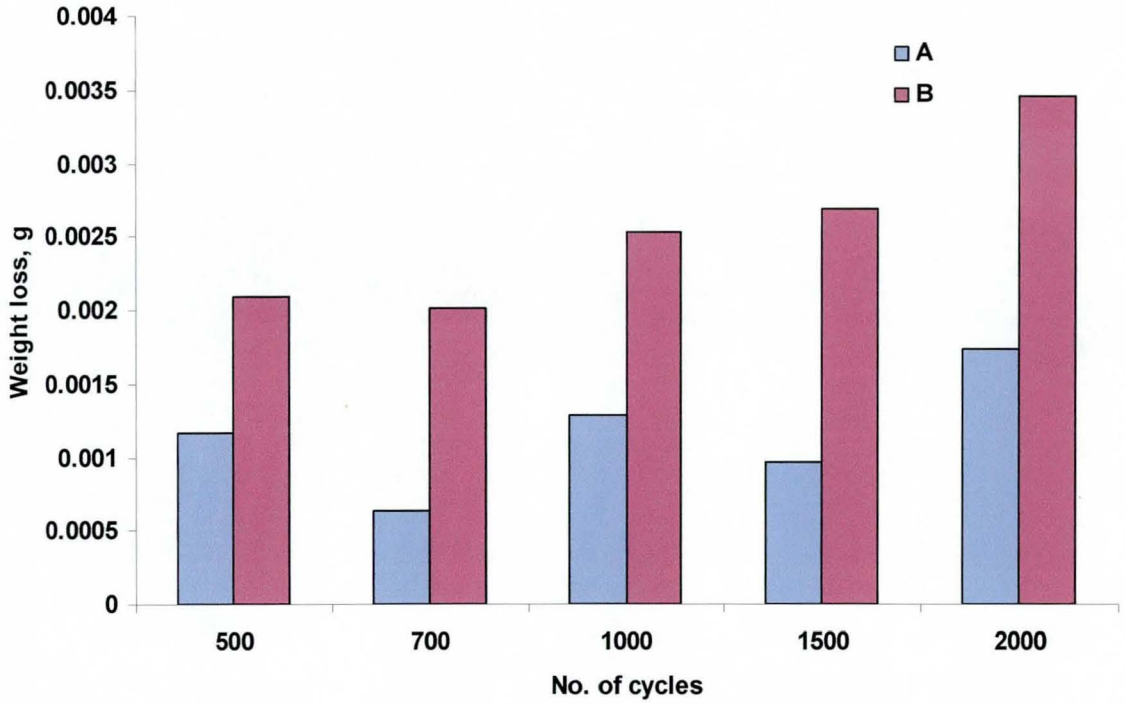

Figure 11.1 **Wear behaviour of zinc with increasing number of cycles for loads of (A) 0.8 N and (B) 2.9 N.**

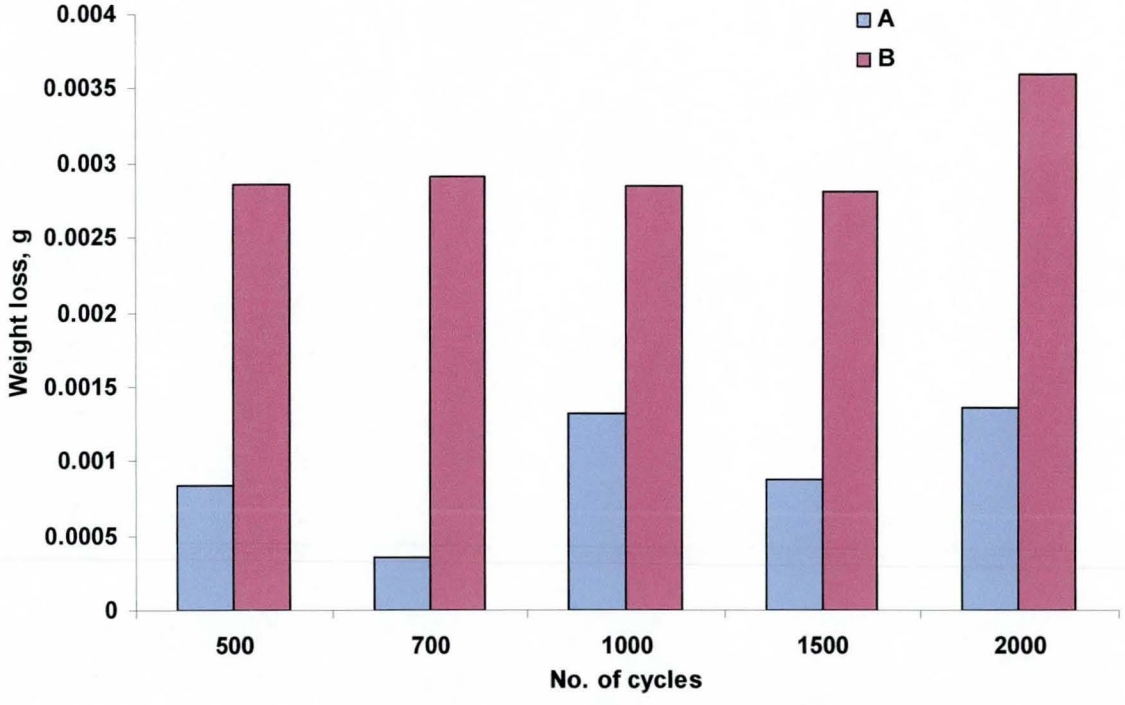

Figure 11.2 **Wear behaviour of Zn/SiO_2 coatings with increasing number of cycles for loads (A) 0.8 N and (B) 2.9 N. SiO_2 (20nm) in deposit approximately 5 wt%.**

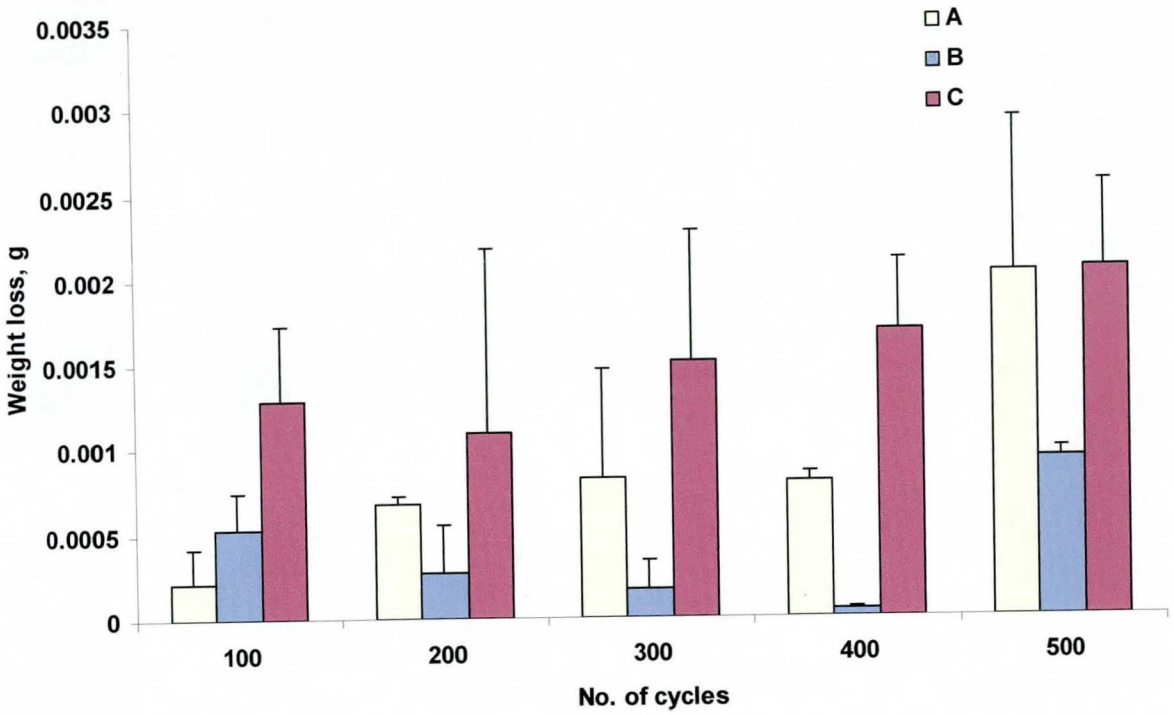

Figure 11.3 **Wear behaviour of Zn-Ni and Zn-Ni/SiO_2 electrodeposits containing different amounts of 20 nm SiO_2 particles. (A) 11% Ni, 0% SiO_2 (B) 11% Ni, 1% SiO_2 (C) 11 % Ni, 11 % SiO_2. Load 10 N.**

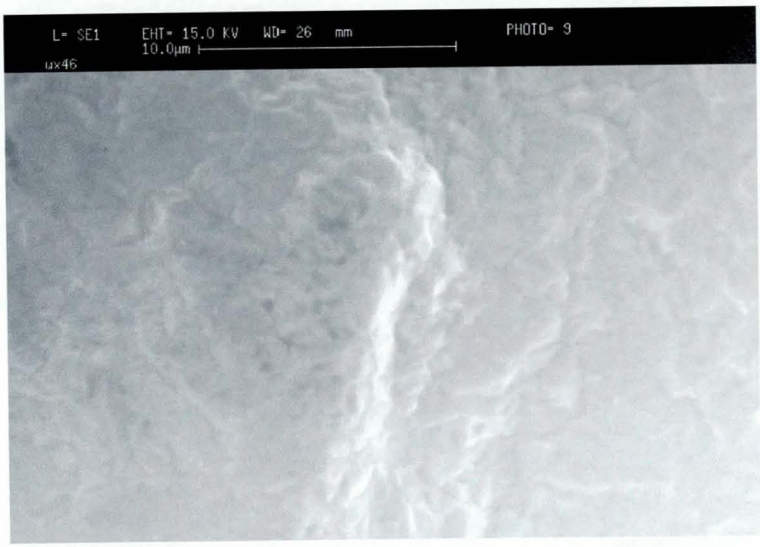

(a)

(b)

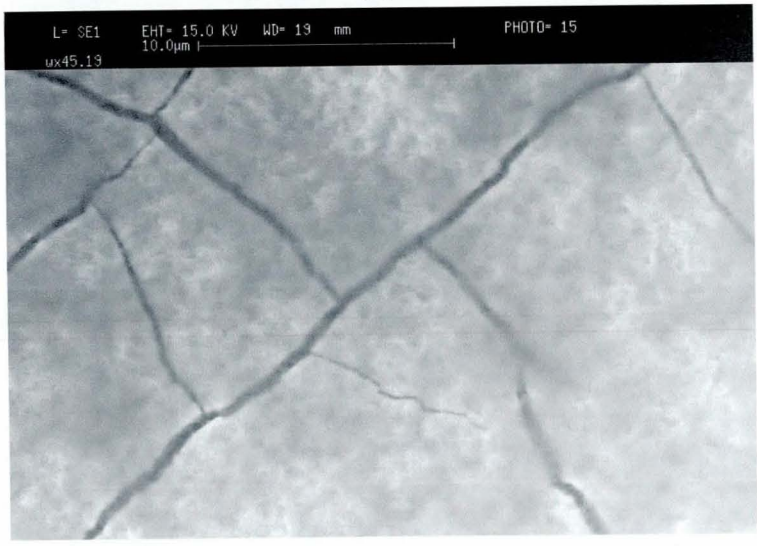

(c)

Figure 11.4 **SEM micrographs showing morphologies of (A) Zn-11%Ni (B) Zn-11%Ni-1%SiO_2 (C) Zn-11%Ni-11%SiO_2. SiO_2 (20 nm).**

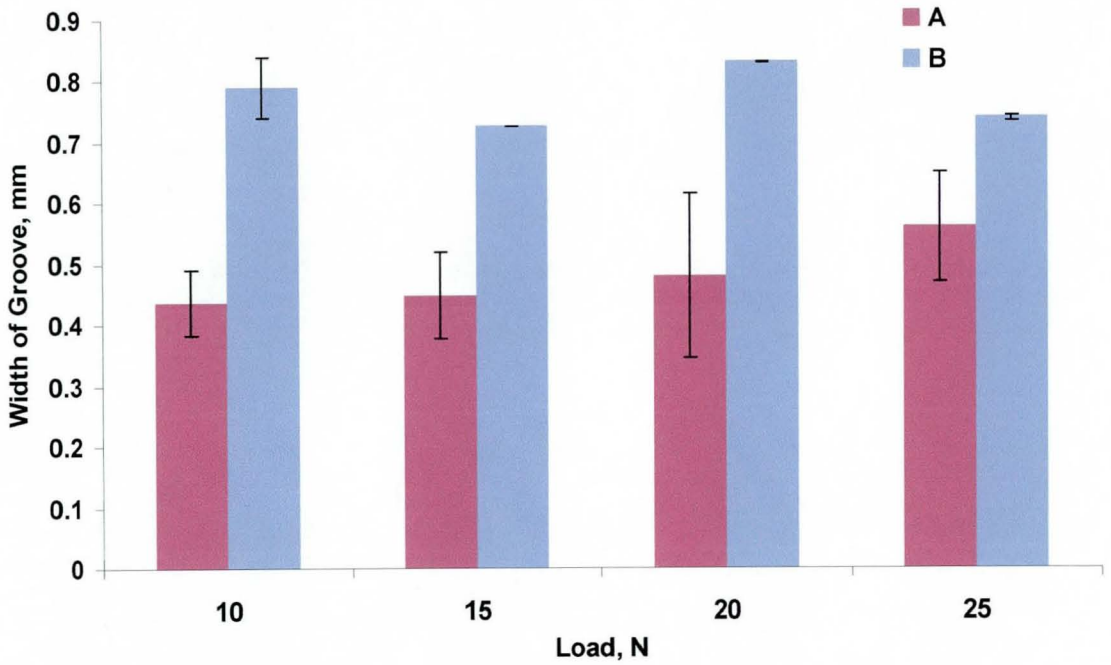

Figure 11.5 **Size of worn Surface of (A) Zn-11 %Ni and (B) Zn-11%Ni-11%SiO_2. SiO_2 (20 nm).**

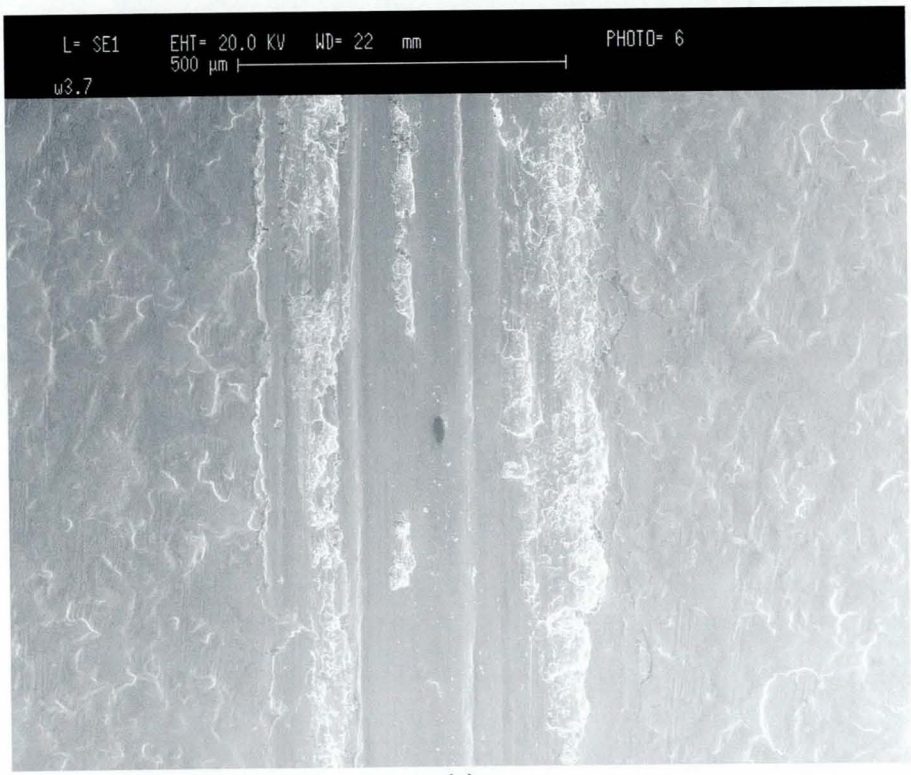

(a)

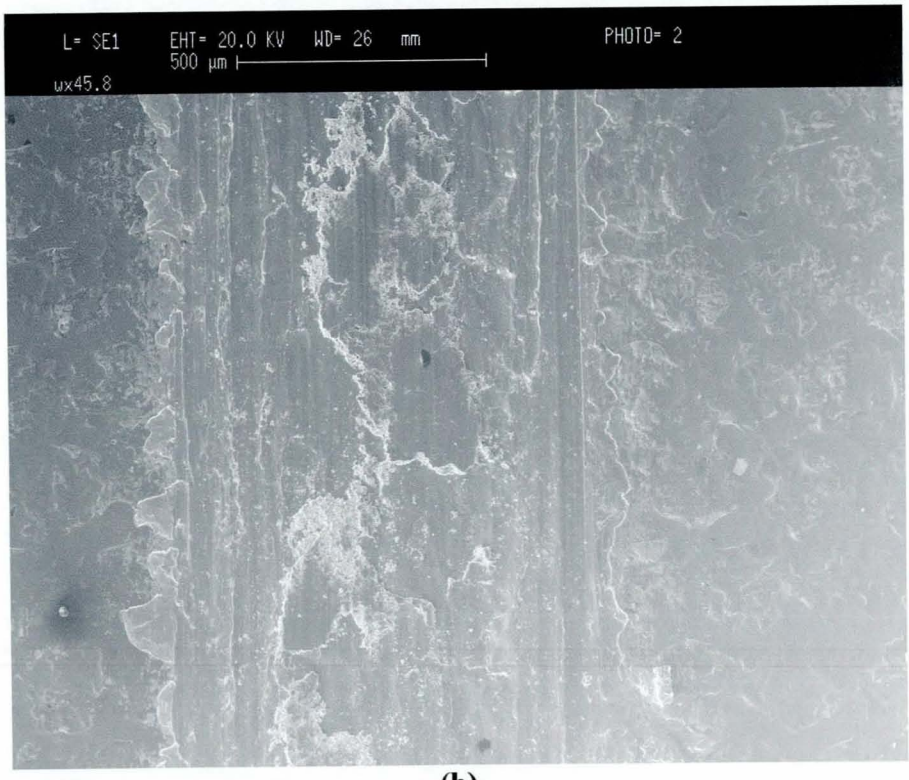

(b)

Figure 11.6 **SEM micrographs of wear surfaces of (a) Zn-11%Ni and (b) Zn-11%Ni-11%SiO_2. Load 20 N and 100 cycles. SiO_2 (20 nm).**

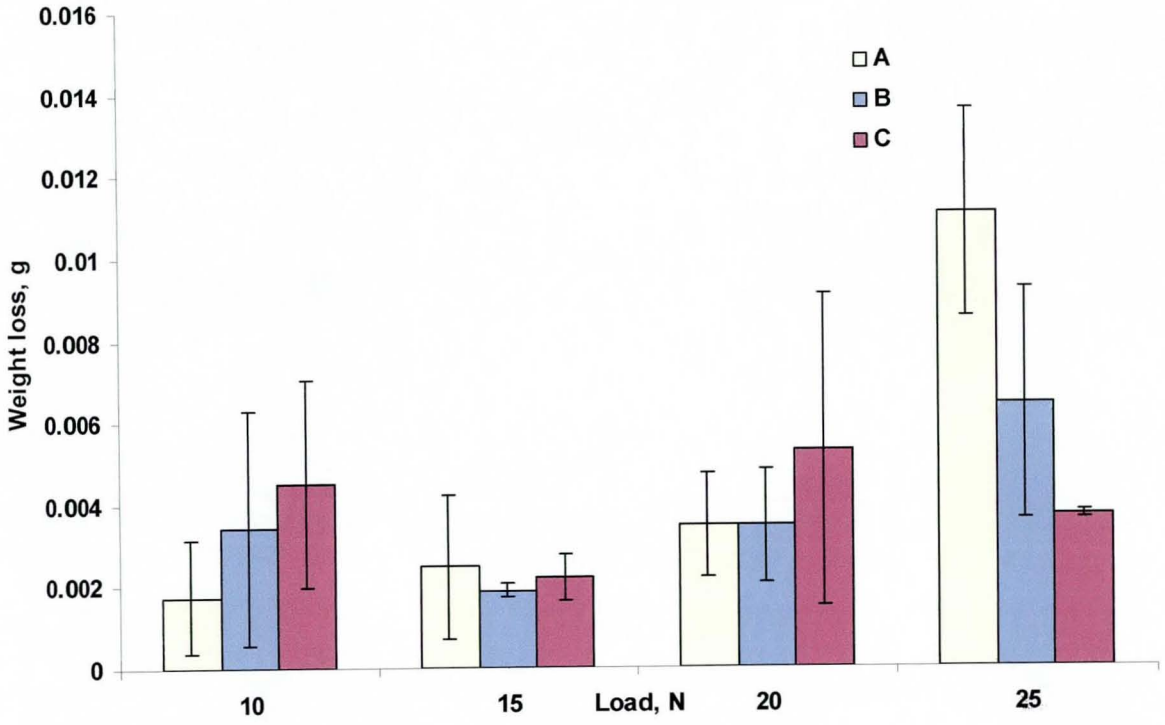

Figure 11.7 **Weight loss versus increasing load for (A) Zn-11%Ni (B) Zn-11%Ni-1%SiO_2 (C) Zn-11%Ni-11%SiO_2. 100 cycles. SiO_2 (20 nm).**

APPENDIX A: Determination of cathode current efficiency of Zn/SiO_2 composite electrodeposits

Cathode current efficiency of Zn/SiO_2 electrodeposits were determined gravimetrically and calculated using the following formulae:

Assuming zinc/silica composite coating has a total weight of W_0 and the weight percentage of silica in the coating is X_1 and zinc is X_2, where $X_1+X_2=100\%$. The weights of silicon, $W_{Si,}$ and zinc, W_{Zn}, in the coating can therefore be deduced as follows;

$$W_{Si} = \frac{W_0 X_1}{60} \times 28 \tag{1}$$

$$W_{Zn} = W_0 X_2 \tag{2}$$

The weight percentage of silicon obtained by EDAX is

$$X^* = \frac{W_{Si}}{W_{Si} + W_{Zn}} \times 100\% \tag{3}$$

Substituting Equations (1) and (2) into (3), one obtains

$$X^* = \frac{\frac{W_0 X_1}{60} \times 28}{\frac{W_0 X_1}{60} \times 28 + W_0 X_2} \times 100\% = \frac{0.467 X_1}{0.467 X_1 + (1 - X_1)} \times 100\% = \frac{0.467 X_1}{1 - 0.533 X_1} \times 100\% \tag{4}$$

Rearranging Equation (4),

$$X_1 = \frac{X^*}{0.467 + 0.533 X^*} \times 100\% \tag{5}$$

Equation 5 can be used for the calculation of weight percentage of silica (X_1) in the coating from the weight percentage of silicon (X^*) obtained by EDAX.

CCE calculation:

$$CCE = \frac{W_{Zn}}{W_T} \times 100\% = \frac{W_0 X_2}{\frac{ItM_{Zn}}{nF}} \times 100\% = \frac{nFW_0 X_2}{ItM_{Zn}} \times 100\% \tag{6}$$

Available online at www.sciencedirect.com
SCIENCE DIRECT
Surface & Coatings Technology 200 (2006) 5921–5930
SURFACE & COATINGS TECHNOLOGY
www.elsevier.com/locate/surfcoat

Behaviour of Zn-SiO_2 electrodeposition in the presence of *N,N*-dimethyldodecylamine

Tolumoye J. Tuaweri, G.D. Wilcox *

Institute of Polymer Technology and Materials Engineering, Loughborough University, Loughborough, Leicestershire, LE11 3TU, UK

Received 15 April 2005; accepted in revised form 8 September 2005
Available online 18 November 2005

Abstract

Zn-SiO_2 composite electrodeposits have been produced from a sulphate bath. The effects of process parameters such as current density, agitation, particle loading and deposition time on the rate of particle incorporation are presented. It was shown that the amount of SiO_2 embedded in the coating is dependent not only on the rate of agitation but also on the type of agitation. The effect of particle size was extensively investigated. It was found that the level (wt.%) of larger particles (2 μm) in the deposits was higher than that of smaller ones (20 nm) produced under similar experimental conditions. A study of the influence of *N,N*-dimethyldodecylamine (NND) as a surface-active additive is also presented. Cathodic polarisation studies show that addition of SiO_2 to the bath increased the zinc deposition current densities whilst the presence of NND in the bath seemed to inhibit the rate of zinc deposition. However, it was established that the addition of *N,N*-dimethyldodecylamine significantly improved the rate of particle incorporation for larger particles. Morphological characteristics of Zn-SiO_2 electrodeposits produced under various electrodeposition conditions are also presented.

Keywords: Zinc; Silica; Corrosion; Wear; Electrodeposition; Composite electrodeposit; *N,N*-dimethyldodecylamine

1. Introduction

Zinc has long been utilised as a sacrificial coating to protect steel from corrosion. However, the life span of such coatings is limited due to the aggressive nature of some environments, particularly those containing industrial pollutants. Consequently, considerable efforts are being made to improve their corrosion resistance [1]. The synergistic relationship between corrosion and wear in most cases has made it increasingly important for the development of coatings capable of conferring considerable resistance to both phenomena.

The electrocodeposition of suspended inert particles into a growing metal matrix seems to offer a possible solution to this problem and has attracted research interest due to their unique functional properties such as improved corrosion [2–7] and wear resistance [8–10], lubricity [11,12] semiconductor properties [13], magnetic properties and superconduction [14]. The electrocodeposit properties obtained generally depend on the type of particulate inclusion. Most composite coatings contain micron-sized particles, although there is growing interest in the codeposition of nanoparticles [15] because of their increasing availability, coupled with the ability to produce surfaces with superior hardness, corrosion and wear resistance. The advantages of electrocodeposition over other coating methods are the uniformity of deposition for complex shapes, reduction of waste encountered in dipping or spraying techniques, low level of contamination, the ability to process parts continuously [11], high production rates, low initial capital investment requirements and easy transfer from the research laboratory to existing infrastructure in electroplating and electroforming industries [9]. However, composite electrocodeposition is not without its drawbacks. Fransaer et al. [16] reported that in aqueous plating electrolytes, particles easily agglomerate due to the compression of the diffuse double layer surrounding the particles by their high ionic strength. It was also noted that this effect is more pronounced for particles of submicron size as the shearing forces on the agglomerates, created by the agitation of the plating bath, decrease with particle size. As a consequence the codeposition of agglomerated particles takes place and the anticipated mechanical, chemical and/or physical properties of the composite coatings are not achieved. Hydration forces [17]

* Corresponding author.
E-mail address: g.d.wilcox@lboro.ac.uk (G.D. Wilcox).

0257-8972/$ - see front matter © 2005 Elsevier B.V. All rights reserved.
doi:10.1016/j.surfcoat.2005.09.023

may also be possible hindrances to particle codeposition. This would explain why highly hydrophilic materials such as oxides, have a small tendency to codeposit, while hydrophobic materials such as polymers, graphite, codeposit readily [16]. Silica is hydrophilic and therefore falls into this group of oxides that are difficult to codeposit. In an attempt to overcome this difficulty, the influence of *N,N*-dimethyldodecylamine (NND) surfactant was explored in this work. It has been reported that the use of surfactants can allow a controlled composition of deposit to be achieved [18]. It has also been confirmed that suitable surfactants could not only improve the stability of a suspension (by increasing the wettability and surface charge of suspended particles) but also enhance the electrostatic adsorption of suspended particles on a cathode surface by increasing their positive charge [19]. However, there are also penalties associated with the use of surface-active materials, which, in inappropriate concentrations, can interfere with incorporation through excessive adsorption on the cathode surface. Free surfactant can also be incorporated in the electrodeposited layer and can cause adverse changes in the mechanical properties of the electrodeposit such as high internal stress and brittleness [18]. Hence the need for careful selection of these surface-active additives and the quantity added to the bath.

The electrocodeposition of Zn-SiO_2 has been reported [2–6]. Takahashi et al. [6] also reported the effect of SiO_2 colloid on the electrodeposition of zinc–iron group metal alloy composites. According to them, SiO_2 has a negative zeta potential, and therefore its electrophoresis to the cathode cannot be expected. However, a phenomenon of induced codeposition was observed, since SiO_2 increased the percentage of Fe, Co, or Ni in the alloys and the iron group metal cations simultaneously accelerated the codeposition of SiO_2 [6]. For enhanced codeposition of ceramic particles, the effect of various types of electrodeposition parameters have previously been reported such as agitation [10,18], surfactants in the bath [7,10,18–21]. However, it is apparent that few investigators have reported on the codeposition enhancement mechanism of NND surfactant on zinc-silica composite electrodeposition. This work therefore, seeks to investigate the codeposition behaviour of Zn-SiO_2 in the presence of this surfactant under various conventional electrodeposition parameters such as agitation, current density, particle size and particle concentration in the bath.

2. Experimental

The electrodeposition was carried out with an acid sulphate zinc bath of standard laboratory reagents containing 250 g/l of $ZnSO_4 \cdot 7H_2O$ and 80 g/l of Na_2SO_4.The effect of several parameters such as presence of *N,N*-dimethyldodecylamine ($CH_3(CH_2)_{11}N(CH_3)_2$)—97% (Aldrich), use of agitation, particle size, particle bath concentration, deposition time and mechanism of codeposition were studied. The range of current densities and pH was 1 to 30 A/dm^2 and 2.0–2.5, respectively. Bath temperature was 50 °C. Silica particles of approximately 20 nm in aqueous suspension and 2 μm particles were used as received from Alfa Aesar, see Fig. 1a and b. Instead of coating particles

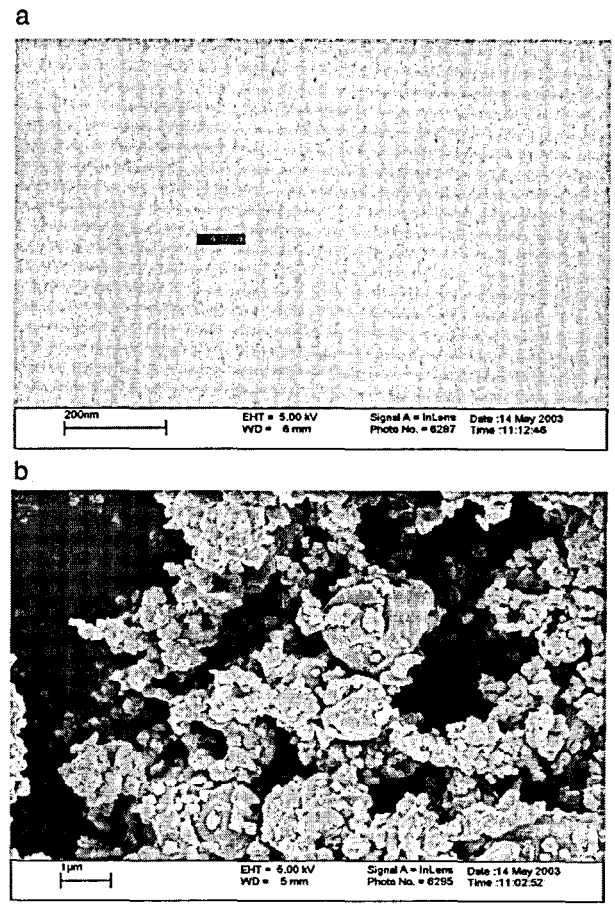

Fig. 1. SEM micrographs of (a) 20 nm and (b) 2 μm particles of silica.

with NND before addition to the electroplating bath, the surface-active agent was added directly into the individual baths since the particles were received in two different forms: colloidal (20 nm) and powder (2 μm). This anomaly could have made it difficult to modify their surfaces with NND in a consistent manner prior to electroplating bath make-up. Agitation was effected using a mechanical stirrer at various speeds of rotation and vibro-agitation with a vibromixer [22]. The diameter of the perforated plate attached to the vibromixer, which effected the agitation, was 4.5 cm. A zenith variac supplied power to the vibromixer.

Coatings were electrodeposited onto mild steel. Prior to electrodeposition, the mild steel panels were first cathodically cleaned in a bath containing 25 g/l of NaOH, 25 g/l of Na_2CO_3 and 50 g/l of Na_3PO_4 and then etched in 50% v/v (SG 1.18) hydrochloric acid for approximately 20 s, washed in running tap water and then in de-ionised water. They were then transferred immediately into the bath for plating to avoid re-oxidation of the surface. All the electrodeposition experiments were carried out galvanostatically using DC currents both at high and low current densities. The anode material was 99% zinc foil.

Coating compositions and morphologies were analysed using a scanning electron microscope (SEM) and a Field Emission Gun Scanning Electron Microscope (FEGSEM) both fitted with an X-ray energy dispersive analysis system. The weight

percentage of silicon in the deposits was analysed by the EDX analyser and converted to the weight percentage of silica.

3. Results and discussions

3.1. Parameters affecting the rate of particle incorporation

3.1.1. Effect of increasing current density

The relationship between current density and rate of particle incorporation with different particle sizes is presented in Fig. 2. For both sizes of particles, a peak in particle incorporation was achieved at 15 A/dm^2. Further increase in current density resulted in initially lower rates of incorporation for both sizes of particles. However, at higher current densities of about 30 A/dm^2 there was a further increase in particle incorporation for the 2 μm particles. Although produced at higher current densities, the trend is similar to other reported composite electrodeposition systems [10,11,23]. It has been reported [11] that particle incorporation behaviour, as a function of current density, can be divided into several regions: initially a region where incorporation increases sharply reaching a maximum value, followed by a sharp decrease in incorporation, then a region where incorporation is fairly constant, and then another decrease as mass transport-limited conditions are approached. Fig. 2 further supports the authors [11] that the regions where the amounts of incorporation sharply increase or decrease with current density are sensitive to particle size. Various explanations have been given for such deposition behaviour. In some cases it is considered that, up to the maximum current density where incorporation occurs, codeposition is controlled by mass transfer [24,25]. In other systems, it is suggested that, before the maximum, the process is controlled by adsorption of the particles, while an increase in current density results in more rapid deposition of the metal matrix and fewer particles are embedded in the coating [23]. In Fig. 2, therefore, the sharp increase in particle incorporation for each type of particle before the maximum point could indicate a fast mechanism of SiO_2 incorporation and beyond the maximum, metal deposition possibly dominates the codeposition process.

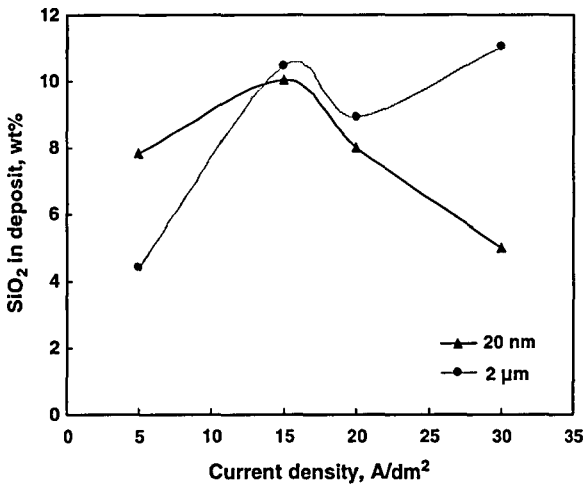

Fig. 2. Relationship between cathode current density and rate of particle incorporation for 20 nm and 2 μm particles with 13 g/l bath loading and amplitude of agitation 0.55 mm.

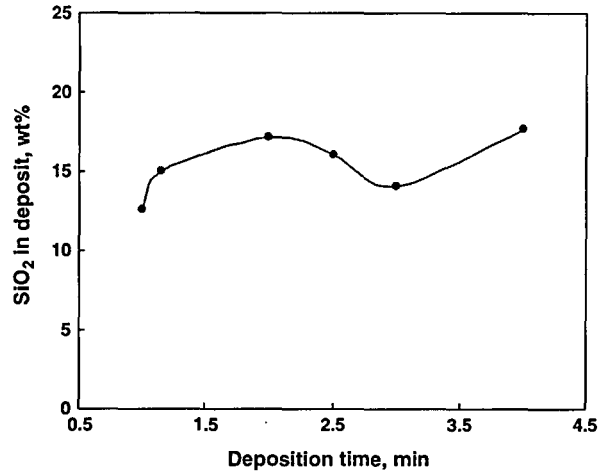

Fig. 3. Effect of increasing deposition time on rate of particle incorporation from a bath containing SiO_2 (2 μm) 80 g/l, amplitude of vibration 1.8 mm, current density 30 A/dm^2.

The rate of particle incorporation with increasing deposition time at a constant current density of 30 A/dm^2 is shown in Fig. 3. The trend of incorporation indicates that there is insignificant increase in the rate of particle incorporation with increase in deposition time. This indicates a relatively uniform rate of incorporation within the specified duration for approximately 1 μm depth from the surface of the coating (energy dispersive X-ray analysis approximate analysis volume). For each current density, there is probably a maximum deposition time limit for particle incorporation beyond which no further increase in the rate of particle incorporation takes place. This is possibly associated with increase in cathode surface pH and subsequent hydroxide formation. On the cathode, $Zn(OH)_2$ is formed due to hydrogen evolution and subsequent pH increase [6]. Since the isoelectric point shifts towards negative values at higher pH, it might be reasonable to suggest that the longer the plating time, the higher the pH at the cathode surface and therefore the possibility of a lower isoelectric point and negative zeta potential which could promote the agglomeration of particles. Consequently, this could lead to lower rates of particle incorporation. However, it has been reported by other investigators [5] that the codeposition of silica is negligible at low pH and increases with increasing pH of the electrolyte.

3.1.2. Effect of bath agitation on particle incorporation

Different types of solution agitation have been reported [26]. Vibratory agitation was given particular attention in the present work because it has one special virtue—it is particularly effective in composite electroplating where it is necessary to maintain second phase particles in suspension in such a way that they can be systematically and quantitatively incorporated in the electrodeposit [22].

Fig. 4 shows the relationship between rate of bath agitation and the level of particle incorporation for a fixed bath particle concentration of 13 g/l and particle size of 2 μm. Rate of

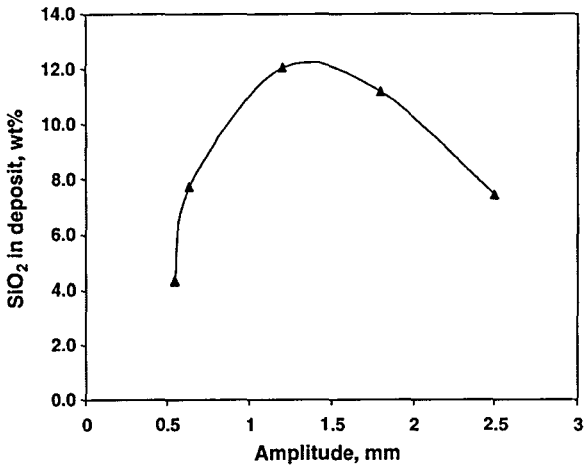

Fig. 4. Effect of vibratory agitation on the rate of particle incorporation. Current density 5 A/dm^2, SiO_2 (2 μm) 13 g/l, pH 2, T=50 °C.

particle incorporation visibly increased until it attained a maximum at an amplitude of about 1.5 mm and then decreased gradually with further increase in agitation. The decrease in incorporation rate has previously been attributed to the collision factor [27]. When the quantity of the transferred particles is too great to be completely entrapped by the growing matrix, the free particles (i.e. those that are neither adsorbed nor incorporated) collide with the incoming particles. This collision factor results, therefore, in a decrease in the rate of incorporation [28]. Muller et al. [10] reported that at low rotation speeds the fluid flow induced by a RDE is not capable of transporting all the particles to the cathode and, when the rotation speed is too high, the rate of particle removal becomes greater than that of attachment at sites on the electrode [29]. Kalantary and Gabe [30] reported that an increase in vibratory agitation should increase the degree of incorporation. However, excessive agitation reduces incorporation as particles are swept away from the surface before incorporation can take place. The results presented in Fig. 4 seem to agree with these authors. For a vibratory system of agitation, residence time of the particles on the cathode is important and seems to also determine the rate of particle incorporation. In a RDE system, increasing the rotational speed effectively reduces the residence time of the particle at the electrode surface, further inhibiting incorporation [11]. Such behaviour is similar to the vibratory system. The increase in particle incorporation from an amplitude of 0.5 to 1.5 mm indicates a faster reduction of adsorbed species, since the shortened residence time results in an increase in codeposition. However, at higher values of agitation the residence time does become an issue again as the reduction of the adsorbed species cannot keep pace with increased supply of particles, and incorporation is reduced. In general if the agitation is too low, particles in the bath may not disperse completely, except when their density is low. On the other hand, if the agitation is too high, particles will not have sufficient time to get attached to the surface and this results in poor particle incorporation [31]. It has been suggested that the stirring speed should be optimised based on the size of the second phase particles to be incorporated [31]. For the purpose of comparison, two types of agitation are presented in Fig. 5. It is obvious that the rate of particle incorporation was significantly improved for the vibratory agitation as opposed to magnetic stirring. A possible explanation is that there is a tendency for particles to remain longer (high residence time) within the same amplitude of vibration due to the reciprocal motion of the perforated plate causing a rotational motion with the commencement of eddy patterns at amplitudes of about 0.62 mm [30]. The fluid rotational motion is circular in a vertical plane thereby allowing particles to remain longer within the vicinity of the cathode and consequently becoming occluded in the growing metal matrix. If the forces acquired due to the vibratory motion are greater than that of a slow horizontal flow (magnetic stirring), which is assumed in this work to be perpendicular to the vibratory motion, the particles could remain longer within the same amplitude and hence become enveloped into the growing metal matrix. On the contrary, magnetic stirring induces a horizontal flow which has the tendency to sweep away particles from the surface of the cathode consequently reducing their residence time which could lead to poorer rates of incorporation. Mechanical agitation has been shown to result in lower incorporation due to its directional flow recently by other researchers [31].

3.1.3. Effect of N,N-dimethyldodecylamine on rate of particle incorporation

Alteration of the surface, via the adsorption of surfactant species, markedly promotes the incorporation of inclusions [18]. Helle and Walsh [18] reported that in nickel–diamond composite electrodeposition, the zeta potential was negative in the absence of surfactant but became less negative as the level of cationic surfactant was increased. At a solution level of approximately 8 mg of surfactant per gram of diamond the zeta potential was zero and hence there was no net charge on the particle. At higher surfactant levels, the zeta potential became increasingly positive, allowing the amount of diamond powder incorporated into the deposit to be enhanced due to the increasing positive charge on the particles. A similar trend of

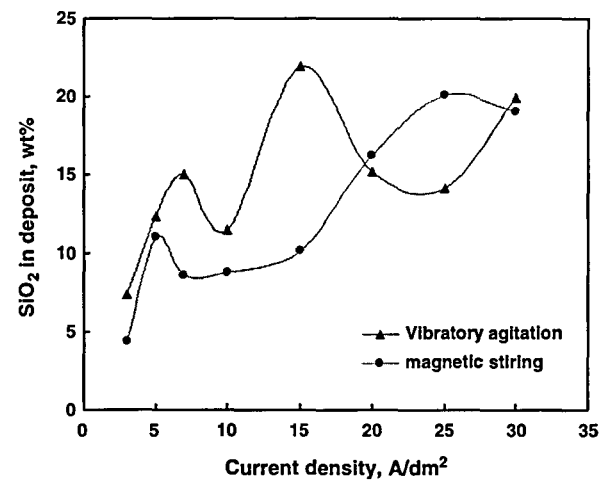

Fig. 5. Relationship between rate of particle incorporation and current density with different types of bath agitation. SiO_2 (2 μm) 60 g/l.

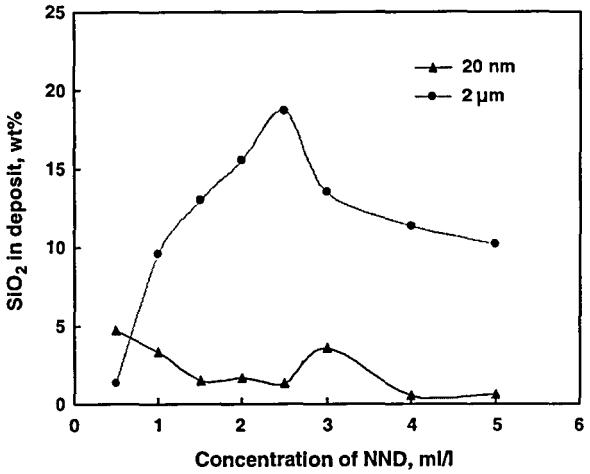

Fig. 6. Effect of *N,N*-dimethyldodecylamine (NND) on the rate of particle incorporation for 20 nm and 2 μm particles. Current density 30 A/dm^2, SiO_2 50 g/l, amplitude of vibration 1.8 mm.

improved incorporation is observed in Fig. 6 which shows that increasing the bath concentration of NND improves the rate of particle incorporation for 2 μm sized particles. There was no significant increase in the incorporation of 20 nm particles, rather a slight decreasing trend was observed. The increase in particle incorporation of the 2 μm particles attained a maximum value at 2.5 ml/l NND. Beyond this concentration, a sharp decrease in incorporation was observed with further increase in the bath concentration of NND. At low concentrations of NND, the silica particles may not have acquired sufficient positive charge to prevent their aggregation [7]. On the other hand, at optimum concentrations (2.5 ml/l) of NND, the particles may have acquired sufficient positive charge that could lead to de-aggregation due to electrostatic repulsion sufficient to stabilise them in the solution. Similar observations have previously been reported [20] with cetyl trimethyl ammonium bromide (CTAB). Reasons for the selective improvement of incorporation rates for the larger against the smaller sized particles have been addressed by several investigators, although a clear theory is not apparent. However, it might be reasonable to consider the surface area to volume ratio of the different sizes of particles. For the same volume and bath loading of the separate types of particles, the surface area available for possible adsorption of NND could be larger for smaller particles than that of larger ones. This could lead to excessive amounts of NND on the smaller particles due to the larger area of adsorption consequently causing electrostatic repulsion and therefore reduced rate of incorporation. It could also be associated with the hydrophilic characteristics of SiO_2 and difference in momentum of the particles. Nowak et al. [32] reported that for both flotation and codeposition processes a solid particle approaches an interface and rupture of the aqueous film between the particle and the interface must occur to allow the capturing of the particle. The momentum acquired from the prevalent (electrophoretic, electroosmotic and hydrodynamic) forces in the bath, may not be large enough for the 20 nm particles to penetrate and hence rupture the aqueous film between the particle and the interface for them to be captured at the interface. Fransaer et al. [17] proposed hydration or structural forces as the adhesion force governing particle incorporation. This repulsion force arises from the work required to remove the ordered hydration layers at the solid–liquid interfaces for solids coming into close contact. Hence it was argued [29] that the hydrophobic nature of the adsorbed cetylpyridium chloride dimers diminishes the hydration forces and enhances polystyrene codeposition. Based on the proposals elsewhere [17,32], it might be reasonable to consider that for incorporation of particles to occur, they must have sufficient terminal momentum to either overcome the ordered hydration forces or rupture the aqueous film between the particle and the interface. Since this momentum is a function of particle mass and velocity just before incorporation, particles with reasonably large momentum might be able to rupture the aforementioned forces much more easily than their smaller counterparts and hence incorporate better. It is also noteworthy, that at optimum conditions of 2.5 ml/l NND, 50 g/l of 2 μm particles and an amplitude of 1.8 mm, the rate of particle incorporation was slightly over twice the rate of incorporation without NND (see Fig. 7).

3.1.4. *Effect of particle size on rate of incorporation*

From Figs. 6 and 8, it is obvious that rate of incorporation is largely dependent on the particle size. The presence of NND did not cause any significant increase in the rate of incorporation for 20 nm particles since the maximum incorporation observed was approximately 5 wt.% for deposition with or without NND in the bath. While for the same conditions for 2.0 μm particles, up to approximately 19 and 14 wt.% of silica was deposited with or without NND in the bath, respectively. The larger particles were found to produce higher silica content in the coatings under all experimental conditions. These observations seem to agree with previous works [16,33,34] on the Ni/SiC system, which suggest that codeposition of particles

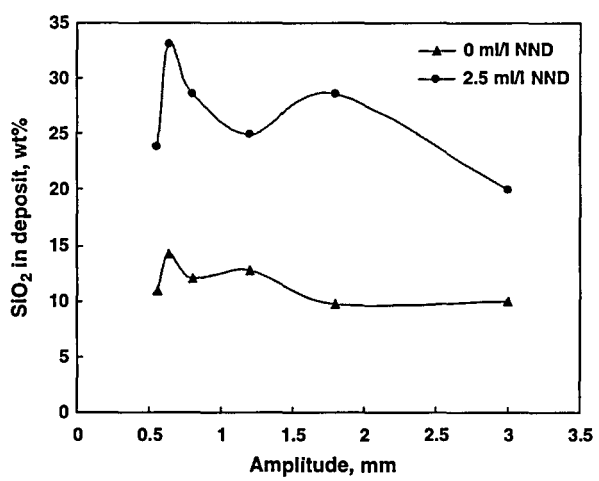

Fig. 7. Effect of *N,N*-dimethyldodecylamine (NND) on rate of particle incorporation for 2 μm particles. Current density 30 A/dm^2, SiO_2 50 g/l, NND 2.5 ml/l, amplitude of vibration 1.8 mm.

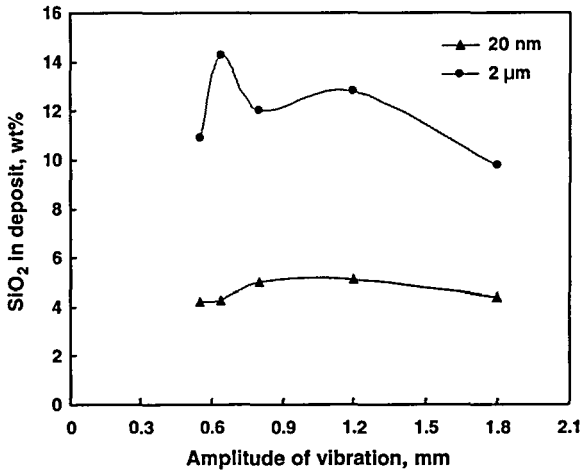

Fig. 8. Effect of agitation on the rate of particle incorporation for 20 nm and 2 μm particle without NND. Current density 30 A/dm^2, SiO_2 50 g/l.

decreases with decrease in particle size. In aqueous plating electrolyte particles easily agglomerate due to compression of the diffuse double layer surrounding the particles by the high ionic strength. This effect is more pronounced for particles of submicron size as the shearing forces on the agglomerates, created by agitation of the plating bath, decrease with particle size [16]. This may also have contributed to the low rate of incorporation of the 20 nm particles. However, considering the large difference in particle size ratio of 20 nm:2 μm being 1:100, the number of 20 nm particles codeposited must be greater but their overall mass deposited less. Recently, Garcia et al. [35] reported that for a given number density of particles in an electroplating solution for three different SiC particle sizes, namely 5, 0.7, and 0.3 μm, the number density of particles rather than volume fraction of SiC in the coating increases with decreasing particle size. However, Hou et al. [36] argue that the assumption of the mono-dispersed particles in the plating solution is not realistic since the agglomeration of SiC particles must occur significantly to decrease the free energy in the system.

FEGSEM micrographs as shown in Fig. 1(a) and (b) reveal that the 2 μm particles had fairly irregular geometries whilst the 20 nm particles were round shaped. The geometry of irregularly shaped particles tends to provide better interlocking with other codepositing particles and with the metal matrix and hence could become readily incorporated into the growing metal matrix. It has been reported that angular shaped particles will have a greater tendency to adhere to the surface upon impingement than round ones [31]. However, Apachitei et al. [37,38] have shown that spherically shaped alumina particles resulted in better incorporation than irregular ones. In addition, Fig. 1b shows a range of particle sizes many nowhere near 2 μm. The use of such uneven particle size distribution could lead to the production of inhomogeneous composite electrodeposits. Non-uniform size distribution in such deposits could affect the anticipated properties and performance, which could be desired, may not be achieved. An uneven dissolution rate of the electrodeposits could occur, when in contact with a corrosive medium, due to the high level of irregular particle size present at various sites.

3.1.5. Effect of electrolyte particle loading on particle incorporation

The effect of bath concentration of SiO_2 particles is shown in Fig. 9. There are obviously two distinct trends of incorporation. Up to the bath concentration of approximately 100 g/l of silica particles, there is an obvious increasing trend. However, beyond this concentration, the incorporation behaviour takes an increasing trend but with an oscillating response. This is probably due to the fact that beyond 100 g/l, the particle concentration in the bath would have been high enough to induce localised agglomeration, which could lead to uneven distribution of particles in the coatings. Consequently, the analytical probe may have picked either pockets of agglomerates giving high peaks or regions of low incorporation with lower peaks for coatings produced beyond 100 g/l hence the sinusoidal response beyond this concentration. The trend of incorporation indicates an overall increase with increasing bath concentration for the 2 μm particles. The observations seem to agree with other investigators [6] that SiO_2 contents in the composite electrodeposits increased with an increase in its concentration in the bath. However, a high concentration of silica particles in the electro-galvanising bath deteriorates its stability, causes cohesion or precipitation of silica particles, and generally reduces the service life of the electro-galvanising bath. In addition, solution resistance in the electro-galvanising bath could become unnecessarily high, resulting in poorer current efficiency and increased consumption of electric power for electro-galvanising [4].

The agglomeration of SiO_2 particles at high bath concentration was observed with the 20 nm particles. Fig. 10 shows SEM surface and cross-sectional views of a zinc-silica electrodeposit from a bath concentration of 104 g/l of 20 nm particles deposited at 30 A/dm^2. Analysis using the SEM revealed two

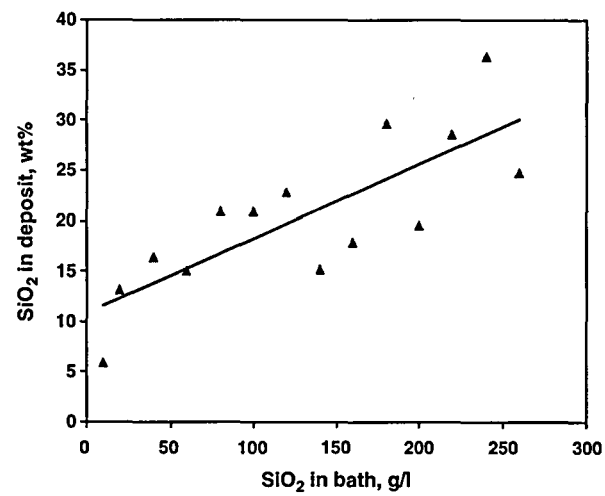

Fig. 9. Relationship between bath concentration of SiO_2 and weight percentage of SiO_2 in deposit. Particle size 2 μm and current density 30 A/dm^2.

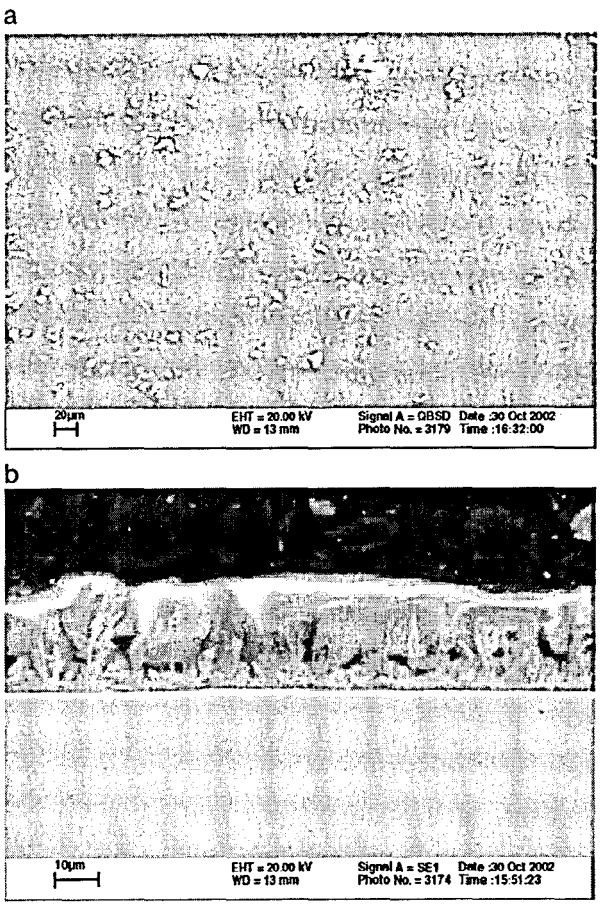

Fig. 10. SEM micrographs of (a) surface morphology and (b) cross-sectional area of zinc-silica electrodeposit. SiO_2 (20 nm) 104 g/l, current density 30 A/dm^2, agitation 500 rpm and pH 2.

distinctly deposited layers—an under layer of dendritic zinc matrix and a top layer of SiO_2. Dendritic growth behaviour in composite electrodeposition has been reported [8]. The surface morphology (see Fig. 10a) was also analysed and the white patches were identified as zinc and the darker portions gave strong silicon peaks. The high overpotential may have increased the rate of Zn^{2+} reduction on the cathode, which could cause an increase in pH of the cathode. Increase in pH is thought to cause the agglomeration of particles. Consequently, the agglomerated particles may have become adsorbed as the top layer preventing further zinc deposition. This indicates that excessive addition of nano-sized silica particles in an aqueous bath could result in an adsorbed layer of silica rather than codeposition. Although, the properties of such deposits were not investigated further, they could exhibit high porosity due to insufficient metal matrix in the top layer to provide the desired metal–particle bonding.

4. Cathodic polarisation studies

Cathodic polarisation studies were carried out on mild steel to aid a mechanistic understanding of the separate influences of NND and SiO_2 on zinc electrodeposition.

Mild steel panels were polarised from their open circuit potential. Both dilute and concentrated baths were used for studying the effect of SiO_2 while only a dilute bath was used in the case of NND. Dilute electrolytes were employed in order to achieve well-defined deposition behaviour in the polarisation curves as opposed to solutions with high zinc levels where metal reduction peaks are less clear [12]. As can be seen from Fig. 11, both dilute and concentrated electrolytes had similar behaviours in the presence of SiO_2 particles. The results from Fig. 11 indicate that there are two main reduction reactions for H^+ and Zn^{2+} forming H_2 and Zn, respectively. The zinc appears to deposit at potentials below −1000 mV vs SCE. Activity prior to this is attributed to oxygen reduction and possibly hydrogen evolution. Increased activity following zinc reduction is due to concurrent hydrogen evolution. Fig. 11 also indicates that there was an increase in the zinc deposition current densities for the baths with silica particles. This trend could support the assumption that when silica particles are added into a zinc bath, the zinc ions tend to adsorb onto the surface of the SiO_2 particles [39], migrate to the cathode and consequently increase the zinc deposition current density due to higher concentration of zinc ions around the cathode. The adsorption of zinc ions onto SiO_2 has been reported [40]. The authors attributed the mechanism of cation adsorption to proton release and noted that adsorption of zinc ions on silica increases with increase in pH of the solution up to 7 and then decreases. However, these observations may not be the same with other composite electrodeposition systems as it has been reported that SiC powder would not significantly affect the electrochemical reduction of nickel ions in the watts bath [27]. Simmons [12] reported a slightly different trend with the zinc/PTFE baths. He stated that upon addition of PTFE to the zinc electrolyte, the whole polarisation curves appeared to shift to more cathodic potentials (i.e. for a given potential the current density became slightly lowered). A similar trend to Simmons [12] was observed in the present investigations when NND was added to the zinc baths (Fig. 12). NND also causes a reduction in the zinc deposition signal, which appears to be approximately proportional to its bath concentration. A

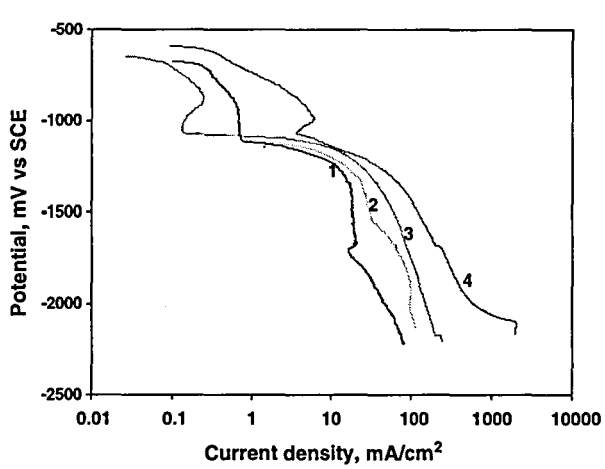

Fig. 11. Cathodic polarisation for mild steel in zinc, and zinc-silica electroplating solutions containing (1) 10 g/l $ZnSO_4 \cdot 7H_2O$; (2) 10 g/l $ZnSO_4 \cdot 7H_2O$, 13 g/l SiO_2; (3) 250 g/l $ZnSO_4 \cdot 7H_2O$; (4) 250 g/l $ZnSO_4 \cdot 7H_2O$, 13 g/l SiO_2.

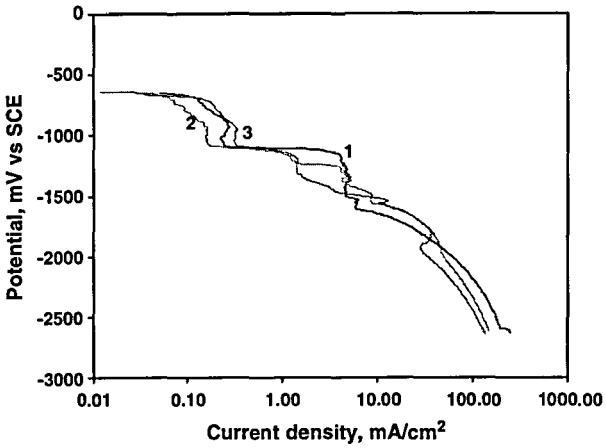

Fig. 12. Cathodic polarisation curves obtained for mild steel in 10 g/l $ZnSO_4 \cdot 7H_2O$, 80 g/l Na_2SO_4 solutions with (1) 0 ml/l NND, (2) 0.04 ml/l NND, (3) 0.2 ml/l NND.

possible explanation for such behaviour is that NND present in the solution competes with zinc cations for active sites on the electrode and particle surfaces. When there is sufficient NND adsorbed onto these surfaces, the zinc deposition current density decreases. Alternatively, the NND could become adsorbed onto the electrode surface thereby blocking off and consequently preventing further deposition of zinc hence the diminishing current densities as the concentration of NND in the bath increases.

5. Morphological studies of zinc-silica electrodeposits

The morphology of a zinc-silica electrodeposit produced with 20.0 nm particles is presented in Fig. 13. As can be seen the electrodeposit consists of crystals with distinct sequential layer-by-layer stacking of hexagonal platelets with their bases parallel to each other and to the surface of the substrate thereby forming columns of crystals. The parallel alignment of hexagonal plane crystals of about 1 μm to the surface of the substrate has been reported by other investigators [2].

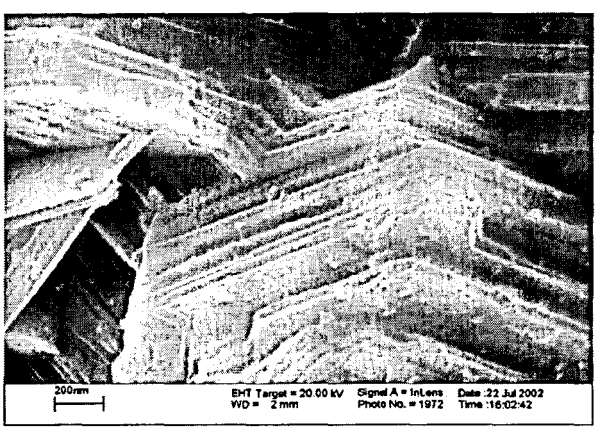

Fig. 13. SEM micrograph of zinc-silica electrodeposited at a current density of 30 A/dm^2, pH 2.6, SiO_2 (20 nm) 26 g/l and agitation 800 rpm.

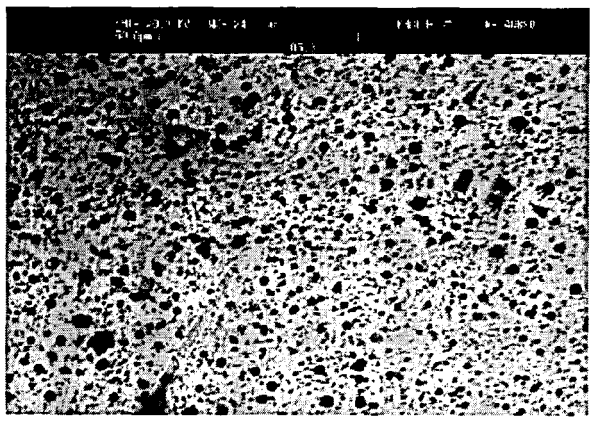

Fig. 14. Surface morphology of zinc-silica electrodeposit containing 21.3 wt.% SiO_2. SiO_2 (2 μm) 50 g/l, current density 30 A/dm^2, agitation 1.8 mm, pH 2.0 and NND 2.5 ml/l.

Fig. 13 further shows the mechanism of codeposition of silica particles onto the zinc crystals. The particles, as can be seen, are randomly incorporated on the sidewalls of the hexagonal crystals. It has been reported [2] that zinc electrodeposits incorporate SiO_2 in two ways. The particles lined up along the macrosteps grow laterally and sweep up the particles to the edge. The randomly dispersed particles remain at their absorbed sites [2]. This described mechanism of codeposition seems to be true as can be seen from Fig. 13. The randomly dispersed particles seem to have initially deposited on the edges of the crystals and then subsequently swept either onto or beneath the surfaces of the laterally stacked layers of hexagonal crystals probably due to the prevalent forces (hydrodynamic, electrophoretic, adsorption and electrostatic) acting on the particles.

Figs. 14 and 15 are surface morphologies of zinc-silica electrodeposits with 24 and 16.8 wt.% of 2 μm silica particles produced from baths containing 2.5 and 1.0 ml/l of NND, respectively. Figs. 14 and 16(a) indicate that NND does not only enhance the codeposition of 2 μm silica particles but also exhibits an acceptable leveling effect of the electrodeposits. Fig. 15 shows a fan-shaped morphology of the zinc-silica

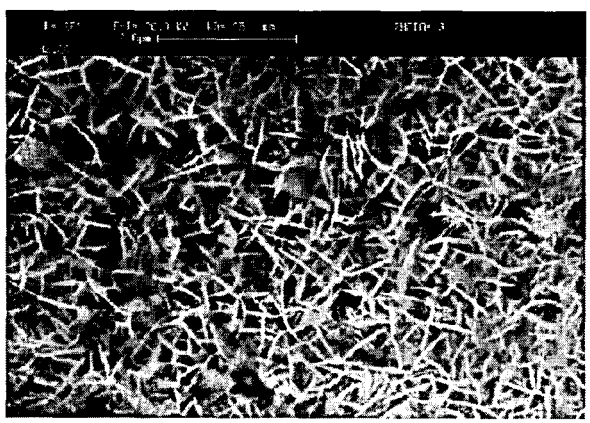

Fig. 15. SEM micrograph of zinc-silica electrodeposit with 15.5 wt.% SiO_2. SiO_2 (2 μm) 50 g/l, current density 30 A/dm^2, agitation 1.8 mm, pH 2.0 and NND 1.0 ml/l.

electrodeposits. Similar fan-shaped zinc-silica morphologies have been reported elsewhere, produced when surfactants have been added to the electroplating bath [7]. The formation of such morphologies is attributed to preferential adsorption of the surfactants on (0002) planes leading to the preferential growth of (1010) zinc planes perpendicular to the (0002) plane. In addition, these deposits could provide sufficient anchor on application of polymer paints. The highly uniform distribution of particles in Figs. 14 and 16 is an indication of the de-aggregation and the enhanced mono-dispersion effect of NND. Minimal agglomeration is observed in these deposits. Being dense and compact, these deposits could exhibit enhanced corrosion resistance if the interfacial bonding between the particles and the metal is strong. However, the effect of non-uniform size distribution of particles on the surface morphology of the deposit is obvious in Fig. 17. There are poor contacts at the interfaces between the larger particles and the metal matrix resulting in porosity. These porous sites are probably due to interfacial stress between the particles and the metal matrix as a result of irregular surface characteristics of the 2 μm particles and could provide suitable sites for the ingress of corrosive species thereby enhancing a quicker mechanism of dissolution.

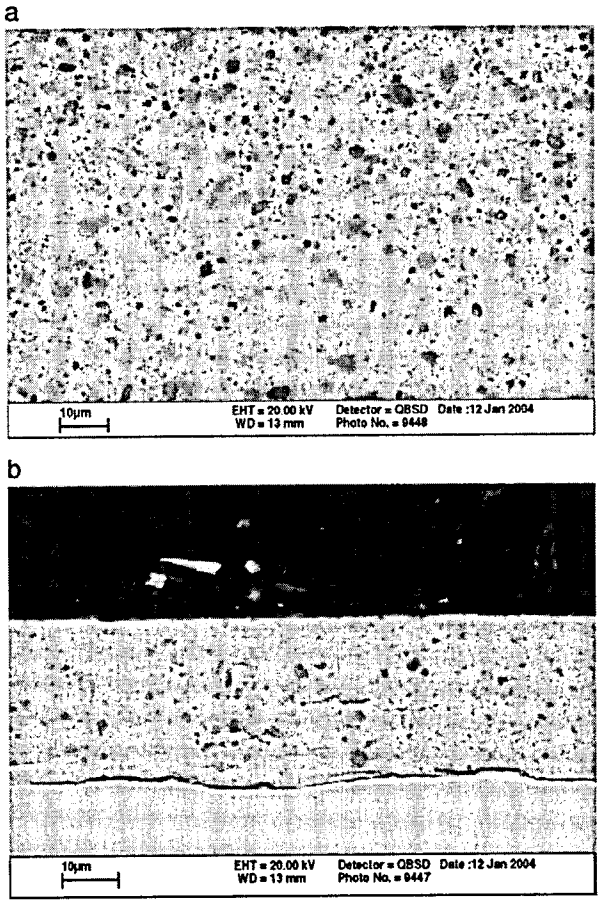

Fig. 16. SEM micrographs (a) surface morphology (b) cross-sectional view of zinc-silica electrodeposit containing 22.8 wt.% SiO_2. SiO_2 (2 μm) 50 g/l, current density 30 A/dm^2, amplitude of agitation 1.8 mm, pH 2.0 and NND 2.5 ml/l.

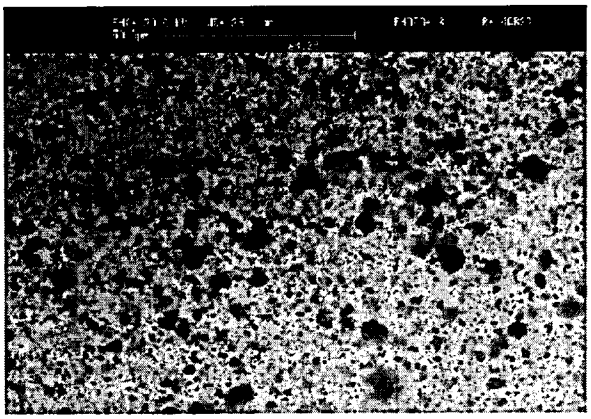

Fig. 17. Surface morphology of zinc-silica electrodeposit containing 33 wt.% of 2 μm SiO_2 particles obtained with 2.5 ml/l of NND in the bath.

In contrast, there are reasonably compact deposits at the sites where smaller particles are deposited. Such locations on the deposit should exhibit better corrosion resistance. Similar results have been reported [41] in a SiC/Ni system. According to these authors, ultra-fine particles, although more difficult to codeposit, produce composite electrodeposits with smoother and better bonding characteristics between SiC and Ni than that in coarse SiC/Ni composites. In many applications, it is therefore recommended that a codeposition of ultra-fine particles with metal is preferable to coarse particles [41].

6. Conclusions

The particle incorporation behaviour of zinc-silica electrocodeposition was found to be significantly dependent on particle size. For nearly all deposition conditions investigated in this work, it was found that the amount (wt.%) of larger particles incorporated was higher than the smaller ones. Not only was the rate of particle incorporation found to be dependent on the magnitude, but also, on the type of agitation. Vibratory agitation is more effective than magnetic stirring in terms of particle incorporation for the conditions of deposition investigated here.

The rate of particle incorporation was also found to improve significantly when *N,N*-dimethyldodecylamine cationic surfactant was added to the zinc-silica electrolytic bath with 2 μm particles. At optimum conditions, electrodeposits with unusually high concentrations as much as 33 wt.% of SiO_2 were produced in the presence of NND with 2 μm size particles. The improved incorporation could probably be attributed to the inhibitive effect of *N,N*-dimethyldodecylamine on the mechanism zinc deposition. Cathodic polarisation studies seem to confirm this inhibitive effect. However, the presence of NND seems to have no positive effects on the rate of incorporation of smaller 20 nm particles. An inhibitive trend was observed for most concentrations of 20 nm particles and concentrations of NND utilised. However, excessive additions of about 104 g/l of 20 nm particles produced electrodeposits with a thick deposited layer of agglomerated SiO_2. Lower particle and bath concentrations of NND may be required to improve the rate of

incorporation and produce an even distribution of 20 nm particles in the electrodeposit.

Finally, it was found with 2 μm particles that deposition time and thickness seem to have little effect on the rate of particle incorporation.

Acknowledgements

The authors wish to thank the sponsors of this project, Bayelsa State Government of Nigeria.

References

[1] N.R. Short, A. Abibsi, J.K. Dennis, Trans. Inst. Met. Finish 67 (1991) 73.
[2] K. Kondo, A. Ohgishi, Z. Tanaka, J. Electrochem. Soc. 147 (2000) 2611.
[3] S. Hashimoto, M. Abe, Corr. Sci. 36 (1994) 2125.
[4] M. Abe, S. Yukimitsu, A. Takeshi, N. Hiroshi, United States Patent, 4,839,241 (June 1989).
[5] M. Kimoto, A. Yakawa, T. Tsuda, R. Kammel, Metall 44 (1990) 1148.
[6] A. Takashi, Y. Miyoshi, T. Hada, J. Electrochem. Soc. 141 (1994) 954.
[7] M. Hiramatsu, H. Kawasaki, Y. Nakayama, T. Omi, Plating Surf. Finish. 74 (7) (1987) 48.
[8] M. Ghorbani, M. Mazaheri, K. Khanogholi, Y. Kharazi, Surf. Coat. Technol. 148 (2001) 71.
[9] U. Erb, Nanostruct. Mater. 6 (1995) 533.
[10] C. Muller, M. Sarret, M. Benbala, Surf. Coat. Technol. 162 (2002) 49.
[11] J.L. Stojak, J.B. Talbot, J. Electrochem. Soc. 146 (1999) 4504.
[12] M. Simmons, Ph.D. Thesis, Loughborough University, 2001.
[13] F. Linder, A. Feltz, J. Eur. Ceram. Soc. 11 (1993) 269.
[14] P. Sarkar, et al., J. Appl. Phys. 69 (1991) 1775.
[15] L. Benea, P.L. Bonora, A. Borello, S. Martelli, F. Wenger, P. Ponthiaux, Jacques Galland, J. Electrochem. Soc. 148 (2001) C461.
[16] J.P. Fransaer, E. Leunis, T. Hirato, J.P. Celis, J. Appl. Electrochem. 32 (2002) 123.
[17] J.P. Fransaer, J.P. Celis, J.R. Roos, J. Electrochem. Soc. 139 (1992) 413.
[18] K. Helle, Frank Walsh, Trans. Inst. Met. Finish. 75 (1997) 53.
[19] A. Hovestad, L.J.J. Janssen, J. Appl. Electrochem. 25 (1995) 519.
[20] C. Filiatre, C. Pignolet, A. Foissy, M. Zembala, P. Warszynski, Colloids Surf., A Physicochem. Eng. Asp. 222 (2003) 55.
[21] A. Hamid, Anti-Corros. Methods Mater. 48 (2001) 235.
[22] M.R. Kalantary, S.A. Amadi, D.R. Gabe, Circuit World 5 (1989) 42.
[23] Z. Wang, Y.Z. Wan, S.M. Zhao, H.M. Tao, X.H. Dong, Surf. Coat. Technol. 106 (1998) 162.
[24] K. Shrestha, I. Miwa, T. Saji, J. Electrochem. Soc. 48 (2001) 85.
[25] C. Kerr, Barker, F. Walsh, J. Archer, Trans. Inst. Met. Finish. 78 (2000) 171.
[26] D.R. Gabe, Trans. Inst. Met. Finish. 81 (2003) 7.
[27] H. Yen, C.C. Wan, Plating. Surf. Finish. 84 (3) (1997) 54.
[28] P.A. Gay, P. Bercot, J. Pagetti, Surf. Coat. Technol. 140 (2001) 147.
[29] A. Hovestad, R.J.C.H.L. Heesen, L.J.J. Janssen, J. Appl. Electrochem. 29 (1999) 331.
[30] M.R. Kalantary, D.R. Gabe, Trans. Inst. Met. Finish. 67 (1989) 28.
[31] J.N. Balaraju, T.S.N. Sankara Narayanan, S.K. Seshadri, J. Appl. Electrochem. 33 (2003) 807.
[32] P. Nowak, R.P. Socha, M. Kaisheva, J. Fransaer, J.P. Celis, Z. Stoinov, J. Appl. Electrochem. 30 (2000) 429.
[33] G. Maurin, A. Lavanant, J. Appl. Electrochem. 25 (1995) 1113.
[34] S.K. Kim, H.J. Yoo, Surf. Coat. Technol. 108-109 (1998) 564.
[35] I. Garcia, J. Fransaer, J.P. Celis, Surf. Coat. Technol. 148 (2001) 171.
[36] K.H. Hou, M.D. Ger, L.M. Wang, S.T. Ke, Wear 253 (2002) 994.
[37] I. Apachitei, J. Duszcyzyk, L. Katgerman, P.J.B. Overkamp, Scr. Mater. 38 (1998) 1347.
[38] I. Apachitei, J. Duszcyzyk, L. Katgerman, P.J.B. Overkamp, Scr. Mater. 38 (1998) 1383.
[39] D. Aslandis, J. Fransaer, J.P. Celis, J. Electrochem. Soc. 144 (1997) 2352.
[40] B. Cabot, A. Foissy, J. Mater. Sci. 33 (1998) 3945.
[41] S. Wang, W.J. Wei, Mater. Chem. Phys. 78 (2003) 574.